博士論文

Doctoral Thesis

Development of Model Updating in 3D AEM to Improve the Numerical Modeling of Existing RC Frame Buildings

（既存の RC フレーム建物の数値モデリングを改善するための 3DAEM でのモデル更新の開発）

TIMSINA KISHOR

ティムシナ キスール

Development of Model Updating in 3D AEM to Improve the Numerical Modeling of Existing RC Frame Buildings

既存の RC フレーム建物の数値モデリングを改善するための
3DAEM でのモデル更新の開発

By
Kishor Timsina
37-207250

A Thesis
Submitted to The University of Tokyo
In partial fulfilment of the Requirements
For
The degree of Doctor of Engineering

Under supervision of
Professor Kimiro Meguro

Department of Civil Engineering
The graduate school of The University of Tokyo
Tokyo, Japan

July 2023

ACKNOWLEDGEMENT

I extend my heartfelt appreciation and deep gratitude to Professor Kimiro Meguro, my esteemed supervisor, for his invaluable contributions to this study. His stimulating ideas, constructive suggestions, enduring patience, and unwavering encouragement have been instrumental in shaping the course of this research.

I am also sincerely grateful to Assistant Professor Chaitanya Krishna of AIT Thailand for his innovative ideas, consistent guidance, unwavering support, and encouragement throughout the research journey.

My sincere thanks go to the members of my thesis committee: Professor Riki Honda, Professor Koichi Kusunoki, Associate Professor Muneyoshi Numada, and Associate Professor Tsukasa Mizutani. Their valuable comments and feedback have significantly enriched the quality of this work.

I express my profound gratitude to Assistant Professor Kenjiro Yamamoto, whose continuous support from the day of my arrival in Japan has been invaluable.

I would like to extend my appreciation to my colleagues at the Meguro and Numada Lab for their friendship, assistance, and moral support, all of which have played a crucial role in completing this thesis.

I am thankful to the Asian Institute of Technology (AIT) and my friends at AIT who provided continuous support during my experiments in Thailand. Moreover, my heartfelt thanks go out to all my friends in Nepal, Japan, and around the world who directly or indirectly supported me during this research.

I am indebted to the secretaries from the Meguro and Numada Laboratory, Ms. Lisa Takakuwa and Ms. Nana Suzuki, for their unwavering assistance throughout this time.

Gratitude must also be extended to the MEXT scholarship program for providing the essential financial support that made this research possible.

Lastly, I dedicate this research work to my beloved parents, Kashinath Timsina and Renuka Timsina, my sister Balika Timsina, and my fiancé Dr. Srijana Neupane. Their constant love and unwavering support have been my guiding light through challenging times and have instilled in me the ambition to pursue higher studies.

I am deeply thankful to all those who have directly or indirectly contributed to my doctoral study. Your support has been invaluable, and I am truly grateful for it.

Kishor Timsina

July 2023

ABSTRACT

In the contemporary built environment, a significant proportion of building structures, particularly Reinforced Concrete (RC) frame buildings, face substantial seismic risk, primarily attributed to substandard construction techniques and non-uniform constituent elements. These non-engineered structures lack durability and resilience due to the absence of essential elements such as sufficient capacity, ductile detailing, and construction quality. To understand the structural status of these buildings and mitigate seismic risk, numerical modeling is essential.

Different numerical techniques, the finite element method (FEM) and discrete element methods (DEM) etc., have demonstrated their efficacy in offering precise numerical modeling. However, constructing numerical models involves uncertainties and assumptions. To validate the results, researchers rely on non-destructive measurements and compare them with the numerical data. Model update approaches, which modify unknown factors, have been introduced to reduce discrepancies between experimental and numerical dynamic characteristics.

Operational modal analysis techniques like frequency domain decomposition (FDD) or stochastic subspace identification (SSI) can extract mode shapes and modal frequencies from ambient vibration measurements, providing valuable inputs for model updating. Despite the abundance of research on finite element (FE) model updating, there is limited research on model updating for low to mid-rise RC buildings with relatively higher stiffness due to infill masonry. Additionally, the Applied Element Method (AEM) proves to be an accurate approach for monitoring structure response but lacks existing numerical model updating techniques.

The thesis aims to address this research gap by exploring numerical model updating technique for low to mid-rise RC buildings, particularly those analyzed using the Applied Element Method, providing insights to enhance seismic resilience and safety in the face of actual

disasters. There are four specific objectives of this research. The first objective is to develop a least square problem for model updating, tailored to these types of structures. The second objective involves integrating the model updating methodology into 3D AEM numerical modeling. The third objective focuses on enhancing the computational efficiency of the 3D AEM tool. Finally, the research aims to perform a seismic vulnerability assessment of an existing building using vibration data, which will help in evaluating its susceptibility to seismic events.

In this research, first, a least square problem for model updating which is suitable for low to mid rise buildings having limited number of operational modal data and limited measurements is developed. The least square problem is formulated calculating the relative residual vector of experimentally measured modal properties and analytical modal properties. The analytical modal properties are calculated using the initial guess of updating parameters for the model updating which is material properties (Young's Modulus/ stiffnesses) for the numerical model of the structure. Using the formulated least square problem as the objective function for the minimization problem, the problem is solved to get the optimum value of updating parameters using Levenberg-Marquardt algorithm. Initially, the model updating implementation is examined for generalized shear frames with various scenarios involving limited measured degree of freedoms (DOFs) and the no. of modes used for model updating, evaluating the accuracy of stiffness updates for structural systems. From this implementation it is understood that, obtaining higher modes in structural analysis becomes challenging and leads to spurious results with increased damping, causing inaccuracies in updating the model. However, it is feasible to update the structural model using a limited number of measured degrees of freedom (DOFs) and modes in operational modal analysis. While frequency parameters can be obtained relatively accurately, mode shape parameters are less precise. In the presence of spurious

modes, giving higher weightage to the residual involving eigenvalues is recommended in the model updating process.

Subsequently, the method is tested on a 3-storey scaled experiment model of a steel frame with bolt-connected joints, inducing damage in different locations by loosening the bolting condition. Ambient vibration measurements are taken in one direction on each floor level, and operational modes and frequencies are obtained using frequency domain decomposition. Through model updating, the storey stiffness of the experiment model is accurately determined, enabling identification of the damage caused by loosening bolts at each storey level. Comparisons between the modal properties of the updated structure and the experimental modal properties validate the accuracy of the model updating process.

One of the objectives of this research is to model real existing structure in 3D AEM. So, it was necessary to improve the current solvers and storage systems used in 3D AEM. With the comparison of different solvers and storage system, parallel direct sparse solver (PARDISO) with triplet storage format using multiple thread of CPU is identified to be the most efficient one and is implemented in 3D AEM.

In the next phase, a four-storey reinforced concrete (RC) frame building representing typical buildings in Nepal is utilized for implementing the model updating methodology. Synthetic data of experimental operational mode shapes and frequencies are obtained by applying frequency domain decomposition to the response of the structure subjected to white noise using actual material properties. The 3D AEM is employed to model the structure with unknown stiffnesses, categorized into three groups: beam/slab, column, and infill wall properties, which serve as the updating parameters. The ARPACK-Arnoldi package integrated in 3D AEM is utilized to obtain analytical modal properties, and the least square problem is formulated based on the residual of experimental and analytical modal properties. The Levenberg-Marquardt

algorithm is applied to minimize the problem and obtain the updating parameters. Comparisons between the Young's Modulus and modal parameters of the updated structure with the assumed values validate the successful implementation of the model updating in 3D AEM, confirming that acceptable error margins can be achieved through this approach.

Next, static and dynamic analysis of the updated numerical model is performed to understand the seismic vulnerability of the structure using 3D AEM. The quantification of the overall damage and local damages are studied successfully in performance criteria based on interstorey drift, frequency degradation and deformation of the structure. The static pushover analysis of the case study structure indicates soft storey behavior, with displacement concentration on the ground floor. This is evident from the higher inter-storey drift ratio on the ground floor compared to upper floors. Failure patterns observed include in-plane shear cracks, on-plane failure of masonry walls, and tensile failure at beam column joints. The frequency degradation curve shows a reduction in stiffness with increasing lateral displacement. The incremental dynamic analysis of the updated 3D AEM model for various ground motions enhances our understanding of the building's seismic performance, providing valuable information on deformation, damage level, and failure mechanisms. These insights can be utilized to optimize the design of structures and improve earthquake resistance.

Finally, the method is then applied to real existing building structures using ambient vibration data measured from the field and analyzed in 3D AEM. The Young's Modulus (stiffnesses) of the structure is considered unknown and assigned random initial values. The elements are grouped into 11 different groups, including floorwise beams/slabs, columns, shear walls, and infill walls, serving as the updating parameters. Comparisons between the Young's Modulus (stiffnesses) and modal parameters of the updated structure with the actual assumptions validate the successful implementation of the model updating in 3D AEM. The study

demonstrates that accurate numerical model updating in 3D AEM is achievable with a limited number of operational modes obtained from the field, but the accuracy heavily depends on the initial guess of the updating parameters. The updated structure is then performed non-linear analysis using static pushover analysis to understand the capacity and performance of the structure.

In conclusion, the least square problem for model updating which is suitable for low to mid rise buildings having limited number of operational modal data and limited measurements is developed and successfully tested for the generalized frame structures. Next, the model updating methodology is successfully integrated in 3D AEM numerical modelling. It is now possible to perform the parameters update for the numerical model for real existing buildings. Also, the computational efficiency of 3D AEM tool is significantly improved with the use of parallelized direct solver (PARDISO), and it is used for performing seismic vulnerability assessment of the real existing building using vibration data using both dynamic and static analysis methods successfully.

Table of Contents

List of figures:

List of tables:

Chapter 1: Introduction

1.1 Background and Motivation

Earthquakes pose a significant risk when combined with substandard built environments, potentially resulting in substantial damage if buildings are unable to withstand the forces generated by seismic events. In the contemporary built environment, a significant proportion of building structures face substantial seismic risk, primarily attributed to substandard construction techniques and non-uniform constituent elements. In recent years, urban and semiurban areas of Indian sub-continent have witnessed rapid growth, with the prevalence of reinforced concrete with masonry infill (RC) buildings increasingly becoming the norm in these regions. One illustrative instance pertains to The National Population and Housing Census (CBS 2012) of Nepal, wherein it has been documented that an estimated more than 500 thousand structures have been classified as reinforced concrete constructions, ranging in height from three to five stories (Figure 1-1) [1]. Over the past few decades, the construction of RC buildings has significantly increased displacing the traditional construction materials, however most of these buildings are non-engineered structures built by untrained masons and owners, lacking adequate capacity, ductile detailing, and construction quality, which significantly limits their durability and resilience [2]. As these buildings are located in seismically very active region, huge damages in these structures have been observed in recent earthquakes (Figure 1-2). In summary, the real world contains a significant number of large buildings situated in regions prone to earthquakes, constructed with subpar practices and varying material properties. These buildings undergo multiple changes over time after their construction. Simulating these scenarios in numerical model to study real-world engineering issues can be quite difficult. Nevertheless, it is imperative to understand the structural state of these buildings to reduce earthquake risk prior to any potential disasters occur.

Figure 1-1: Low to Mid Rise Buildings in Nepal (Photo Courtesy: K. Timsina)

Figure 1-2 : Building Damage in Gorkha Earthquake 2015 (Photo Courtesy: NSET, Nepal)

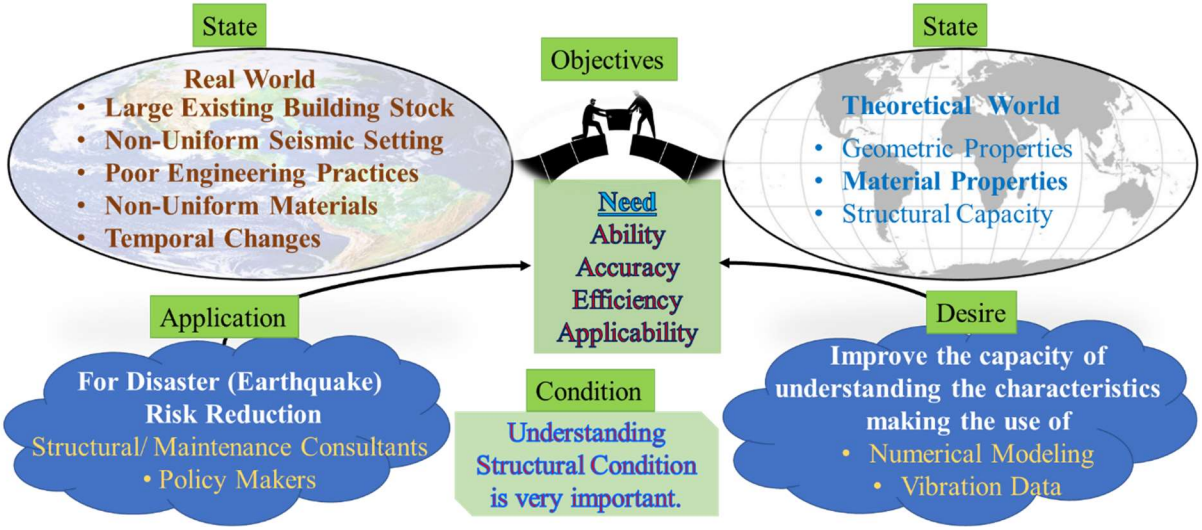

Figure 1-3 : Conceptual representation of the motivation for the research

To facilitate this process, real-world structures are typically transformed into a theoretical realm that allows for easy replication of their behaviour. This entails defining the problems with respect to structural capacities, geometric and material characteristics. Accurately replicating these diverse parameters of real-world structures within an analytical numerical model is necessary to achieve a comprehensive understanding of their behaviour in the face of actual disasters. The motivation of this research is to bridge the gap between real world and theoretical world by improving the capacity of understanding the characteristics of the real world structures through numerical modelling and vibration data with good ability, accuracy, efficiency and applicability, such that the developed model and numerical tool can be utilized by structural consultants and policy makers for earthquake risk reduction (Figure 1-3).

1.2 Review of Existing Literatures

1.2.1 Identification of Material Properties

The three most crucial factors to consider when evaluating a building's state, damage, vulnerability, remaining capacity, and post-earthquake safety are its structural, geometric, and

material properties. The degree to which the material and geometric properties of the structure are predicted or estimated has a significant impact on the accuracy, precision, and practical application of the model. The available drawings/design papers, as well as actual measurements, can be used to determine the structural and geometrical characteristics of the buildings. On contrary, the identification of the material properties has several uncertainties. Theoretically, the idealised concrete is assumed to be homogenous and isotropic, however an actual site situation may be different. It becomes more complicated generally as a result of environmental factors, ageing, and degeneration with time. Since most structures are not engineered and are built incorrectly with numerous human faults, it is impossible to estimate material properties using any engineering judgement based on expert opinion. So, there is a challenge to estimate the material properties accurately for the numerical modelling.

To determine the material properties, there are various non-destructive tests available, including the Schmidt Hammer test and ultrasonic pulse velocity (UPV). However, the existing structures we are working with are generally not engineered, with non-uniform material distribution throughout the structure, making it impossible to achieve a high accuracy using these methods. The precision of the used instruments and their calibration also significantly affects the accuracy of the results [3],[4],[5].

There are existing studies on expert based properties identification, in which assessment is done using different numerical approaches and properties are estimated with certain sets of assumptions [6],[7]. There are some researches, in which, parametric analyses are used to account for uncertainties by randomising the inputs and changing the parameters [8],[9], [10]. With conversation to building owners, masons, or contractors, some studies take into account the building's initial properties[11].

There are several vibration-based methods available to determine material characteristics. Numerous studies have been done to identify the material properties for bridges and detect deterioration using vibration based methods [12], [13] and also in the structural health monitoring of tall buildings with good reliability[14], [15],[16]. Ambient vibration measurements can provide operational modal data in terms of frequencies, and mode shapes which are frequently utilised as experimental inputs to forecast unknown physical parameters. Mode shapes represent the spatial distribution of vibration within a structure for each mode of vibration, while modal frequencies represent the natural frequencies at which a structure vibrates. It is feasible to derive frequencies and mode shapes from ambient vibration data by applying operational modal analysis techniques like stochastic subspace identification (SSI) and frequency domain decomposition (FDD) [17], [18]. The modes identified by operational modal analysis, however, are not scaled mode shapes. We are working with existing, generally stiffer low- to mid-rise buildings. The higher modes and modal characteristics of these structures is highly difficult to obtain. Without knowledge of the higher modes, it is challenging to determine the precise material characteristics.

1.2.2 Model Updating Methods

There are many numerical methods like finite element method (FEM)[19], discrete element methods (DEM)[20] etc. can provide good outcome for the problems with accurate numerical modelling. The constitution of numerical models entails numerous uncertainties and assumptions. To verify the experimental results, researchers usually conduct non-destructive measurements and compare them with the numerical data. Model update approaches have been introduced, wherein unknown factors including material properties, and other physical parameters are modified, to reduce disparities between experimental and numerical dynamic characteristics.

Model updating entails changing a numerical model of a structure such that its behaviour matches experimental observations. This is a widely employed technique for assessing structural performance. Mottershead and Friswell [15], [21] and Marwala [22] conducted a study of the various finite element (FE) model update strategies. Two common approaches to model updating are direct and indirect (iterative) methods (Figure 1-4).

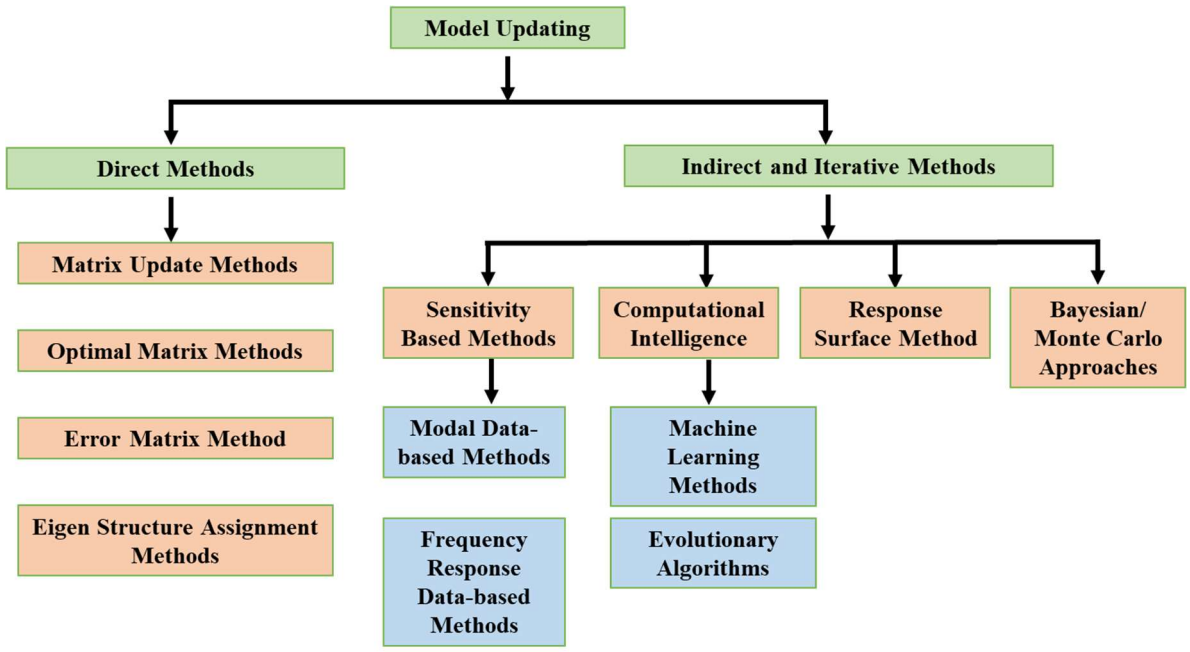

Figure 1-4: Model-Updating Methods

Modal properties of the structure are used in direct methods for model updating. They are regarded as precise and efficient techniques. Some of the existing direct model updating techniques are the eigen structure-assignment [23], optimal-matrix, error-matrix [21], matrix update [24] method. Direct approaches have several drawbacks that make them unreliable, even though they are precise and effective [22]. Direct methods assume that the mathematical model completely encompasses the fundamental physics of the issue at hand. However, this presumption is frequently challenging to meet and does not consider the impact of measurement inaccuracies or fluctuations in observed responses [25]. Due to the aforementioned challenges, direct methods are unsuitable for the purpose of material properties

identification. However, alternative iterative and indirect approaches exist to tackle these issues effectively.

To start with, sensitivity-based techniques involve the analysis of measured responses as deviations from the responses of the initial numerical model of the structure, and the optimization objective function is defined through the use of an error minimization function approach, as described in scholarly literature approach [22],[21]. The underlying assumption of this approach is that the measured responses should closely resemble the computed data obtained from the numerical model. Hence, sensitivity-based approaches are more appropriate when dealing with the structures where the alterations in the actual structure are relatively minor in magnitude. Notable examples of research utilizing sensitivity-based methods include the study of Yu et al.[26] and Sarvi et al. [27].

Next, the Response Surface Method (RSM) is a statistical technique used to establish relationships between predetermined design variables and their corresponding responses, represented as polynomial functions. Through this method, the optimal response can be determined by minimizing the variation between the initial model and the actual measured responses. [22], [28], [29]. Owing to its computational efficiency and applicability, RSM has found widespread usage in model updating applications as evidenced in [28],[29]. However, the statistical approximations employed by RSM cannot accurately identify the location-wise properties [22] and application to large-scale structures warrants further research [29].

Another one, the Bayesian model-updating technique uses Bayes' theorem. The probability distribution of the model is reflected by employing the database set with similar distribution [22]. Monte Carlo approaches are commonly employed to solve Bayesian methods. The outcome of the Bayesian methods is generally accurate without overfitting and simple to execute [30]. The damage identification problems are generally solved using the Bayesian–

model updating. This technique has been successfully applied for damage detection in steel structure [31] and RC bridges [32]. However, the Bayesian model updating methods have certain complexities in solving the integrals resulting high computationally expensive. Furthermore, it is essential to possess prior information about the distributions of the variables to be updated beforehand [22],[30].

Since changing structural parameters to improve the matching between the numerical model and the real structure is essentially an optimisation problem, computational-intelligence techniques are being used more and more for model-updating[22]. This is particularly appealing given the uncertainties involved in updating these parameters. Computational intelligence techniques can generally be classified into two types: machine learning (ML) and evolutionary algorithms (EA). For instance, Fei et al. [33] employed artificial neural network (ANN) models to update using frequency-response for the beam-elements. In another research, ANN is used to update a frame model with frequency data [34].

Evolutionary Algorithms (EAs) are a class of optimization algorithms inspired by the process of natural selection and evolution. They are commonly used for solving complex optimization problems, including model updating and parameter estimation tasks. These algorithms are better for the large structure with high damage as it does not require gradient calculation for objective function [35],[36].

Numerous studies in the literature delve into FEM and measurement of ambient-vibration and model updating for masonry constructions [37], [38],[39], precast structures [40], steel structures [41], [42], and buildings [43], [44], [45]. Moreover, for the buildings, Weber et. al. [46] used forced-vibration data in sensitivity-based model-updating for a two storey RC frame building. Similarly, Shiradhonkar and Shrikhande [47], applied the sensitivity method with Tikhonov regularization for updating the parameters of 7 storey 2D RC frame model. Akhlaghi

et.al. [48] uses ambient-vibration data in Bayesian model-updating of a four-story infilled RC frame building with damage. Besides these, there are very limited research model updating of the low to mid rise (3-7 stories) Reinforced Concrete (RC) buildings with relatively higher stiffness due to infill masonry, in which only limited no. of modal properties can be obtained from ambient vibration although there are plenty of research on FE model updating in recent years.

1.2.3 Numerical Analysis Tools

Earthquakes cause a variety of damages to buildings and civil infrastructure. One of the most significant areas of research is structural collapse as it causes severe damage in the structures and also causes human casualties. To study the structural behaviour there are many existing methodologies. Due to limitation in the depiction of fractures and separation in the elements, methods based on the assumption that the material is continuous, such as Finite Element Method (FEM) [49], are unable to execute the collapse analysis accurately[50]. The Extended Distinct Element Method (EDEM) and the Distinct Element Method (DEM), which use discrete elements to represent structures, may track the behaviour of a structure collapsing, although they are less precise than FEM before cracking [51],[52]. However, Applied Element Method (AEM) represents a precise and effective approach for monitoring the behaviour from the zero loading until the point of ultimate failure, encompassing crack propagation and separation of structural components. This approach offers reliable accuracy and ease of use in terms of material-modelling in a reasonable timeframe [53]. Even though, AEM has the edge over FEM for collapse analysis, the numerical model updating for the AEM model is non-existence.

The forthcoming obstacle in the domain of numerical analysis tools pertains to the aspect of computational efficiency. Specifically, the Applied Element Method (AEM) encounters a

noteworthy challenge in its ability to conduct expeditious simulations for the large-scale structural problems with the large no. of elements. The computational efficiency result in lengthy simulation times due to the limitation of the existing solvers integrated in the AEM tool hindering engineers from exploring complex design and conducting multiple iterations.

1.3 Problem Statement

The current methods of Operational Modal Analysis (OMA) have limitations when it comes to capturing the full range of modes in low to mid-rise buildings and hence resulting less accuracy in model updating. To overcome this, optimization schemes are necessary to increase the accuracy and effectiveness of the analysis. Furthermore, performing model-updating using OMA does not provide scaled mode shapes, so a different formulation is required to obtain more accurate results. Next, numerical modelling of non-engineered or non-uniform components is essential, and it requires a powerful tool with a large number of elements, such as high-performance computing for Applied Element Method.

1.4 Research Objectives and Expected Outcomes

The objective of the research is to develop a model updating method with the ability to perform realistic numerical modelling in 3D AEM accurately and efficiently.

The specific objective of the research can be explained as following:

- Develop a least square problem for model updating which is suitable for low to mid rise buildings having limited number of operational modal data and limited measurements.
- Integrate model updating methodology in 3D AEM numerical modelling.
- Improve the computational efficiency of 3D AEM tool.
- Perform seismic-vulnerability assessment of the real existing building by using vibration data.

1.5 Proposed Methodology

This research consists of four distinct stages. Stage 1 focuses on the identification of modal parameters, encompassing two sub-stages: Stage 1 (α) involves the determination of analytical modal parameters by performing modal analysis on the three-dimensional (3D) Applied Element Method (AEM) of the building structure. Stage 1 (β) involves the experimental modal parameters identification by analyzing ambient vibration data collected from existing buildings.

Stage 2 involves the development and implementation of a model updating methodology. This methodology addresses the least square problem for model updating, specifically tailored for low to mid-rise buildings with limited operational modal data and measurements. It is applied to both idealized shear frames and experimental frames.

Stage 3 entails the integration of the model updating method into the 3D AEM and its implementation for the identification of material properties, which serve as input parameters for the 3D AEM model.

Finally, Stage 4 focuses on the 3D AEM modeling and analysis of the updated numerical model. The first part of this stage is dedicated to improving the computation efficiency of the solver in the 3D AEM tool. While, second part involves conducting seismic vulnerability assessments on existing buildings using the updated properties within the 3D AEM framework.

In summary, the research scope encompasses two parts: the development of a comprehensive system for vulnerability assessment using vibration data, comprising Stages 1 (α), 2, 3, and 4; and the application of this system to assess the vulnerability of existing buildings using ambient vibration data, comprising Stages 1 (β), 2, 3, and 4.

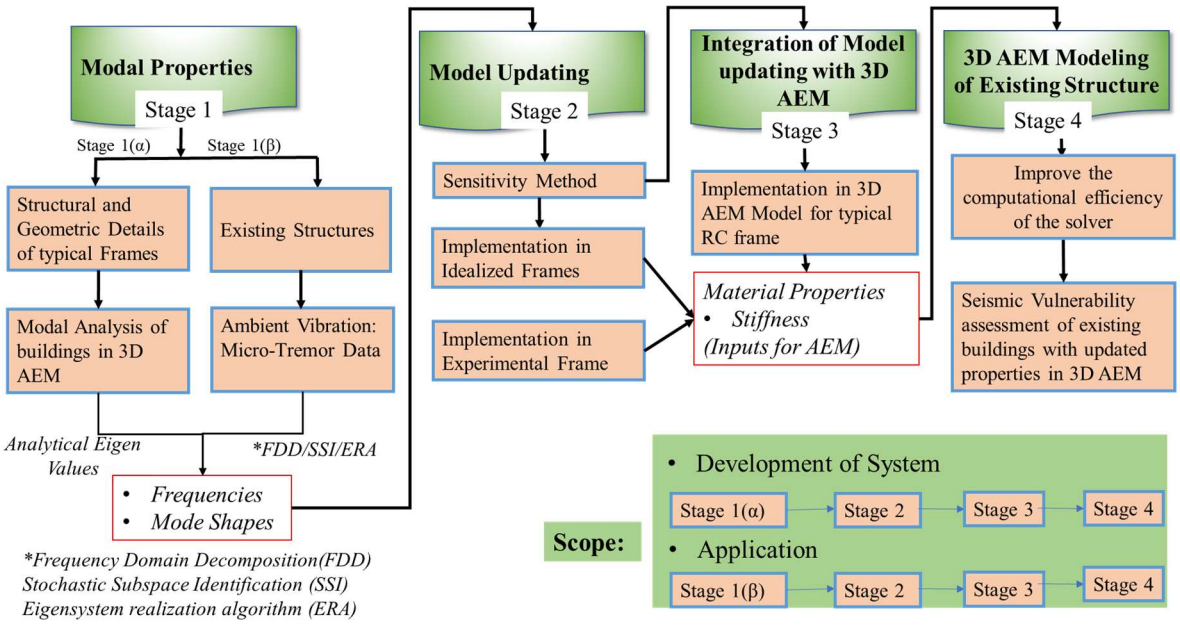

Figure 1-5: Flow of the Research

1.6 Research Significance

This research holds significant importance in the field of earthquake engineering and structural analysis. By aiming to develop a model updating method that can perform realistic numerical modelling in 3D AEM (Applied element method) accurately and efficiently, this study addresses a crucial need in the field. The development of a least square problem specifically tailored for low to mid-rise buildings with limited operational modal data and measurements is a significant contribution, as it enables engineers to update structural models effectively even when modal data and measurements are limited. The integration of this model updating methodology into 3D AEM numerical modelling further enhances the accuracy and reliability of seismic response predictions. Additionally, the improvement in computational efficiency of the 3D AEM tool has practical implications by reducing the time and computational resources required for simulations, making it more accessible for seismic vulnerability assessments. Ultimately, the research's significance lies in its potential to advance the field of earthquake

engineering by providing an efficient and accurate tool for assessing seismic vulnerability of buildings, leading to improved design practices and the creation of safer structures.

1.7 Organization of Thesis

The research is organized with seven chapters and the contents of the chapters are summarized as following:

Chapter 1: Introduction

This chapter serves as the introduction to the research, encompassing background information and problem statements, along with a comprehensive literature review of related previous studies, while also defining the research objectives, scope, and framework. The thesis aims to develop a model updating method with the ability to perform realistic numerical modeling in 3D Applied Element Method (AEM) accurately and efficiently, providing insights to enhance seismic resilience and safety in the face of actual disasters. There are four specific objectives of this research. The first objective is to develop a least square problem for model updating, tailored to these types of structures. The second objective involves integrating the model updating methodology into 3D AEM numerical modeling. The third objective focuses on enhancing the computational efficiency of the 3D AEM tool. Finally, the research aims to perform a seismic vulnerability assessment of an existing building using vibration data, which will help in evaluating its susceptibility to seismic events. There are total 7 chapters in the thesis.

Chapter 2: Sensitivity-based model-updating method.

It discusses development of a least square problem for model updating which is suitable for low to mid rise buildings having limited number of operational modal data and limited measurements. The least square problem is formulated calculating the relative residual vector

of experimentally measured modal properties and analytical modal properties. The analytical modal properties are calculated using the initial guess of updating parameters for the model updating which is material properties (Young's Modulus/ stiffnesses) for the numerical model of the structure. Using the formulated least square problem as the objective function for the minimization problem, the problem is solved to get the optimum value of updating parameters using Levenberg-Marquardt algorithm. The model updating implementation is examined for generalized shear frames with various scenarios involving limited measured degree of freedoms (DOFs) and the no. of modes used for model updating, evaluating the accuracy of stiffness updates for structural systems.

Chapter 3: Implementation of the sensitivity-based model-updating for an experimental model.

In this chapter, the successful implementation of a model-updating method for an experimental model is presented. The objective of this method is to identify storey stiffness and detect damage within the model using operational modal data acquired through ambient vibration measurements in the laboratory. Through the analysis, it is discovered that changes in storey stiffness can provide valuable insights into the extent of damage, specifically the decrease in stiffness resulting from the loosening of bolts on a particular floor. This understanding allows us to quantify the damage experienced by the structure. The results of this study demonstrate the efficacy of the developed model updating method in accurately identifying damage in terms of stiffness at different locations within the structure.

Chapter 4: 3D AEM integration of the sensitivity-base model updating.

At first, this chapter includes the theoretical explanation of numerical analysis tool 3D AEM, and its validation for static and dynamic analysis using experiment results from previous research. The objective of this research is to model real existing structure in 3D AEM. So, it is

necessary to improve the current solvers and storage systems used in 3D AEM. With the comparison of different solvers and storage system, parallel direct sparse solver (PARDISO) with triplet storage format using multiple thread of CPU is identified to be the most efficient one and is implemented in 3D AEM.

Furthermore, this chapter discussed the methodology of 3D AEM integration of the sensitivity-based model updating. A successful implementation of the model updating for the 4 storey RC frame building to prepare the 3D AEM model is performed in this chapter. Synthetic data of experimental operational mode shapes and frequencies are obtained by applying frequency domain decomposition to the response of the structure subjected to white noise using actual material properties. The 3D AEM is employed to model the structure with unknown stiffnesses, categorized into three groups: beam/slab, column, and infill wall properties, which serve as the updating parameters. The ARPACK-Arnoldi package integrated in 3D AEM is utilized to obtain analytical modal properties, and the least square problem is formulated based on the residual of experimental and analytical modal properties. The Levenberg-Marquardt algorithm is applied to minimize the problem and obtain the updating parameters. Comparisons between the Young's Modulus and modal parameters of the updated structure with the assumed values validate the successful implementation of the model updating in 3D AEM.

Chapter 5: Seismic vulnerability of the updated model structure using 3D AEM

This chapter is about static and dynamic analysis of the updated numerical model to understand the seismic vulnerability of the structure using 3D AEM. The quantification of the overall damage and local damages are studied in performance criteria based on interstorey drift, frequency degradation and deformation of the structure.

Chapter 6: Implementation of the model updating in real structure

This chapter discusses the implementation of the model updating in the real building structure by using the ambient vibration data measured from the field and perform the analysis in 3D AEM. The Young's Modulus (stiffnesses) of the structure is considered unknown and assigned random initial values. The elements are grouped into 11 different groups, including floorwise beams/slabs, columns, shear walls, and infill walls, serving as the updating parameters and the updated values of the parameters are obtained from the 3D AEM model updating. The updated structure is then performed non-linear analysis using static pushover analysis to understand the capacity and performance of the structure.

Chapter 7: Conclusion and Future Scope

This chapter is the summary and conclusion part describing the limitation of the study and future recommended studies relevant to this research.

Chapter 2: Sensitivity-based model updating method

2.1 Introduction

The current state of research indicates that there is a gap in the existing research regarding the process of updating models of building structures, specially where there are limited numbers of unscaled operational measured modes, as well as a restricted number of measured degrees of freedom (DOFs). This chapter represents the theoretical foundations of sensitivity-base model updating along with its application in idealized shear frames for reinforced concrete (RC) structure with limited number of measured modes and limited measurements are tested with the model updating method.

2.2 Theoretical Development

One of the iterative and indirect methods for model updating is sensitivity-based approaches, which involve estimating differences in model parameters based on their impact on the modal characteristics of the system. This process relies on gauging the sensitivity of the modal properties with respect to adjustments in the model parameters [54].

Experimentally measured modal properties; frequencies (ω), and mode shapes (Φ) are used as input for model updating. These properties are often obtained from ambient-vibration collected on structure of interest. Several techniques exist for extracting modal properties from ambient vibration data. In this research, the Frequency Domain Decomposition (FDD) approach is employed to extract the frequency components and vibration modes from the collected data. The FDD method entails acquiring vibration signals, subjecting them to Fast Fourier Transform (FFT) processing to obtain the frequency spectrum, and then applying FDD to identify the mode shapes. A comprehensive representation of the intricacies of the Frequency Domain Decomposition (FDD) method is available in the literature[17].

Hereafter, $\lambda_{exp}=(\omega^2)$ and $\{\Phi\}_{exp}$ are the experimental eigenvalues and mode shape vectors respectively. Let us consider, 'nmodes' no. of modal parameters is obtained from the Frequency Domain Decomposition (FDD) of measurement data.

The subsequent step involves determining the physical parameters (P) to update in the model of the structure. The physical parameters refer to the properties of the structure that can be adjusted or modified to better match the real behaviour. These physical parameters may include material properties like density, Young's modulus, as well as geometric properties like length, width, and thickness of structural elements. The present study involves updating the global stiffness matrix$[K]_{global}$ of the structure by adjusting the Young's Modulus (E) of the materials utilized in its construction.

If the values of updating parameters are large, the accumulation of the errors will increase with the updating. So, the relative value of the parameters (x) is considered to be updated.

$$\{x\}_j = \frac{\{P_u\}_j - \{P_0\}}{\{P_0\}} \tag{2-1}$$

Where, $\{x\}_j$ is vector containing relative values of updating parameters in j-th iteration of optimization, $\{P_u\}_j$is the vector containing values of physical parameters to be updated, and $\{P_0\}$is vector containing initial guess of physical parameters.

Let us consider Young's Modulus (E) to be the updating physical parameter (P). We can calculate the stiffness of each dofs based on the value of Young's Modulus. Based on equation (2-1) stiffness value for each degree of freedom (dof) is calculated as:

$$\{K\}_j = \{K_0\}(1 + \{x\}_j) \tag{2-2}$$

Where, $\{K\}_j$is vector containing values of stiffness for each dofs, and $\{K_0\}$is vector containing initial stiffness values for each dofs. The global stiffness matrix $[K]_g$ for the numerical model is constructed based on these stiffness values. Let us consider, mass [M] to be a known

parameter. A generalized eigen value problem $[K]_g\{\Phi\}=\lambda[M]\{\Phi\}$ is solved using ARPACK (Arnoldi package) in FORTRAN90[55]. The solution of this generalized eigenvalue problem involves finding the eigenvalues λ and the corresponding eigenvectors $\{\Phi\}$ such that the equation above is satisfied. ARPACK uses the Arnoldi algorithm to find a few eigenvalues and eigenvectors of the generalized eigenvalue problem[55]. First an orthonormal basis for the Krylov subspace of $[K]_g$ and [M] using the Arnoldi algorithm is constructed. The Krylov subspace is defined as:

$Kp = span\{b, K_gb, K_g^2b, ..., K_g^{(p-1)}b\}$, where b is an initial vector, and p is the order of the Krylov subspace. The Arnoldi algorithm then generates a Hessenberg matrix H with respect to this basis, which is similar to the generalized eigenvalue problem matrix pair (K_g, M) and has the same eigenvalues. The eigenvalues of H are computed using standard techniques, and the corresponding eigenvectors are then transformed back into the original basis to obtain the generalized eigenvectors of (K_g, M). This method is useful when dealing with large matrices where it is computationally expensive to identify all eigenvalues and eigenvectors. The eigenvalues and eigenvectors obtained from the analytical analysis solving generalized eigen value problem is hereafter denoted by λ_{ana} and $\{\Phi\}_{ana}$ respectively.

Next, a relative residual vector which consists of differences between experimental and analytical eigen values and mode shape vectors are calculated. A. Teughels [56] has suggested to use the relative residual for the eigenvalues to get the similar weightage for the eigenvalue residual, as higher eigen value will have higher residual and will impact the optimization process.

$$res(\lambda) = \frac{(\lambda_{exp})_i - (\lambda_{ana}(x))_i}{(\lambda_{exp})_i}, i = 1, nmodes \quad (2\text{-}3)$$

Similarly, let us consider 'm' no. of measured dofs in the structure. The mode shape vectors from the experiment and analytical are normalized with the largest absolute modeshape vector

of each mode. The analytical mode shapes vectors are sequenced in the same order of measured experimental data, so that the residuals of mode shape correspond to the same dofs.

$$(\Phi_{exp}^{norm})_i = \frac{(\Phi_{exp})_i}{(\Phi_{exp})_{i,max}}, i = 1, nmodes \tag{2-4}$$

$$(\Phi_{ana}^{norm}(x))_i = \frac{(\Phi_{ana}(x))_i}{(\Phi_{ana}(x))_{i,r}}, i = 1, nmodes \tag{2-5}$$

'r' is the dof where experiment has maximum amplitude of mode shape vector in the mode corresponding mode.

The residual vector for the modeshape can be written as:

$$res(\Phi) = (\Phi_{exp}^{norm})_i - (\Phi_{ana}^{norm}(x))_i,\ i = 1, nmodes \tag{2-6}$$

Since, the reference degree of freedom where the mode shape amplitude is maximum in each mode is normalized to one. The dimension of the residual vector associated with each mode shape decreases by one size for each mode.

The complete residual vector can be represented as:

$$res(x) = \begin{pmatrix} res(\lambda) \\ \vdots \\ res(\Phi) \end{pmatrix} = \begin{pmatrix} \frac{(\lambda_{exp})_i - (\lambda_{ana}(x))_i}{(\lambda_{exp})_i} \\ \vdots \\ (\Phi_{exp}^{norm})_i - (\Phi_{ana}^{norm}(x))_i \end{pmatrix}, i = 1, nmodes \tag{2-7}$$

The weightage factor vector of wt(λ) and wt(Φ) is used for controlling the influence of residuals in the optimization.

$$res(x) = \begin{pmatrix} res(\lambda).wt(\lambda) \\ \vdots \\ res(\Phi).wt(\Phi) \end{pmatrix} = \begin{pmatrix} \frac{(\lambda_{exp})_i - (\lambda_{ana}(x))_i}{(\lambda_{exp})_i}.wt(\lambda) \\ \vdots \\ (\Phi_{exp}^{norm})_i - (\Phi_{ana}^{norm}(x))_i.wt(\Phi) \end{pmatrix} \tag{2-8}$$

A least square problem is formulated based on the residual vectors calculated in equation (2-8) and the minimization of the least square problem yields the updated value of the parameter (x). The objective function for the optimization problem is represented by:

$$f(x) = Minimize\ (x)\ for\ \|res(x)\|_2^2$$

$$= \sum_{i=1}^{n_{modes}} \left(\frac{(\lambda_{exp})_i - (\lambda_{ana}(x))_i}{(\lambda_{exp})_i}.wt(\lambda) \right)^2 + \left(\left(\Phi_{exp}^{norm} \right)_i - (\Phi_{ana}^{norm}(x))_i.wt(\Phi) \right)^2 \tag{2-9}$$

There are numerous optimization algorithms to solve the least square problem. Further, Levenberg Marquardt Algorithm is used for the optimization[57]. The method works by iteratively adjusting the parameters of the function being optimized to minimize the sum of the squares of the residuals, which are the differences between the predicted values of the function and the actual data points.

In each iteration, the algorithm evaluates gradient of the objective function and the curvature of function, which are used to determine the step size and direction for the parameter update. The Levenberg-Marquardt method uses a damping factor to balance the step size between a gradient descent step and a Gauss-Newton step to get the optimum value of the updating parameter (x) for that iteration. The $(j+1)^{th}$ iteration value of the updating parameter can be represented by:

$$x(j+1) = x(j) - (\nabla^2 f(x(j)) + \Lambda I)^{-1} \nabla f(x(j) \quad (2\text{-}10)$$

Where, $\nabla f(x(j)) =$ Gradient (sensitivity) of objective function for j^{th}-iteration.

$\nabla^2 f(x(j))$= Curvature of objective function for j^{th}-iteration.

Λ= Damping factor to switch between gradient descent and Gauss Newtonian method

The optimization iteration is continued until it converges to the optimum value.

The updated value of the parameter can be thus obtained by substituting the optimized value of x in equation (2-1) or (2-2).

2.3 Case Studies for Model Updating

2.3.1 Case Study Properties

The sensitivity-based model updating is conducted on simplified four storey RC shear frames (Figure 2-1). This process involved changing the damping in the frame for 1% and 5%, the number of modes considered to be two and three, and the number of measured dofs from some to all. The model updating utilizes operational modal data. The storey stiffnesses of the structure of each floor are updating parameters. The updating parameters are then compared to

theoretically calculated storey stiffnesses. Theoretical storey stiffness and lumped masses of the structure are:

$(\text{Lumped Mass})_{1\text{-}4\text{storey}}$: [5.54,4.08, 4.08,2.62] ton

$(\text{Storey Stiffness})_{1\text{-}4\text{storey}}$: [24336.16, 24336.16,20129.21,18960.70] KN/m

Table 2-1 : Different scenario of case studies

SN	Storeys	No. of DOF Measured	No. of Modes	Damping
1	4	4,3,2	2 and 3	1% and 5%

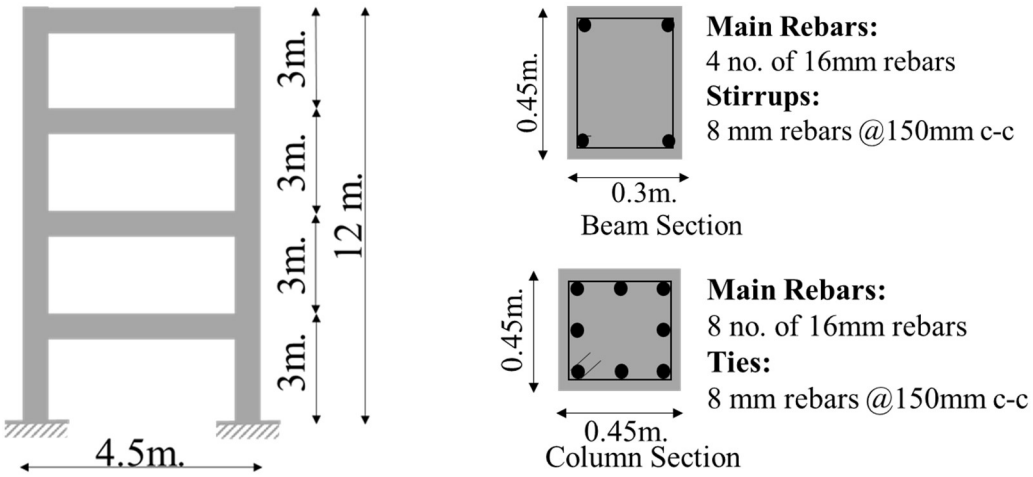

Figure 2-1: Properties of case study frame

2.3.2 Operational Modal Data

A synthetic ambient vibration data as a response of each floor of the frame with damping 1% and 5% is created by applying white-noise of 0.01hz-100hz for 120 seconds with sampling rate of 100hz (Figure 2-2). The operational modal frequency and modeshape data for the frame is extracted using of the Frequency Domain Decomposition (FDD) of the ambient vibration data (Figure 2-3) and (Figure 2-4).

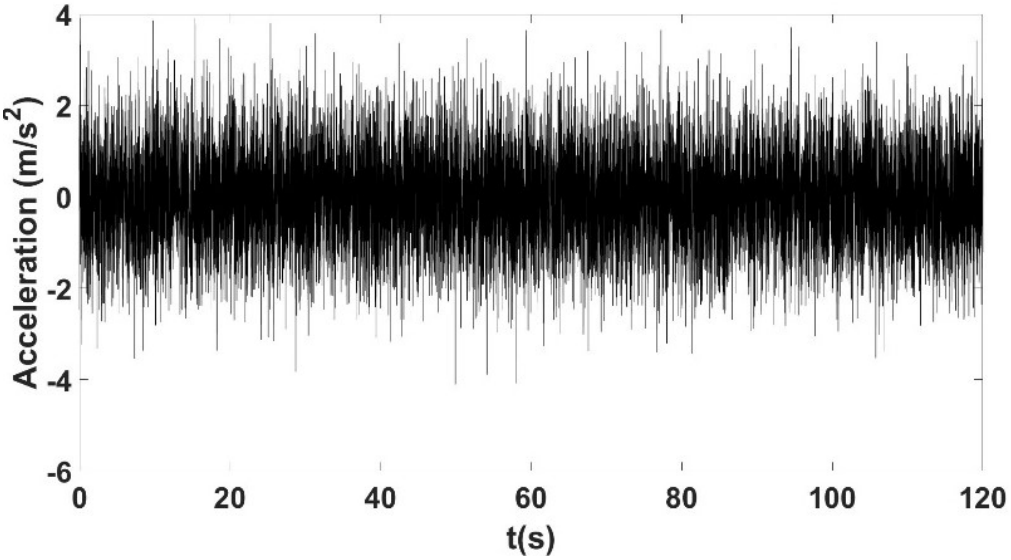

Figure 2-2: White Noise

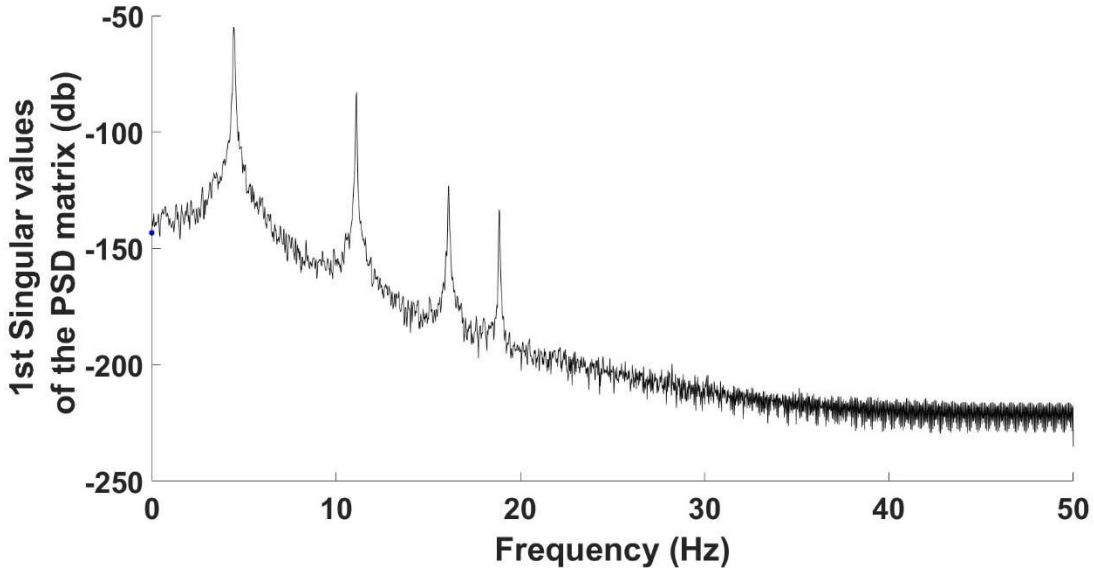

Figure 2-3: 1st Singular Values of Power Spectrum Density (PSD) plot for 1% damping

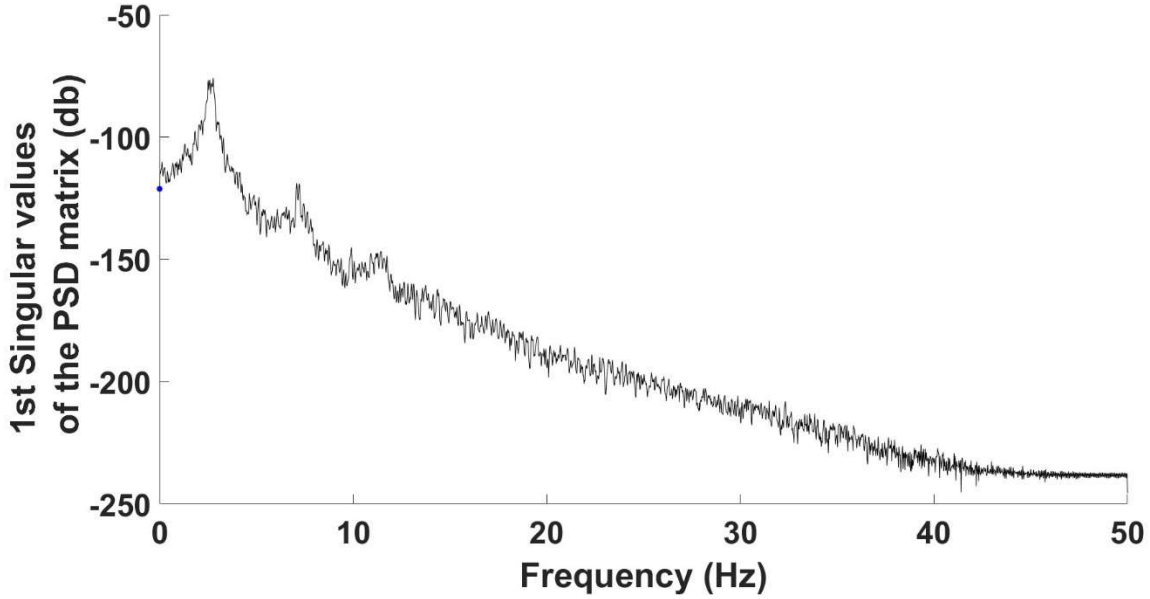

Figure 2-4 : 1st Singular Values of Power Spectrum Density (PSD) plot for 5% damping

Table 2-2 : Mode shape vectors and frequencies obtained from FDD

	Mode Shape Vectors (1% damping)			**Mode Shape Vectors (5% damping)**		
	Mode 1	**Mode 2**	**Mode 3**	**Mode 1**	**Mode 2**	**Mode 3**
DOF 1	-0.2322	-0.5790	-0.5058	-0.2302	-0.5601	-0.4853
DOF 2	-0.4218	-0.4640	0.2790	-0.4204	-0.4626	-0.1192
DOF 3	-0.5829	0.1693	0.3995	-0.5831	0.1274	0.0577
DOF 4	-0.6545	0.6443	-0.6716	-0.6557	0.5724	-0.4651
Frequency	4.41hz	11.10hz	16.16hz	4.54hz	11.10hz	16.04hz

The frequencies and modeshape vectors displayed in (Table 2-2) are further used as an experimental modal data for performing the model updating. The subsequent analysis employs solely the real component of the eigenvalues. Nevertheless, it is noted, the modeshape data for the third mode exhibits a relatively higher value in the imaginary component, specifically for the third mode of a 5% damped structure. (Figure 2-5) and (Figure 2-6) depict the Argand

diagram, which illustrates the real and imaginary components of the modeshape vectors for both the 1% and 5% damped structures.

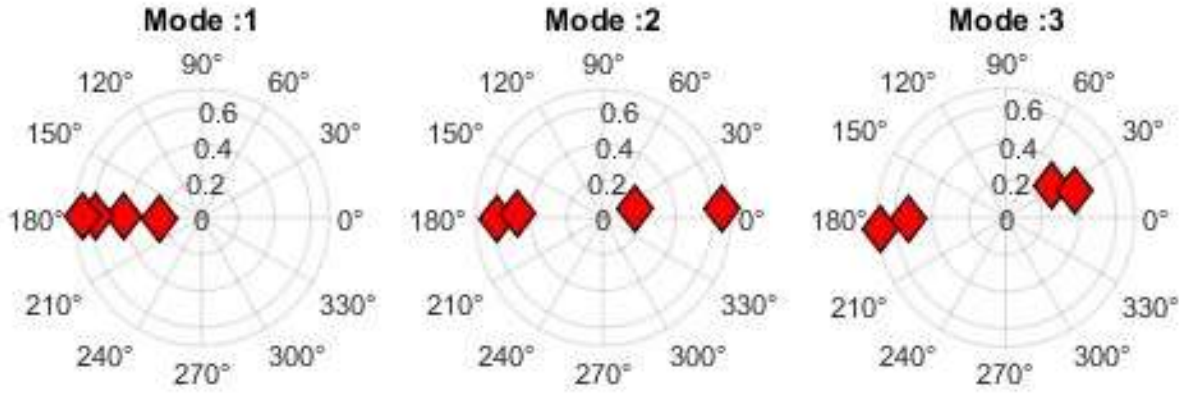

Figure 2-5 : Argand diagram of the mode shapes (real and imaginary) for 1% damping

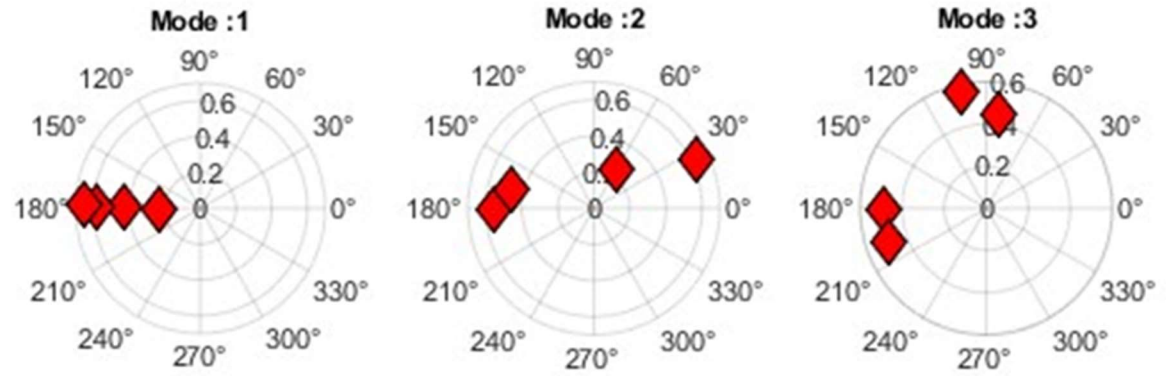

Figure 2-6 : Argand diagram of the mode shapes (real and imaginary) for 5% damping

2.3.3 Results of model updating

With the baseline stiffness of frame guessed to be 20000KN/m in each storey, the model updating is performed for the structure. The result of model updating compared with the actual stiffness for 1% and 5% damping in the frame, two and three modes, and some to all the number of measured dofs as shown in the (Figure 2-7) and (Figure 2-8). The result summary is also represented in (Table 2-3).

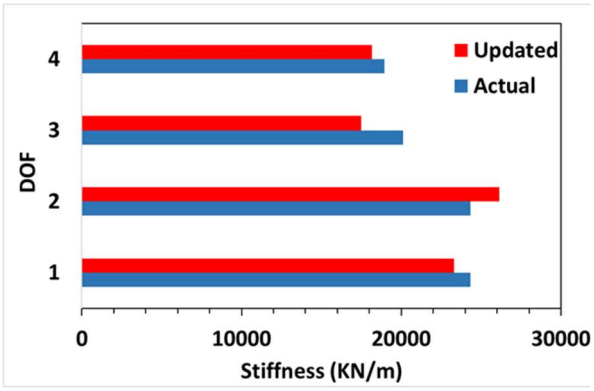

2 Dofs and 2 Modes Measured

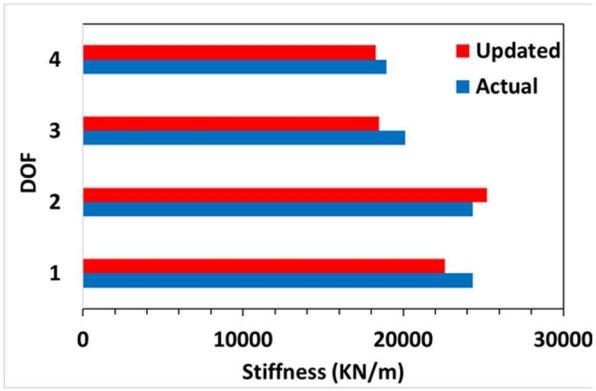

3 Dofs and 2 Modes Measured

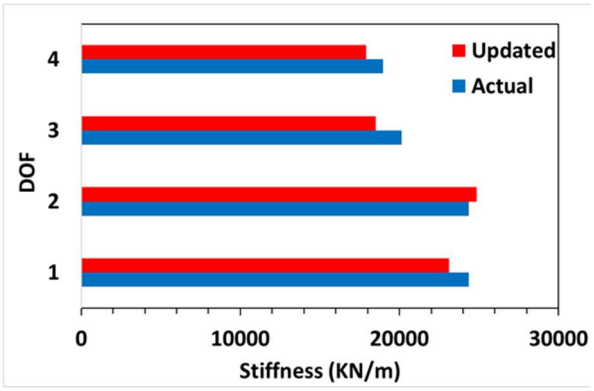

All Dofs and 2 Modes Measured

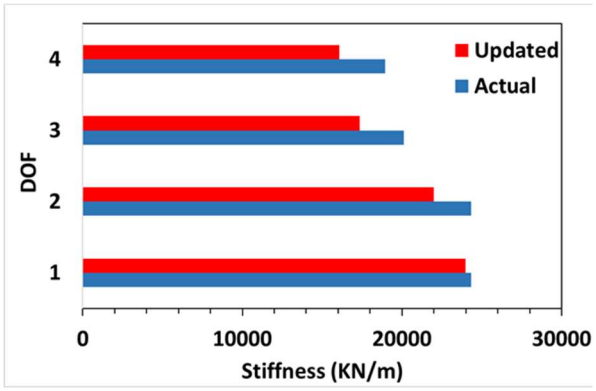

2 Dofs and 3 Modes Measured

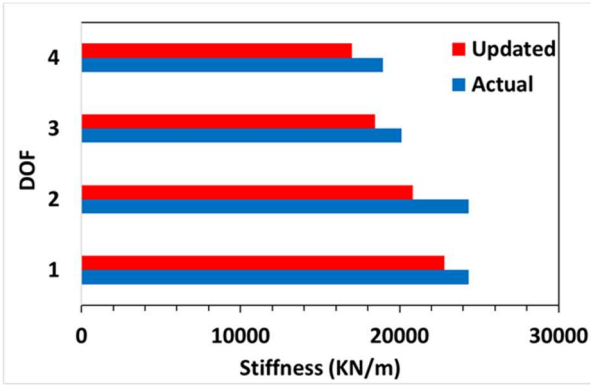

3 Dofs and 3 Modes Measured

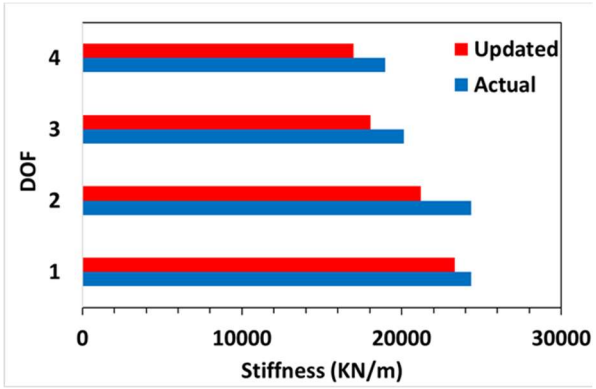

All Dofs and 3 Modes Measured

Figure 2-7 : Comparison of model updating results of 1% damped structure with actual value

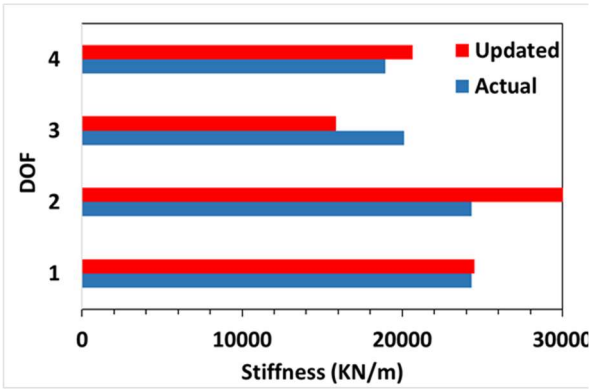

2 Dofs and 2 Modes Measured

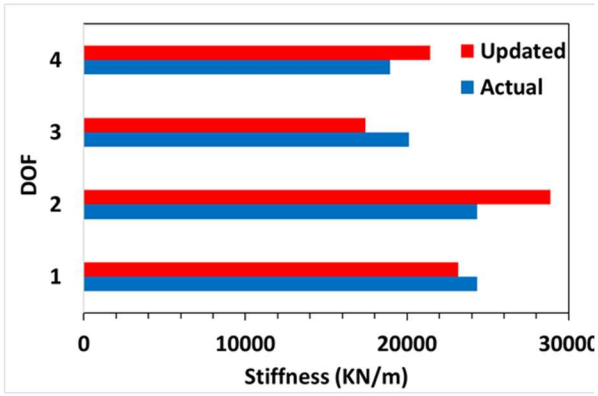

3 Dofs and 2 Modes Measured

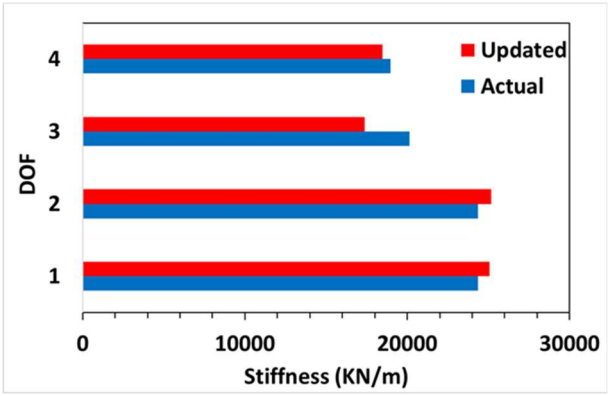

All Dofs and 2 Modes Measured

Figure 2-8 : Comparison of model updating results of 5% damped structure with actual value

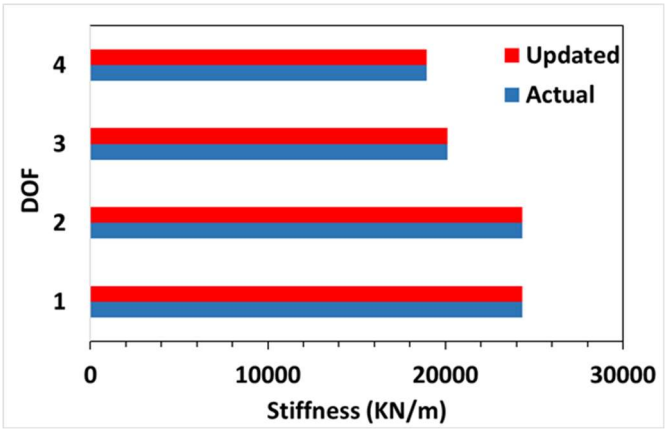

Figure (9):

Figure 2-9 : Comparison of model updating results obtained from the eigen value analysis data as experimental data with actual value

Table 2-3 : Model updating result comparison.

SN	Frame	Percentage of error in updating parameter				
		1% of damping		5% of damping		Eigen Value Analysis
		n.m.=2	n.m. =3	n.m.=2	n.m. =3	n.m.=2
1	4-dof*	5.170	9.420	5.650	---	Less than 0.1
2	3-dof*	6.210	9.840	12.490	---	Less than 0.1
3	2-dof*	7.260	10.060	15.020	---	Less than 0.1

Where, *: measured dof; and n.m.: number of modes;

In the context of a structural system possessing a damping ratio of 1%, the use of two modes for the purposes of model updating, in conjunction with the acquisition of measurement data from all four degrees of freedom, yields a stiffness update within 5.17% margin of error. Conversely, a reduced no. of measured degree of freedoms correspondingly results in increased margins of error, with stiffness update errors of 6.21% and 7.21% respectively being observed for scenarios involving measurements from 3 and 2 degrees of freedom. When employing three modes for the purpose of updating the aforementioned structure possessing 1% damping, the associated error margin for model updating increases to 9.42%, under the condition that four degrees of freedom are measured. The error margin further escalates to 9.84% and 10.06% when measurement data is acquired from only three or two degrees of freedom, respectively.

Analogously, in the case of frame with a damping ratio of 5%, the utilization of two modes for the purpose of model updating, in combination with measurement data collection from all four degrees of freedom, culminates in a stiffness update characterized by a margin of error of 5.65%. Conversely, a reduction in the no. of measured degree of freedoms results in commensurate increases in the margin of error. Specifically, scenarios involving measurement data collection from three or two degrees of freedom were found to exhibit stiffness update errors of 12.49% and 15.02%, respectively. Notably, due to issues concerning the clarity of

third mode shape data pertaining to the 5% damping structural system, said data was not incorporated in the updating process.

2.4 Discussion and Conclusion

The sensitivity-base model updating has been successfully implemented to the RC shear frame using only a few degrees of freedom for measurement and limited number of operational modes in a reasonable error margin. Nevertheless, obtaining higher mode poses challenges, and as the structure's damping increases, these higher modes can become more unreliable, leading to inaccuracies in the updating process. Moreover, the accuracy of the model updating is heavily reliant on precise modal parameters. While frequency is acquired with higher accuracy compared to modeshape, and if the modes are deemed unreliable, it is recommended to assign greater importance weight to the residual with eigenvalue during the updating procedure.

Chapter 3: Implementation of the sensitivity-base model updating method for an experimental model

3.1 Introduction

One of the iterative and indirect methods for model updating is sensitivity-based approaches, which involve estimating differences in model parameters based on their impact on the modal characteristics of the system. In the previous chapter, the structural model updating was done by utilizing an optimization-based sensitivity method for the buildings using operational modal data. We discussed the sensitivity method with numerical optimization for model updating of building structures, especially where there are limited numbers of unscaled operational measured modes, as well as a restricted no. of measured degree of freedoms (DOFs).

This chapter presents the implementation of the same approach to update a three-storey experimental steel frame by utilizing operational modal data. The steel frame is constructed in laboratory setup with the bolted joint in each floor level. The bolting condition of each floor is changed to induce damage in a particular floor. The ambient vibration of the frame is measured in each floor level for every damaged condition and operational modal properties; frequency and mode shapes of the frame are obtained. Using the limited modal properties of the experimental frame, sensitivity-based model updating is performed to obtain the change in storey stiffness of structure and damage of the frame is quantified.

3.2 Experimental Setup

A three-storey steel frame is assembled by utilizing distinct steel components, depicted in Figure 3-1. The interconnection of columns on each floor and the attachment of the slab are facilitated through the implementation of gusset plates and steel angles, securely fastened using

bolts (details in Annex 1). The specific dimensions and geometric characteristics of each component are detailed in Table 3-1.

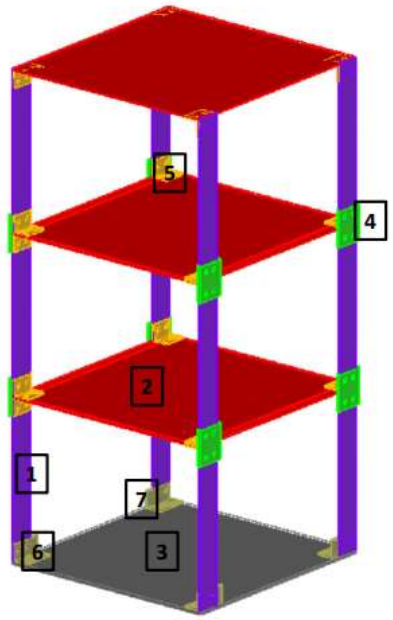

Table 3-1: Geometric Properties of the Frame

Item No.	Quantity	Description	Dimension
1	12	Column	PL 500 mm x 70 mm x 5 mm
2	3	Slab	PL 690 mm x 700mm x 5 mm
3	1	Base Plate	PL 700 mm x 700 mmx10 mm
4	8	Gusset Plate	PL 90 mm x 110 mm x 5mm
5	20	Steel Angles (L-shape)	L 50 mm x 50 mm x 3 mm
6	2	Steel Angles (L-shape)	L 50 mm x 50 mm x 3 mm
7	2	Steel Angles (L-shape)	L 50 mm x 50 mm x 3 mm

Figure 3-1: Details of experiment frame

The steel frame is fabricated within the laboratory facility, with its base securely affixed to a rigid foundation (Figure 3-2). To monitor and assess the frame's vibrational characteristics, uni-directional sensors are strategically placed on each floor, measuring the ambient vibrations experienced by the frame along the designated direction specified in (Figure 3-2). In order to deliberately introduce damage to a specific floor, the bolting condition of that floor is intentionally altered through the controlled process of loosening and tightening. Figure 3-3 presents the three distinct scenarios examined in the present study: an undamaged state, characterized by the complete tightening of the bolts, and two damaged conditions characterized by the loosening of bolts, one on the 1st floor and the other on the 2nd floor.

The experimental frame is idealized to a shear frame as shown in Figure 3-4. The mass of the frame is measured and lumped to the floor level (Table 3-2).

Table 3-2 : Lumped Mass of the Experimental Frame

SN	Floor	Mass
1	First floor	18.04 Kg
2	Second floor	18.02 Kg
3	Third floor	18.08 Kg

Figure 3-2 : Experimental setup of the frame

Case 1: Undamaged Frame Case 2: Damaged first floor Case 3: Damaged second floor

Figure 3-3 : Case study frames

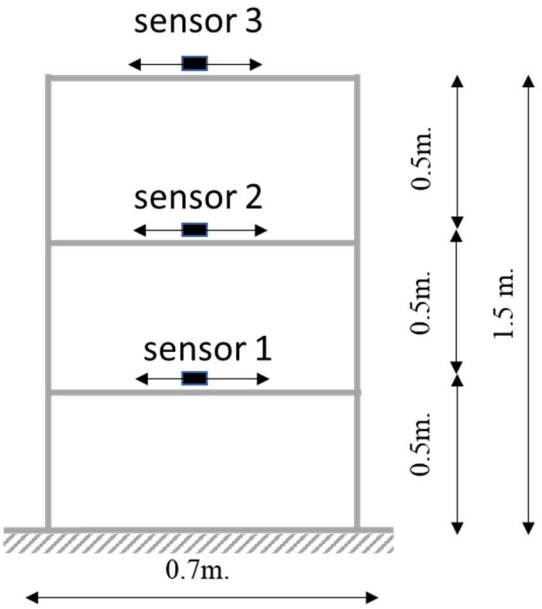

Figure 3-4 : Idealized Shear frame representation of the experimental frame

3.3 Ambient Vibration Data from the Experiment

The ambient vibration data is measured using unidirectional sensor in all three floors in the direction shown in Figure 3-2. During the experiment, the sensor captured and recorded the acceleration response of the structure. This response represents the magnitude and frequency of the vibrations experienced by the structure. By analysing this data, we can gain insights into the dynamic behaviour like frequencies, and modeshapes characteristics of the steel frame

under ambient conditions. Three different cases, first with the tight bolting condition and another with loosening the bolt to induce damage in a particular floor are assessed.

The Figure 3-5, Figure 3-6, and Figure 3-7 show the filtered and corrected ambient vibration responses for each floor, alongside the transformation of the time-domain response into the frequency domain by the use of Fast Fourier Transform (FFT). These figures illustrate the undamaged scenario, as well as the cases involving bolt loosening in the first and second floors, respectively.

3.3.1 Case 1: Undamaged Case

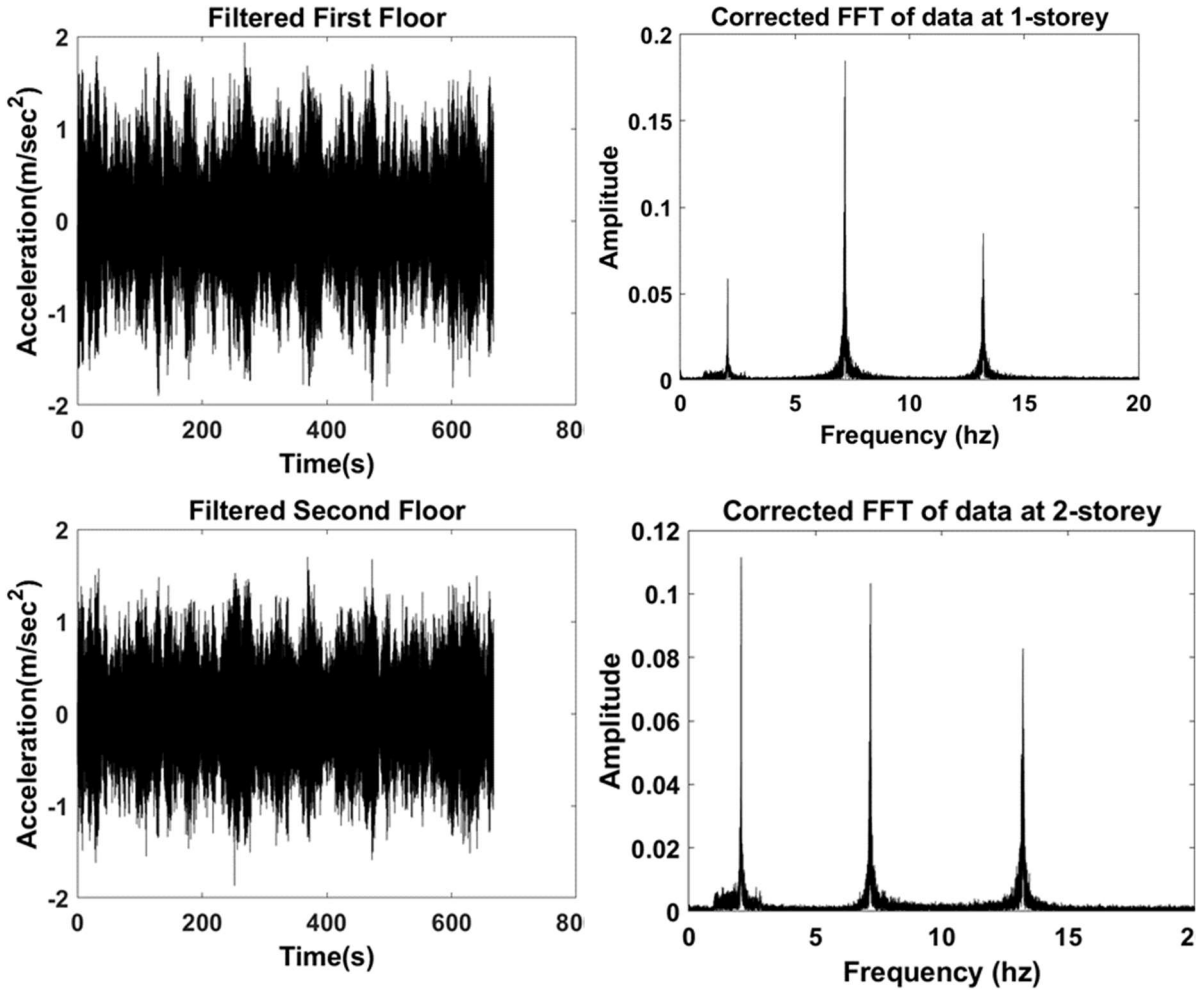

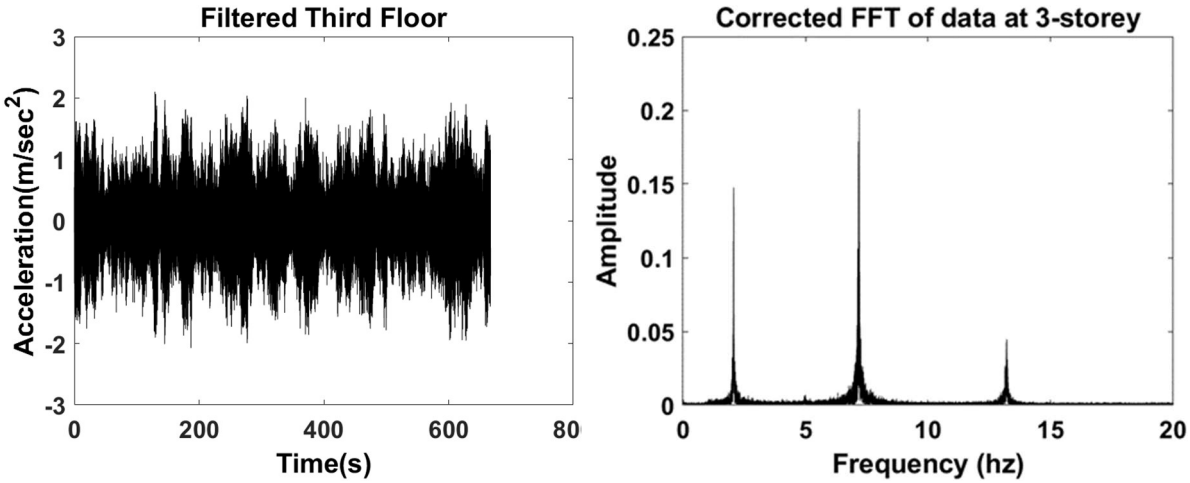

Figure 3-5 : Filtered ambient vibration response of each floor and Fast Fourier transform of undamaged frame.

3.3.2 **Case 2:** Damaged Case (First Floor)

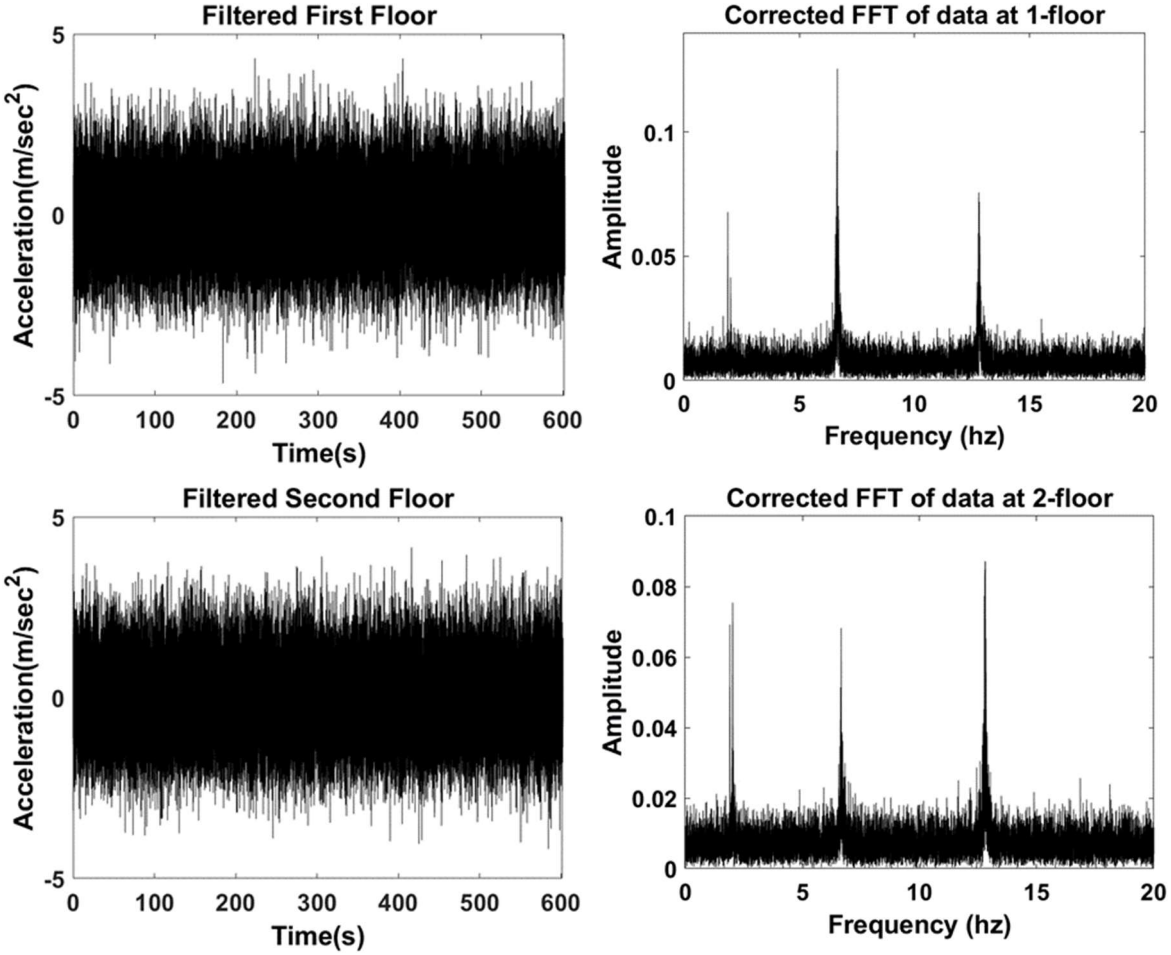

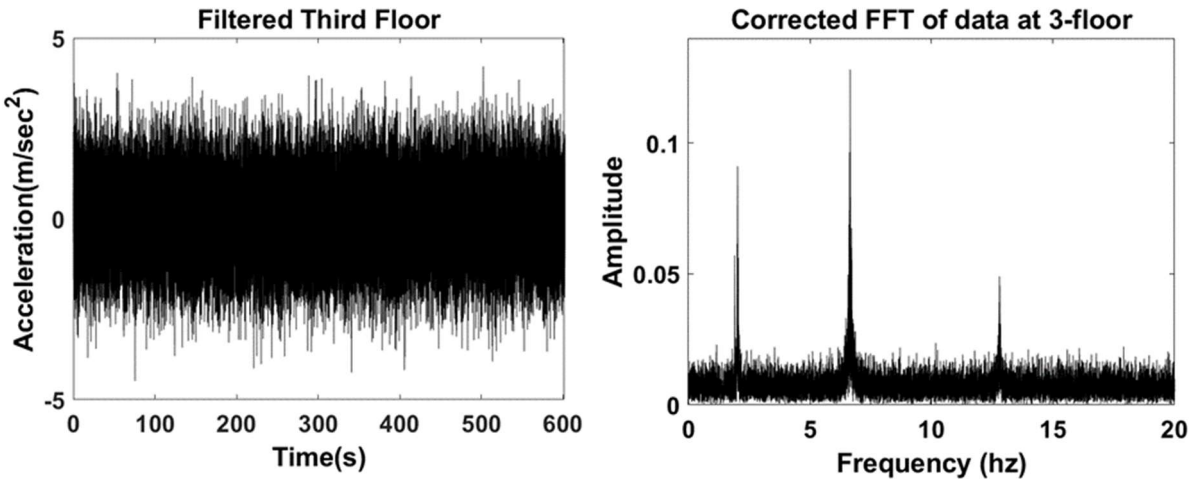

Figure 3-6 : Filtered ambient vibration response of each floor and Fast Fourier transform of damaged frame at first floor.

3.3.3 **Case 3: Damaged Case (Second Floor)**

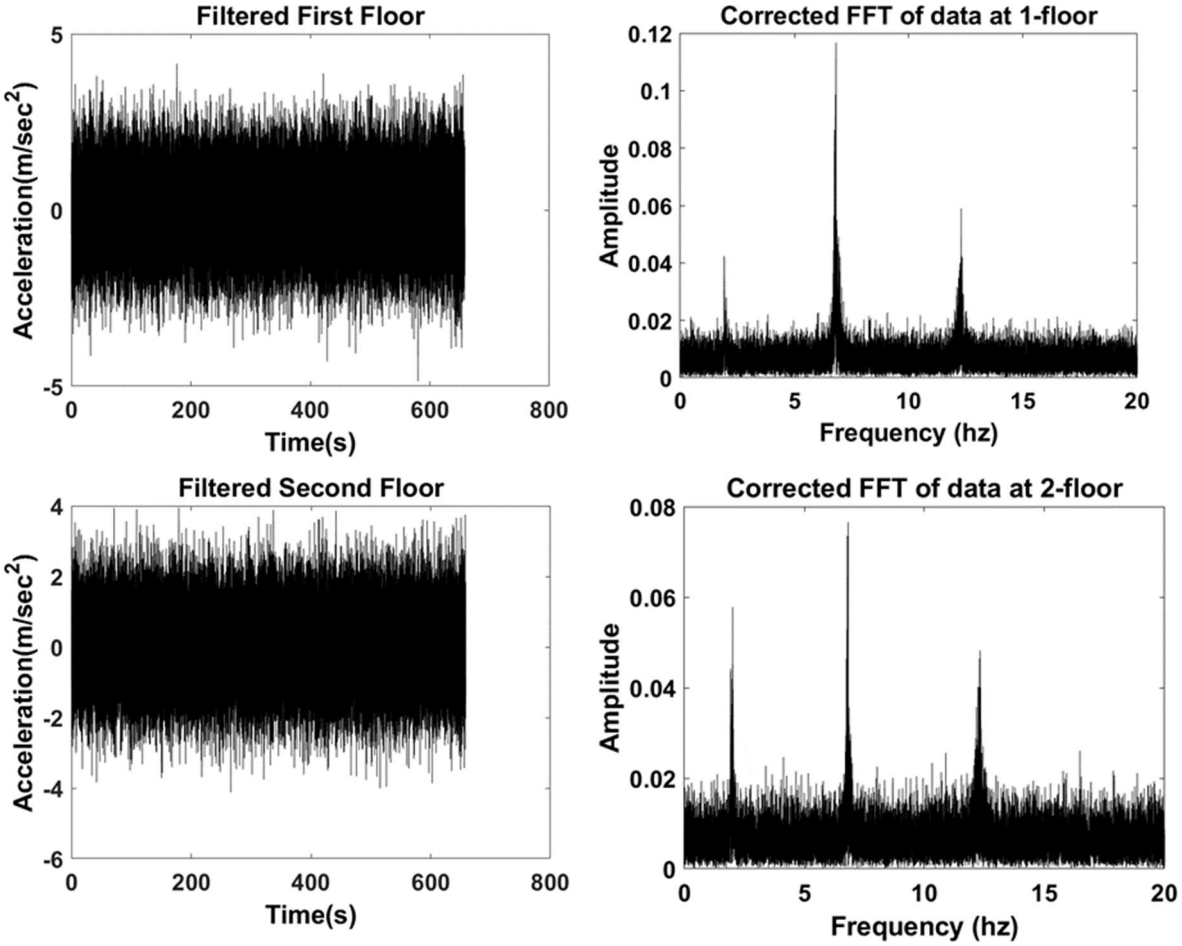

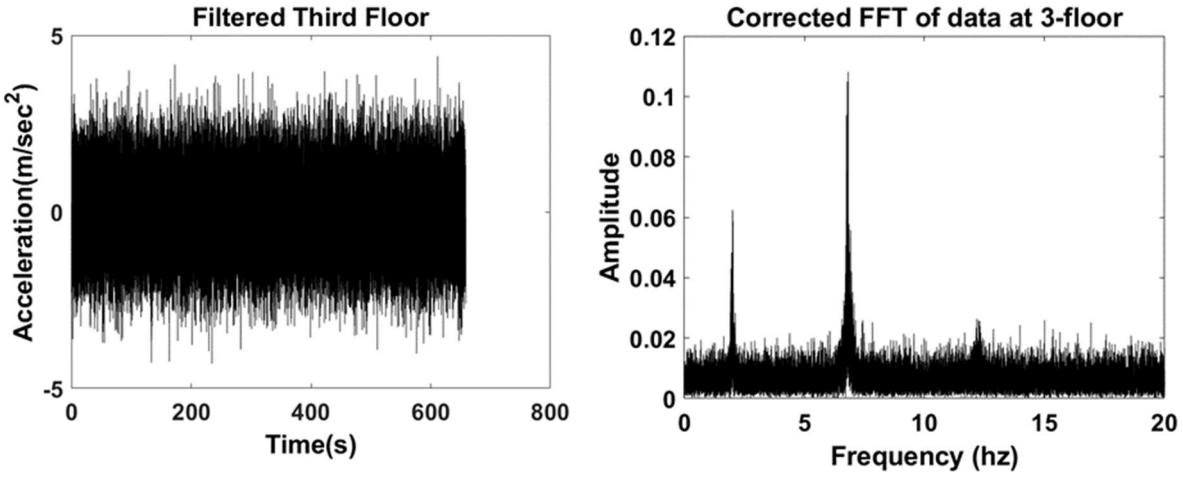

Figure 3-7 : Filtered ambient vibration response of each floor and Fast Fourier transform of damaged frame at second floor.

3.4 Operational Modal Analysis (OMA) using FDD

In this study, the ambient vibration data collected from the three-floor steel frame for all three cases, the Frequency Domain Decomposition (FDD) method [17] is employed for OMA. First step, the time-domain acceleration response data is converted into the frequency domain using a fast Fourier transform. This transformation results in a power spectral density function which provides information about the distribution of energy across different frequencies. Next, the FDD algorithm is used to decompose the power spectral density (PSD) function to a set of individual peaks, each corresponding to a vibration mode. The identified peaks in the spectra correspond to resonant frequencies of the frame. The 1st Singular value of the Power Spectral Density (PSD) matrix for Case-1, Case-2, and Case-3 are represented in Figure 3-8, Figure 3-10, and Figure 3-12 respectively. Once the peaks are identified, the FDD method estimates the modal parameters associated with each mode, including the natural frequency, and mode shape. These estimates are depicted in Figure 3-9, Figure 3-11 and Figure 3-13 as well as Table 3-3,Table 3-4 and Table 3-5 for Case-1, Case-2 and Case-3 respectively.

3.4.1 **Case 1**: Undamaged Case

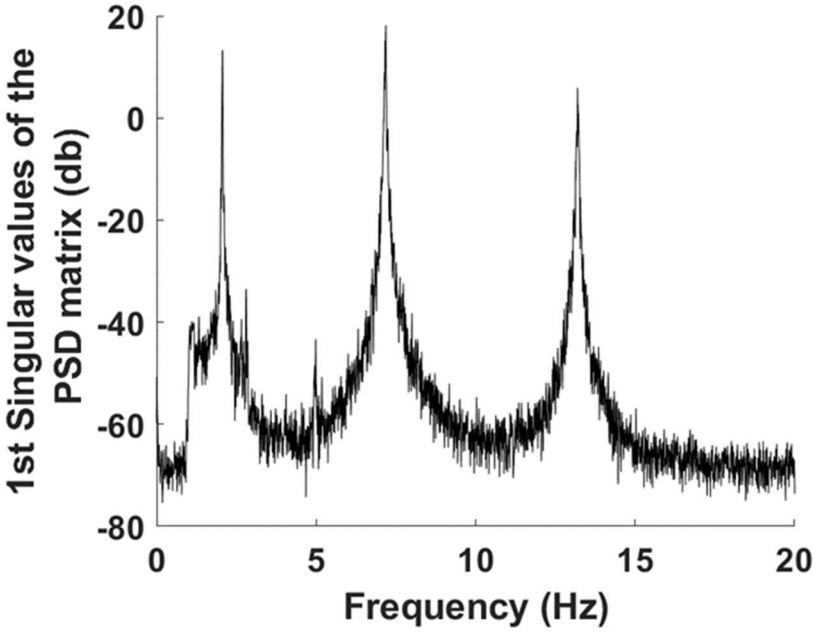

Figure 3-8 : 1st Singular value of the PSD matrix of undamaged frame (Case-1)

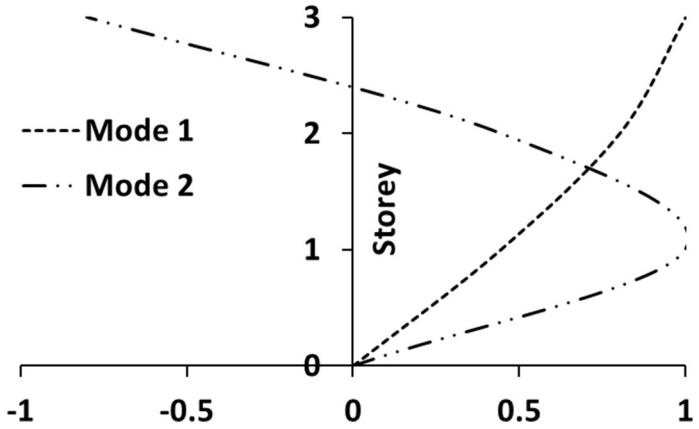

Figure 3-9 : Mode Shapes of undamaged experimental frame obtained from OMA (Case-1)

Table 3-3: Modal parameters of the undamaged experimental frame

	Mode Shape	
	Mode 1	**Mode 2**
First floor	0.4440	1
Second floor	0.8016	0.4461
Third floor	1	-0.800
Frequencies	2.30Hz	7.19 Hz

3.4.2 Case 2: Damaged Case (First Floor)

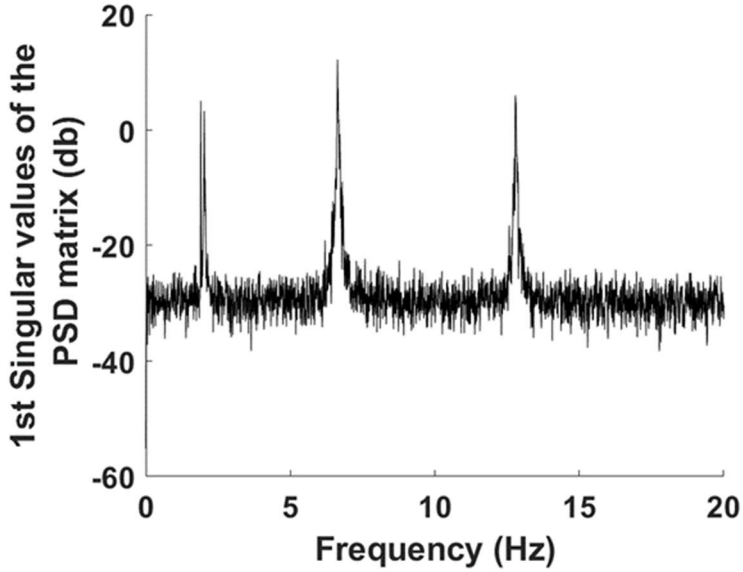

Figure 3-10 : 1st Singular value of the PSD matrix of damaged frame in first floor(Case-2)

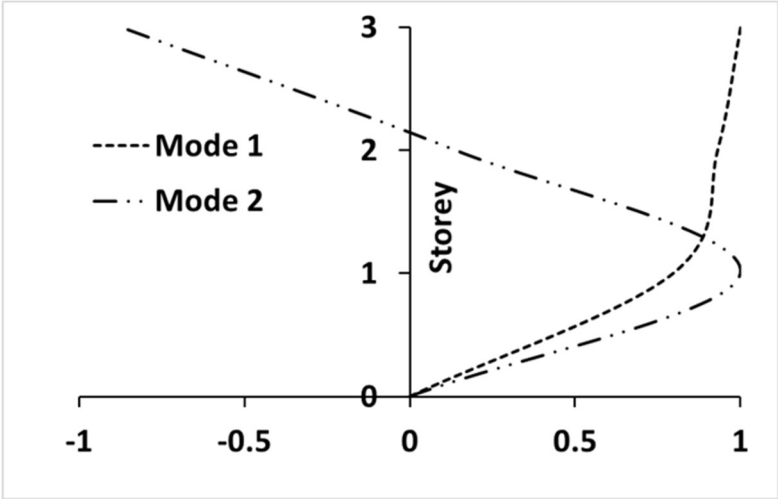

Figure 3-11 : Mode Shapes of damaged experimental frame in first floor obtained from OMA (Case-2)

Table 3-4: Modal parameters of the damaged experimental frame in first floor

	Mode Shape	
	Mode 1	**Mode 2**
First floor	0.796124538	1
Second floor	0.930352931	0.137692308
Third floor	1	-0.875384615
Frequencies	1.904Hz	6.630Hz

3.4.3 Case 3: Damaged Case (Second Floor)

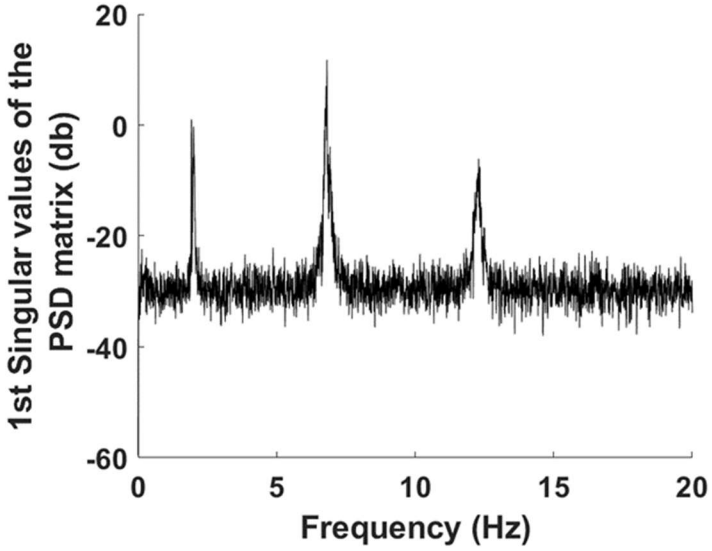

Figure 3-12 : 1st Singular value of the PSD matrix of damaged frame in second floor (Case-3)

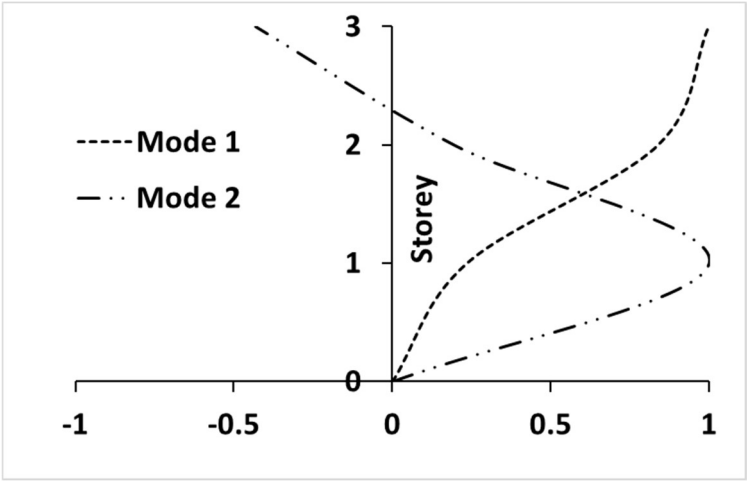

Figure 3-13 : Mode Shapes of damaged experimental frame in second floor obtained from OMA (Case-3)

Table 3-5: Modal parameters of the damaged experimental frame in second floor

	Mode Shape	
	Mode 1	**Mode 2**
First floor	0.235	1
Second floor	0.8402	0.1947
Third floor	1	-0.4320
Frequencies	1.9287Hz	6.8176Hz

3.5 Model Updating of Experimental Frame

The sensitivity method for model updating discussed in the previous chapter is implemented to perform the model updating of the experimental frame to obtain the storey stiffness of the frame idealized as shown in Figure 3-4. The sensitivity-based model updating methodology aims to improve the accuracy of a structural model by iteratively adjusting its physical parameters based on experimental measurements. Experimental modal properties (frequencies and modeshapes) are extracted from ambient vibration data using FDD. The physical parameters, storey stiffness, is selected for updating. With an initial guess of the updating parameter (x), a global stiffness matrix is constructed, and a generalized eigenvalue problem is solved to obtain analytical eigenvalues and modeshapes. The definition of the updating parameter (x) is discussed in previous chapter. Residual vectors are then calculated to quantify the differences between the experimental and analytical results. An objective function to minimize the sum of squared residuals is formulated, and the Levenberg-Marquardt algorithm is further deployed for optimization. The algorithm iteratively adjusts the parameter values until convergence is reached.

3.6 Results and Discussion

Modal parameters of the first 2 modes were used for the model updating to obtain the storey stiffness of the frame. The initial guess for each floor's stiffness was provided, and the parameters were updated through the model updating. The updating parameters (x) were used to calculate the corresponding updated stiffness values. For each floor, initial guess of the stiffness is 15000 N/m.

3.6.1 Case 1: Undamaged Case

In reference to Case 1, wherein the frame remains undamaged, the process of model updating has yielded updated stiffness values for the first, second, and third storeys, amounting to 26460

N/m, 26850 N/m, and 27570 N/m, respectively, as indicated in Table 3-6. Subsequently, a comparison was made between the experimentally obtained eigenvalues and their corresponding updated counterparts. The discrepancy observed between the experimentally obtained and updated eigenvalues for mode 1 was -8.91%, while for mode 2, it was 10.89%, as presented in Table 3-7. Furthermore, the error between experimentally obtained and updated eigen vectors is within 10% as shown in Table 3-8. The iterative optimization process successfully achieved convergence to the optimal solution after 13 iterations, as illustrated in Figure 3-14 and Figure 3-15.

Table 3-6 : Updated Storey Stiffness of the Experimental Frame

Floor	Initial Guess	Updating Parameter (x)	Updated Stiffness
1	15000	0.764	26460
2	15000	0.79	26850
3	15000	0.838	27570

Table 3-7: Comparison of experimental and updated eigen values

	Eigen Values		
	Experiment	**Updated**	**Error%**
Mode 1	203.40	209.536	-3.02%
Mode 2	2083.86	2016.905	3.21%

Table 3-8: Comparison of experimental and updated eigen vectors

	Experiment		Updated		ERROR %	
	Mode 1	**Mode 2**	**Mode 1**	**Mode 2**	**Mode 1**	**Mode 2**
DOF1	0.4440	1	0.453	1	-2.01%	0.00%
DOF2	0.8016	0.4461	0.809	0.409	-0.92%	8.32%
DOF3	1	-0.8	1	-0.782	0.00%	2.25%

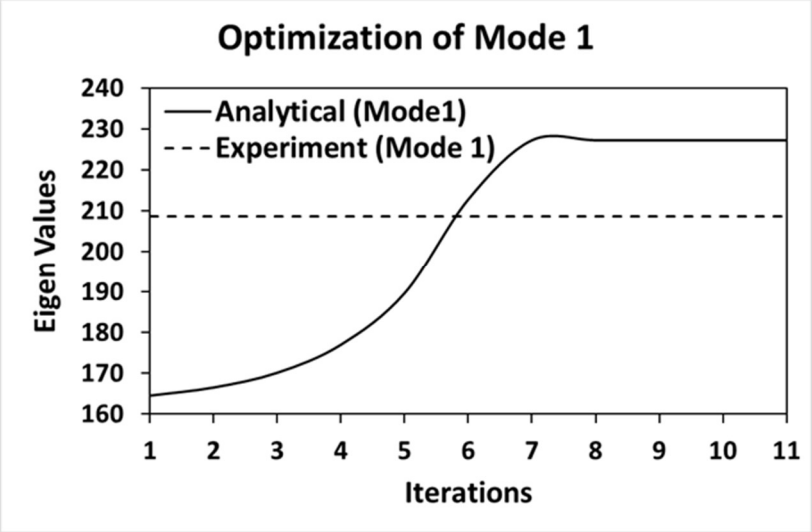

Figure 3-14 : Eigen Values for mode 1 in each iteration of optimization (case 1)

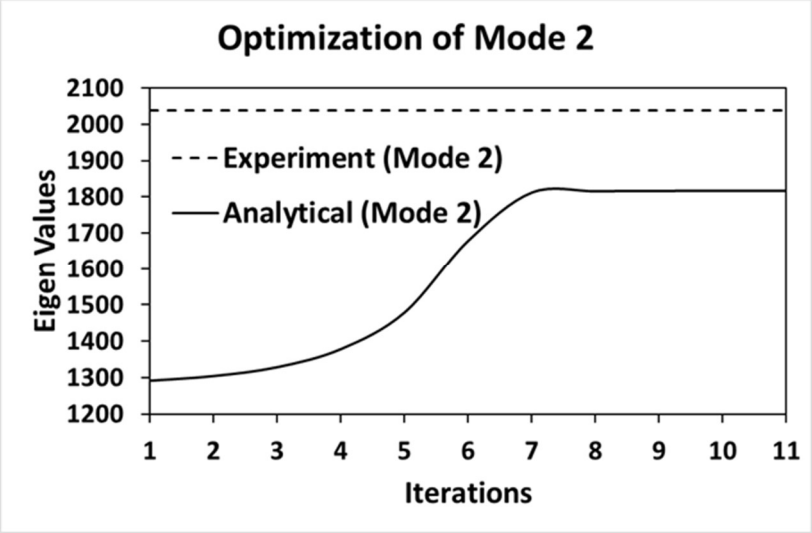

Figure 3-15 : Eigen Values for mode 2 in each iteration of optimization (case 1)

3.6.2 Case 2: Damaged Case (First Floor)

In relation to Case 2, wherein the frame experiences damage at the first floor, the model updating process has resulted in revised stiffness values for the first, second, and third storeys, measuring 9066 N/m, 27210 N/m, and 27360 N/m, respectively, at the conclusion of the optimization procedure as demonstrated in Table 3-9. The observed reduction in storey stiffness for the first floor enables successful identification of both the location and magnitude of the damage. Subsequently, a comparison was conducted between the experimentally obtained eigenvalues and eigenvectors and their corresponding updated counterparts. The

discrepancy observed between the experimentally obtained and updated eigenvalues for mode 1 was 2.80%, while for mode 2, it was -2.65%, as presented in Table 3-10. Additionally, the error between the experimentally obtained and updated eigenvectors was found to be within 10%, as depicted in Table 3-11. The iterative optimization process successfully achieved convergence to the optimal solution after 13 iterations, as shown in Figure 3-16 and Figure 3-17.

Table 3-9 : Updated Storey Stiffness of the Experimental Frame

Floor	Initial Guess	Updating Parameter (x)	Updated Stiffness
1	**15000**	**-0.3956**	**9066**
2	15000	0.814	27210
3	15000	0.824	27360

Table 3-10: Comparison of experimental and updated eigen values

	Eigen Values		
	Experiment	**Updated**	**Error%**
Mode 1	142.97	138.9668	2.80%
Mode 2	1733.59	1779.579	-2.65%

Table 3-11: Comparison of experimental and updated eigen vectors

	Experiment		Updated		ERROR %	
	Mode 1	**Mode 2**	**Mode 1**	**Mode 2**	**Mode 1**	**Mode 2**
DOF1	0.7961	1	0.732	1	8.05%	0.00%
DOF2	0.9303	0.1377	0.908	0.152	2.40%	-10.39%
DOF3	1	-0.8754	1	-0.868	0.00%	0.84%

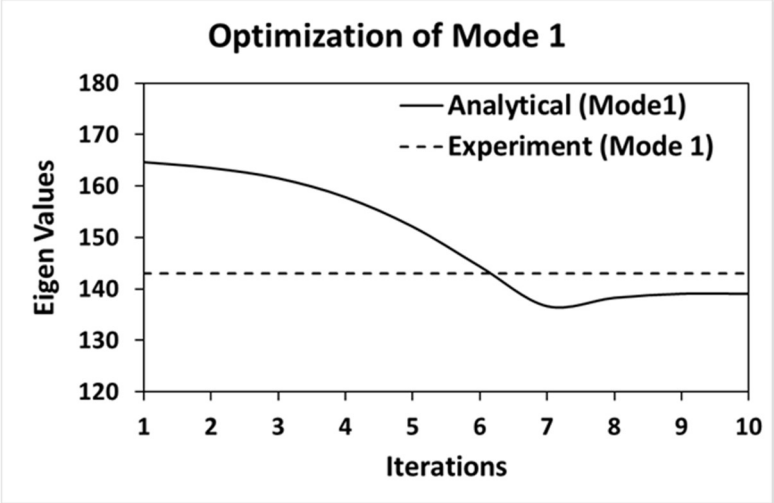

Figure 3-16 : Eigen Values for mode 1 in each iteration of optimization (case 2)

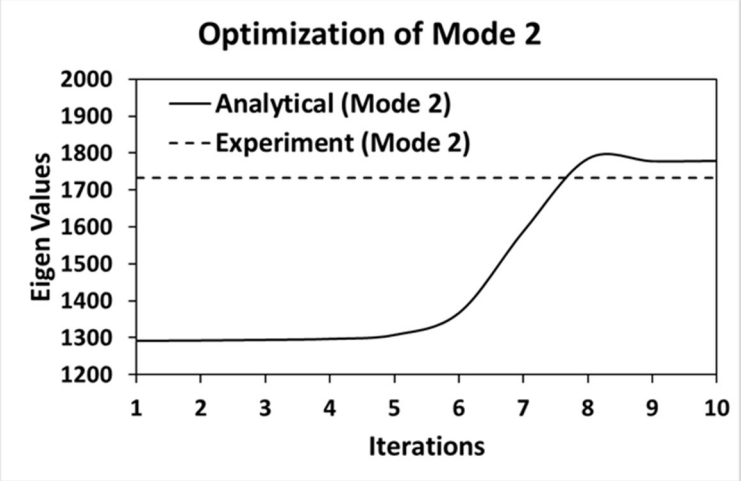

Figure 3-17 : Eigen Values for mode 2 in each iteration of optimization (case 2)

3.6.3 Case 3: Damaged Case (Second Floor)

In the context of Case 3, involving a damaged frame at the second floor, the model updating process has yielded updated stiffness values for the first, second, and third storeys, which amounted to 26400 N/m, 7650 N/m, and 21300 N/m, respectively, at the conclusion of the optimization phase, as presented in Table 3-12 . The observed reduction in storey stiffness specifically on the second floor indicates the location of the damage. Moreover, the stiffness reduction to 7650 N/m provides a quantification of the extent of the damage. Subsequently, a comparative analysis was performed between the experimentally obtained eigenvalues and eigenvectors and their respective updated counterparts. The observed errors between the

experimentally obtained and updated eigenvalues were -1.67% for mode 1 and 1.72% for mode 2, as indicated in Table 3-13. Furthermore, the error between the experimentally obtained and updated eigenvectors fell within 10%, as demonstrated in Table 3-14. The iterative optimization process successfully achieved convergence to the optimal solution after 13 iterations, as illustrated in Figure 3-18 and Figure 3-19.

Table 3-12 : Updated Storey Stiffness of the Experimental Frame

Floor	Initial Guess	Updating Parameter (x)	Updated Stiffness
1	15000	0.76	26400
2	**15000**	**-0.49**	**7650**
3	15000	0.42	21300

Table 3-13: Comparison of experimental and updated eigen values

	Eigen Values		
	Experiment	**Updated**	**Error%**
Mode 1	146.7	149.15	-1.67%
Mode 2	1833.098	1801.49	1.72%

Table 3-14: Comparison of experimental and updated eigen vectors

	Experiment		Updated		ERROR %	
	Mode 1	**Mode 2**	**Mode 1**	**Mode 2**	**Mode 1**	**Mode 2**
DOF1	0.2350	1	0.212	1	9.81%	0.00%
DOF2	0.8402	0.1947	0.873	0.2077	-3.90%	-6.68%
DOF3	1	-0.4320	1	-0.393	0.00%	9.03%

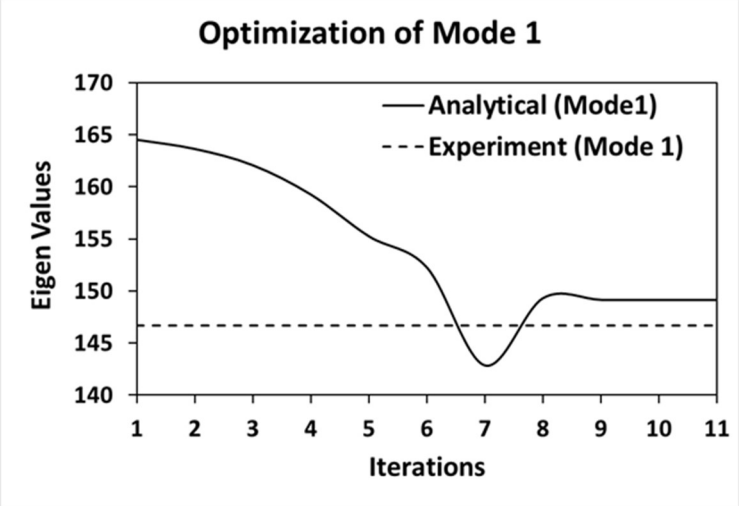

Figure 3-18 : Eigen Values for mode 1 in each iteration of optimization

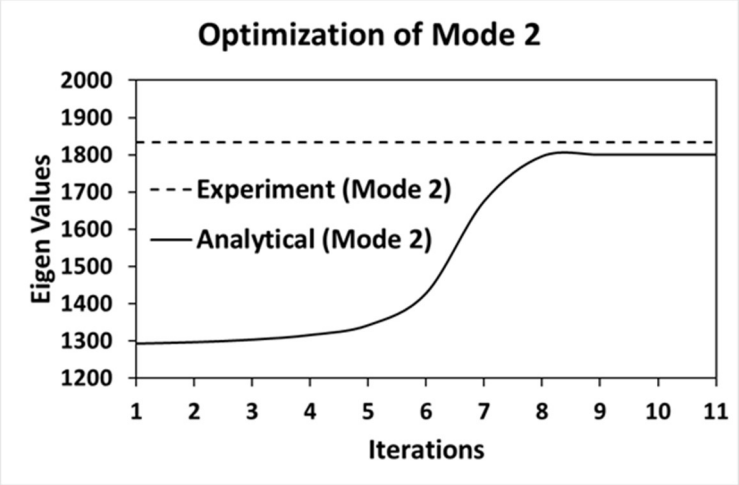

Figure 3-19 : Eigen Values for mode 2 in each iteration of optimization

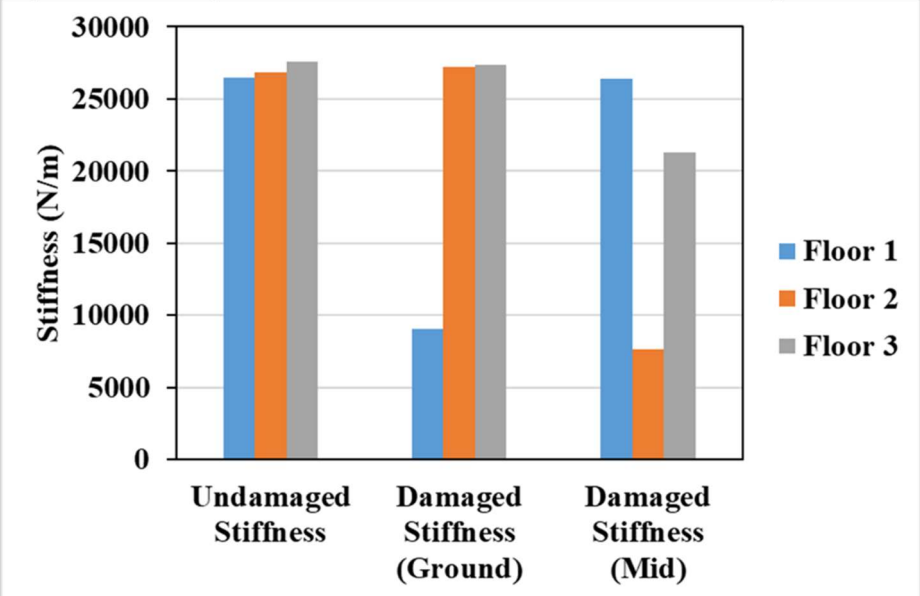

Figure 3-20 : Comparison of the storey stiffnesses for different cases

3.7 Discussion and Conclusion

In conclusion, the successful implementation of a sensitivity-base model updating approach for an experimental steel frame to determine the storey stiffness of the frame using only two modal parameters. It is understood by analyzing the changes in storey stiffness, it is possible to understand and quantify the damage in a specific floor caused by the loosening of a bolt (Figure 3-20). In other words, the decrease in storey stiffness can be attributed to the damage in that particular floor. The study serves as proof that the model updating method, which was discussed in a previous chapter, can be effectively utilized to identify damage in terms of

stiffness at various locations within a structure. This suggests that this model updating method is a reliable tool for detecting and assessing damage in different parts of a structure based on changes in stiffness properties.

Chapter 4: 3D AEM integration of the sensitivity-based model updating

4.1 Introduction

In this chapter, we delve into the theoretical development of the Applied Element Method (AEM) and its subsequent validation in elastic analysis, static analysis, and dynamic analysis. The elastic validation of AEM involves comparing the results from elastic analysis in AEM with theoretical calculations ensuring its reliability and accuracy in predicting structural behavior. Furthermore, the static validation assesses AEM's capability to accurately capture the response of structures under pushover loading condition, with comparisons made against experimental data. Additionally, the dynamic validation focuses on the dynamic response of structures subjected earthquake ground motion analyzed in AEM and compare with the experimental results.

Furthermore, in this chapter, the computational efficiency of three different solvers; direct solver with skyline storage format, iterative solver with triplet storage format and parallel direct sparse solver (PARDISO) with triplet storage format, are discussed and compared implementing in 3D AEM.

Next, the integration of sensitivity-based model updating in the 3D Applied Element Method (AEM) represents a significant advancement in the field of structural analysis. The model updating method discussed in previous chapter offers a powerful approach to calibrate numerical models using measured modal data, while the 3D AEM provides a sophisticated framework for accurately representing complex structures. By combining these two methodologies, the aim is to refine the numerical model by optimizing (minimization) the disparities between the model predictions and experiment observations, ultimately enhancing

the accuracy and reliability of structural simulations. This chapter delves into the integration of sensitivity-based model updating within the 3D AEM, highlighting the key steps involved and the potential benefits it offers for improved structural modeling and analysis.

4.2 Theoretical Development of Applied Element Method

Numerical methods for structural analysis can be divided into two categories: continuum-based models like the Finite Element Method (FEM) [19]and discrete element techniques like the Rigid Body and Spring Model (RBSM)[58] and the Extended Distinct Element Method (EDEM)[51].

The FEM[19], a continuum-based method, faces limitations when dealing with separation between structural elements. It can answer whether the structure will fail or not but struggles to predict the collapse process accurately.

Discrete element techniques, like RBSM[58] and EDEM[51], offer a simpler way to simulate cracking but have drawbacks. RBSM cannot analyze the structure up to complete collapse, while EDEM can do so but lacks the FEM's accuracy in small deformation ranges. The cumulative errors resulting from repeated calculations make it difficult to accurately predict the failure behavior using the current EDEM method. As a result, the EDEM can only provide insights into "how the structure collapses."

On the other hand, the Applied Element Method (AEM) is an effective and precise approach for capturing the intricate behaviour of structures throughout various stages, encompassing initial zero loading to collapse, all within a practical timeframe. The method achieves reliable accuracy by employing relatively simple material models. A fundamental aspect of the AEM involves dividing the structures into discrete elements interconnected by springs in normal and tangential direction. Consequently, the occurrence of failure within these elements can be

simulated by monitoring failure of connecting springs. This failure is determined once the computed stress derived from spring forces surpasses the critical principal stress thresholds [59].

The Figure 4-1 shows a sample of meshing for 3D AEM model divided into small square elements. The Figure 4-2 and Figure 4-3 shows two elements which is connected with springs (one normal and a pair of shear springs) positioned at various contact points around the faces of these elements. Every spring fully captures the stress and deformation within a specific region of the analyzed elements. The stiffness of each spring is calculated as:

$$K_n = \frac{\mathrm{E}d_1 d_2}{a}; \qquad K_{1s,2s} = \frac{\mathrm{G}d_1 d_2}{a} \tag{4-1}$$

where, "d_1" and "d_2": width and thickness of representative area of each spring

"a" : length of same representative area,

"E": Young's modulus

"G": Shear modulus

The equation (4-1) expresses that each spring corresponds to the stiffness of an area with dimensions (d_1*d_2) and length (a) of the material being studied. Assuming the spring connects with the centreline of the element's normal stiffness K_n, Shear stiffnesses $K_{1s,2s}$ is calculated. Each elements have 6 degree of freedoms and these dofs represents the elements' rigid body motion Figure 4-3. While the overall motion of the element behaves as a rigid body, its internal deformations are accounted for through the deformation of springs surrounding each element. This setup ensures that the shape of the individual element remains unchanged throughout the analysis, preserving its rigidity. However, the collective behavior of the elements can exhibit deformable characteristics due to the spring-based representation of internal deformations.

The size of local stiffness matrix is 12x12. Equation (4-2) represents the upper one quadrant of the matrix. The details are illustrated in Figure 4-3.

	1	2	3	4	5	6
1	$K_nN_x^2+K_{1s}S_{1x}^2+K_{2s}S_{2x}^2$	$N_xK_nN_y+S_{1x}K_{1s}S_{1y}+S_{2x}K_{2s}S_{2y}$	$N_xK_nN_z+S_{1x}K_{1s}S_{1z}+S_{2x}K_{2s}S_{2z}$	$K_nN_x(R_yN_z-R_zN_y)+K_{1s}S_{1x}(R_yS_{1z}-R_zS_{1y})+K_{2s}S_{2x}(R_yS_{2z}-R_zS_{2y})$	$K_nN_x(R_zN_x-R_xN_z)+K_{1s}S_{1x}(R_zS_{1x}-R_xS_{1z})+K_{2s}S_{2x}(R_zS_{2x}-R_xS_{2z})$	$K_nN_x(R_xN_y-R_yN_x)+K_{1s}S_{1x}(R_xS_{1y}-R_yS_{1x})+K_{2s}S_{2x}(R_xS_{2y}-R_yS_{2x})$
2	S(1,2)	$K_nN_y^2+K_{1s}S_{1y}^2+K_{2s}S_{2y}^2$	$N_yK_nN_z+S_{1y}K_{1s}S_{1z}+S_{2y}K_{2s}S_{2z}$	$K_nN_y(R_yN_z-R_zN_y)+K_{1s}S_{1y}(R_yS_{1z}-R_zS_{1y})+K_{2s}S_{2y}(R_yS_{2z}-R_zS_{2y})$	$K_nN_y(R_zN_x-R_xN_z)+K_{1s}S_{1y}(R_zS_{1x}-R_xS_{1z})+K_{2s}S_{2y}(R_zS_{2x}-R_xS_{2z})$	$K_nN_y(R_xN_y-R_yN_x)+K_{1s}S_{1y}(R_xS_{1y}-R_yS_{1x})+K_{2s}S_{2y}(R_xS_{2y}-R_yS_{2x})$
3	S(1,3)	S(2,3)	$K_nN_z^2+K_{1s}S_{1z}^2+K_{2s}S_{2z}^2$	$K_nN_z(R_yN_z-R_zN_y)+K_{1s}S_{1z}(R_yS_{1z}-R_zS_{1y})+K_{2s}S_{2z}(R_yS_{2z}-R_zS_{2y})$	$K_nN_z(R_zN_x-R_xN_z)+K_{1s}S_{1z}(R_zS_{1x}-R_xS_{1z})+K_{2s}S_{2z}(R_zS_{2x}-R_xS_{2z})$	$K_nN_z(R_xN_y-R_yN_x)+K_{1s}S_{1z}(R_xS_{1y}-R_yS_{1x})+K_{2s}S_{2z}(R_xS_{2y}-R_yS_{2x})$
4	S(1,4)	S(2,4)	S(3,4)	$K_n(R_yN_z-R_zN_y)^2+K_{1s}(R_yS_{1z}-R_zS_{1y})^2+K_{2s}(R_yS_{2z}-R_zS_{2y})^2$	$K_n(R_yN_z-R_zN_y)(R_zN_x-R_xN_z)+K_{1s}(R_yS_{1z}-R_zS_{1y})(R_zS_{1x}-R_xS_{1z})+K_{2s}(R_yS_{2z}-R_zS_{2y})(R_zS_{2x}-R_xS_{2z})$	$K_n(R_yN_z-R_zN_y)(R_xN_y-R_yN_x)+K_{1s}(R_yS_{1z}-R_zS_{1y})(R_xS_{1y}-R_yS_{1x})+K_{2s}(R_yS_{2z}-R_zS_{2y})(R_xS_{2y}-R_yS_{2x})$
5	S(1,5)	S(2,5)	S(3,5)	S(4,5)	$K_n(R_zN_x-R_xN_z)^2+K_{1s}(R_zS_{1x}-R_xS_{1z})^2+K_{2s}(R_zS_{2x}-R_xS_{2z})^2$	$K_n(R_zN_x-R_xN_z)(R_xN_y-R_yN_x)+K_{1s}(R_zS_{1x}-R_xS_{1z})(R_xS_{1y}-R_yS_{1x})+K_{2s}(R_zS_{2x}-R_xS_{2z})(R_xS_{2y}-R_yS_{2x})$
6	S(1,6)	S(2,6)	S(3,6)	S(4,6)	S(5,6)	$K_n(R_xN_y-R_yN_x)^2+K_{1s}(R_xS_{1y}-R_yS_{1x})^2+K_{2s}(R_xS_{2y}-R_yS_{2x})^2$

(4-2)

The local stiffness matrix of each pair of springs is then aggregated to obtain the global stiffness matrix. The equation of motion is then solved incrementally:

$$\mathbf{M}\Delta\ddot{Y}+\mathbf{C}\Delta\dot{Y}+\mathbf{K}\Delta Y=\Delta\mathbf{F} \quad (4\text{-}3)$$

ΔY= incremental displacements

$\Delta\dot{Y}$= incremental velocities

$\Delta\ddot{Y}$ =incremental accelerations

M = global mass matrix,

C = damping matrix,

K = global stiffness matrix,

ΔF = incremental force.

Newmark-beta methodology is used to solve this problem. The details of Applied Element Method (AEM) are discussed in flowchart Figure 4-4.

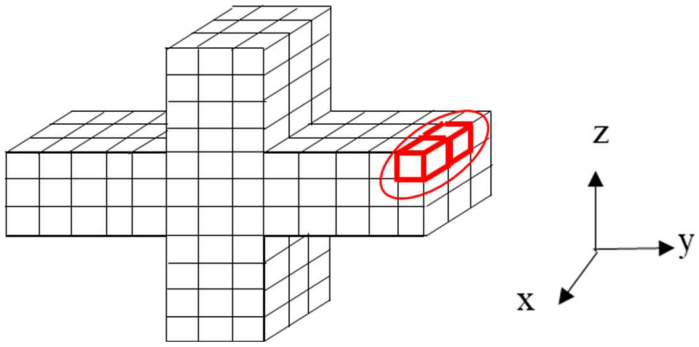

Figure 4-1 : Sample of 3D AEM meshing

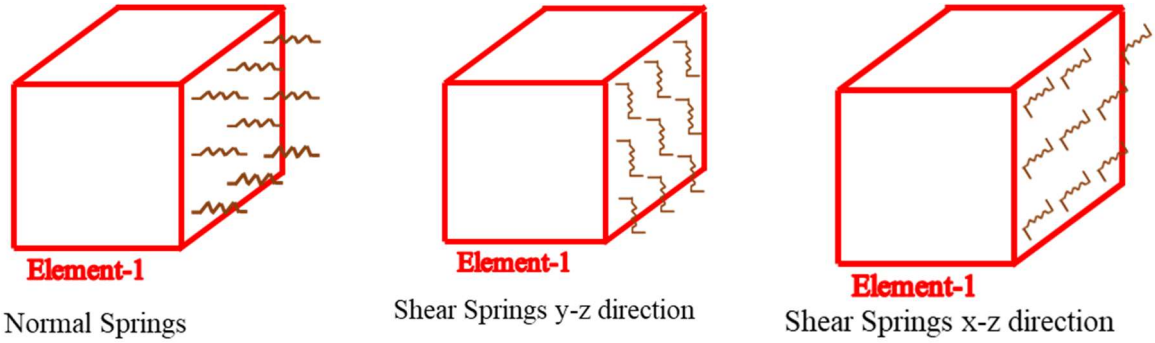

Figure 4-2: Spring distributions

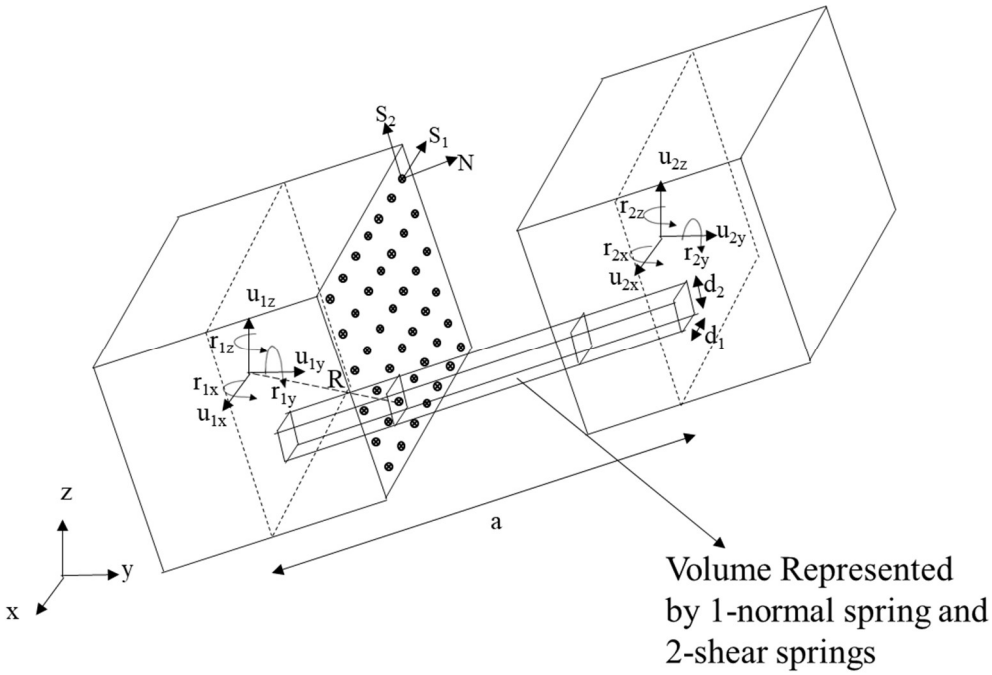

Figure 4-3 : Spring distribution, area of influence of each spring and degree of freedoms

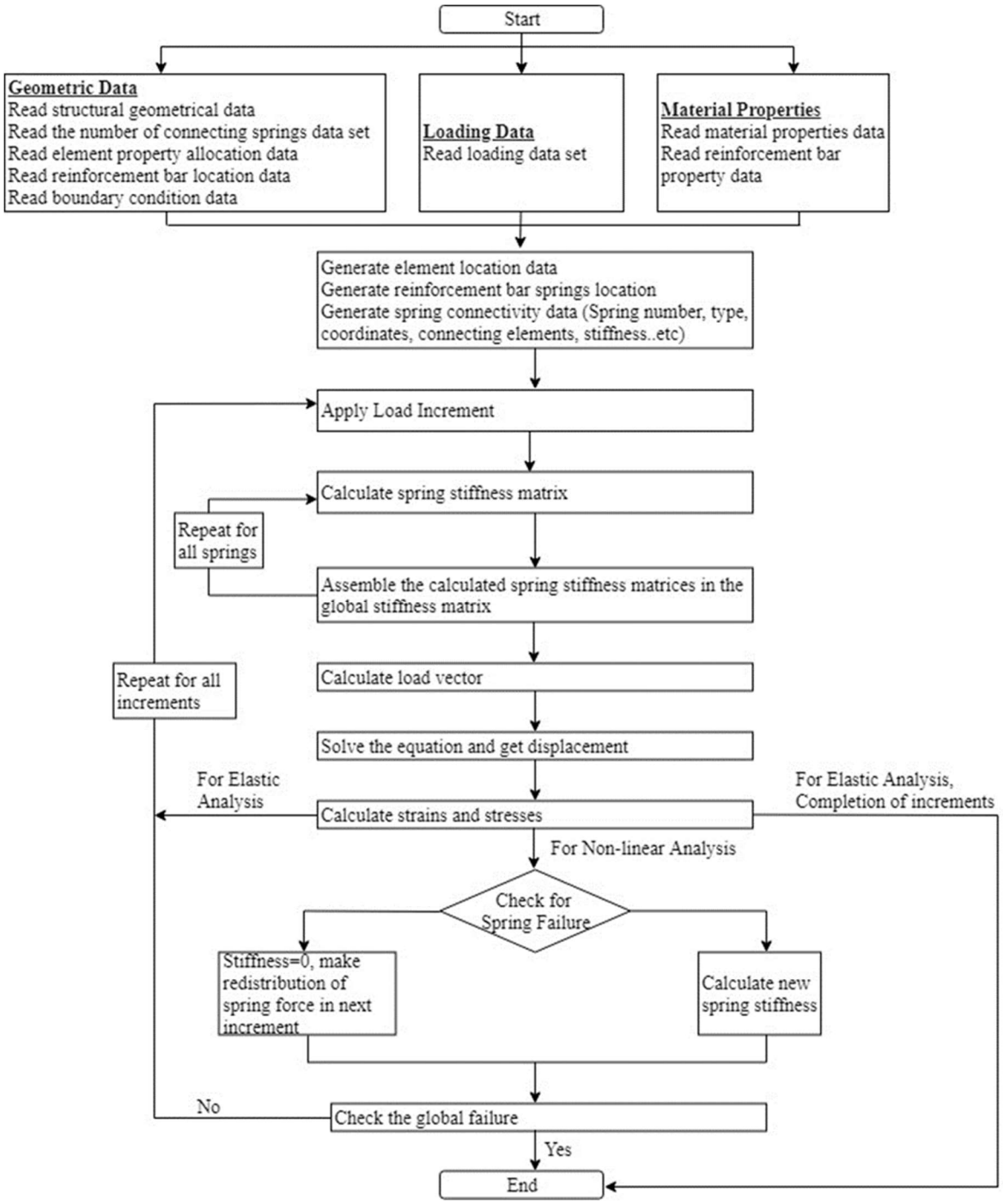

Figure 4-4 : Flowchart of Elastic and Non-linear Analysis in Applied Element Method (AEM) [59], [60]

4.3 Validation of Numerical Tool

The present study involves the redevelopment of the applied element method (AEM) tool for three-dimensional numerical analysis of structures, utilizing the FORTRAN 90 programming language. Subsequently, the numerical tool is subjected to validation for various scenarios,

namely the elastic case, static case, and dynamic case, which will be discussed in the subsequent sub-sections.

4.3.1 Elastic Validation

The validation process for the numerical tool used to simulate elastic loading involves analyzing a cantilever beam Figure 4-5. The frame's geometrical and material characteristics are detailed in Table 4-1.

Table 4-1: Properties of beam under validation

Length	3 m
Cross Section	0.3m. x 0.3 m.
Young's Modulus, (E)	$2.49 * 10^8$ N/m^2

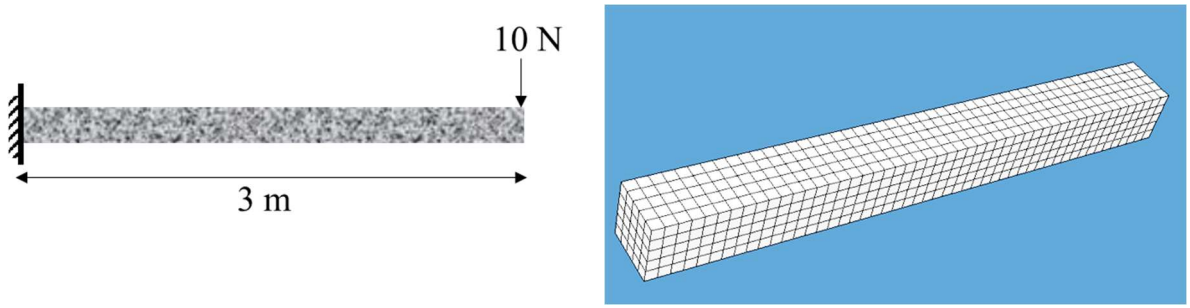

Figure 4-5: Case study cantilever beam for elastic validation

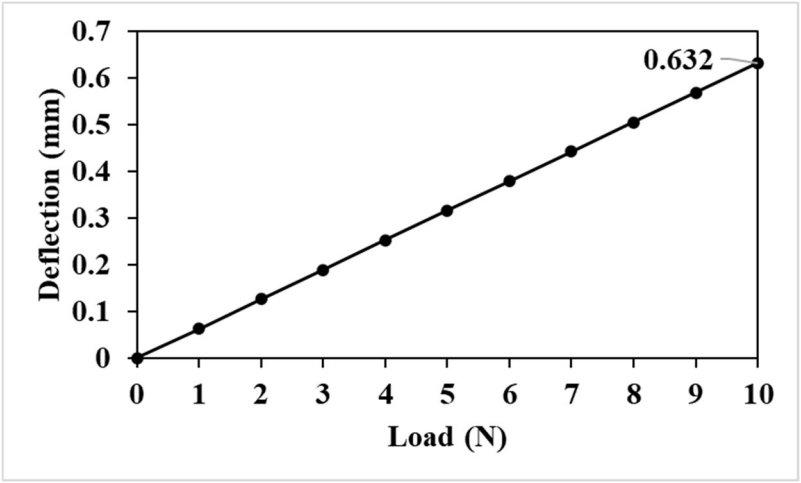

Figure 4-6 : Load-Displacement plot for the elastic analysis

A 10N of load at the free end of the cantilever beam is applied in the 10 timesteps in 3D AEM. The maximum deflection at the free end is identified from the AEM analysis is 0.632 mm (Figure 4-6). Manually calculating the deflection for a cantilever beam with point load at the end is given by:

$$\delta(at\ the\ end\ of\ cantilever) = \frac{PL^3}{3EI} = 6.33*10^{-3}\ \text{m}\ .$$

The theoretical and numerical analysis results show a strong agreement, confirming the accuracy and reliability of the numerical tool.

4.3.2 Static Validation

To validate the 3D AEM tool for the static case, we analyzed a frame (Figure 4-7) previously tested by K. Muto [61]. The result from 3D AEM numerical simulation is compared with the experiment result. The frame's geometric characteristics are listed in Table 4-2, while its material characteristics can be found in Table 4-3.

Table 4-2: Geometrical characteristics of the frame

Length of bay (m.)	2.310m
Height of frame (m.)	1.460m
Details of Columns	0.25mx0.25m, 8 no. of 16mm reinforcement bars with 6 mm stirrups at 200mm center to center
Details of Beam	0.18mx0.25m, 4no. of 16mm reinforcement bars with 6 mm stirrups at 200mm center to center

Table 4-3: Material characteristics of the frame

Young's Modulus of concrete, (N/m^2)	$2.49 * 10^{10}$
Yield strength of rebars (N/m^2)	$4.53*10^8$
Poison's ratio	0.2

Tensile Strength, (N/m^2)	$1.471 * 10^6$
Compressive Strength, Fc (N/m^2)	$1.824 * 10^7$
Material Density (Kg/m^3)	2400
Connecting springs in each face	81
Element Numbers	2350
Size of elements (m)	0.05

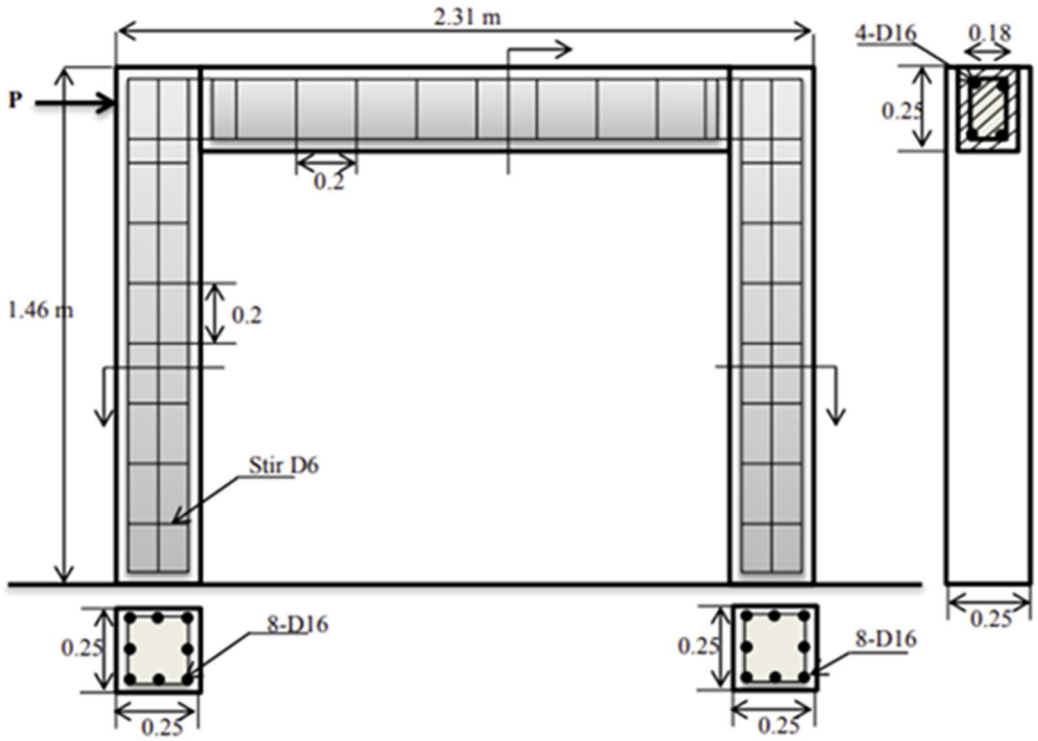

Figure 4-7: Case study frame for static validation

In 2000 consecutive time increments, a static pushover displacement of 0.0090m is exerted at the top part of the frame. Figure 4-8 illustrates the correlation between the applied load and deformation, computed using a numerical tool. This numerical analysis is then compared to experimental data conducted by K. Muto [61]. The comparison reveals a substantial concurrence between the two sets of results, indicating good agreement. Moreover, in Figure 4-9, the deformed shape and crack location obtained from the numerical model closely match those observed in the experimental setup shown in Figure 4-10.

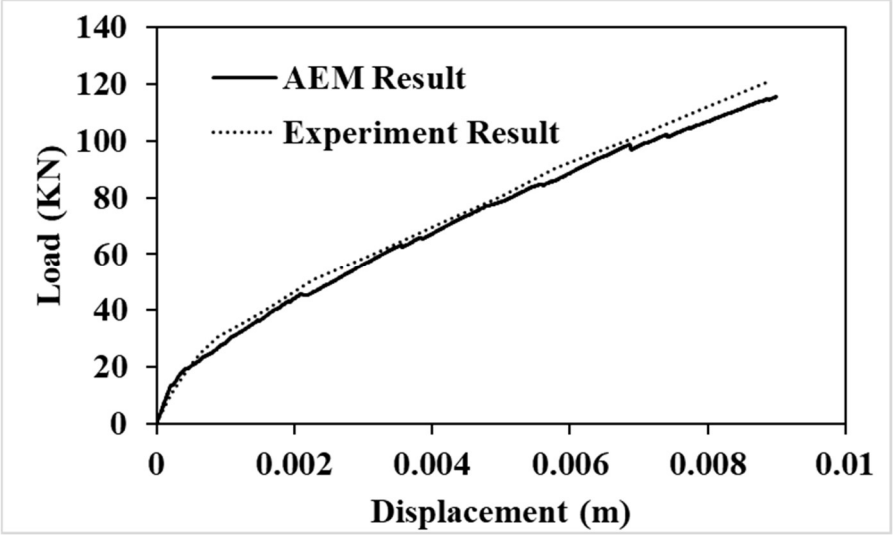

Figure 4-8 : Force-Displacement relation for the static analysis case-study frame

Figure 4-9 : Deformed Shape and failure pattern of RC Frame from 3D AEM simulation (Illustration Scale: 5)

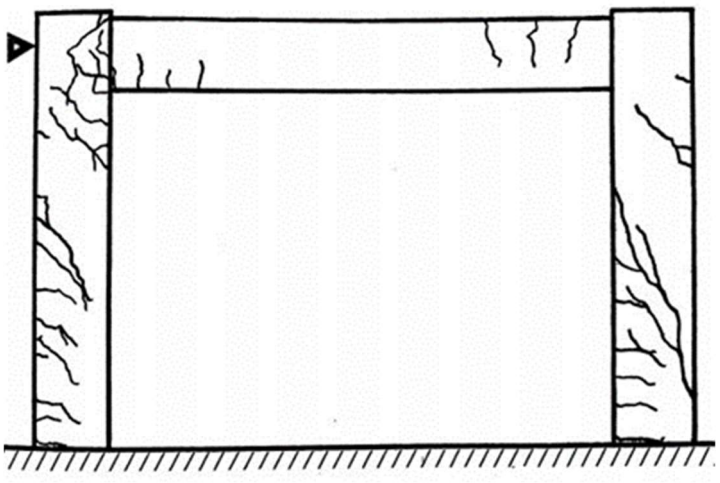

Figure 4-10 : Failure Pattern of RC Frame from experiment[61]

4.3.3 Dynamic Validation

For the validation of the numerical tool developed based on AEM for dynamic loading case a frame shown in Figure 4-11 : Case study frame for dynamic validation [62], [63] verified through analytical and experimental study by A. Filiatrault et.al. has been analysed [62],[63]. Table 4-4 displays the material characteristics of the frame being analyzed.

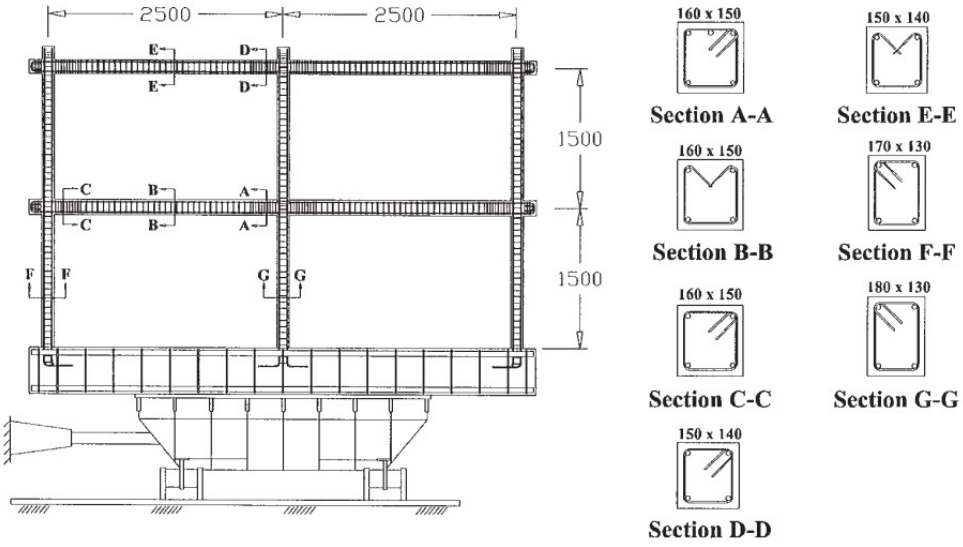

Figure 4-11 : Case study frame for dynamic validation [62], [63]

Table 4-4 : Material Properties of frame under analysis

Longitudinal reinforcing steel	Young's Modulus of reinforcement= 224.6 Gpa, Yield strength of reinforcement = 438 Mpa Yield strain of reinforcement = 0.001950, Tensile strength of reinforcement =601.00 Mpa Ultimate strain of reinforcement= 0.1990
Transverse reinforcing steel	Yield strength of transverse steel= 750.00 Mpa Tensile strength of transverse steel =900.00 Mpa
Concrete for structure with nominal ductility	Young's Modulus of concrete = 25.20 Gpa, Compressive strength of concrete= 31Mpa, Poisson's ratio of concrete=0.17

The Figure 4-12 shows the AEM model of the frame under analysis. The frame is modelled with 2728 cubical elements of size 4 cm each. Each face of the elements are connected with 81 springs.

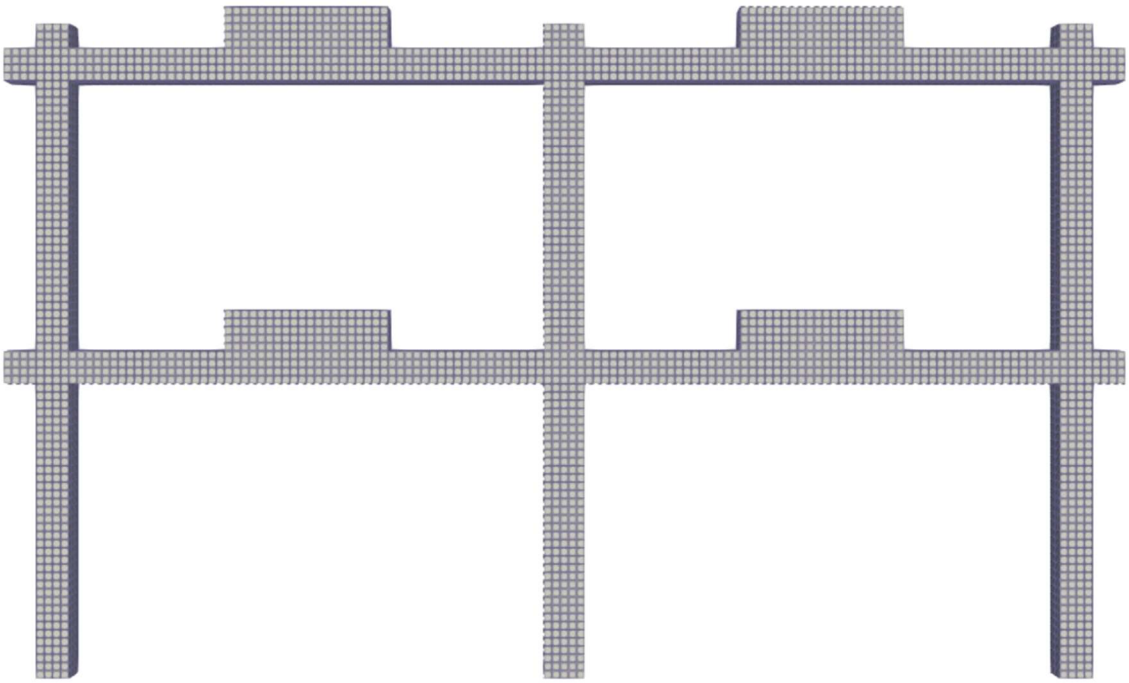

Figure 4-12 : AEM model of the frame under dynamic validation

For the experiment, researchers utilized the N04W ground motion component of 1949 Western Washington Earthquake from the recording station in Olympia of Washington. The numerical simulation in AEM is conducted for the 30-second significant duration of this ground motion.

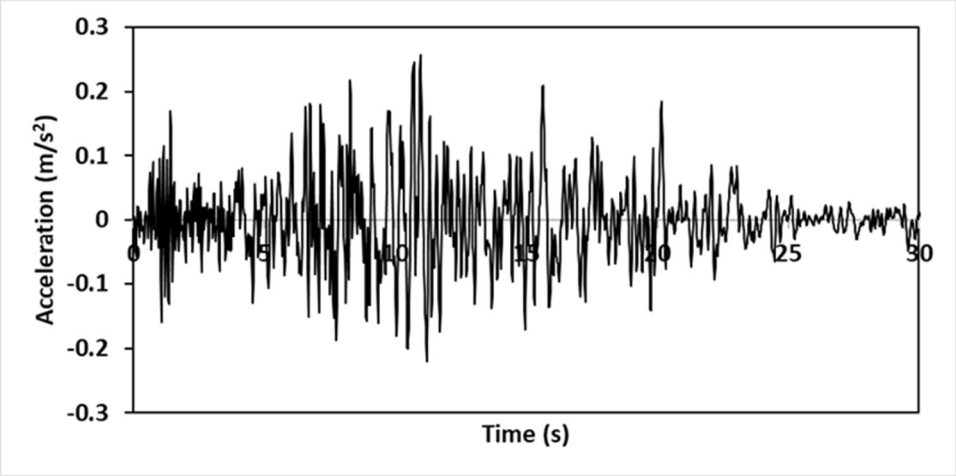

Figure 4-13 : Western Washington Earthquake ground motion

The top floor displacement response for this ground motion has been plotted and compared in Figure 4-14 and Figure 4-15. The response calculated from the numerical tool shows a good agreement with the experimental result. Maximum roof displacement is observed to be ± 40mm, which exactly matches with the experiment result. Also, the crack location from the numerical model agrees well with the experiment (Figure 4-16). The cracks are located at the joint of beam and column and base of the column, which is also similar to that of experiment.

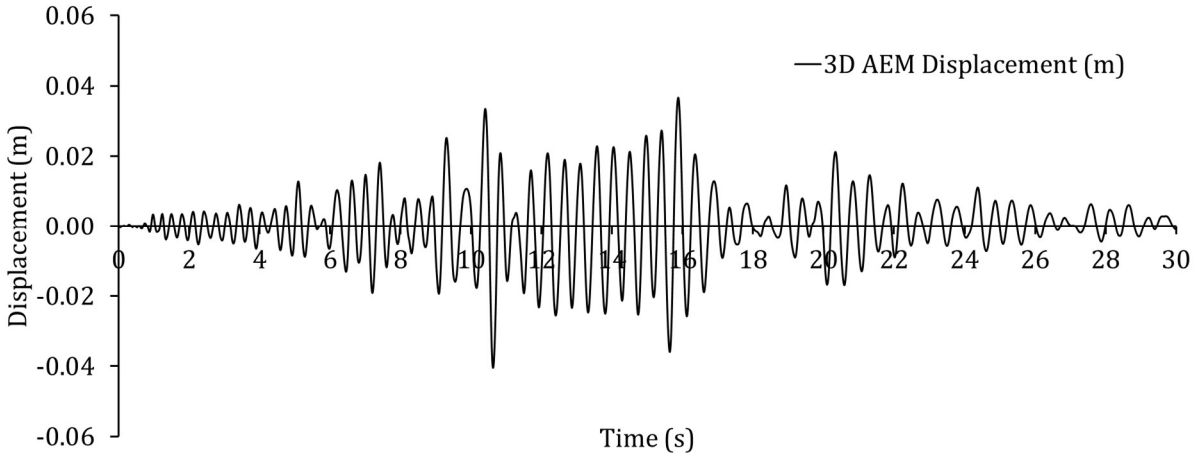

Figure 4-14 : Top floor displacement response in AEM

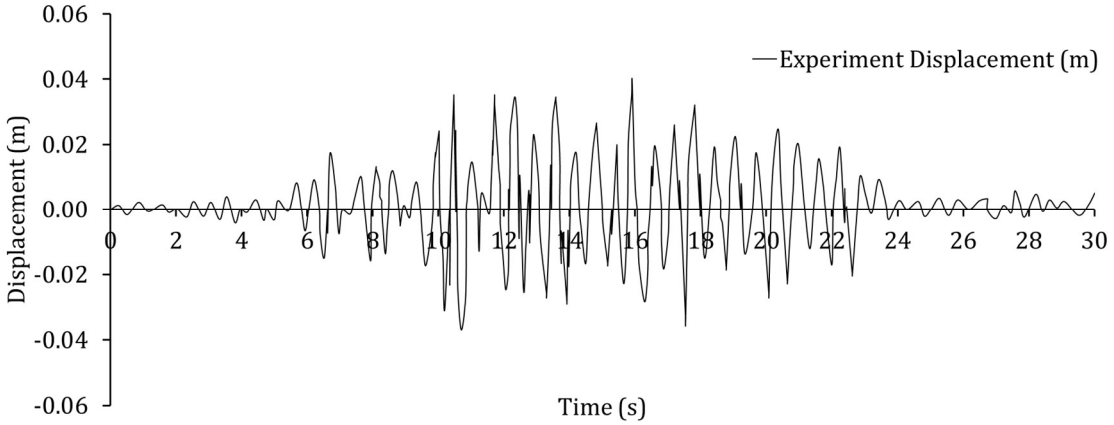

Figure 4-15 : Top floor displacement response by experimental analysis by Filiatraut et. al. [62],[63]

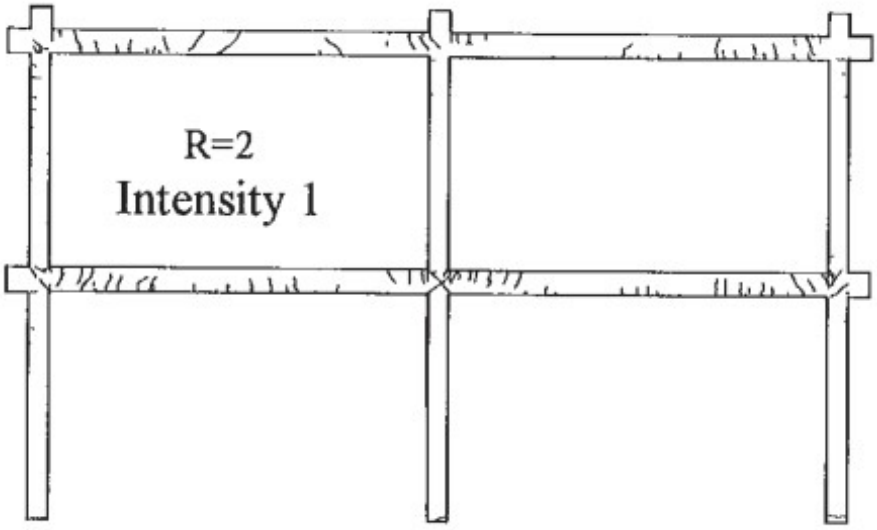

Figure 4-16 : Crack location in Experiment

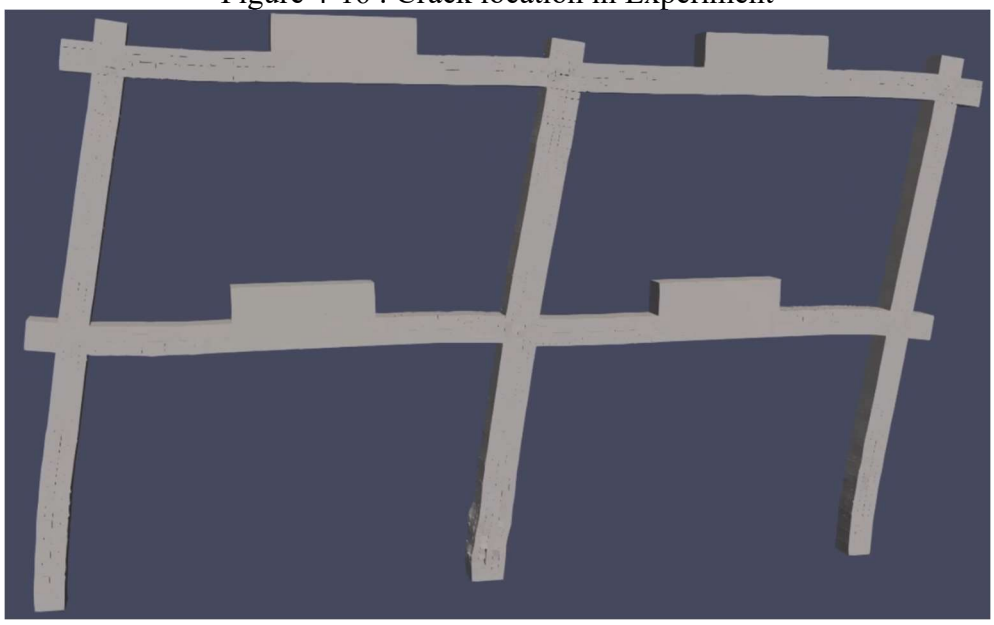

Figure 4-17 : Deformation of the frame in AEM

4.4 Computational Efficiency of the Tool

The displacement measurement (x) in each dof can be calculated solving the linear equation $\{F\}=[K]\{x\}$. Where, $\{F\}_{nx1}$ is vector containing the external force applied to n-degree of freedoms and $[K]_{nxn}$ is highly sparse and symmetric global stiffness matrix and $\{x\}_{nx1}$ is the displacement vector. Numerous solvers are available to solve this linear equation. Three solvers: direct solver with skyline storage format, iterative solver with triplet storage format and parallel direct sparse solver with triplet storage format, used in the Fortran 90 implementation with GNU compiler of AEM to solve the linear equation $\{F\}=[K]\{x\}$ since its development.

Direct solver with skyline storage format, generally implemented using gaussian elimination method, is a type of linear equation solver used in numerical analysis and computational mathematics [64]. It is designed specifically for solving sparse matrices that have a symmetric, positive definite structure. This solver exploits the sparsity pattern of the matrix to reduce the no. of computations required to solve the system of equations. Direct solver with skyline storage format is commonly used in a wide range of applications, including finite element analysis. They are particularly useful when the matrix is sparse and large and when the sparsity pattern is irregular. However, this solver can be computationally expensive, especially when the matrix is not well-conditioned or when the sparsity pattern is highly irregular[65].

Though there are numerous iterative solvers, in this paper, the Generalized Minimum Residual (GMRES) algorithm for the iterative method for solving large-scale sparse-linear systems is used. The GMRES algorithm is designed to work well for large-scale sparse linear systems that are difficult to solve by direct methods such as Gaussian elimination. The GMRES algorithm works by constructing an orthonormal basis for the Krylov subspace and then solves the least squares problem of finding the vector that minimizes the residual over the Krylov subspace [66],[67],[68]. It is widely used in computational fluid dynamics, structural mechanics, and

numerical optimization. This iterative method is used in conjunction with the triplet storage format, in which the triples are stored in a one-dimensional array, with each triple taking up three consecutive elements in the array. The array is ordered first by row, then by column, so that all the nonzero elements in a given row are stored together. One advantage of the triplet storage format is that it is easy to modify elements from the matrix, since each element is represented as a separate triple due to which the large numbers of zeros in the sparse matrix can be eliminated.

Next, PARDISO, a parallel direct sparse solver, represents a software library employed for the solution of extensively sparse linear systems of equations through direct method. PARDISO is designed to solve the linear equations in a parallel and efficient manner on modern computer architectures [69]. It is particularly well-suited for solving the linear equations with highly sparse matrices that arise in the structural analysis problem. Different storage formats can be used with this solver, however, in this study triad storage format is used for analysis.

In this section, the computational efficiency of three different solvers; direct solver with skyline storage format, iterative solver with triplet storage format and parallel direct sparse solver (PARDISO) with triplet storage format, are discussed and compared. The computational device employed for the task features an Intel Core i9-10850K processor with a base clock speed of 3.6 GHz, which possesses 10 cores and 20 threads. Additionally, the device is equipped with DDR4 memory in the form of two 16 GB modules, operating at a frequency of 3200 MHz.

4.4.1 Theoretical Description of the study

The problem addressed in this chapter includes the numerical solution of a system of linear equations, {F}=[K]{x}, arising from numerical analysis of the structural system in 3D AEM. The [K] matrix in the linear system has nxn sized highly sparse, and symmetric matrix structure.

First method, the direct solver with skyline storage format is a methodology to solve a symmetric, positive definite (SPD) linear system using Cholesky factorization. The Cholesky factorization is a special case of Gaussian elimination that decomposes the SPD matrix [K] into a lower triangular matrix [L] such that $[K] = [L][L]^T$. The direct solver with skyline storage format uses the skyline structure of the matrix to reduce the no. of computations required to perform the Cholesky factorization and solve the linear system. The process involves initializing [L] as a zero matrix, computing the diagonal and off-diagonal elements of [L] using a particular ordering of the rows and columns of [K], and solving the linear system using forward and backward substitution [64].

Second method, iterative solver with the GMRES algorithm is an iterative method used to solve a sparse linear system of the form {F}=[K]{x}, where [K] is a large, sparse, and symmetric matrix, and {F} is a known vector. The [K] matrix stored in triplet storage format. The orthonormal basis Q_k for a Krylov subspace of [K] and {F} using the Arnoldi iteration is constructed and then solves the least squares problem to identify the vector x which minimalizes the residual $||F - Kx||_2$ over Q_k. The GMRES algorithm can be restarted to improve convergence and is useful for solving large-scale sparse linear systems, especially for non-symmetric matrices that are challenging to solve by direct methods[68].

Last method, the PARDISO solver is a direct, sparse matrix solver that utilizes parallel processing to solve large-scale linear equations which involves the factorization of a sparse matrix into lower [L] or upper [U] triangular matrices. It is designed to be highly efficient on modern computer architectures, including multi-core processors and high-performance computing clusters. In our implementation, the PARDISO solver is used with [K] matrix stored in triplet format. The factors L and U of a sparse matrix [K] using symbolic and numerical factorization. The symbolic factorization analyses the structure of [K] to determine the non-zero part of [L] and [U], while the numerical factorization computes their numerical values

using a pivoting strategy for stability. Once the factors are computed, PARDISO uses forward and backward substitution to solve the linear system. PARDISO is highly efficient and scalable, with parallel processing capabilities and support for different matrix formats[69].

In these three methods as discussed in previous paragraphs, two types of storage formats are used. First one, the skyline matrix storage format [70],[71], also known as the profile matrix or the border matrix, is a way to store symmetric and sparse matrices. Figure 4-18 shows a sample of matrix storage in skyline format. In this format, only the non-zero elements on and below or above the diagonal are stored, as well as the indices of the initial non-zero component in each row. This can greatly reduce the storage requirements for sparse matrices with a significant number of zeros below the diagonal. Second one, triplet storage[72] is a popular format for storing sparse matrices in computer science and linear algebra. The triplet format is used to efficiently store matrices where most of the elements are zero i.e., highly sparse matrices. Figure 4-19 shows a sample of matrix storage in triplet format. In the triplet format, the non-zero component of the matrices are stored in compressed form along with their corresponding row and column indices. The system of storage has three arrays, one array containing values and other two containing column index and row index.

In this paper, these three methods are tested for their computational efficiency with 6 different structural analysis case studies of a concrete block in 3D AEM with $[K]_{nxn}$ matrix with 'n' ranging from 1080 to 32560 (Figure 4-20).A pushover load {F} of 0.1m in 10 timesteps is applied at the top-most part of the model to perform the analysis. The average time taken for solving {F}=[K]{x} to get the displacement vector {x} is recorded and compared. For the method using PARDISO solver, each of the 6 cases are solved using 4, 8, 12, 16, and 20 CPU threads.

	a11												
	a21	a22											
	a31=0	a32	a33										
	a41=0	a42	a43=0	a44									
	a51	a52=0	a53=0	a54	a55								
	a61=0	a62=0	a63	a64=0	a65	a66							
Row array	1	2	5	2	3	4	3	6	4	5	5	6	6
Column array	1	1	1	2	2	2	3	3	4	4	5	5	6
Value array	a11	a21	a51	a22	a32	a42	a33	a63	a44	a54	a55	a65	a66

Figure 4-18 : Triplet Storage Format

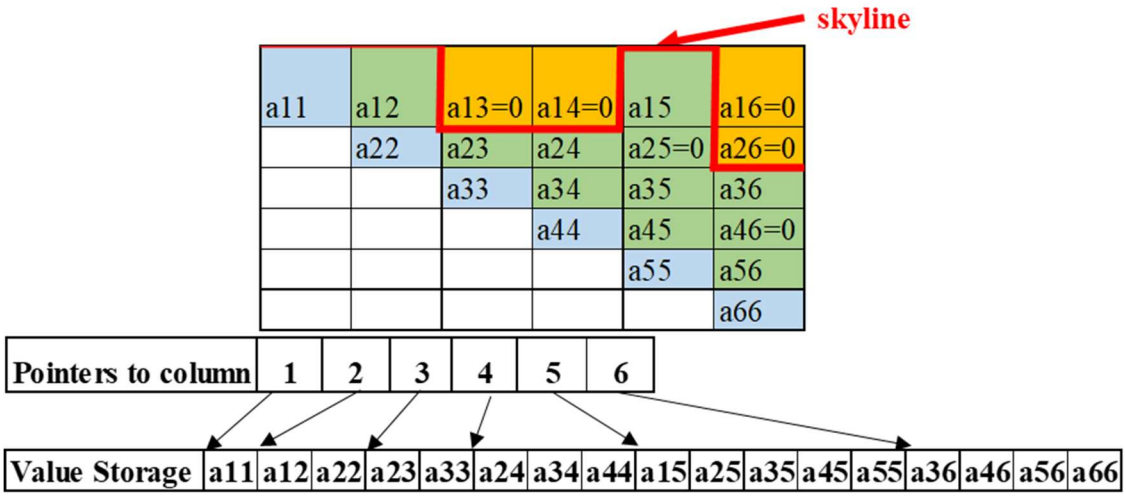

Figure 4-19 : Skyline Storage Format

Case 1: (n=1080)

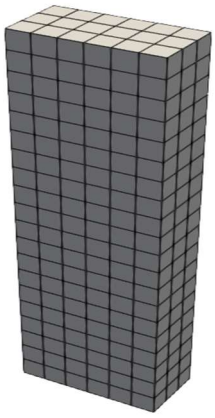

Case 2: (n=2160)

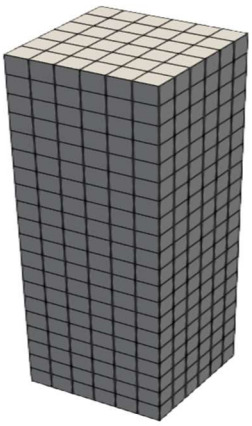

Case 3: (n=4320)

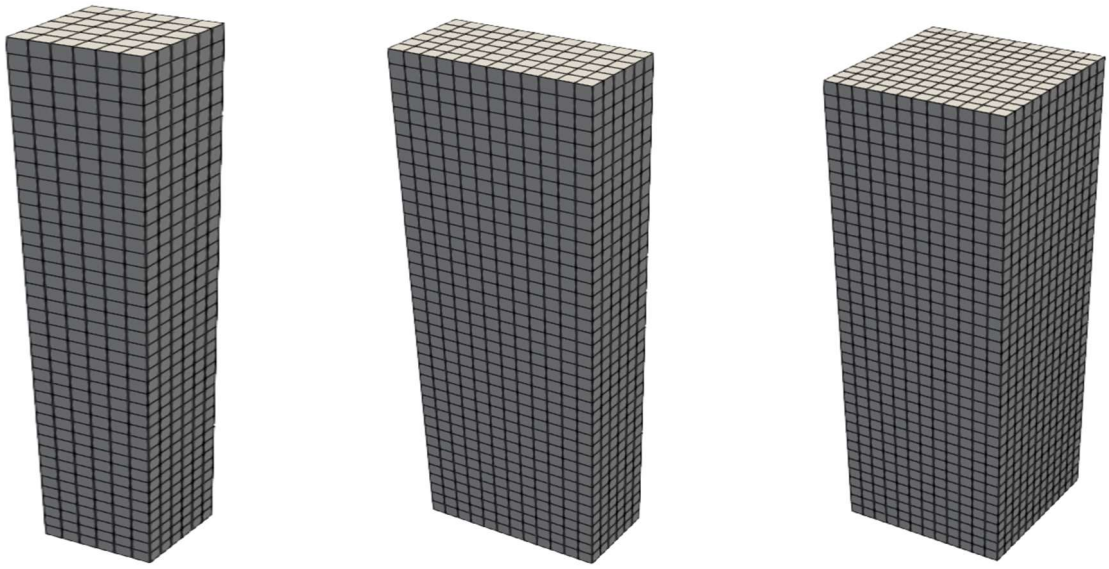

Case 4: (n=8640) Case 5: (n=17280) Case 6: (n=34560)

Figure 4-20: Case Studies

4.4.2 Results from the different solvers

The results of the comparison of computational efficiency of linear solvers on matrices of varying sizes in 3D AEM are presented in the Table 4-5 and Figure 4-21. Three solvers, Direct solver with skyline storage format, Iterative Linear Solver (GMRES), and Parallel direct sparse solver (PARDISO) with different numbers of CPU threads, are evaluated.

For smaller matrices (1-2), Direct solver with skyline storage format appears to be the fastest, with computational times ranging from 0.0144 seconds for a 1080x1080 matrix to 0.047 seconds for an 4320x4320 matrix. With the increase in size of matrix, The Skyline Direct Linear Solver becomes slower compared to other solvers. For matrix size 34560x34560, skyline format of storage of [K] matrix exceeds the allowable storage capacity.

Iterative Linear Solver (GMRES) also performed well, with computational times ranging from 0.0492 seconds for a 1080x1080 matrix to 34.76 seconds for an 34560x34560 matrix. However, it is slower compared to the direct linear solver, it can handle the higher size of matrices.

On the other hand, the Parallel direct sparse solver (PARDISO) has better results compared to other two solvers. The computational times (in seconds) for solving matrices of different sizes (1-6) using the Parallel direct sparse solver (PARDISO) with varying numbers of CPU threads

(4-20) is shown in Table 4-5 and Figure 4-22. The solver was able to solve larger matrices more efficiently using more CPU threads. For smaller matrices (1-4), the computational times were generally lower and did not vary significantly with the number of CPU threads. For larger matrices (5-6), the computational times decreased significantly with the use of more CPU threads, with the fastest times achieved using 20 CPU threads. The fastest computational time achieved for the largest matrix (34560x34560) was 0.762 seconds with 20 CPU threads.

Table 4-5 : Comparison of Computational Efficiency of Different Solvers

S N	Size of [K] matrix (nxn)	Time (sec.) for each solution						
		Direct Linear Solver	Iterative Linear Solver (GMRES)	Parallel direct sparse solver (PARDISO)				
				4-CPU threads	8- CPU threads	12-CPU threads	16-CPU threads	20-CPU threads
1	1080x1080	0.0144	0.0492	0.0415	0.0408	0.033	0.0315	0.022
2	2160x2160	0.047	0.295	0.2015	0.098	0.0833	0.078	0.071
3	4320x4320	0.354	0.738	0.218	0.1252	0.0467	0.043	0.0405
4	8640x8640	0.624	1.265	0.3057	0.2006	0.1848	0.1930	0.1870
5	17280x17280	8.6405	7.8208	0.4725	0.421	0.3532	0.35	0.3422
6	34560x34560	***	34.76	1.5655	0.929	0.79	0.766	0.762

*** : skyline format of storage of [K] matrix exceeds the allowable storage capacity.

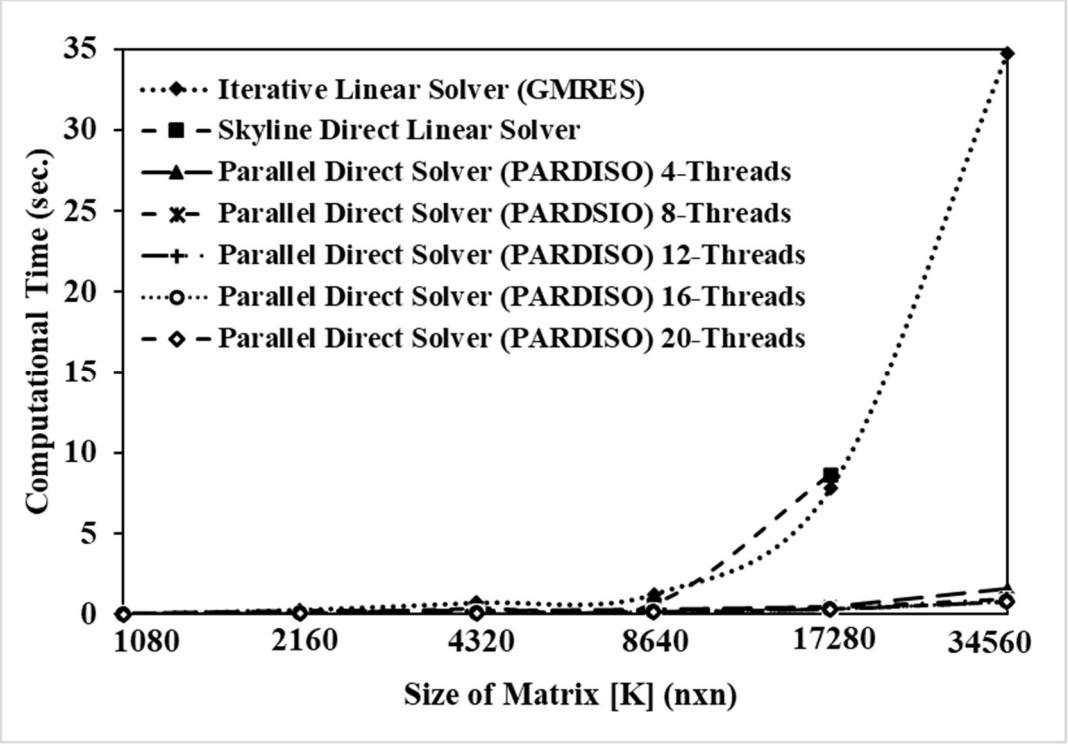

Figure 4-21: Comparison of Computational Efficiency

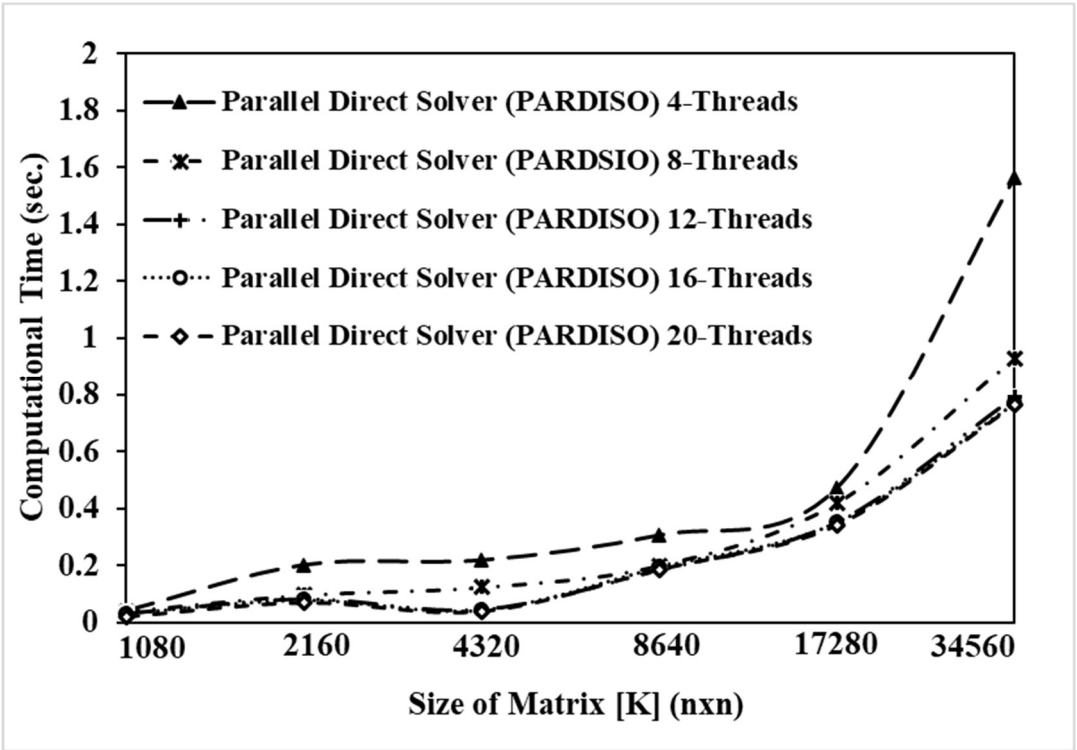

Figure 4-22 : Comparison of Computational Efficiency (Parallel solvers)

4.4.3 Key Findings and Interpretations of the comparative study of solvers

The direct solver with skyline storage format can handle smaller size problems very efficiently, however with the increase in size of problem, skyline storage system cannot handle the problem. However, triplet format requires less memory than skyline format, especially for matrices that are very sparse. This is because triplet stores only the non-zero values and their indices, while skyline stores the diagonal elements and the upper triangular matrix elements. Triplet format allows for faster matrix-vector multiplication compared to skyline format, especially for matrices with a large number of rows. This is because the triplet format can take advantage of the cache hierarchy of modern processors and optimize memory access. With the use of parallel solvers in conjunction with triplet storage format would significantly increase the computational efficiency, specially for the structural analysis where [K] matrix would be large and highly sparse.

Two conclusions are derived from this paper. Firstly, the triplet format is a more efficient and versatile storage format for highly sparse matrices compared to skyline format. Secondly, the choice of linear solver depends on the size of the matrix and the computing resources available. For smaller matrices, Direct solver with skyline storage format and Iterative Linear Solver (GMRES) may be options, while for larger matrices, the parallel direct sparse solver (PARDISO) with multiple CPU threads may provide the best computational efficiency.

4.5 3D AEM integration of the sensitivity-based model updating

4.5.1 Methodology

The 3D AEM formulation is discussed in the previous section. The non-linear analysis and collapse behaviour can be handled very efficiently in 3D AEM. Once the structures' material properties in terms of young's modulus is obtained accurately from the field, it is possible to replicate behaviour of the structure through AEM numerical model. The operational modal data through the ambient vibration measurement from the field in conjunction with the numerical model updating in AEM can capture the on-field property of the structure. This will help to conduct efficient and accurate vulnerability assessment of large building stocks. For this regard, the model updating procedure described in the previous section is integrated into 3D Applied Element Method FORTRAN90 implementation. The overall flowchart of the procedure is represented in Figure 4-23.

In the context of materials characterization, it is imperative to commence the analysis by offering an initial estimation of material properties, specifically Young's modulus. The initial step is to prepare an Applied Element Model for the as built geometric properties of the structure providing a preliminary guess for the material properties (Young's Modulus (E_0)). This parameter serves as a fundamental indicator of a material's stiffness and its ability to resist deformation when subjected to external forces. Furthermore, it is crucial to assign a corresponding GroupID to each element group based on their distinct material properties. This categorization facilitates the classification and organization of materials into homogeneous clusters, enabling efficient data management and subsequent analysis. The elements of the numerical model are grouped based on their material properties. Each of them is assigned a group identity that corresponds to its respective material property group.

Young's modulus $\{E_0\}_i \in \mathbb{R}(i = 1, ngr)$ (4-4)

The coefficient denoted as x_{ij}, which governs the update of parameters, as specified in the equation, is distinctly defined for individual groupings of elements. This provision allows for a systematic treatment of each element group, ensuring that the updating process is tailored to the unique characteristics and properties exhibited by these specific groups. By employing such a well-defined coefficient, the parameter updating procedure is effectively executed, leading to enhanced accuracy and precision in the analysis of the elements within their respective groups.

Coefficient of updating parameters (x_{ij}) for each group

$$x_{ij} = \frac{E_i - E_{i0}}{E_{i0}} \ (i = 1, ngr, \ j = 0, niter) \tag{4-5}$$

Where "ngr" is no. of element groups, "niter" is iteration number for optimization.

The initial guess of coefficients of updating parameters (x_{i0}) are important for the convergence of the optimization.

Next is to calculate the local stiffness matrix for each connecting springs. In order to determine the initial local stiffness matrix for each connecting spring, we need to calculate the normal stiffness (K_n), shear stiffness in direction-1 (K_{1s}), and shear stiffness in direction-2 (K_{2s}).

K_n : Normal stiffness of spring = $E_{i0}(1 + x_{ij})$ *d_1*d_2/a (4-6)

K_{1s} : Shear stiffness of spring in direction-1 = $G_{i0}(1 + x_{ij})$ *d_1*d_2/a (4-7)

K_{2s} : Shear stiffness of spring in direction-2 = $G_{i0}(1 + x_{ij})$ *d_1*d_2/a (4-8)

Where , Shear Modulus $G = \frac{E}{2(1+\upsilon)}$ (4-9)

The details of the notations d_1, d_2 and a are discussed in Figure 4-3.

In the 3D AEM structural problem, the local stiffness matrix has an important role in identifying the behavior of individual elements within the system. The local stiffness matrix represents the stiffness properties of an element in its local coordinate system. It is a 12x12 square matrix that captures the relationships between the displacements and the forces acting on the element. The entries of the local stiffness matrix are determined by the material characteristics, geometrical characteristics, and connectivity of elements.

The local stiffness matrix can be represented by $K_{local} = \begin{bmatrix} \boldsymbol{K_{11}} & K_{12} \\ K_{21} & K_{22} \end{bmatrix}_{12x12}$ (4-10)

$\boldsymbol{K_{11}}$ can be expressed as discussed in previous chapter:

	1	2	3	4	5	6
1	$K_nN_x^2+K_{1s}S_{1x}^2+K_{2s}S_{2x}^2$	$N_xK_nN_y+S_{1x}K_{1s}S_{1y}+S_{2x}K_{2s}S_{2y}$	$N_xK_nN_z+S_{1x}K_{1s}S_{1z}+S_{2x}K_{2S}S_{2z}$	$K_nN_x(R_yN_z-R_zN_y)+K_{1s}S_{1x}(R_yS_{1z}-R_zS_{1y})+K_{2S}S_{2x}(R_yS_{2z}-R_zS_{2y})$	$K_nN_x(R_zN_x-R_xN_z)+K_{1s}S_{1x}(R_zS_{1x}-R_xS_{1z})+K_{2S}S_{2x}(R_zS_{2x}-R_xS_{2z})$	$K_nN_x(R_xN_y-R_yN_x)+K_{1s}S_{1x}(R_xS_{1y}-R_yS_{1x})+K_{2S}S_{2x}(R_xS_{2y}-R_yS_{2x})$
2	S(1,2)	$K_nN_y^2+K_{1s}S_{1y}^2+K_{2s}S_{2y}^2$	$N_yK_nN_z+S_{1y}K_{1s}S_{1z}+S_{2y}K_{2S}S_{2z}$	$K_nN_y(R_yN_z-R_zN_y)+K_{1s}S_{1y}(R_yS_{1z}-R_zS_{1y})+K_{2S}S_{2y}(R_yS_{2z}-R_zS_{2y})$	$K_nN_y(R_zN_x-R_xN_z)+K_{1s}S_{1y}(R_zS_{1x}-R_xS_{1z})+K_{2S}S_{2y}(R_zS_{2x}-R_xS_{2z})$	$K_nN_y(R_xN_y-R_yN_x)+K_{1s}S_{1y}(R_xS_{1y}-R_yS_{1x})+K_{2S}S_{2y}(R_xS_{2y}-R_yS_{2x})$
3	S(1,3)	S(2,3)	$K_nN_z^2+K_{1s}S_{1z}^2+K_{2s}S_{2z}^2$	$K_nN_z(R_yN_z-R_zN_y)+K_{1s}S_{1z}(R_yS_{1z}-R_zS_{1y})+K_{2S}S_{2z}(R_yS_{2z}-R_zS_{2y})$	$K_nN_z(R_zN_x-R_xN_z)+K_{1s}S_{1z}(R_zS_{1x}-R_xS_{1z})+K_{2S}S_{2z}(R_zS_{2x}-R_xS_{2z})$	$K_nN_z(R_xN_y-R_yN_x)+K_{1s}S_{1z}(R_xS_{1y}-R_yS_{1x})+K_{2S}S_{2z}(R_xS_{2y}-R_yS_{2x})$
4	S(1,4)	S(2,4)	S(3,4)	$K_n(R_yN_z-R_zN_y)^2+K_{1s}(R_yS_{1z}-R_zS_{1y})^2+K_{2s}(R_yS_{2z}-R_zS_{2y})^2$	$K_n(R_yN_z-R_zN_y)(R_zN_x-R_xN_z)+K_{1s}(R_yS_{1z}-R_zS_{1y})(R_zS_{1x}-R_xS_{1z})+K_{2S}(R_yS_{2z}-R_zS_{2y})(R_zS_{2x}-R_xS_{2z})$	$K_n(R_yN_z-R_zN_y)(R_xN_y-R_yN_x)+K_{1s}(R_yS_{1z}-R_zS_{1y})(R_xS_{1y}-R_yS_{1x})+K_{2S}(R_yS_{2z}-R_zS_{2y})(R_xS_{2y}-R_yS_{2x})$
5	S(1,5)	S(2,5)	S(3,5)	S(4,5)	$K_n(R_zN_x-R_xN_z)^2+K_{1s}(R_zS_{1x}-R_xS_{1z})^2+K_{2s}(R_zS_{2x}-R_xS_{2z})^2$	$K_n(R_zN_x-R_xN_z)(R_xN_y-R_yN_x)+K_{1s}(R_zS_{1x}-R_xS_{1z})(R_xS_{1y}-R_yS_{1x})+K_{2S}(R_zS_{2x}-R_xS_{2z})(R_xS_{2y}-R_yS_{2x})$
6	S(1,6)	S(2,6)	S(3,6)	S(4,6)	S(5,6)	$K_n(R_xN_y-R_yN_x)^2+K_{1s}(R_xS_{1y}-R_yS_{1x})^2+K_{2S}(R_xS_{2y}-R_yS_{2x})^2$

The procedure for creating the global stiffness matrix $[K]_{global}$ involves several steps. Initially, we assemble the stiffness matrices of individual elements and correctly position them within

the global-stiffness matrix, utilizing the element connectivity information. This process involves mapping the degrees of freedom of each element and element groups to their corresponding locations in the global system. Summing up the contributions from all element groups leads us to the final global stiffness matrix. This highly sparse stiffness matrix is stored in triplet storage format.

$$([K]_{global})_{k,l} = \sum_{i=1}^{n_{gr}} [K_{local}]_i \,,\ 1 \le i \le ngr,\ 1 \le k \le ndof, 1 \le l \le ndof \tag{4-11}$$

$$Where,\ [K]_{global} = f(x)$$

The Arnoldi Method is an iterative algorithm that allows for the identification of a selected no. of eigenvalues and eigenvectors of a given matrix. ARPACK[55], a widely used software library, provides an efficient implementation of the Arnoldi Method, enabling researchers and practitioners to obtain eigenvalues and eigenvectors with high accuracy and computational efficiency. When coupled with the Applied Element Method (AEM), the ARPACK algorithm becomes a versatile tool for investigating the eigenvalue properties of complex systems. The analytical eigen value analysis using Arnoldi Method (ARPACK) implemented in AEM is performed for the following generalized eigen-value problem.

$$[K]_{global}\{\Phi_{ana}\} = \lambda_{ana}\,[M]\{\Phi_{ana}\} \tag{4-12}$$

where $[K]_{global}$ represents the global stiffness matrix, $[M]$ represents the mass matrix, $\{\Phi_{ana}\}$ is the vector of the analytical mode shapes, and λ_{ana} is the corresponding eigenvalue. The mass matrix [M] is calculated based on the material density property and assumed to be constant with the time.

The solution of this generalized eigen value analysis is:

$$(\lambda_{ana})_{k,1}, 1 \leq k \leq ndof$$

$$(\Phi_{ana})_{k,l},\ 1 \leq k \leq ndof, 1 \leq l \leq ndof$$

$$Where,\ \lambda_{ana}\ and\ \Phi_{ana} = f(x) \tag{4-13}$$

The experimental modal data ($\lambda_{exp}=(\omega^2)$ and $\{\Phi\}_{exp.}$) are obtained from the frequency domain decomposition of response measured at each floor of the structure. The modal frequencies provide insight into the frequencies of vibration exhibited by structure, while the modeshapes describe the spatial distribution of these vibrations across each floor. It's important to note that the measurement locations for these modal parameters are limited to a specific number of degrees of freedom ("mndof ≤ ndof"), which refers to the no. of sensors or measurement locations used. Additionally, the no. of modes obtained ("nmodes ≤ ndof") reflects the maximum number of distinct vibration patterns identified in the data.

$$(\lambda_{exp})_{k,1}, 1 \leq k \leq mndof$$

$$(\Phi_{exp})_{k,l},\ 1 \leq k \leq mndof, 1 \leq l \leq nmodes \tag{4-14}$$

Corresponding degree of freedom in numerical model are mapped to experimental measurements. This allows us for element level of model updating in the numerical model from the limited no. of measurement data. The eigenvalues corresponding to measured dofs in experimental observations (λ_{exp}) are initially arranged in an array, followed by the unmeasured degrees of freedom. The same ordering scheme applies to the mode shapes.

$$\lambda_{ana} = \begin{Bmatrix} \lambda_{ana,1} \\ \lambda_{ana,2} \\ \vdots \\ \lambda_{ana,nmodes} \\ \lambda_{ana,nmodes+1} \\ \vdots \\ \lambda_{ana,ndof} \end{Bmatrix} \begin{matrix} \} \text{ Measured} \\ \\ \\ \\ \} \text{ Unmeasured} \\ \\ \end{matrix} \tag{4-15}$$

$$\Phi_{ana} = \begin{bmatrix} \overbrace{\Phi_{ana,(1,1)} & \Phi_{ana,(1,2)} & \cdots & \Phi_{ana,(1,mndof)}}^{\text{Measured}} & \overbrace{\cdots & \Phi_{ana,(1,ndof)}}^{\text{Unmeasured}} \\ \Phi_{ana,(2,1)} & \Phi_{ana,(2,2)} & \cdots & \Phi_{ana,(2,mndof)} & \cdots & \Phi_{ana,(2,ndof)} \\ \vdots & \vdots & \vdots & \vdots & \vdots & \vdots \\ \Phi_{ana,(nmodes,1)} & \Phi_{ana,(nmodes,2)} & \ddots & \Phi_{ana,(nmodes,mndof)} & \ddots & \Phi_{ana,(nmodes,ndof)} \\ \vdots & \vdots & \vdots & \vdots & \vdots & \vdots \\ \Phi_{ana,(ndof,1)} & \Phi_{ana,(ndof,2)} & \cdots & \Phi_{ana,(ndof,mndof)} & \cdots & \Phi_{ana,(ndof,ndof)} \end{bmatrix} \begin{matrix} \} \text{Measured} \\ \\ \\ \\ \} \text{Unmeasured} \end{matrix} \tag{4-16}$$

The Φ_{ana} and Φ_{exp} are normalized by setting their maximum value to unity for the measured dofs, aligning analytical and experimental data on a similar scale.

$$\Phi_{ana} = \begin{bmatrix} \overbrace{\Phi_{ana,(1,1)} & \Phi_{ana,(1,2)} & \cdots & \Phi_{ana,(1,mndof)} = 1}^{\text{Measured}} & \overbrace{\cdots & \Phi_{ana,(1,ndof)}}^{\text{Unmeasured}} \\ \Phi_{ana,(2,1)} & \Phi_{ana,(2,2)} & \cdots & \Phi_{ana,(2,mndof)} = 1 & \cdots & \Phi_{ana,(2,ndof)} \\ \vdots & \vdots & \vdots & \vdots & \vdots & \vdots \\ \Phi_{ana,(nmodes,1)} & \Phi_{ana,(nmodes,2)} & \ddots & \Phi_{ana,(nmodes,mndof)} = 1 & \ddots & \Phi_{ana,(nmodes,ndof)} \\ \vdots & \vdots & \vdots & \vdots & \vdots & \vdots \\ \Phi_{ana,(ndof,1)} & \Phi_{ana,(ndof,2)} & \cdots & \Phi_{ana,(ndof,mndof)} = 1 & \cdots & \Phi_{ana,(ndof,ndof)} \end{bmatrix} \begin{matrix} \} \text{Measured} \\ \\ \\ \\ \} \text{Unmeasured} \end{matrix} \tag{4-17}$$

Calculate relative residual vector of experimental and analytical modal data ($res(x)$) from the measured data.

$$res(x) = \begin{pmatrix} \dfrac{(\lambda_i{}^{exp} - \lambda_i{}^{ana}(x))}{\lambda_i{}^{exp}} w_{\lambda i} \\ \vdots \\ \left(\dfrac{\phi_{i,l}^{exp,M}}{\phi_{i,r}^{exp,M}} - \dfrac{\phi_{i,l}^{ana,M}(x)}{\phi_{i,r}^{ana,M}(x)} \right) w_{\phi i} \end{pmatrix}, \; i = 1, nmodes, \; l = 1, mndof, \; r = mndof \tag{4-18}$$

The weightage for eigenvalue and mode shape residuals $w_{\lambda i}$ and $w_{\phi i}$ in model updating is a subjective decision that depends on analysis purpose, confidence in the measured data, and characteristics of the structure. Assigning weightage involves considering the relative importance of eigenvalues and mode shapes in achieving the analysis objectives. Equal weightage is a common approach, but optimization techniques or expert judgment may be used to determine optimal weightage values.

The objective function f(x) with the least square problem based on residuals of modal parameters is formulated as follows:

$$minimize\ f(x) = \sum_{i=1}^{n_{modes}} \left(\frac{({\lambda_i}^{exp} - {\lambda_i}^{ana}(x))}{{\lambda_i}^{exp}} w_{\lambda i} \right)^2 + \left(\left(\frac{\phi_{i,l}^{exp,M}}{\phi_{i,r}^{exp,M}} - \frac{\phi_{i,l}^{ana,M}(x)}{\phi_{i,r}^{ana,M}(x)} \right) w_{\phi i} \right)^2 \quad (4\text{-}19)$$

In order to find the value of updating parameters (x) and subsequently the material properties (Young's modulus (E)) and Stiffness Matrix of the structure for the (j+1)-th iteration, the Levenberg-Marquardt algorithm [57] is employed. This algorithm is a robust optimization method specifically designed for analyzing non-linear least squares problem. This method merges the strengths of both the steepest descent and Gauss-Newton methods while incorporating a damping factor to regulate the step size during each iteration. Through an iterative process of updating variable values, its primary goal is to do minimization of the objective function and ultimately discover optimal solution to given problem.

$$x_{j+1} = x_j - (\nabla^2 f(x_j) + \Lambda I)^{-1} \nabla f(x_j)\ ,\ j = iteration\ number,\ size\ of\ x\ is\ (1, ngr) \quad (4\text{-}20)$$

Where,

x_j represents the vector of variables at iteration j. Its size is 1×ngr, where ngr is the number of updating element groups.

$\nabla f(x_j)$: gradient of the function '*f*' evaluated at x_j.

This gradient is a vector of partial derivatives (Jacobian) of '*f*' w.r.t each variable in x_j. It represents the sensitivity of the objective-function '*f*' w.r.t each of the parameters x_j.

$\nabla^2 f(x_j)$: Hessian matrix of the function '*f*' evaluated at x_j. The Hessian matrix is second-order partial derivatives of objective function '*f*' w.r.t the variables x_j.

'I' represents the identity matrix of size *ngr*×*ngr* and Λ is damping-factor which is scalar value to adjust the step size in each iteration.

At the end of the optimization, the structure would be accurately replicated, and it would be ready for the further analysis.

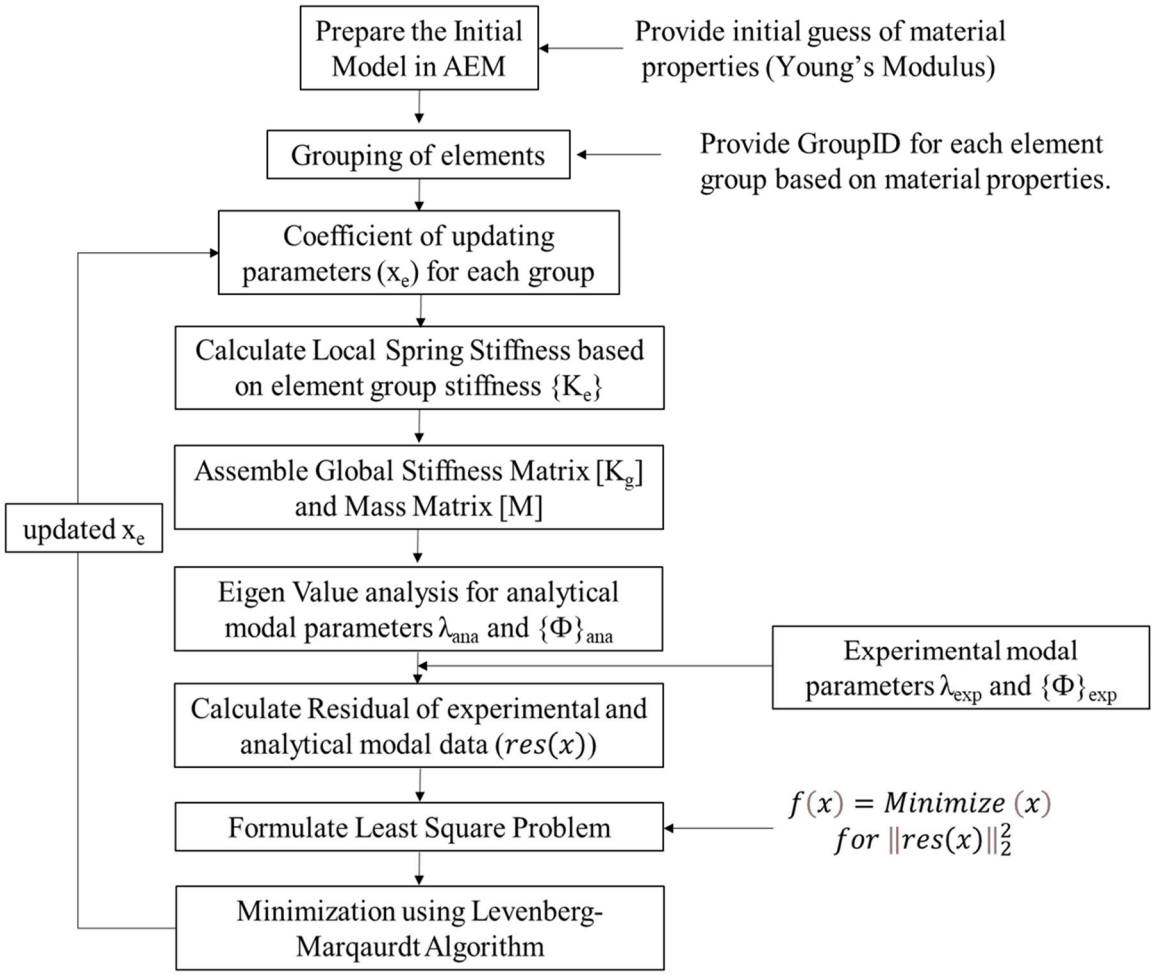

Figure 4-23 : AEM integration of model updating

4.5.2 Case Study Frame

The study involves the testing of a sensitivity-based model updating technique integrated into the 3D AEM framework, utilizing a sample of four-storey RC frames with infilled masonry, as illustrated in Figure 4-24. The building properties were selected to represent a typical soft storey structure in Nepal, as documented in a survey conducted by [38]. The geometrical and material characteristics of frames are tabulated in Table 4-6.

Table 4-6: Geometrical and Material Characteristics of the case study frame

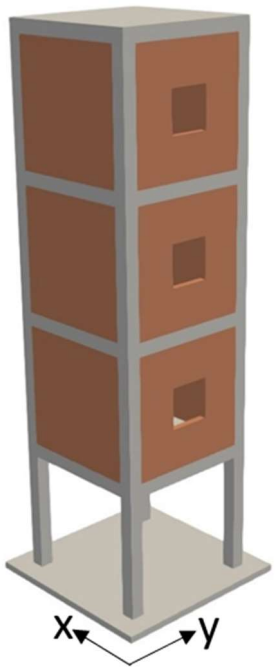

Figure 4-24 : 4-storey RC frame

Geometric Properties	
Length of Bay, (m.)	3 m
Height of floor (m.)	3 m
Detail of columns	0.30m x 0.30m, 8 no. of 16mm reinforcement bars and 8 mm stirrups at 200mm center to center
Detail of beams	0.30m x 0.45m, 4 no. of 16mm reinforcement bars and 8 mm stirrups at 200mm center to center

Material Properties			
Properties	Column	Beam/Slab	Masonry
Young's Modulus E (N/m^2)	$2.23 * 10^{10}$	$1.94 * 10^{10}$	$1.58 * 10^{10}$
Poisons Ratio	0.2	0.2	0.2
Tensile strength, (N/m^2)	$2.0 * 10^6$	$1.5 * 10^6$	$1.0 * 10^6$

	Compressive strength, (N/m^2)	$2.0 * 10^7$	$1.5 * 10^7$	$1.0*10^7$
	Density of Material (Kg/m^3)	2400	2400	1900
	No. of connecting springs	81	81	81
	Size of elements (m)	0.15	0.15	0.15

The structure is discretized in 8184 elements of 0.15m sizes each in 3D AEM. The elements are grouped into three groups for column, beam/slab and masonry wall respectively. The material properties of three groups of elements are the physical properties to be found through model-updating methodology considered in this chapter.

4.5.3 Experimental operational modal data for the case study frame

A synthetic ambient vibration data as a response of each floor of the frame with damping 1% is created by applying white noise of 0.01hz to 100hz for 120 seconds with sampling rate of 100hz Figure 4-25. Frequencies and modeshapes of the structure are identified by doing FDD of the ambient vibration data thus obtained from the response of the structure due to white noise Figure 4-26.

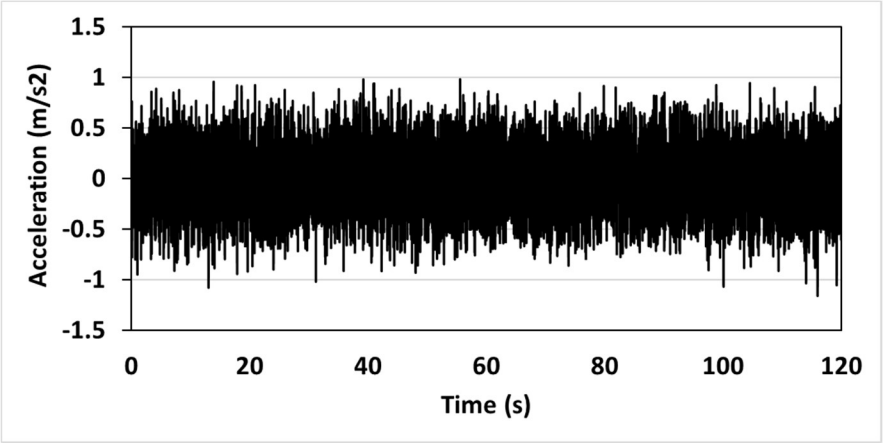

Figure 4-25 : White Noise

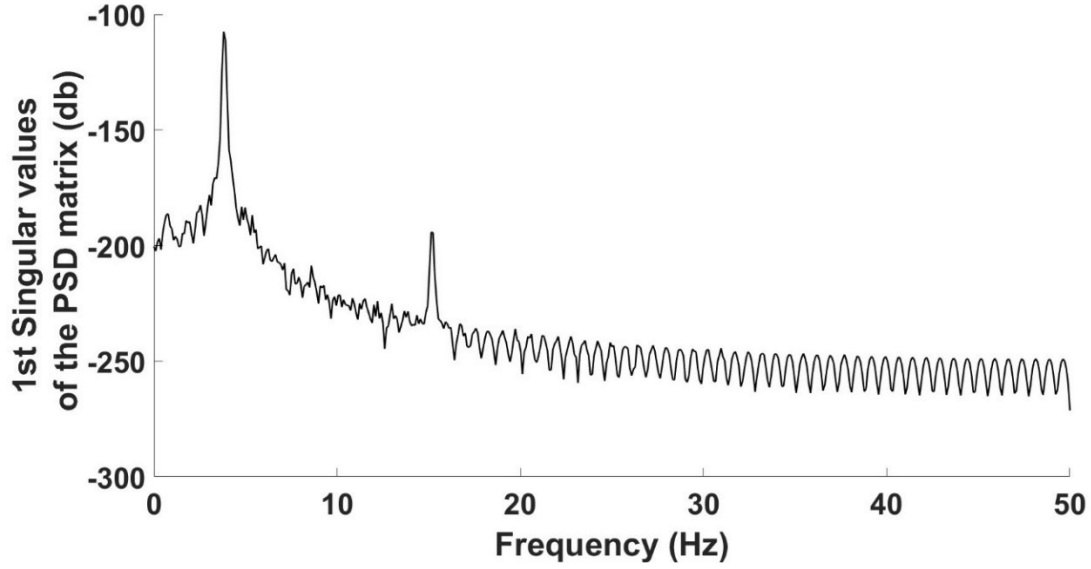

Figure 4-26 : 1st Singular Values of Power Spectrum Density (PSD) Y-direction

Table 4-7: Mode shape vectors and frequencies obtained from FDD (Y-direction)

	Mode Shape Vectors		**Mode Shape Vectors (Normalized to the maximum amplitude)**	
	Mode 1	**Mode 2**	**Mode 1**	**Mode 2**
First Floor	-0.4235	0.6408	0.741	-0.932
Second Floor	-0.4711	0.2836	0.824	-0.412
Third Floor	-0.5215	-0.1900	0.912	0.276
Fourth Floor	-0.5716	-0.6876	1.000	1.000
Frequency	3.8384 hz	16.2611 hz		

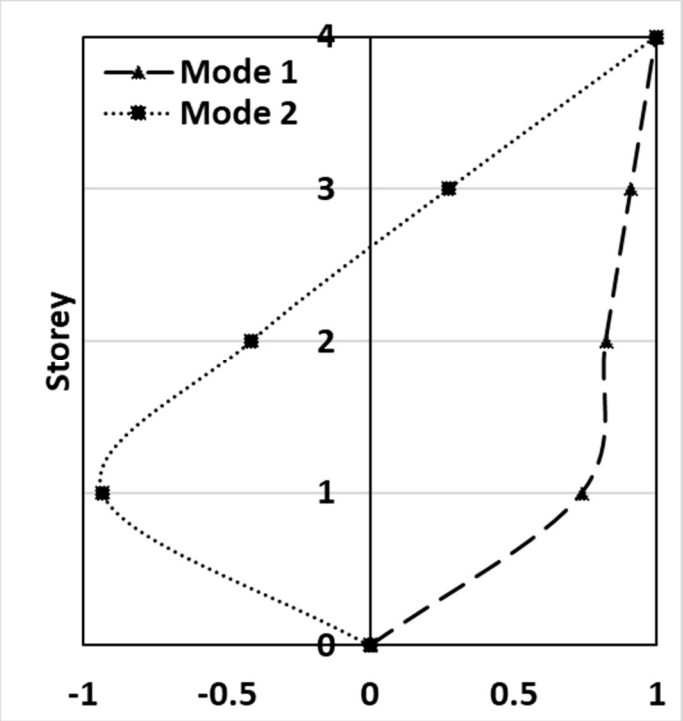

Figure 4-27 : Mode Shapes (Y-direction)

The frequencies and mode shape vectors displayed in Table 4-7, Figure 4-27 and are further used as an experimental modal data for performing the model updating.

4.5.4 Result of model updating

The preliminary value of the young's modulus is guessed to be $2.10*10^{10}$ N/m^2, $1.80*10^{10}$ N/m^2, $1.40*10^{10}$ N/m^2 for column, beam/slab and masonry wall element group respectively. The initial coefficient of all three updating parameters is assumed to be 0.001 and equal weightage for all the parameters are provided. The updated parameters (Young's Modulus) values after the model updating using the developed method is shown in Table 4-8.

Table 4-8 : Young's Modulus of the updated structure

	Youngs' Modulus *10^5 (KN/m^2)			
SN	**Experiment (Exact)**	**Initial Guess**	**Updated**	**Error %**
Column	223	210	229.60	2.95%
Beam/Slab	194	180	196.87	1.48%
Wall	158	140	160.41	1.52%

Similarly, the frequency of the updated structure is obtained within the error margin of 1.83% as shown in Table 4-9.

Table 4-9 : Comparison of frequency of the updated structure

	Frequency (Hz)			**Error %**
	Experiment	**Initial Guess**	**Updated**	
1st Mode	3.8384	3.75	3.899	1.585%
2nd Mode	16.2611	15.81	16.557	1.83%

On the other hand, the updated mode shape vectors are obtained within the error margin of 3.45% in comparison with the experimental mode shape of the structure as shown in Table 4-10 and Figure 4-28.

Table 4-10 : Comparison of mode shape of the updated structure

	Mode Shape Vectors (Experimental)		**Mode Shape Vectors (Updated)**		**Error %**
	Mode 1	**Mode 2**	**Mode 1**	**Mode 2**	
First Floor	0.741	-0.932	0.757	-0.958	2.77%
Second Floor	0.824	-0.412	0.878	0.431	4.53%
Third Floor	0.912	0.276	0.934	0.267	-3.45%
Fourth Floor	1.000	1.000	1.000	1.000	-

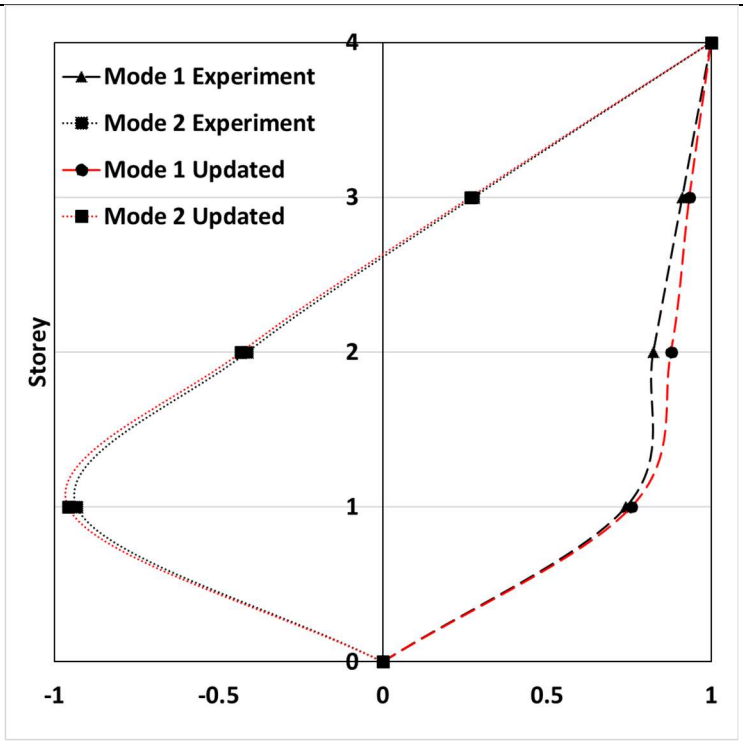

Figure 4-28 : Comparison of Mode Shapes (Y-direction)

4.5.5 Discussions and Conclusions

The findings of the present study yield several noteworthy conclusions. Firstly, the model updating of the numerical model in 3D AEM can be achieved with an acceptable error margin. Secondly, the incorporation of additional measurement data can potentially enhance the accuracy of model updating methodology. However, this is crucial to be mindful of presence of spurious higher modes in the experimental data that may lead to erroneous results. Thirdly, the results of this case study demonstrate that even with a limited no. of modes obtained from field, an accurate numerical model can be updated using the proposed method. Fourthly, the correctness of the model updating process is heavily related on the initial guess of the updating parameters. Although the Levenberg-Marquardt algorithm can improve convergence by circumventing local minima, a significant deviation of the preliminary guess from accurate values of updating parameters may prevent convergence altogether. Therefore, obtaining an initial guess as close as possible through empirical calculations is essential. Lastly, the grouping of the elements constitutes another critical aspect of the model updating process in 3D AEM. The no. of unknowns or updating parameters should not exceed the number of equations of residuals. Therefore, grouping the elements in a manner that groups together the same material properties and keeping the number of groups within permissible limits is crucial. If the elements of each critical location are grouped together, the model updating process can yield a good match between the AEM model and the existing structure.

Chapter 5: Seismic vulnerability assessment of the updated model structure using 3D AEM

5.1 Introduction

The seismic vulnerability assessment of buildings and structures is a crucial step for ensuring the safety and resilience of buildings and infrastructure systems in earthquake-prone regions. In this chapter, we present a comprehensive seismic vulnerability assessment of an updated model structure using the 3D AEM. The 3D AEM is a powerful numerical technique that allows realistic simulation of the structural response by incorporating the nonlinear behavior of materials and the interaction of different components in structure [60].

The updated model structure from previous chapter is considered in this study for the vulnerability assessment. To understand the non-linear behaviour of structure, static pushover analysis and single-ground motion incremental dynamic analysis has been performed. The quantification of the overall damage and local damages are studied in performance criteria based on interstorey drift, frequency degradation and visual deformation of the structure. The findings from this study provides broader knowledge of the seismic performance of structures and can be used to inform design guidelines, retrofit strategies, and risk mitigation measures.

5.2 Static Pushover Analysis

Static pushover analysis is an effective method to assess the performance and vulnerability of the structures. This analysis method allows engineers to evaluate the behaviour of a building under incremental lateral loads, providing insights into the structural behaviour, capacity, and potential failure modes. The static pushover analysis is performed on a 4-storey soft-storey

reinforced concrete (RC) frame building in this study. The goal is to acquire a comprehensive knowledge of the building's seismic performance and identify critical weak points.

5.3 Case study frame and Numerical Model

The numerical model, which includes updated material properties, is constructed in a three-dimensional (3D) Applied Element Method (AEM). The model consists of 8184 elements with an element size of 0.15 meters Figure 5-1. Representing the material properties of each element nine springs are incorporated in each face of the element. To understand the performance of the structure for lateral load, non-linear static pushover analysis is performed for the structure. It involves subjecting the structure to increasing levels of displacement controlled lateral loads (P) of 0.24m in 4000 timesteps in a static manner. This analysis accounts for the non-linear performance of the structure and provides an estimation of the capacity and deformation demands of the structure during lateral loading. The response of the structure is calculated at each load level, considering the non-linearities of both materials and structural connections. The result provides an approximation of lateral force-displacement relationship, commonly known as the pushover curve. The interstorey drift ratio and the frequency degradation with the increase in load are evaluated as the performance indicators. The critical locations and the weaknesses of the structure along with the damage pattern are discussed.

So, in summary following four performance indicators are studied:

1. Lateral force-displacement relationship
2. Interstorey drift ratio
3. Frequency degradation
4. Damage pattern and location

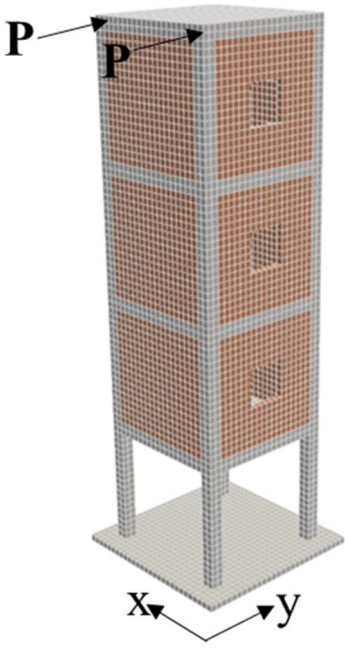

No. of Elements: 8184

No. of springs in each face of structure: 9

Lateral Pushover (P) : 0.24 m at the top of structure

Pushover timesteps: 4000 steps

Figure 5-1 : 3D AEM model of the structure with element discretization

5.4 Result of Static Pushover Analysis

The frame exhibits linear behavior until reaching a lateral drift at the roof of 0.048 m under a lateral load of 9.28 KN at location (a) on the force-displacement curve (Figure 5-3). Beyond this load, the frame exhibits soft storey behavior, with displacement concentration occurring on the ground floor of the structure. The slight drop in the force-displacement curve at location 'a' can be attributed to the occurrence of a crack in the infill wall on the first floor (Figure 5-2-location (iii) and (iv)). Another sudden drop in the force-displacement curve is observed at location (c) of the force-deformation curve, which can be attributed to the occurrence of a crack

at the joint of the beam-column on the first floor. Beyond this load, all deformation is concentrated on the open ground floor, which leads to soft storey failure. The soft storey behavior of structure is further evidenced by an inter-storey drift ratio of 0.88% on the ground floor compared to 0.24% at the top of the frame at location ‘a’, which increases to over 5% at the ground floor compared to 0.91% at the top floor at location ‘e’ (Figure 5-4). The structure exhibits typical failure patterns, including in-plane shear cracks at location (iii) and on-plane failure of the masonry wall at location (iv) of Figure 5-2. Additionally, tensile failure at the beam column joint at location (ii) and some tensile cracks at the base of the column at location (i) were observed.

Furthermore, an observation was made on the frequency degradation (Figure 5-5). The frequency of the structure decreases with increasing lateral displacement, indicating structural failure and a reduction in stiffness. As the frequency of the structure is determined based on the eigenvalue analysis in each loading step, this curve is good representation of the stiffness degradation of the structure. A sudden rise in frequency occurs at a lateral push of around 0.07 m, which corresponds to location ‘c’ in the force-displacement curve. This is attributed to the recontact of separate elements during the failure that occurred at location ‘c’.

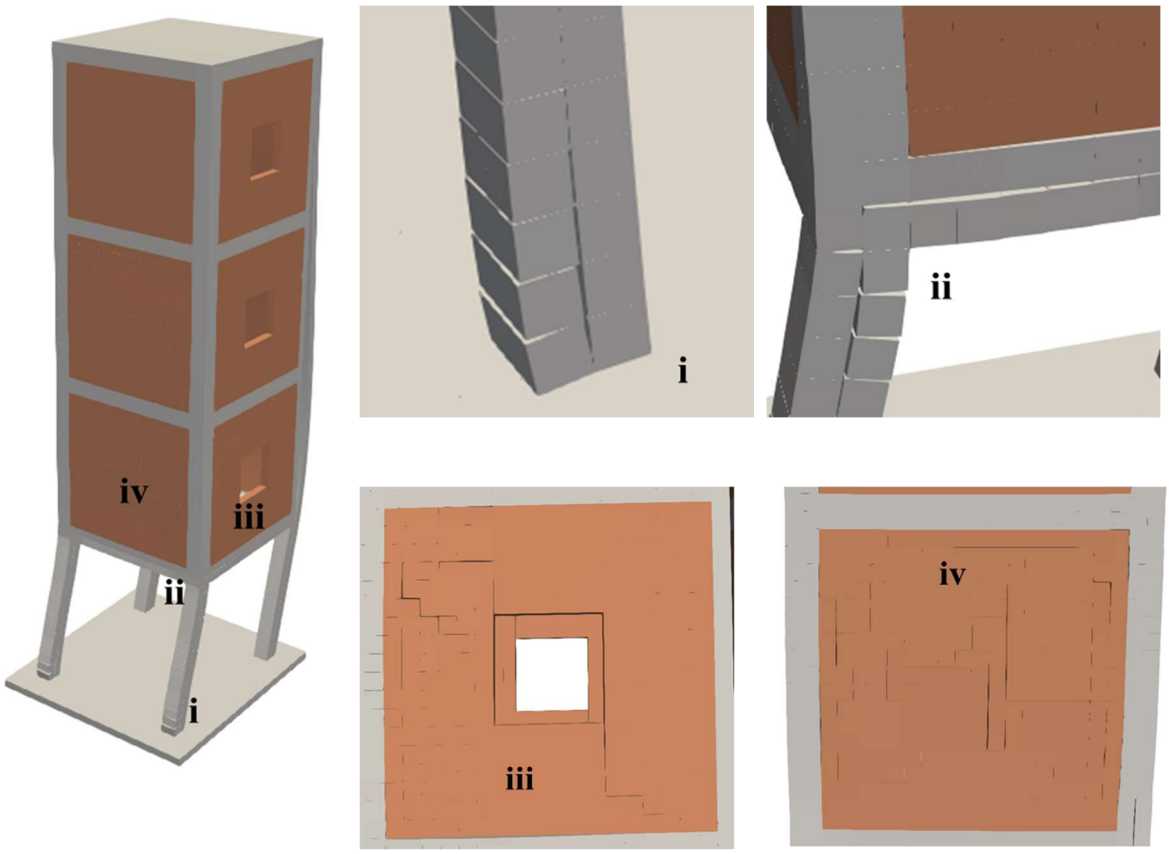

Figure 5-2 : Final deformation and crack pattern (at ‘e’)

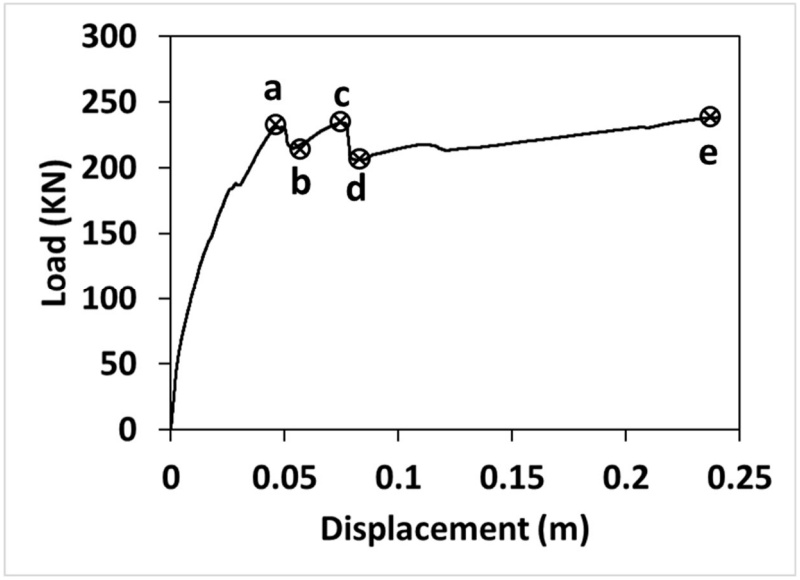

Figure 5-3 : Force-Displacement (Capacity) Curve

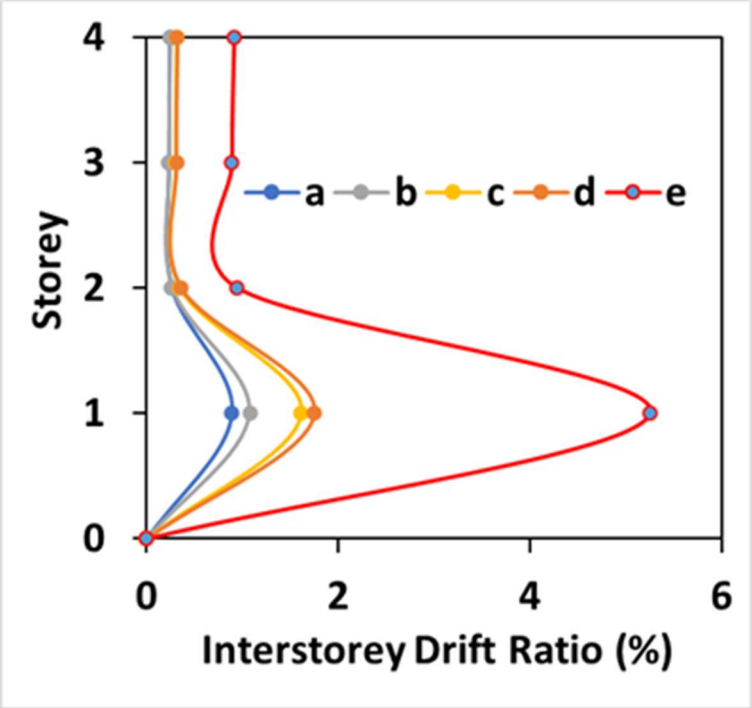

Figure 5-4 : Interstorey-drift ratio

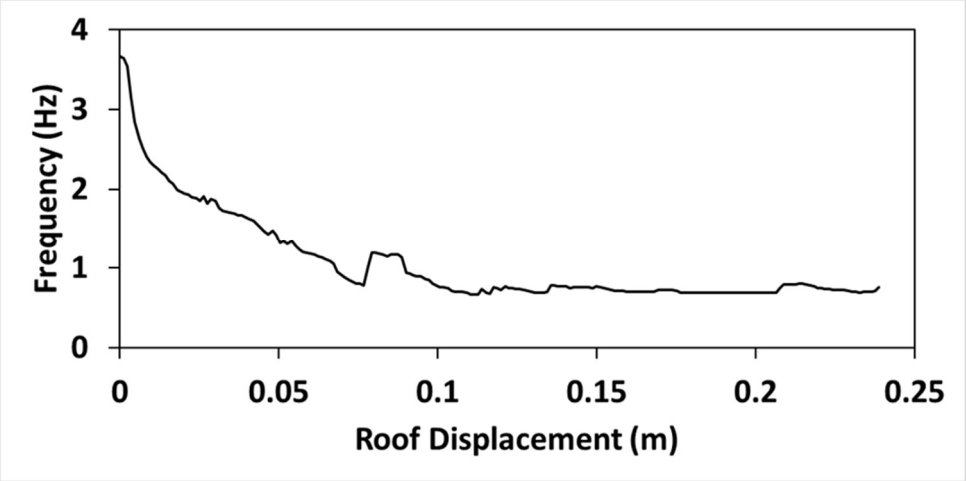

Figure 5-5 : Frequency degradation of the frame

5.5 Dynamic Analysis of the Structure

The concept of Incremental Dynamic Analysis (IDA) revolutionizing the field of structural engineering and seismic design [73]. IDA is a methodology that aims to provide a complete

understanding of the behaviour of the structure under varying levels of ground motion intensity. IDA involves analyzing ground motion records with increasing levels of intensity in a step-by-step manner.

There are two main approaches to IDA: single IDA and multiple IDA. In this research, single IDA is performed. The single IDA process begins with selecting a ground motion that represent the similar frequency property to that of the structure. The ground motion is then scaled to different intensities using appropriate scaling laws. For each intensity level, nonlinear time-history analysis is performed, and the structural response is evaluated. This analysis captures the dynamic characteristics of the structure and provides valuable information about its response characteristics, such as inter-story drifts, base shear, and ductility demands.

By incrementally increasing the intensity of ground motion, IDA allows engineers to observe how the structure responds to different levels of seismic excitation. This approach provides crucial insights into the structure's performance and helps identify critical levels of ground motion that may lead to structural damage or failure. Through IDA, engineers can gain a deeper understanding of the structural vulnerabilities and limitations, enabling them to make informed decisions regarding design modifications, retrofit strategies, or performance-based design.

5.6 Case Study Frame and Numerical Model

The numerical model details for the dynamic analysis are same as discussed in static pushover analysis (Figure 5-1).

Incremental Dynamic Analysis (IDA) involves subjecting the structure to a progressive sequence of ground motions with increasing intensity. The primary objective of IDA is to assess how the structure responds to various levels of ground motion intensity and to ascertain

its performance at each level. The fundamental frequency of the structure is 3.899 hz. So, an earthquake with similar predominant frequency is selected for the IDA. The San-Fernando Earthquake has the predominant frequency of around 3.84 hz, so it is selected for this study (Figure 5-6) illustrates the response spectrum of the earthquake. In single-ground motion Incremental Dynamic Analysis (IDA), the structure undergoes a step-by-step analysis, by applying a single earthquake ground motion that is gradually scaled to various intensities. The ground motion intensity is progressively augmented till structure either attains its ultimate limit state or meets a predefined performance threshold. In this case, the ground motion is scaled down and scaled up to get the different intensity level. The significant duration of the earthquake which covers Arias Intensity of 0.1-99% is calculated to be 32.99 sec. as shown in Figure 5-8. The Arias Intensity (IA) quantifies the magnitude of ground motion by evaluating the time-integral of the squared ground acceleration [74]. The ground motion data is then truncated for the significant duration as shown in Figure 5-9.

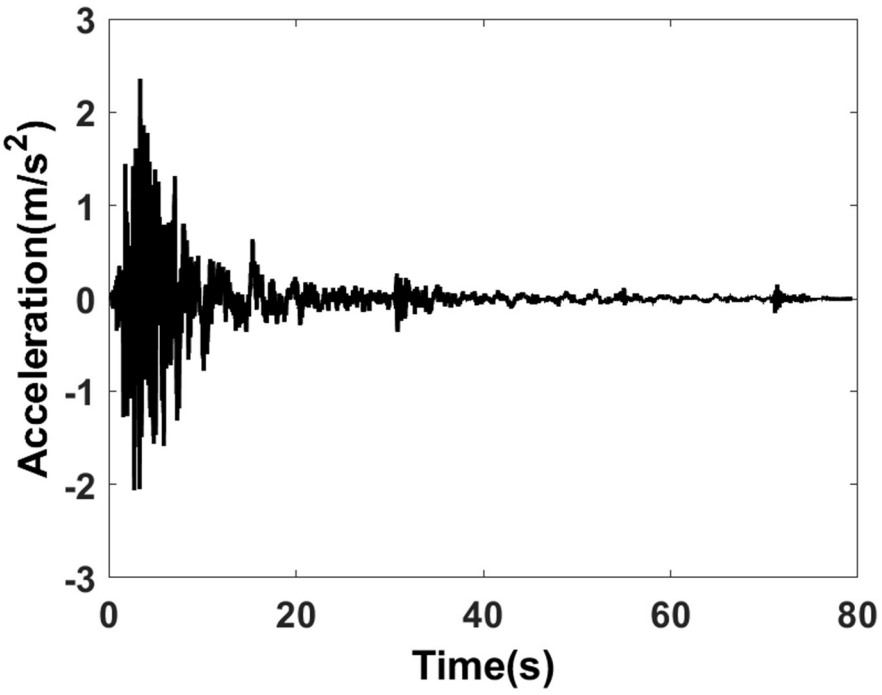

Figure 5-6 : San Fernando Earthquake Ground Motion

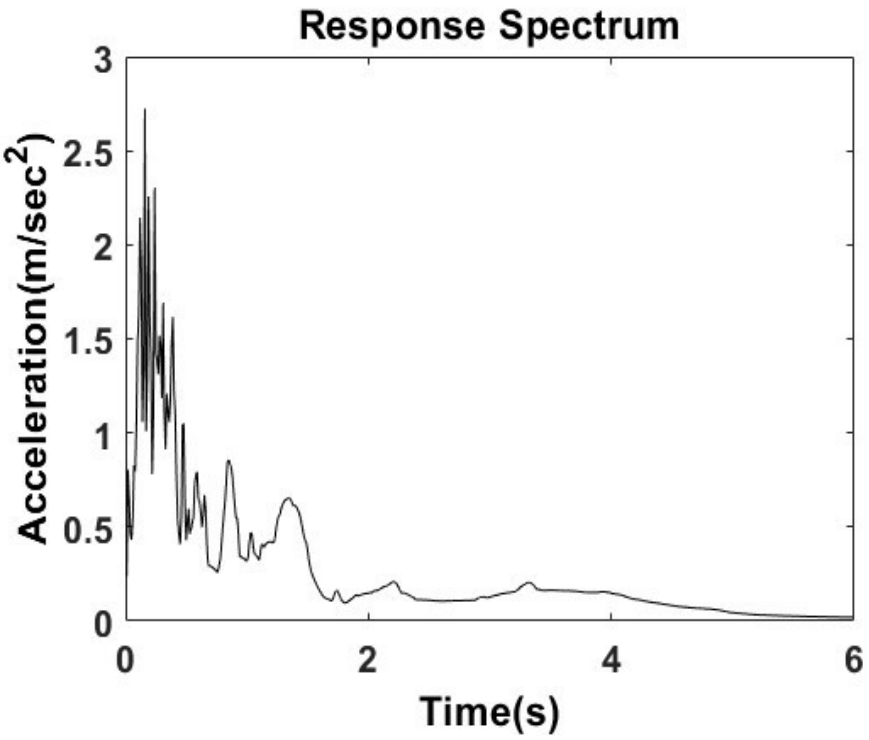

Figure 5-7 : Response Spectrum

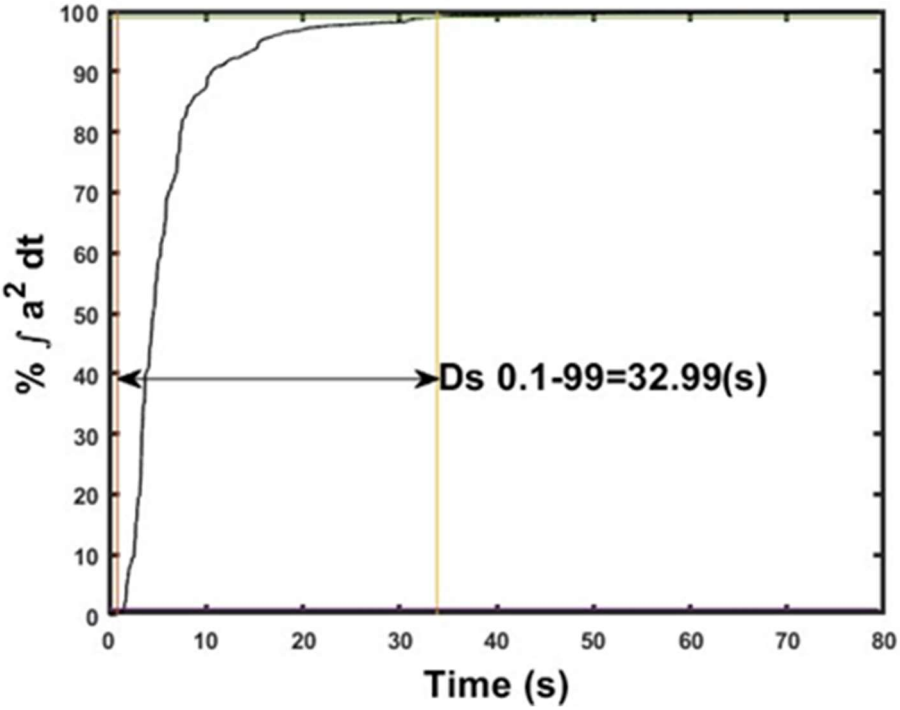

Figure 5-8 : Significant Duration

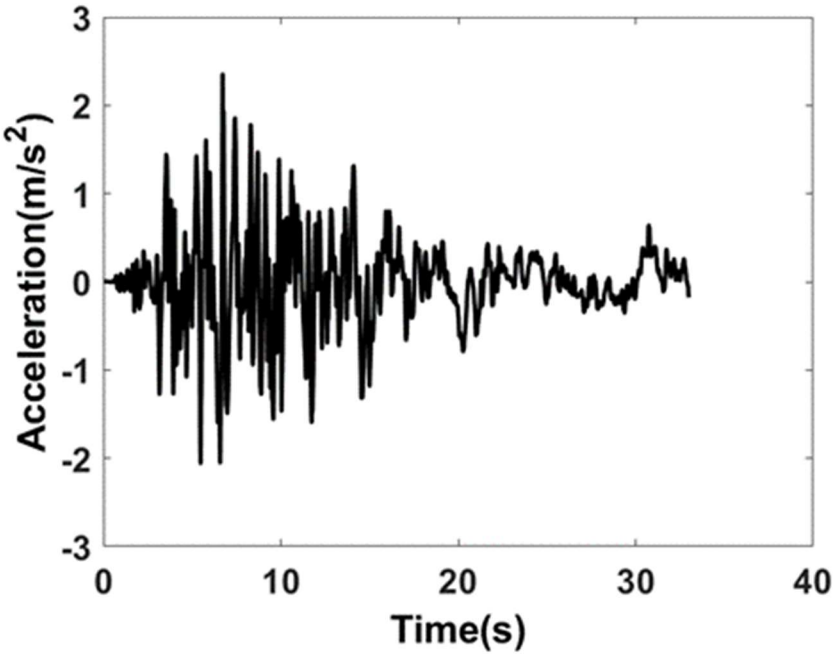

Figure 5-9 : Truncated Ground Motion

The JMA intensity of this earthquake is calculated to be 5.34 (Figure 5-10) using the relation of ground acceleration with JMA intensity proposed by K.T. Shabestari and F. Yamazaki. (2001)[75]. This method involves utilizing a reference acceleration value, denoted as "a_0" with a total period (τ) exceeding 0.3 seconds.

Intensity in JMA scale: $I_{JMA}= 2.0 \log(a_0) + 0.94$ (5-1)

Using this relation, the ground motion of San Fernando earthquake has been scaled up and scaled down to JMA 3.5, JMA 4.5, JMA 5, JMA 5.5, JMA 6 and JMA 6.5 as an instrumental intensity. The ground motion time history is plotted in Figure 5-11.

Throughout the analysis process, the structure's response is assessed based on its maximum inter-story drift ratio and floor displacements at various intensity levels. By interpreting the analysis results, it becomes possible to pinpoint the critical components of the structure that are at the highest risk of damage and evaluate the overall seismic performance of the entire building.

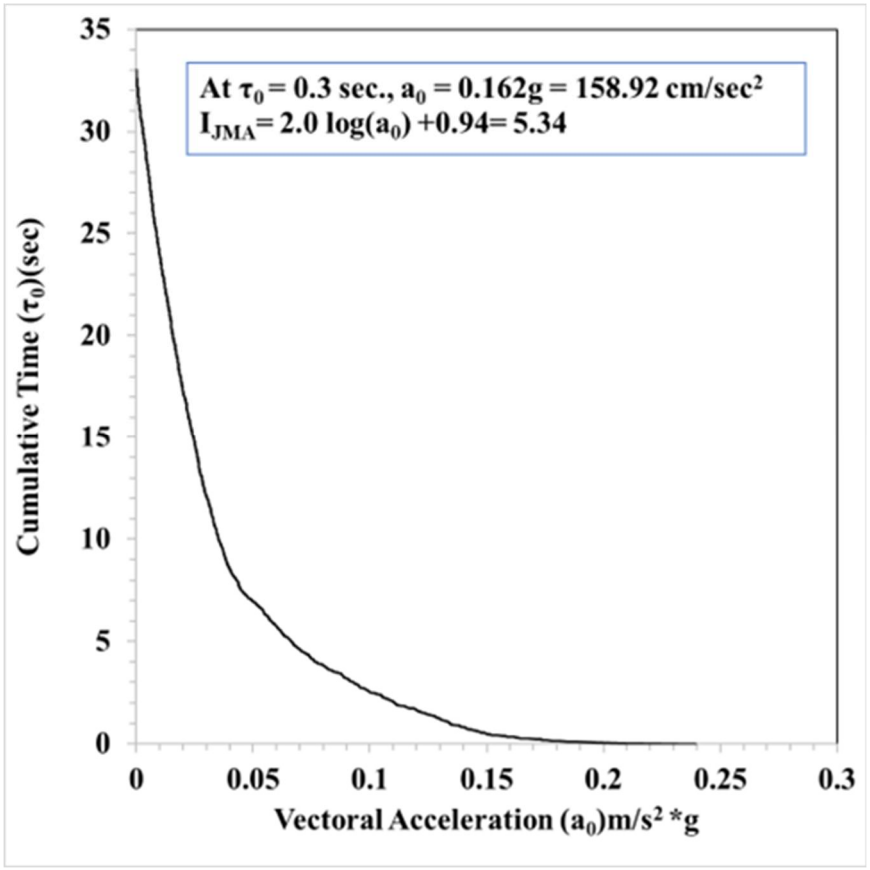

Figure 5-10 : Calculation of JMA intensity

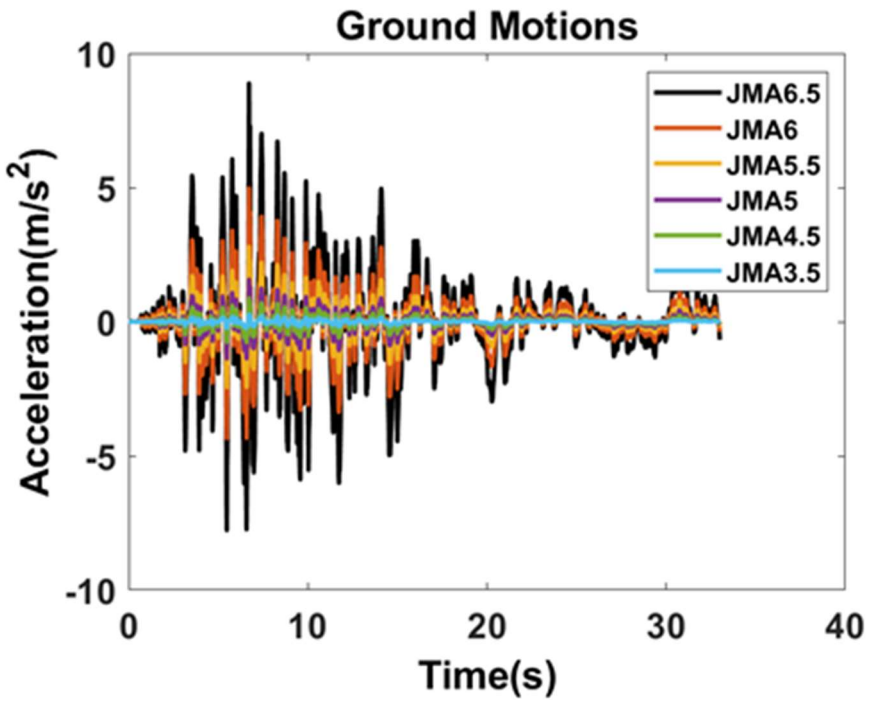

Figure 5-11 : Scaled ground motions

5.7 Results of Incremental Dynamic Analysis

In this research, an updated numerical model of a building was analysed for a range of ground motions, varying from 3.5 JMA to 6.5 JMA instrumental intensity. The response of the structure at each floor level was measured for each intensity ground motion. Figure 5-12 to Figure 5-17 compares the response at each floor level and Figure 5-18 compares the maximum interstorey drift ratio for the 3.5-6 JMA ground motion. The results indicate that the deformation is concentrated on the ground floor, making it a soft storey building. No failures were observed for 3.5 JMA and 4.5 JMA ground motions. The interstorey drift ratio is 0.3% at the ground floor, compared to 0.026% at the top floor for 4.5 JMA ground motion. However, significant failure in the ground floor columns and upper floor masonry wall was observed for 5 JMA ground motion. The interstorey drift ratio was 0.87% at the first(ground) floor and 0.024% at the top floor. Extensive damage in first(ground) floor columns and higher response was observed for the ground motion of 5.5 JMA with an inter-storey drift ratio of 2.63% at the ground floor and 0.041% at the top floor. The structure underwent large deformation on the firs(ground) floor, and heavy damage was seen for the 6 JMA ground motion, leading to collapse due to soft storey failure. The maximum interstorey drift ratio was observed to be 4.99% at the first(ground) floor and 0.13% at the top floor for 6 JMA ground motion. The study concludes that the structure collapses within 7 seconds for ground motion greater than 6.5 JMA.

The Incremental Dynamic Analysis (IDA) curve of maximum interstorey drift ratio with respect to each intensity level is shown in Figure 5-19. The damage grade 1-5 categorized based on the EMS scale of damage grade is employed to classify the damage level of the structure in each level of ground motion. The structure is within damage grade 1 (D1) with very minor cracks in the structure for JMA 3.5-4.5 ground motions. While for ground motion between 4.5-5 JMA has damage grade (D2) damage. Similarly, for ground motion 5-5.5 JMA has significant

failure on the ground floor resulting damage grade of D3-D4. With the ground motion higher than the 5.5 JMA, the structure undergoes damage grade of D5 and followed by complete collapse. The deformation and damage of the structure for each intensity level is shown in Figure 5-21 to Figure 5-25 .

Figure 5-20 illustrates how the structure's frequency degrades over time for different levels of ground motion intensity. With the increase in intensity level the frequency degradation is also high. The frequency degradation ratio (FDR), a ratio of final fundamental frequency and initial frequency of the structure after application of ground motion is tabulated in Table 5-1. The structure with FDR value 1 is considered to be structure with no damage and with the decrease of the FDR value the damage level of the structure will be higher.

5.7.1 Response at 3.5 JMA ground motion

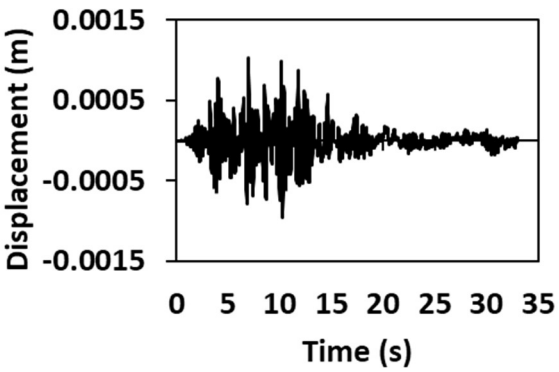

First (Ground) floor response

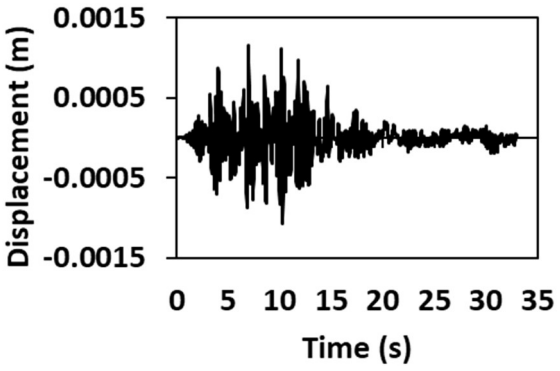

Second floor response

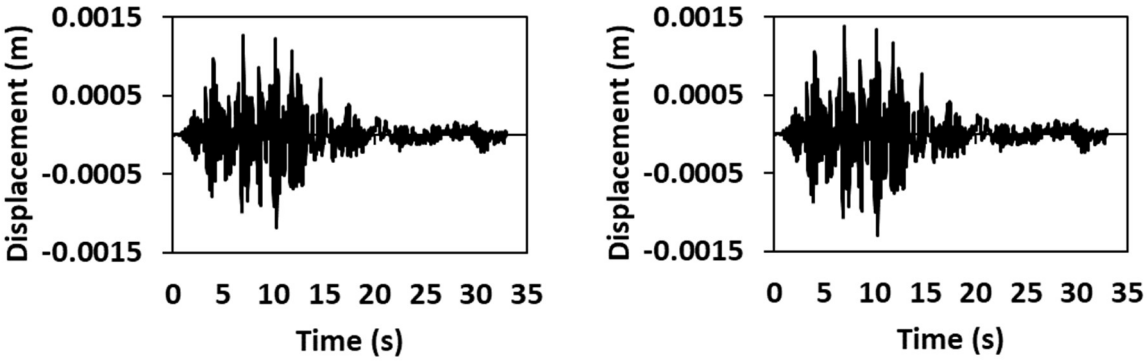

Third floor response Fourth floor response

Figure 5-12 : Floor Responses for 3.5 JMA Ground Motion

5.7.2 Response at 4.5 JMA ground motion

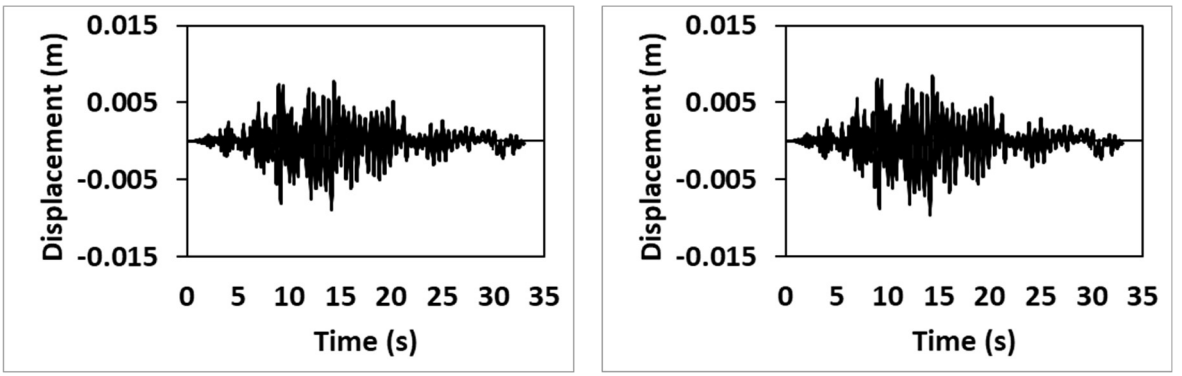

First (Ground) floor response Second floor response

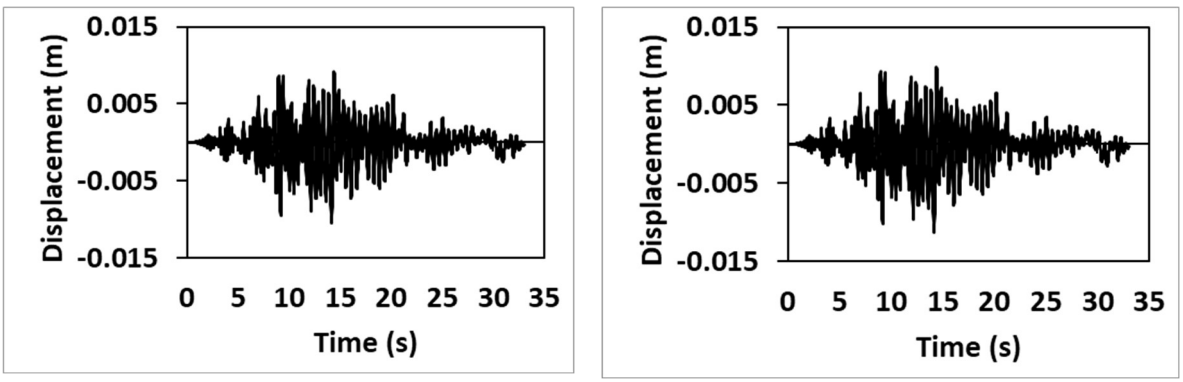

Third floor response Fourth floor response

Figure 5-13 : Floor Responses for 4.5 JMA Ground Motion

5.7.3 Response at 5 JMA ground motion

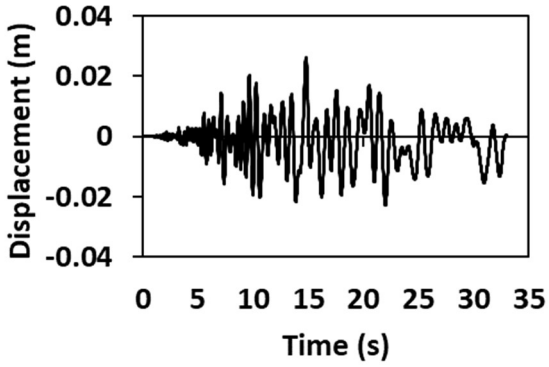

First (Ground) floor response

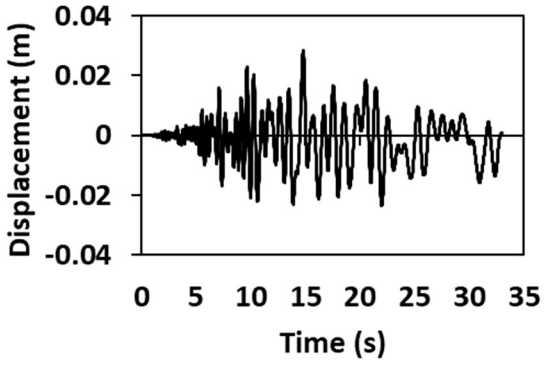

Second floor response

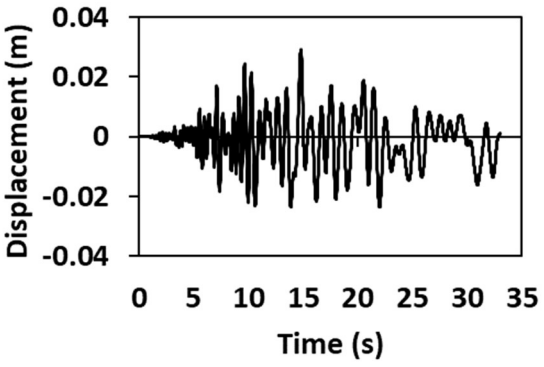

Third floor response

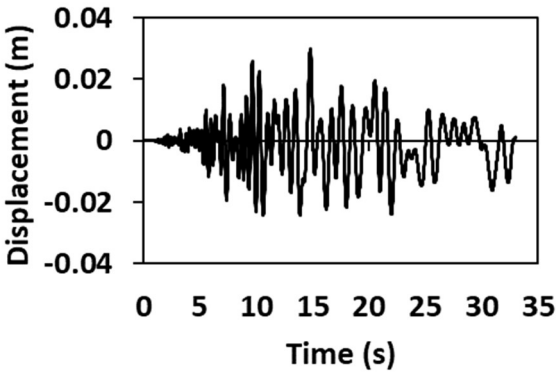

Fourth floor response

Figure 5-14 : Floor Responses for 5 JMA Ground Motion

5.7.4 Response at 5.5 JMA ground motion

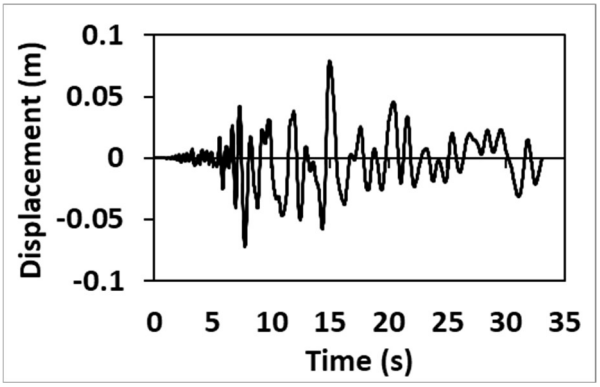

First (Ground) floor response

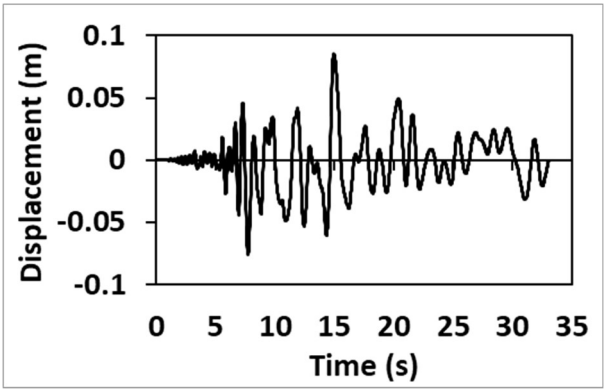

Second floor response

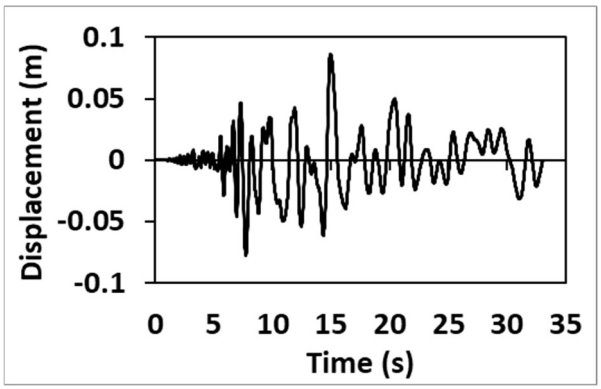

Third floor response

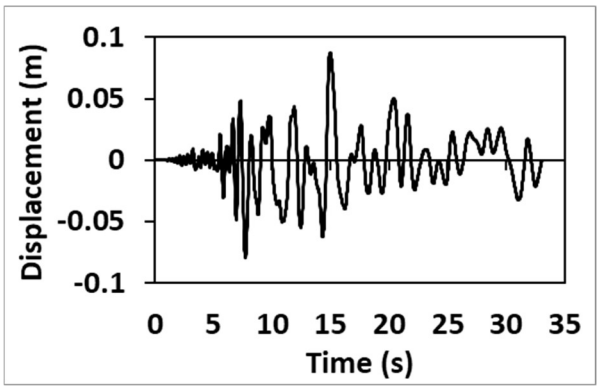

Fourth floor response

Figure 5-15 : Floor Responses for 5.5 JMA Ground Motion

5.7.5 Response at 6 JMA ground motion

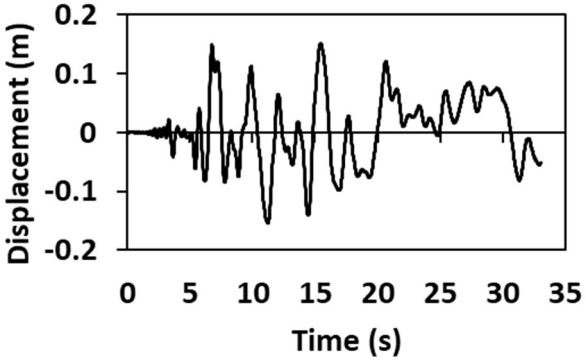

First (Ground) floor response

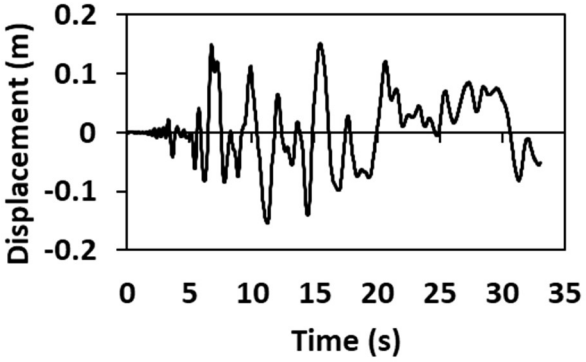

Second floor response

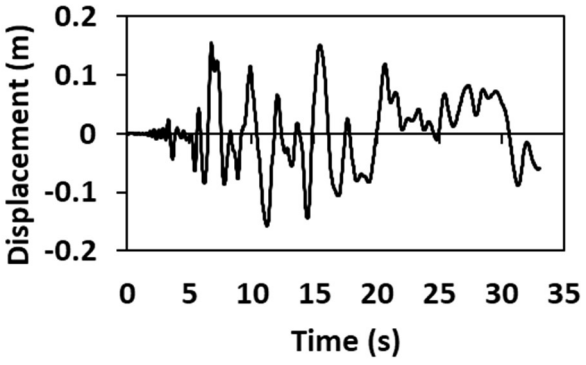

Third floor response

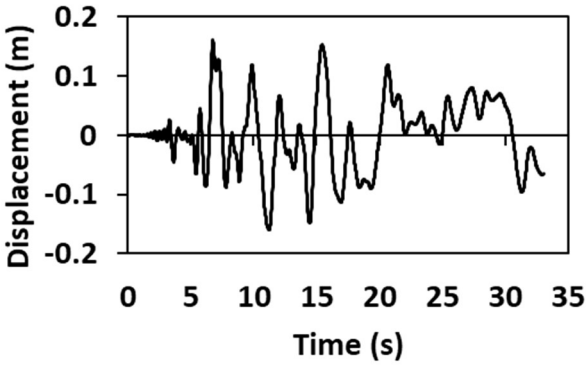

Fourth floor response

Figure 5-16 : Floor Responses for 6 JMA Ground Motion

5.7.6 Response at 6.5 JMA ground motion

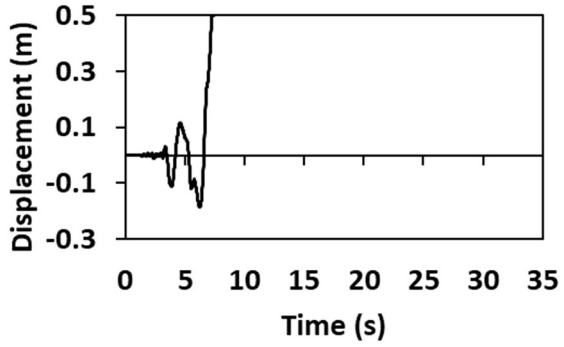

First (Ground) floor response

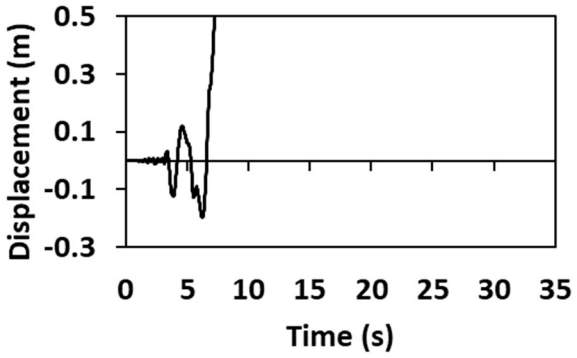

Second floor response

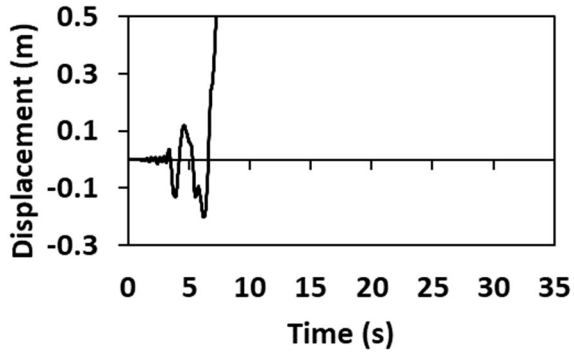

Third floor response

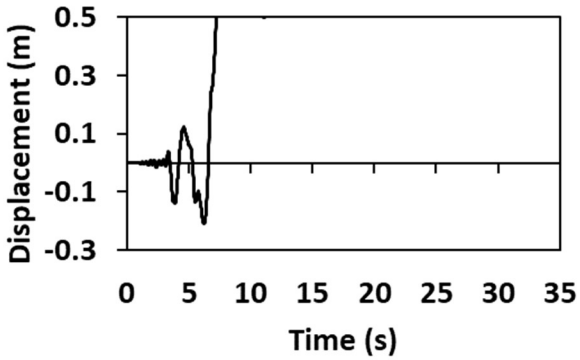

Figure 31(d): Fourth floor response

Figure 5-17 : Floor Responses for 6.5 JMA Ground Motion

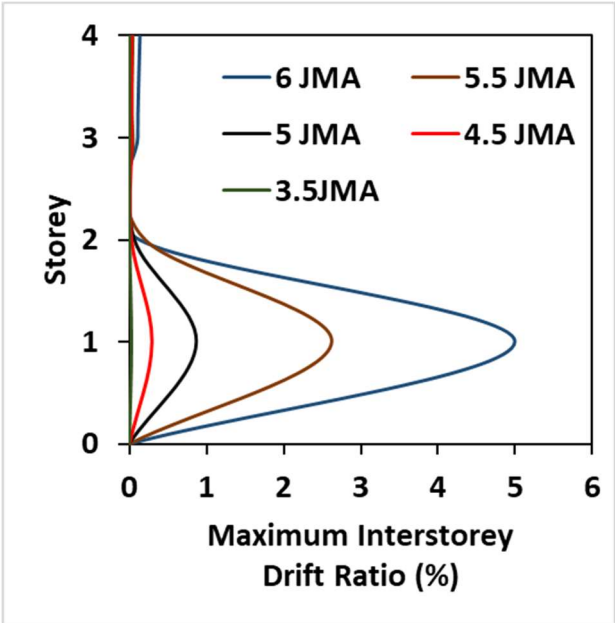

Figure 5-18 : Maximum Interstorey Drift Ratio

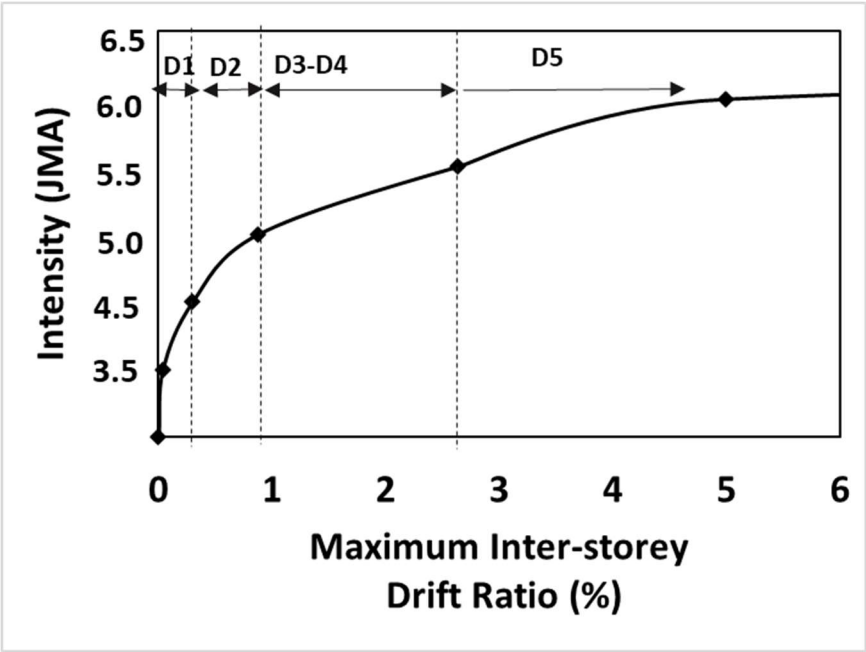

Figure 5-19 : Maximum Interstorey Drift Ratio with respect to Intensity (JMA)

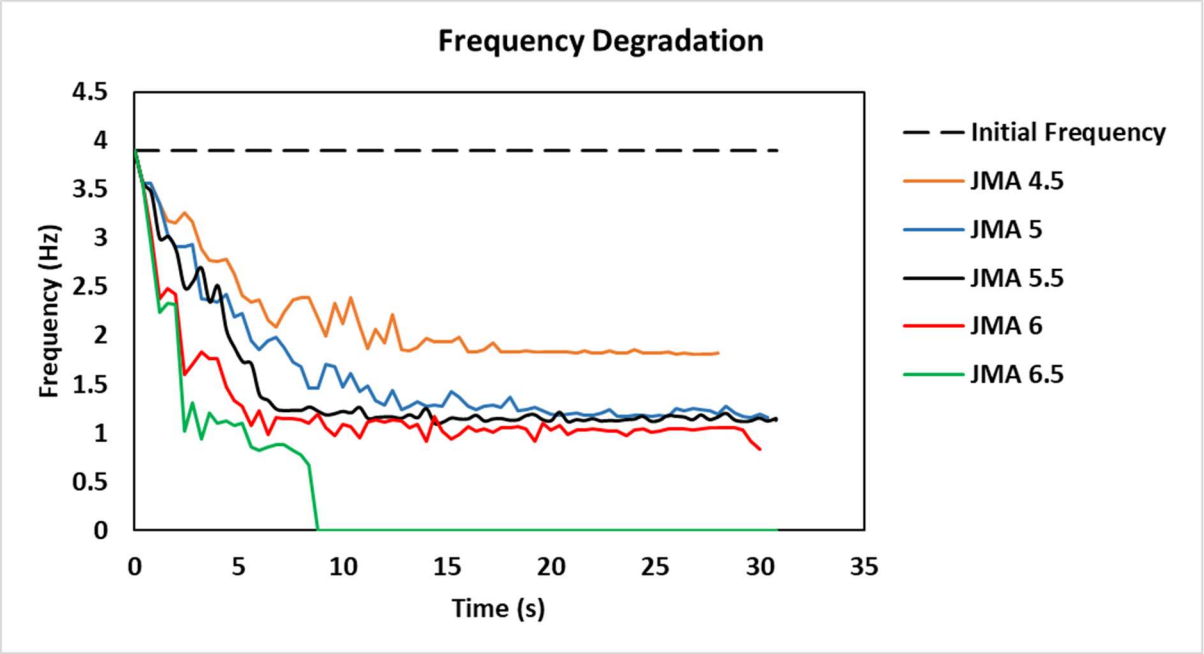

Figure 5-20 : Frequency Degradation Curve for Different Intensities

Table 5-1: Frequency Degradation Ratio

SN	Intensity	Fundamental Frequency (hz)	Frequency degradation ratio (FDR)
1	**Initial structure**	3.899	1
2	**3.5 JMA**	3.899	1
3	**4.5 JMA**	1.83	0.469351116
4	**5 JMA**	1.15	0.294947422
5	**5.5 JMA**	1.13	0.289817902
6	**6 JMA**	0.83	0.212875096
7	**6.5 JMA**	0 (complete collapse)	0

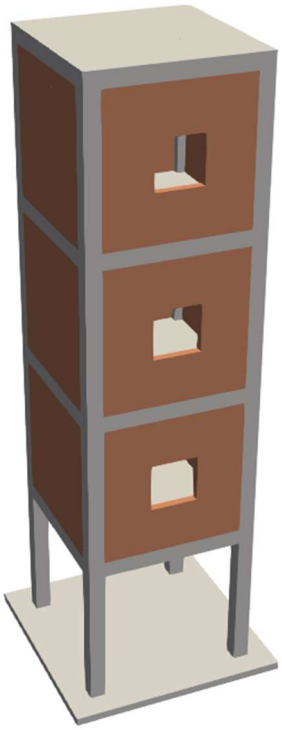

Figure 5-21: Damage pattern for JMA 3.5 and JMA 4.5 ground motion

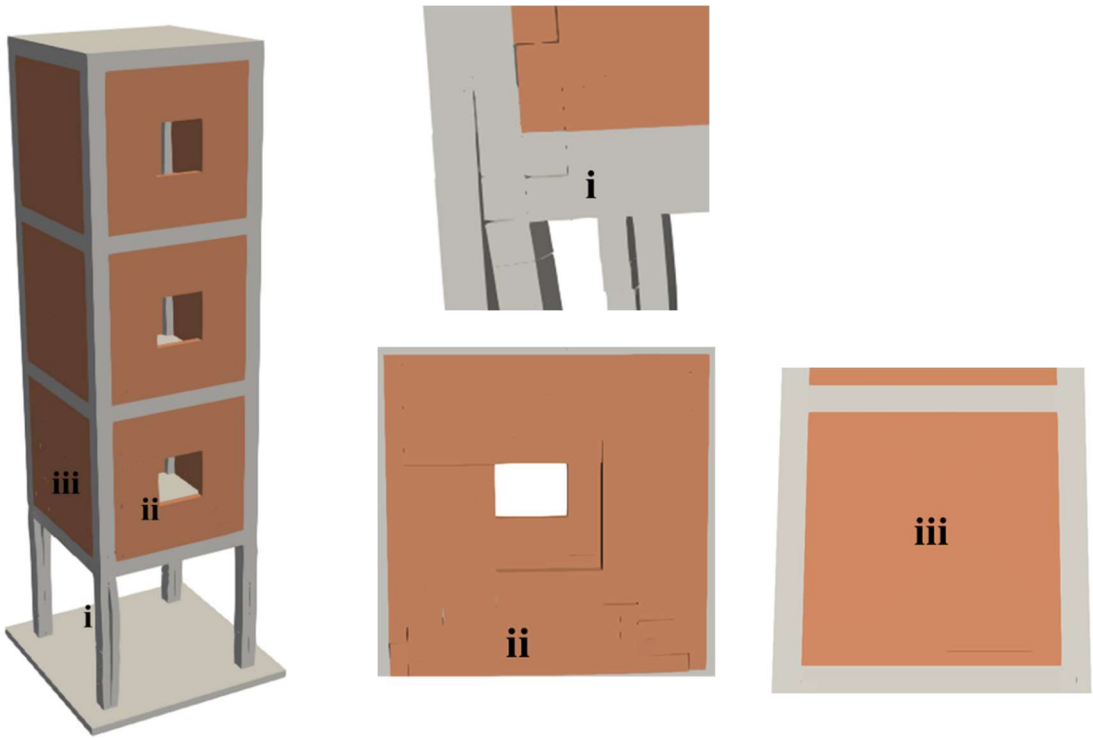

Figure 5-22: Damage JMA 5

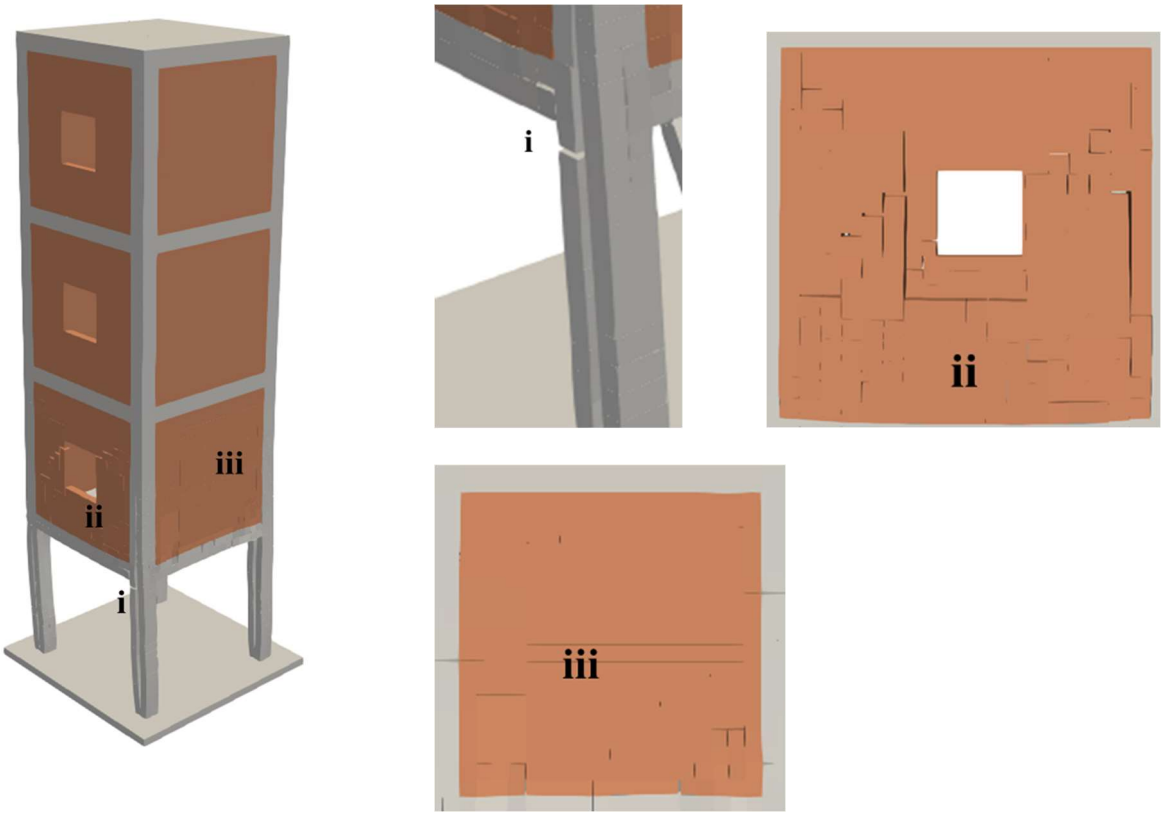

Figure 5-23 : Damage JMA 5.5

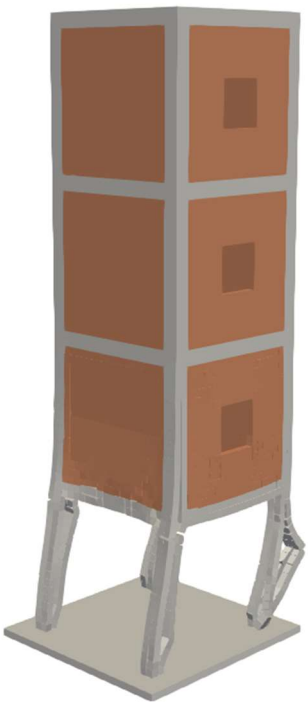

Figure 5-24 : Damage JMA 6

Figure 5-25 : Damage JMA 6.5

5.8 Conclusion

Using the model updating procedure, the existing structures can be modelled accurately in 3D AEM. To understand the non-linear behaviour and seismic capacity of the existing structures static or dynamic non-linear analysis has been performed and behaviour of the structure for different cases has been studied.

The static pushover analysis performed in the structure indicates that the structure exhibits soft storey behavior with displacement concentration occurring on the ground floor. The soft storey behavior is evidenced by the inter-storey drift ratio, which is significantly higher on the ground floor comparing to the upper floor. The failure patterns observed in the structure include in-plane shear cracks, on-plane failure of the masonry wall, and tensile failure at the beam column joint. The frequency degradation curve indicates a reduction in stiffness with increasing lateral displacement.

The incremental dynamic analysis of the updated 3D AEM model of the building for a range of ground motions, as described in this chapter, is of significant importance for enhancing our understanding of the performance of building under seismic loading. This can be very useful for determining the deformation, damage level, and failure mechanism of a structure. The IDA curve of maximum interstorey drift ratio with respect to each intensity level, deformation and damage of the structure for each intensity level, and frequency degradation ratio (FDR) provide valuable information which will be useful for the optimized design of structures and improvement in performances during earthquakes.

Chapter 6: Implementation of the 3D AEM Model Updating for Existing Structure

6.1 Introduction

In this chapter, the 3D AEM integrated model updating method is used for updating an existing reinforced concrete (RC) frame structure. The method employed is iterative and indirect, involving the estimation of changes in the modeling parameters by considering the sensitivity of modal characteristics to these parameters. This method proves particularly useful in scenarios where there is a limited no. of measured unscaled operational modes and a restricted no. of measured dofs. The previous chapter explored the application of this optimization-based sensitivity method for updating structural models in various scenarios involving different types of building structures, utilizing operational modal data but it was not applied for the real existing structure.

This chapter employs the same methodology to update a real three-storey RC frame structure in 3D AEM. The objective is to update the numerical model by utilizing operational modal data. Throughout the process, ambient vibration measurements are conducted at multiple critical locations on each floor of the RC building. This enables the acquisition of operational mode shapes and frequencies, for the structure. By employing these limited modal properties obtained from the existing RC frame, model updating in three-dimensional AEM is performed.

6.2 Case Study Building

The building in this study is an existing three-storey RC frame building referred to as "ST2," situated within the premises of the Asian Institute of Technology (AIT) in Thailand. Constructed in 1979, the building has undergone consistent maintenance measures, leading to

its commendable operational state. The photographs in the Figure 6-1 and Figure 6-2 show perspective of the building under study.

Figure 6-1 : Front perspective view of the building

Figure 6-2 : Back perspective view of the building

The building has an overall dimension of 24 meters by 13.43 meters, and it is characterized by 2 x 7 bays in two directions. The individual bay lengths range from 4 meters to 4.35 meters. Comprising three storeys, each storey maintains a consistent height of 2.6 meters. The typical column size is 0.20x0.20 m. and the beam dimension are 0.20x0.50 meters. Furthermore, the slab thickness throughout the building is 0.1 meters. The building's geometric details, including its dimensions and specific structural elements, are provided in Figure 6-3, Figure 6-4, Figure 6-5 and Figure 6-6. The summary of the building properties is shown in

Table 6-1.

Table 6-1: Characteristics of the Building

Age of building	44 Years
Overall Dimension	24 m x 13.43 m
No. of Bays	2 x 7
Bay Lengths, L (m.)	4 m- 4.35 m
No. of Storey	3
Storey height H (m.)	2.6 m
Typical Column Details	0.20m x 0.20m (Rebars detail Figure 6-4)
Beam Details	0.20m x 0.50m (Rebars detail Figure 6-5)
Slab Thickness	0.1 m (Rebars detail Figure 6-6)

All other structural drawings of the building can be found in ANNEX-2.

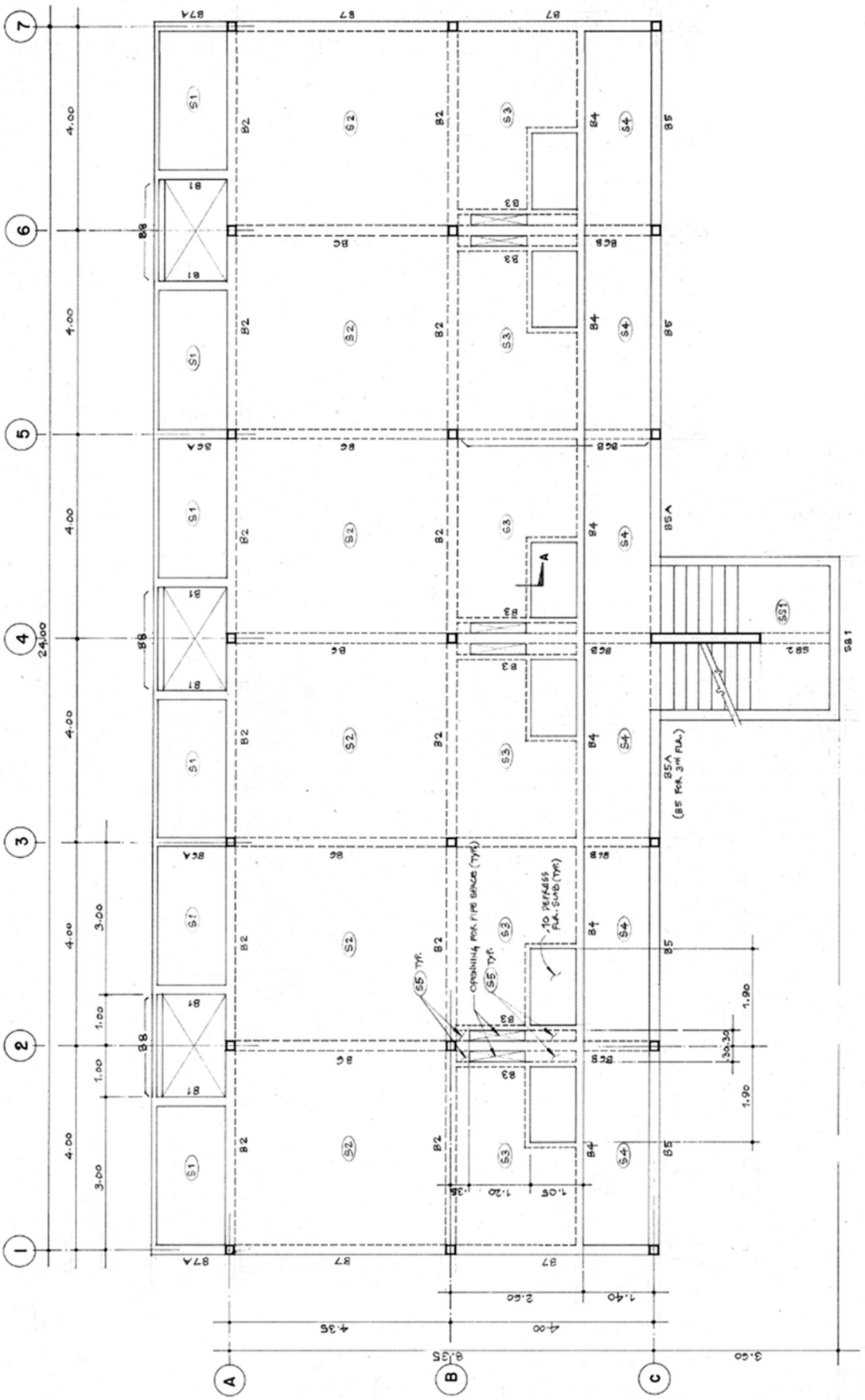

Figure 6-3: Typical Floor Plan (Source: Asian Institute of Technology (AIT), Thailand)

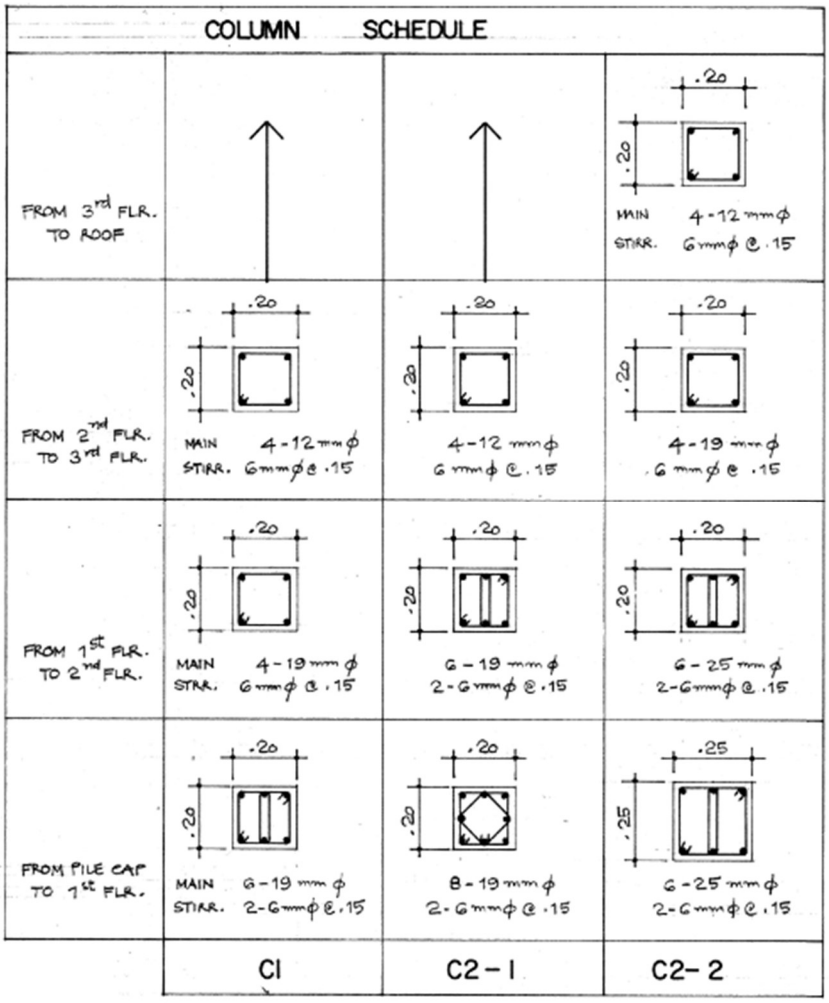

Figure 6-4: Column Schedule of the building (Source: Asian Institute of Technology, AIT)

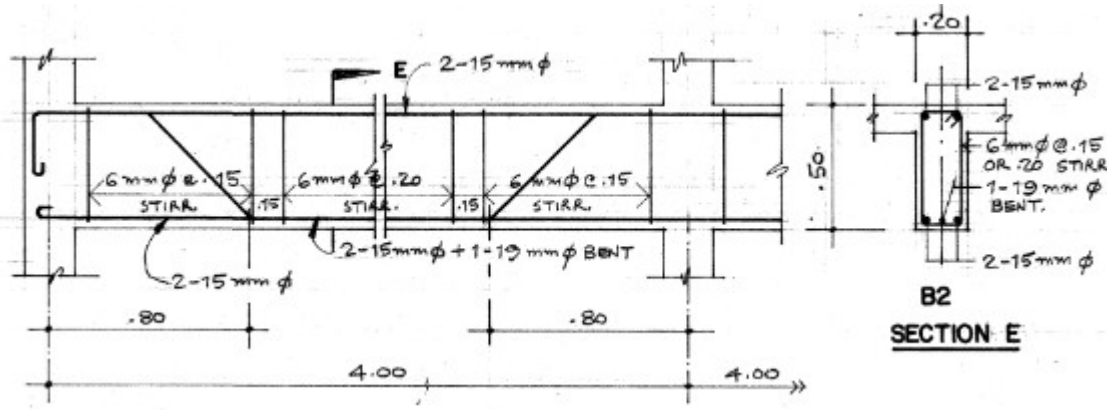

Figure 6-5: Typical beam detailing of building (Source: Asian Institute of Technology, AIT)

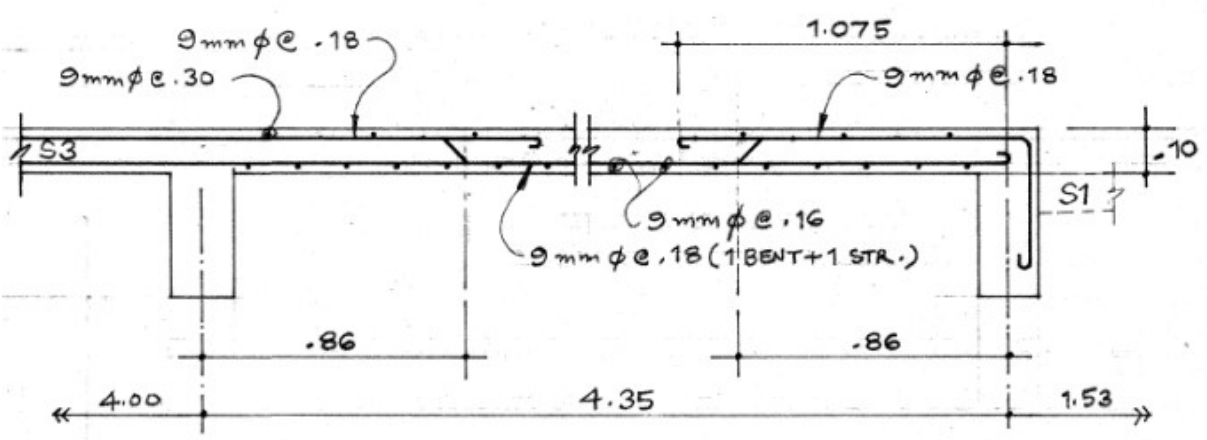

Figure 6-6: Typical slab detailing of the building (Source: Asian Institute of Technology, AIT)

6.3 Limitations and Considerations of the Study

Firstly, the building's rooftop accessibility was limited, with only one location available above the shear wall of the staircase for measurement. Consequently, the measurements of the roof's properties were obtained solely from this particular location.

Secondly, the structural model employed for analysis included solely the RC shear wall, with the load generated by the staircase steps allocated to the corresponding floor beams.

The structure’s global mass matrix was computed based on the material densities. Specifically, the density of concrete is considered to be 2400 Kg/m^3, while the masonry wall was assigned a density of 1900 Kg/m^3. The live load of the structure is not considered for this study.

6.4 Experiment Plan

The ambient vibration test was conducted on two different dates, June 18 and June 27, 2023. The experiment involved a team of eight human resources and aimed to collect data from 16 sets of measurements, comprising 48 total measurement locations. To gather the required data, four GeoDAS 3-directional velocity microtremor sensors were used as measurement sensors, connected to a GeoDAS 10-24 DS Data Acquisition System with a sampling rate of 100 Hz.

Each measurement set lasted for a duration of 1200 seconds. Sample photographs representing the experimental setup are shown in Figure 6-7.

Figure 6-7 : Representative experimental setup photographs during experiment

6.5 Ambient Vibration Data from Field Survey

The microtremor velocimeter sensors placed at various locations on all three floors, as depicted in the Figure 6-8, are utilized to measure the ambient vibration data. The measured locations during the experiment for 16 different sets are illustrated in Table 6-2. The experiment employed a collective of four sensors, wherein each measurement set involved the utilization of one sensor on the ground and three sensors positioned at the beam column joint of each floor. Notably, while the roof was not accessible, it was possible to access the top of the RC shear wall of the staircase at location C-4. The set-13 includes the data which includes the measurement at each floor level and roof.

Table 6-2 : Different sets of measurement location

SN	Measurement Set	Location
1	Set-1	Ground: G and 1-F, 2-F, 3-F: C-1
2	Set-2	Ground: G and 1-F, 2-F, 3-F: B-1
3	Set-3	Ground: G and 1-F, 2-F, 3-F: A-1
4	Set-4	Ground: G and 1-F, 2-F, 3-F: A-2
5	Set-5	Ground: G and 1-F, 2-F, 3-F: B-2
6	Set-6	Ground: G and 1-F, 2-F, 3-F: C-2
7	Set-7	Ground: G and 1-F, 2-F, 3-F: B-4
8	Set-8	Ground: G and 1-F, 2-F, 3-F: A-4
9	Set-9	Ground: G and 1-F, 2-F, 3-F: A-5
10	Set-10	Ground: G and 1-F, 2-F, 3-F: B-5
11	Set-11	Ground: G and 1-F, 2-F, 3-F: C-5
12	Set-12	Ground: G and 1-F, 2-F, 3-F: C-4
13	Set-13	1-F, 2-F, 3-F and Roof: C-4
14	Set-14	Ground: G and 1-F, 2-F, 3-F: C-3
15	Set-15	Ground: G and 1-F, 2-F, 3-F: C-6
16	Set-16	Ground: G and 1-F, 2-F, 3-F: C-7

Throughout the experiment, these sensors captured and documented the response of the structure in terms of velocity. The ambient vibration is measured for 20 minutes for each set of data with the sampling rate of 100 Hz. This recorded response provides information about the intensity and frequency of the vibrations endured by the building. By analyzing this data, we can obtain its frequency and modeshapes, when subjected to ambient conditions.

As a sample, the filtered and corrected ambient vibration response for each floor at for set 7, which is at the center of the building, is shown in Figure 6-9 along with the transformation of the response in time domain to frequency domain using the FFT method.

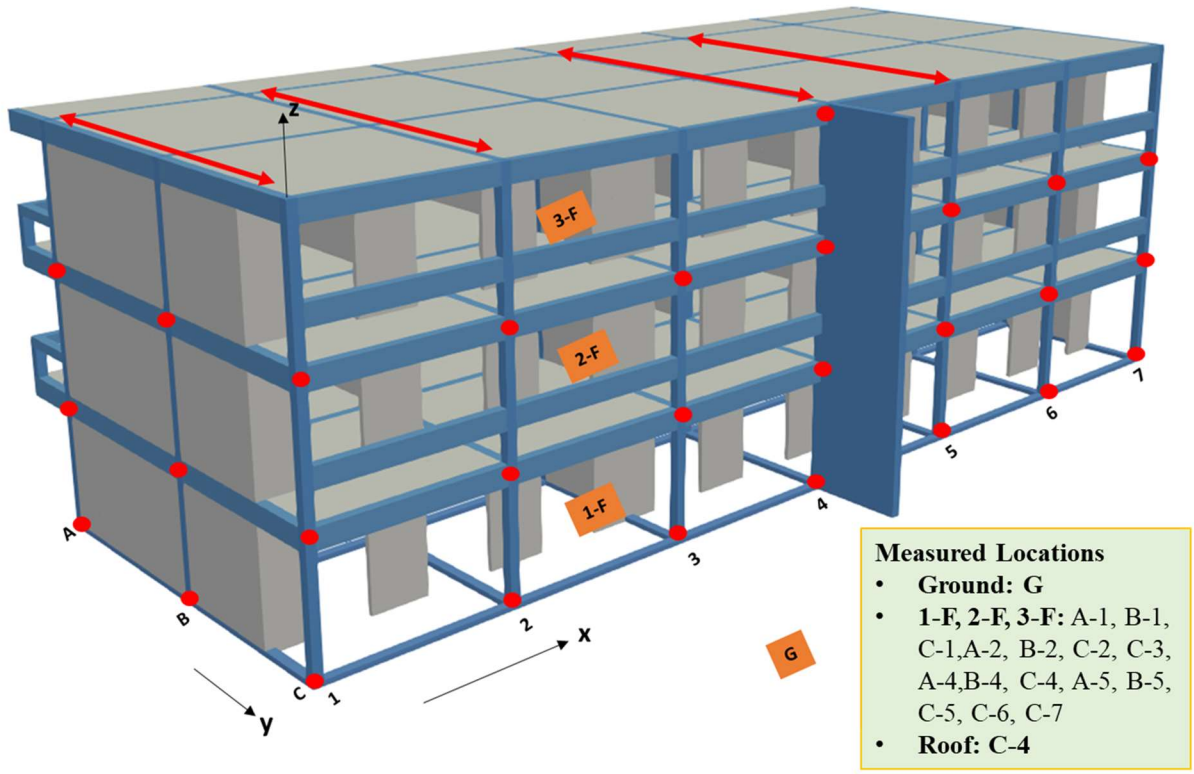

Figure 6-8: Micro-Tremor sensors measurement locations

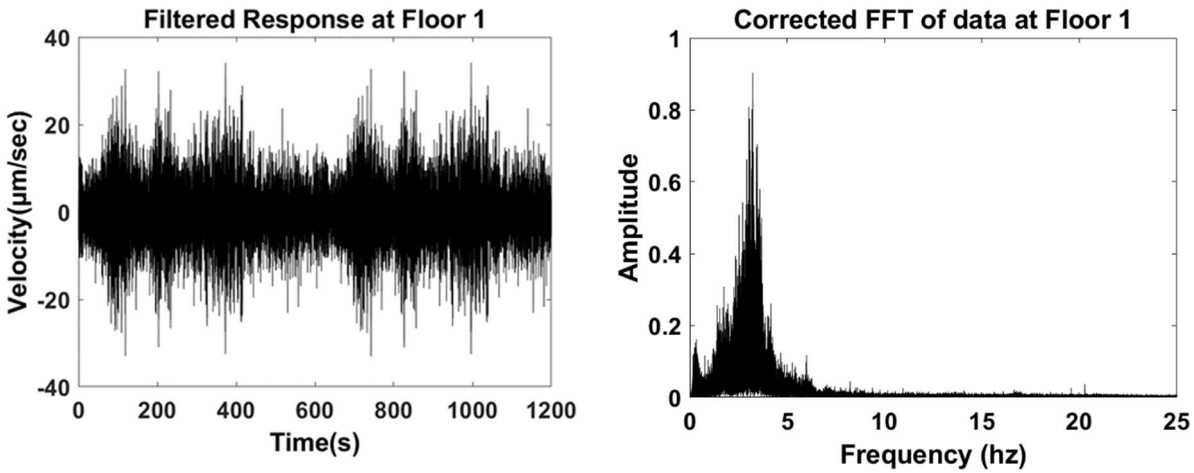

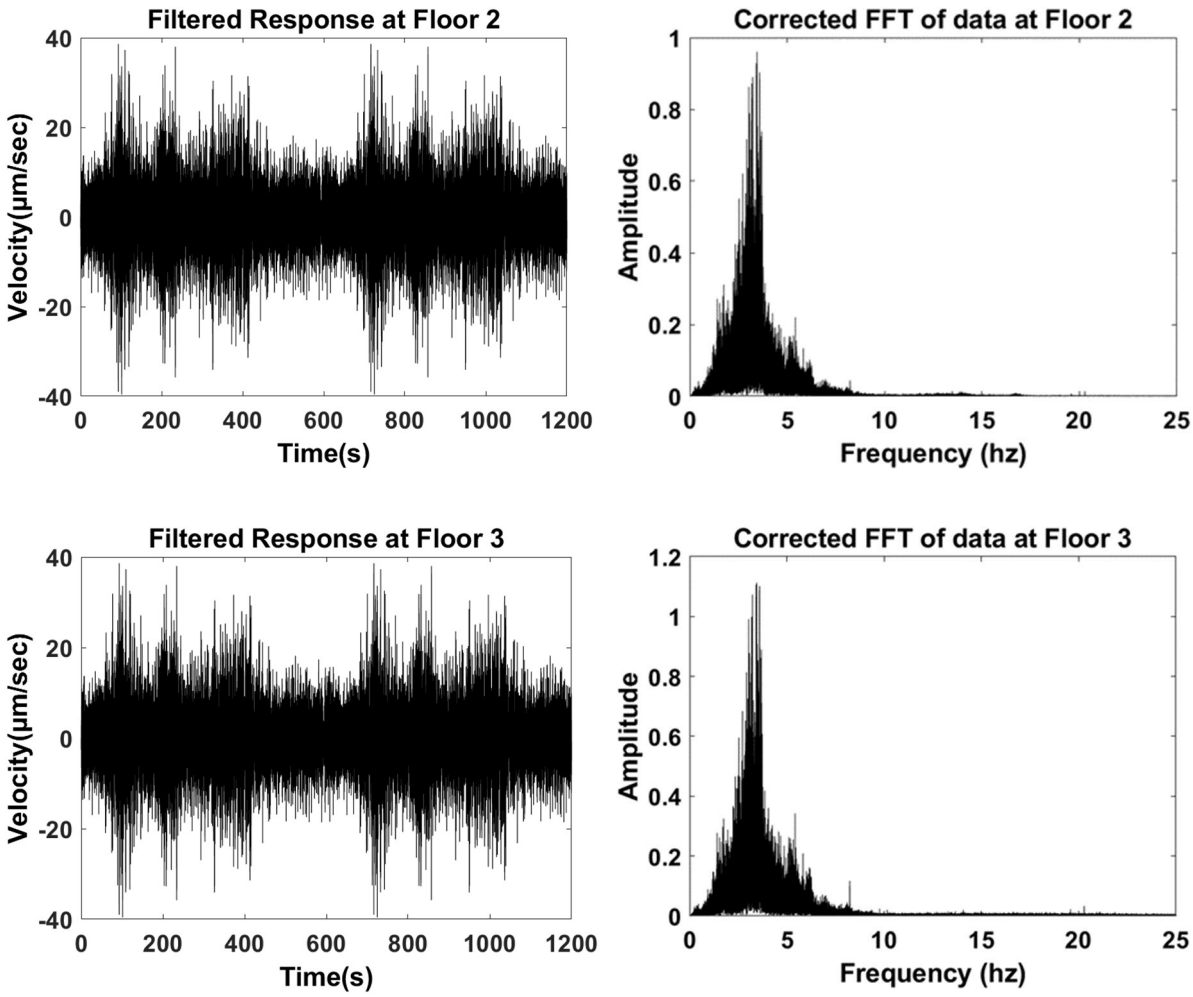

Figure 6-9 : Ambient vibration response and corresponding FFT for set 7 data.

6.6 Operational Modal Analysis Using Frequency Domain Decomposition

The 1st Singular value of the Power Spectral Density (PSD) matrix of the corrected and filtered ambient vibration data set was analyzed. As depicted in Figure 6-10 the peaks observed in the 1st singular value of the PSD matrix elucidate a distinct and prominent first mode of building, with a frequency of approx. 3.35 Hz. The corresponding mode shape of this first mode is provided in Figure 6-12 and Table 2-1. The mode-shape coordinates are normalized to the highest value to be 1. In contrast, the second mode remains indistinct, exhibiting limited clarity. By examining diverse data sets and filtering to eliminate the influence of the first mode, it was possible to identify an approximate frequency of the second mode to be 6.001Hz as observed in the FFT analysis of the data from set 7 (Figure 6-11). However, the modeshape data for the

second mode could not be successfully extracted. Consequently, for the purpose of model updating, the frequency and mode shape data pertaining to the first mode are employed.

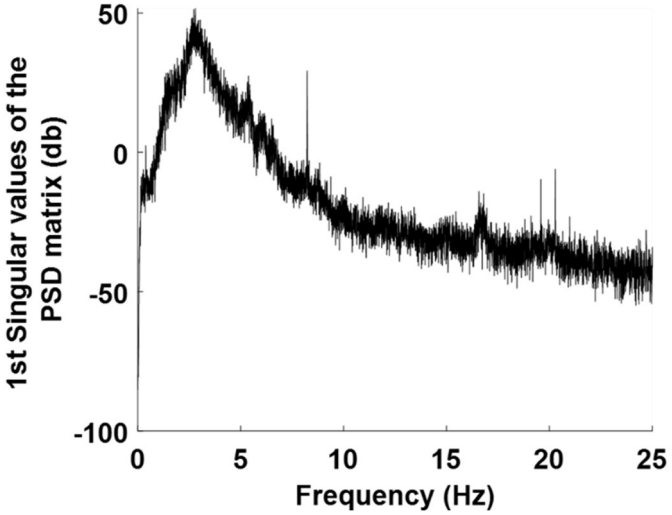

Figure 6-10: 1st Singular value of the Power Spectral Density (PSD) matrix

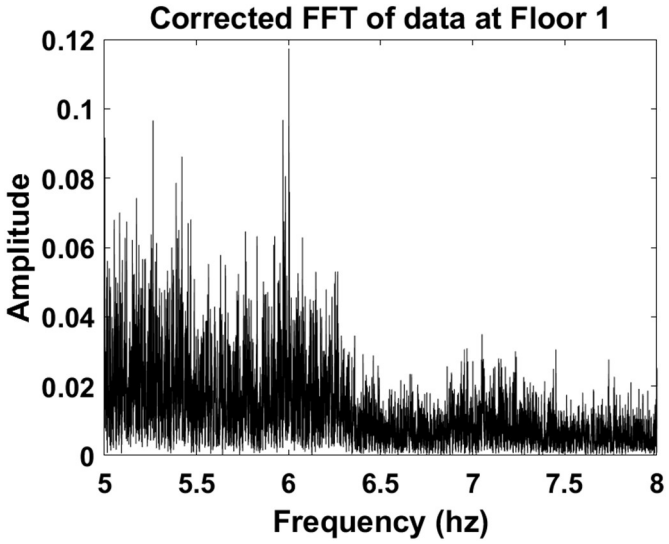

Figure 6-11: FFT of ambient vibration after filtering first mode for set 7 data

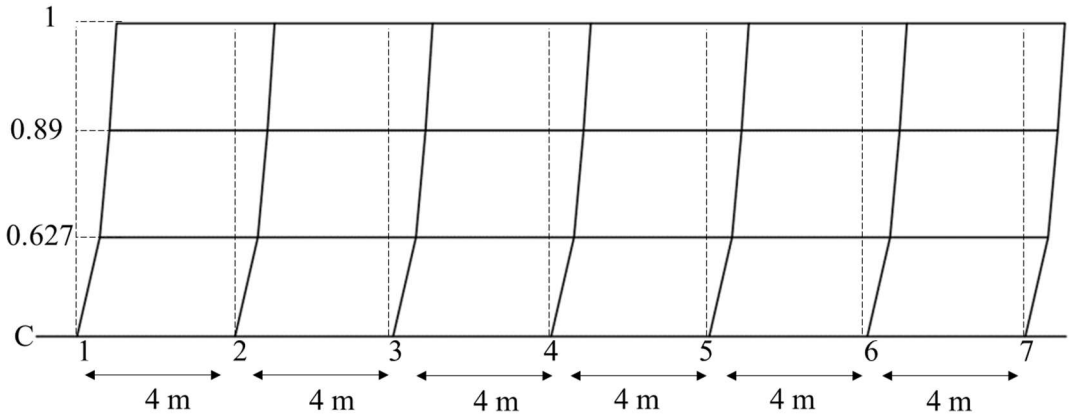

Figure 6-12 : First mode-shape of the building from experiment

Table 6-3 : First mode-shape of the building from experiment at some locations

SN	Location	Experiment (Mode 1)
1	**1-Floor: C-1**	0.0000
2	**2-Floor: C-1**	0.6270
3	**3-Floor: C-1**	0.8904
4	**Roof**	1.0000
5	**1-Floor: B-1**	0.0000
6	**2-Floor: B-1**	0.6002
7	**3-Floor: B-1**	0.9178
8	**Roof**	1.0000
9	**1-Floor: A-1**	0.0000
10	**2-Floor: A-1**	0.6182
11	**3-Floor: A-1**	0.8277
12	**Roof**	1.0000
13	**1-Floor: C-4**	0.0000
14	**2-Floor: C-4**	0.5814
15	**3-Floor: C-4**	0.8837
16	**Roof**	1.0000
17	**1-Floor: B-4**	0.0000
18	**2-Floor: B-4**	0.5938
19	**3-Floor: B-4**	0.9008
20	**Roof**	1.0000
21	**1-Floor: A-4**	0.0000
22	**2-Floor: A-4**	0.6234
23	**3-Floor: A-4**	0.8640
24	**Roof**	1.0000
	Frequency	3.35 Hz

6.7 Model Updating of the Case Study Building using 3D AEM

The structural components of the buildings are grouped together in 11 different groups with similar material properties. The components of the buildings are grouped floorwise into columns, beams and slabs, masonry wall and a separate group for RC shear wall. We are updating the physical parameter young's modulus of each group of structural components to model it accurately in 3D AEM. The details of each group and the initial Young's Modulus for each group is shown in Table 6-4.

Table 6-4 : Different groups of structural components and initial guess of the updating parameters

Parameters	Parameters Group	Initial Guess of Youngs Modulus (N/m^2)
1	Column First Floor	$1.20*10^{10}$
2	Column Second Floor	$1.20*10^{10}$
3	Column Third Floor	$1.20*10^{10}$
4	RC Shear wall staircase	$1.20*10^{10}$
5	Beam and Slab First Floor	$1.00*10^{10}$
6	Beam and Slab Second Floor	$1.00*10^{10}$
7	Beam and Slab Third Floor	$1.00*10^{10}$
8	Masonry Wall First Floor	$6.00*10^{9}$
9	Masonry Wall Second Floor	$6.00*10^{9}$
10	Masonry Wall Third Floor	$6.00*10^{9}$
11	Parapet walls	$6.00*10^{9}$

The initial guess of the young's modulus for the is guessed to be $1.20*10^{10} N/m^2$, $1.00*10^{10}$ N/m^2, $6.0*10^{9}$ N/m^2 for columns/RC shear wall, beams/slabs and masonry walls element group respectively.

With the reference to as built drawings of the building from Asian Institute of Technology (AIT), the structure is modelled in 3D AEM. The 3D AEM modelling properties of the building is shown in Table 6-5. The initial numerical model prepared is shown in Figure 6-13. The initial properties of the material for the building is assigned as Table 6-4.

Table 6-5 : 3D AEM numerical modelling properties

SN	Description	Quantity
1	Element Size	0.1 m
1	No. of Elements	151,178
2	No. of groups of structural components	11
3	Fixed Boundaries	124
4	Springs in each face of the elements	9
5	Total number of degree of freedoms	907,068
6	Size of global stiffness matrix in triplet format	14,545,698
7	No. of Springs	2,842,740

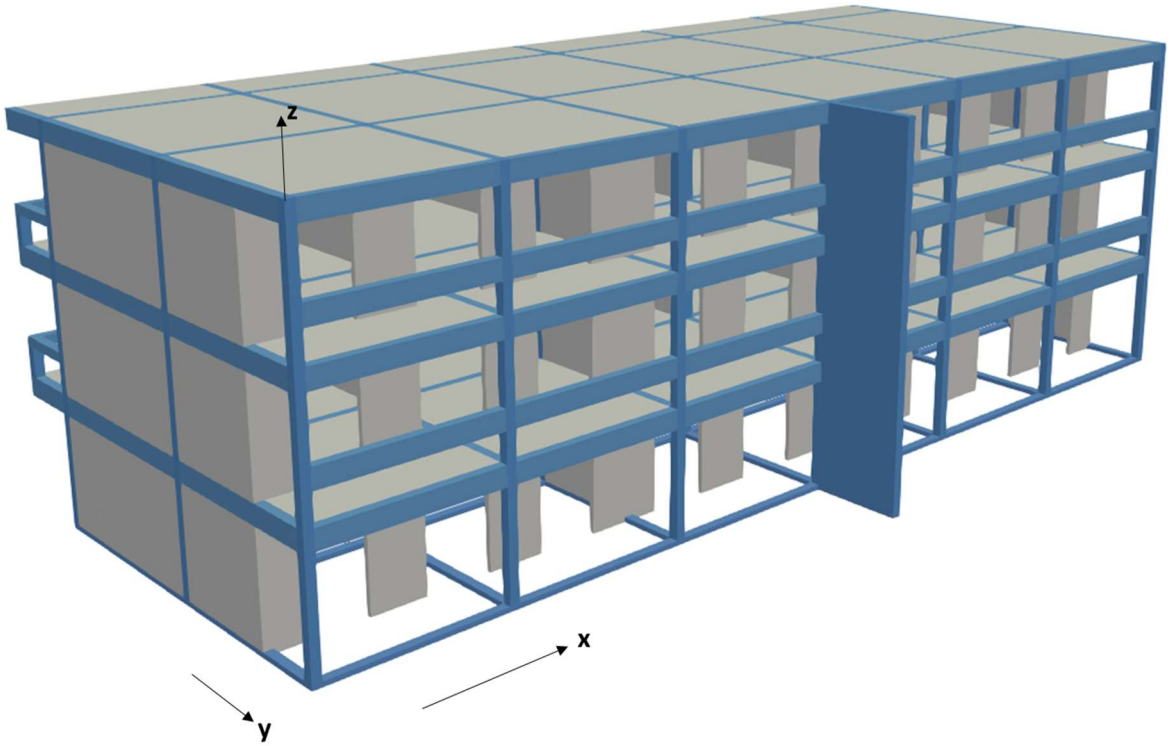

Figure 6-13: 3D AEM numerical model of the case study building

As described in chapter 4, let us recall the following objective function:

$$minimize\ f(x) = \sum_{i=1}^{n_{modes}} \left(\frac{(\lambda_i{}^{exp} - \lambda_i{}^{ana}(x))}{\lambda_i{}^{exp}} w_{\lambda i} \right)^2 + \left(\left(\frac{\phi_{i,l}^{exp,M}}{\phi_{i,r}^{exp,M}} - \frac{\phi_{i,l}^{ana,M}(x)}{\phi_{i,r}^{ana,M}(x)} \right) w_{\phi i} \right)^2 \quad \ldots (6\text{-}1)$$

This objective function is minimized using the Levenberg Marquardt algorithm.

$$x_{j+1} = x_j - (\nabla^2 f(x_j) + \Lambda I)^{-1} \nabla f(x_j)\ ,\ j = iteration\ number,\ size\ of\ x\ is\ (1, ngr) \quad \ldots\ldots\ldots (6\text{-}2)$$

The detail descriptions of these variables are described in chapter 4.

Implementing this algorithm for updating this case study building, at the end of the optimization, the structure would be accurately replicated, and it would be ready for the further analysis. An equal weightage for all the parameters is provided. The updated parameters (Young's Modulus) values after the model-updating using the developed method is shown in Table 6-6.

Table 6-6: Updated Young's Modulus of different parameters group for the case study building

Parameters	**Parameters Group**	**Initial Guess of Youngs Modulus (N/m^2)**	**Updated Value of Youngs Modulus (N/m^2)**
1	Column First Floor	$1.20*10^{10}$	$3.1653*10^{10}$
2	Column Second Floor	$1.20*10^{10}$	$3.1493*10^{10}$
3	Column Third Floor	$1.20*10^{10}$	$3.2160*10^{10}$
4	RC Shear wall staircase	$1.20*10^{10}$	$3.1542*10^{10}$
5	Beam and Slab First Floor	$1.00*10^{10}$	$2.6422*10^{10}$
6	Beam and Slab Second Floor	$1.00*10^{10}$	$2.6349*10^{10}$
7	Beam and Slab Third Floor	$1.00*10^{10}$	$2.6416*10^{10}$
8	Masonry Wall First Floor	$6.00*10^{9}$	$1.5916*10^{10}$
9	Masonry Wall Second Floor	$6.00*10^{9}$	$1.5723*10^{10}$
10	Masonry Wall Third Floor	$6.00*10^{9}$	$1.5934*10^{10}$
11	Parapet walls	$6.00*10^{9}$	$1.5860*10^{10}$

Table 6-7 : Comparison of experimental and updated eigen values

	Eigen Values		
	Experiment	**Updated**	**Error%**
Mode 1	442.59	410.38	7.28%

Table 6-8 : Comparison of experimental and updated eigen vectors

Grid	**Location**	**Exp. (Mode 1)**	**Updated (Mode 1)**	**Error %**	**MAC**
All	**1-Floor**	0	0	0.00%	
C-1	**2-Floor**	0.627	0.5391	14.01%	0.9936
	3-Floor	0.8904	0.8067	9.41%	
B-1	**2-Floor**	0.6002	0.5383	10.31%	0.9965
	3-Floor	0.9178	0.8125	11.47%	
A-1	**2-Floor**	0.6182	0.5433	12.11%	0.9978
	3-Floor	0.8277	0.8199	0.95%	
C-4	**2-Floor**	0.5814	0.5371	7.62%	0.9979
	3-Floor	0.8837	0.8045	8.97%	
B-4	**2-Floor**	0.5938	0.5425	8.64%	0.9975
	3-Floor	0.9008	0.8122	9.83%	
A-4	**2-Floor**	0.6234	0.5453	12.53%	0.9977
	3-Floor	0.864	0.8205	5.03%	
All	**Roof**	1	1	0.00%	

Similarly, the frequency of the updated structure is obtained within the error margin of 7.28% as shown in Table 6-7. On the other hand, the revised mode shape vectors are acquired with an error margin of only 14% when contrasted with the experimental mode shape of the structure. Additionally, the Mode Assurance Criterion (MAC) values for these mode shape vectors surpass 0.99, indicating a substantial alignment between the experimental and computed mode shapes as shown in Table 6-8 and Figure 6-14.

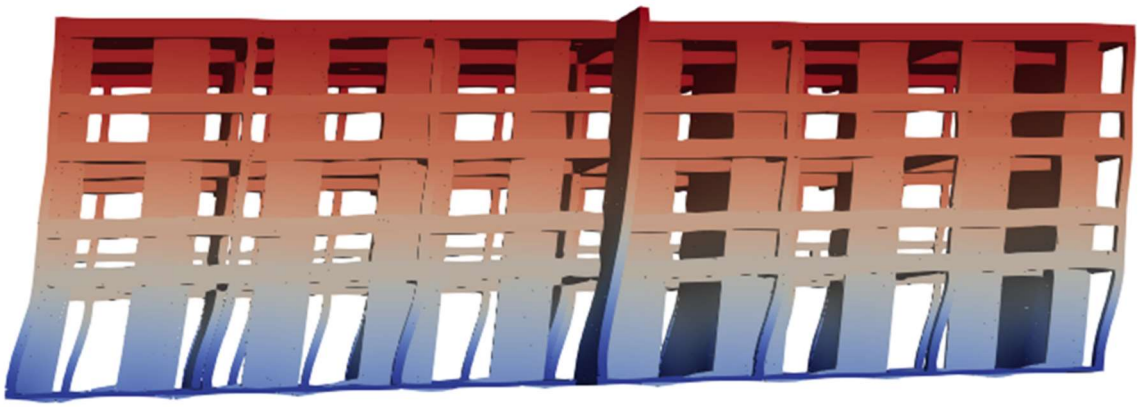

Figure 6-14: First mode shape of the updated structure

6.8 Static Pushover Analysis Using Applied Element Method

Moreover, an in-depth static pushover analysis is executed on the updated 3D AEM model of the building structure under study. The primary goal is to acquire a holistic comprehension of the performance of the building in lateral load and discern critical vulnerabilities. The numerical model of the updated structure is modelled in three-dimensional (3D) Applied Element Method (AEM) incorporating updated material characteristics of the structure under study. The non-linear static pushover analysis involves subjecting the building to incrementally increasing displacement-controlled lateral loads (P) of 0.08m (1% of height of the structure) at the roof level over 700 timesteps in a static manner. By considering the non-linear behavior of the structure, this analysis provides an estimation of the structure's capacity and deformation demands during the earthquake. The displacement response of the structure is evaluated at each load level, accounting for the non-linearities of the materials and structural connections. The resulting analysis yields a lateral force-displacement relationship, commonly referred to as the pushover curve. Performance indicators such as interstorey drift ratio with increasing load are assessed. Furthermore, the critical locations, weaknesses, and damage patterns of the structure are discussed based on the findings of the analysis.

So, in summary following four performance indicators are studied:

1. Lateral force-displacement relationship

2. Interstorey drift ratio

3. Damage pattern and location

6.9 Results and Discussion

The frame exhibits linear behavior until reaching a lateral drift at the roof of 0.0075 m under a lateral load of 501.1 KN at location (a) on the force-displacement curve (Figure 6-15). The slight drop in the force-displacement curve at location ‘a’ can be attributed to the occurrence of a crack in the masonry wall on the first floor (Figure 6-15). As the upper floor has additional masonry walls in the upper floors and also cantilever portion with masonry walls over it, the upper floor is stiffer than the bottom floor. Consequently, another sudden drop in the force-displacement curve is observed at location (c) of the force-displacement curve, which can be attributed to the occurrence of a crack at the joint of the beam column on the ground floor. Beyond this load, all deformation is concentrated on the ground floor, leading to soft storey failure. The soft storey behavior of the structure is further evidenced by an inter-storey drift ratio of over 2.95% at the ground floor compared to 0.73% at the top floor at location ‘e’ (Figure 6-16). The structure exhibits typical failure patterns, including in-plane shear cracks at location (2) and outof-plane failure of the masonry wall at location (3) of Figure 6-18. Additionally, tensile failure at the beam column joint at location (1) and some tensile cracks at the base of the column were observed.

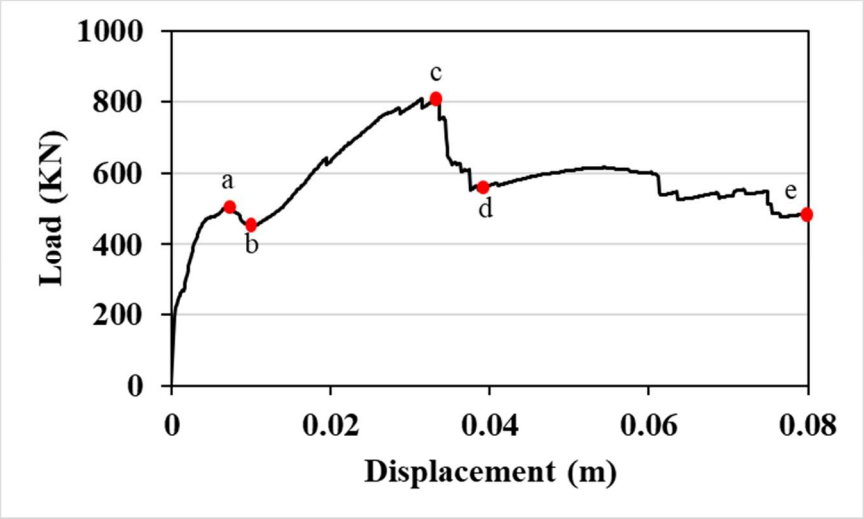

Figure 6-15 : Force-displacement curve at the roof level for the study building

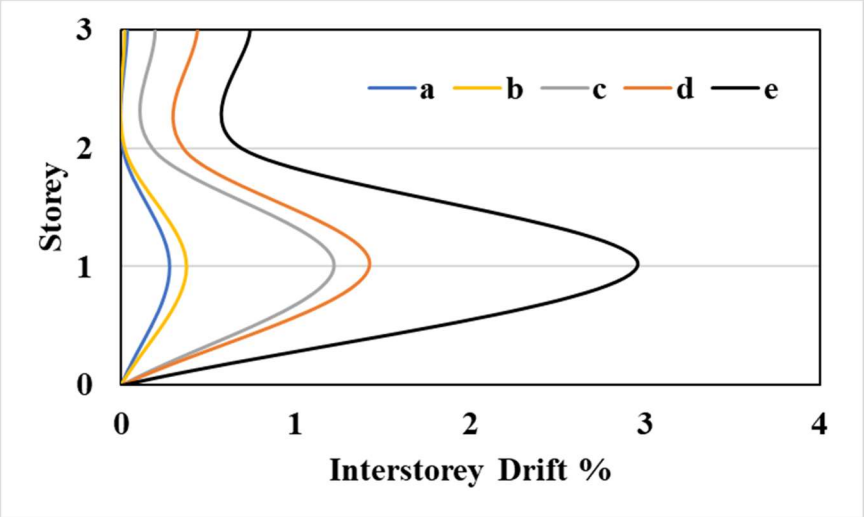

Figure 6-16 : Interstorey drift ratio of the study building

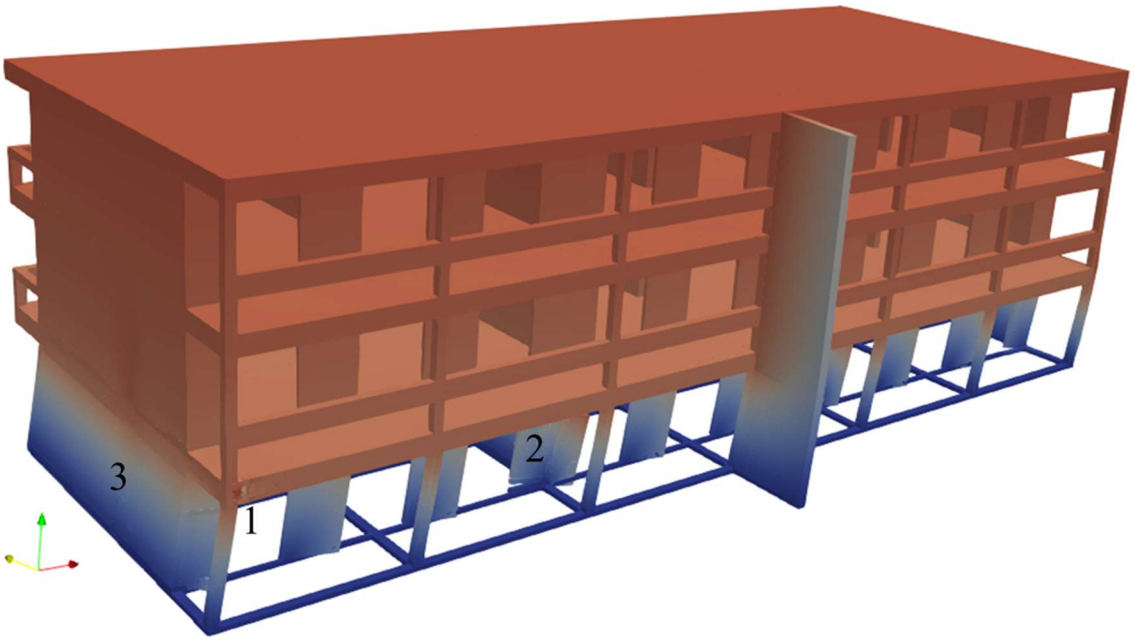

Figure 6-17 : Deformation of the building at the end of the pushover analysis

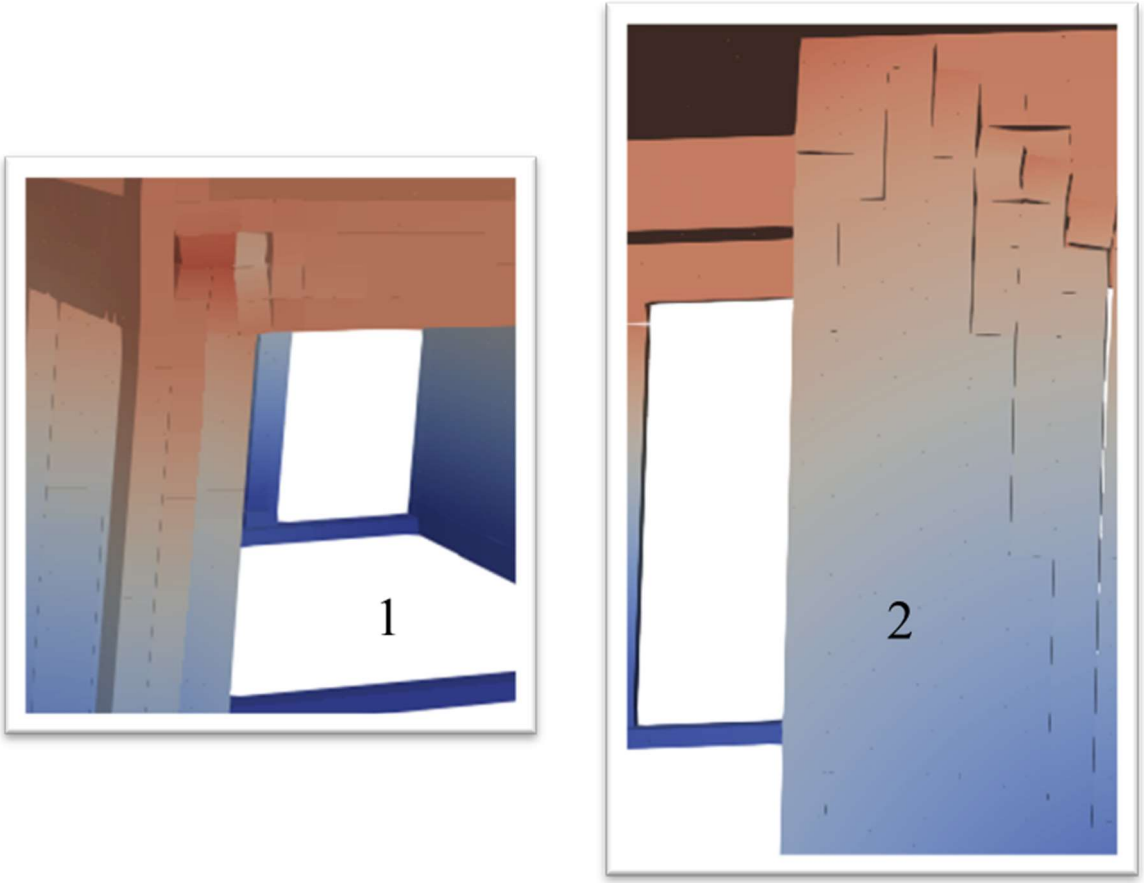

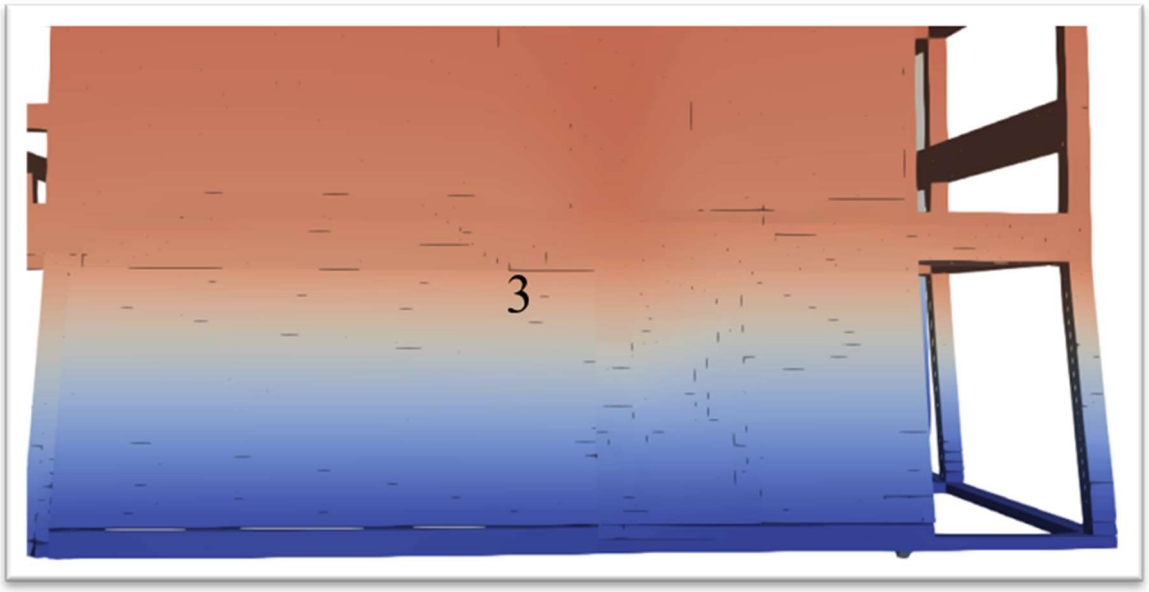

Figure 6-18 : Damage pattern of the building at location (1), (2) and (3)

6.10 Conclusion

Despite the challenging modal identification in this case study, the 3D AEM model updating was successfully accomplished with only one modal frequency and mode shape data. The results showed an acceptable margin of error between the experimental and numerical models. The study encountered specific limitations concerning the measurement locations, which may have implications for the precision of the model updating process. Incorporating supplementary measurement data has the potential to enhance the overall accuracy and reliability of the model updating methodology. Overall, the results of this case study demonstrate that even with a limited number of modes and limited measurements obtained from the field, an accurate numerical model can be updated using the proposed method. In 3D AEM model updating, the proper grouping of elements plays a vital role. To ensure a well-defined solution, the number of unknowns or updating parameters should not exceed the number of residual equations. Given the structure's good condition with no visible damage and regular maintenance, the element grouping was performed thoughtfully, focusing on grouping together elements with

similar material properties. This approach kept the number of groups within acceptable limits based on the available equations. The columns, RC shear walls, beams/slabs, and masonry walls on each floor were grouped separately, resulting in a favorable alignment between real existing structure and the numerical 3D AEM model. To initialize the model-updating parameters (Young's Modulus), engineering judgment was employed. This allowed for an approximate estimation of the actual values and improved the optimization convergence.

The findings derived from the static pushover analysis reveal notable structural damage manifested initially in the ground floor masonry wall, which subsequently culminated in the failure of the beam-column joint and eventual collapse of the entire structure. Notably, the inter-storey drift ratio exhibits a substantial increase on the first(ground) floor comparing to the top floor, following the initial failure of the ground floor wall, thereby imparting behavior akin to a soft storey phenomenon. The observed failure patterns in the structure encompass in-plane shear cracks, on-plane failure of the masonry wall, and tensile failure at the beam-column joint.

Chapter 7: Conclusions and Future Works

7.1 Summary

Firstly, the least square problem for model updating which is suitable for low to mid rise buildings having limited no. of operational modal data and limited measurements is developed and successfully tested for the generalized frame structures.

The sensitivity-based model updating technique has been effectively incorporated into the three-dimensional applied element method (AEM), enabling the utilization of a minimal no. of dofs for measurement and a limited set of modes. This approach facilitates the adjustment of parameters within the numerical model. By employing sensitivity analysis, the method identifies the influence of each parameters on the response of the model, allowing for targeted modifications to improve accuracy and reliability. Through this process, the updated numerical model aligns more closely with the measured data, enhancing its predictive capabilities and ensuring greater fidelity in structural analysis and design.

The 3D Applied Element Method (AEM) is a powerful computational technique that has proven its efficacy in capturing the intricate non-linear behavior of structures, ranging from the early stages of crack initiation to the ultimate point of complete collapse. By employing static or dynamic non-linear analysis, AEM can accurately simulate and predict the response of complex structures subjected to various loading conditions. Unlike traditional methods, AEM accounts for the inherent non-linearities present in the structural materials, allowing for a more realistic representation of their mechanical response. This method leverages the discrete nature of the elements used in its formulation to model the localized behavior of cracks, yielding precise predictions of crack propagation and failure mechanisms.

However, there is always a big challenge of computational efficiency and matrix storage in the 3D AEM tool. To improve the computational efficiency of the 3D AEM tool developed in FORTRAN90 has been tested with three different linear solvers: direct solver with skyline storage format, iterative solver with triplet storage format and parallel direct sparse solver (PARDISO) with triplet storage format. The parallel direct sparse solver (PARDISO) with triplet storage format is found to be the most efficient among all and is used for the developed 3D AEM tool.

Starting with the measurement of the ambient vibration of structure to operational modal analysis, numerical model updating in 3D AEM to seismic vulnerability assessment of the structure a complete system has been developed. Different performance criteria are used to study the vulnerability of the structure. First, the interstorey drift ratio is a crucial parameter for evaluating the damage sustained by each storey in a structure. By measuring the displacement between adjacent floors during an earthquake, it provides a quantitative measure of the structural damage. Additionally, incremental dynamic analysis offers a comprehensive assessment of the structure's overall capacity by subjecting it to progressively increasing ground motion intensities. This analysis technique allows engineers to gauge the structure's ability to withstand seismic forces and determine its performance under varying levels of ground motion. Another essential performance criterion is the Frequency degradation ratio (FDR), which reflects the stiffness degradation of the structure. By quantifying how the structure's natural frequencies change due to damage, FDR provides valuable insights into the global damage suffered by the structure. These performance criteria, namely interstorey drift ratio and FDR, play a significant role in optimizing the design of structures to enhance their seismic performance. Engineers have the opportunity to utilize this information in order to create stronger structures that are capable of withstanding earthquakes more effectively.

The precision of the model updating method relies significantly on initial guess of the updating parameters. When attempting to implement this method in real structures, obtaining the initial guess from a database of similar structures with comparable characteristics, the method can be effectively and successfully applied. This approach allows for a more precise estimation and adjustment of the updating parameters, leading to improved accuracy in the overall analysis or prediction of the real structures under consideration.

7.2 Limitations

There are certain limitations of this studies:

- There were challenges in assessing ambient vibrations of buildings at all critical locations.
- Acquiring higher modes proves to be challenging, and as damping in the structure increases, the accuracy of updates diminishes due to the increased occurrence of spurious higher modes. The accurate identification of higher modes and mode shapes in modal analysis presents inherent difficulties, leading to potential inaccuracies in the results.
- The model updating is based on local optimization using Levenberg-Marquardt algorithm. So, occasionally the optimization process will be impeded by instances of converging towards local minima, primarily attributed to suboptimal initial guesses.
- Presently, our capability is limited to representing the structure in 3D using the Applied Element Method with elements of the same size. Unfortunately, this approach results in an excessive number of elements, which is unnecessary.

7.3 Future Works

7.3.1 Data-driven approach combined with the proposed method for model updating.

The effectiveness of updating a model using the sensitivity method integrated in 3D AEM relies heavily on the preliminary estimation of the updating parameters according to the conclusion of this research. The accuracy and reliability of this methodology are closely tied to the initial guess of the updating parameters, making it a crucial factor for successful implementation in real structures. When the preliminary guess is afar from the actual solution, the optimization process using the sensitivity method can yield to a local minimum, leading to suboptimal results Figure 7-1. To address this issue, it is crucial to have an initial guess for the updating parameters that is close to the solution. One approach to achieve this is by leveraging a comprehensive database of analogous structures. By drawing upon the wealth of information available in such a database, it becomes possible to obtain reasonable approximations for the preliminary values of the updating parameters. This, in turn, enhances the accuracy and applicability of the sensitivity method integrated in 3D AEM when applied to real-world structures.

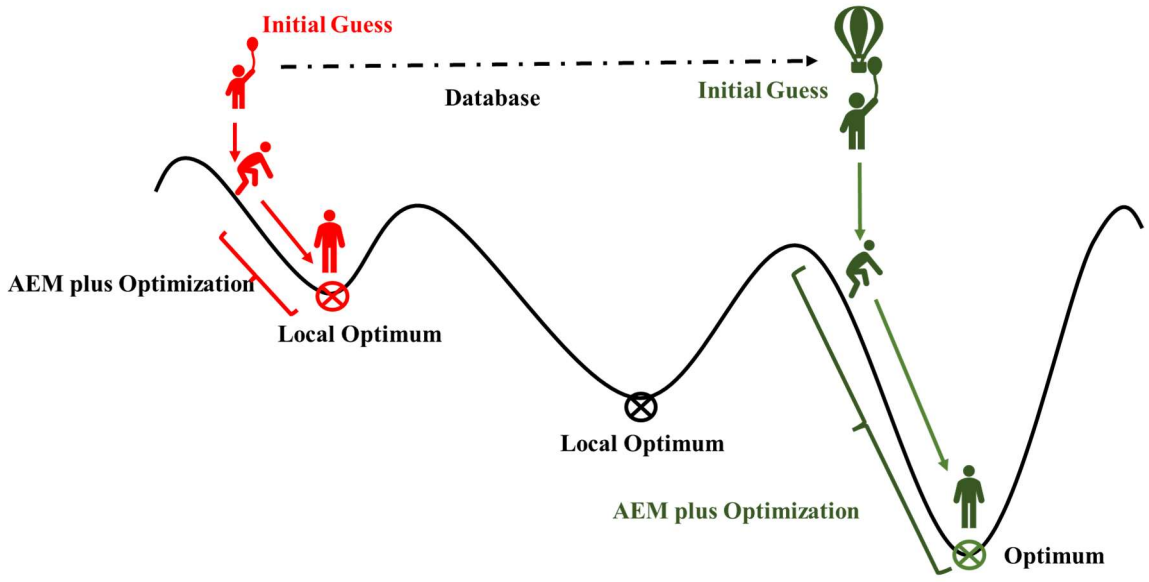

Figure 7-1 : Need of database for increasing accuracy of model updating

7.3.2 Bayesian method for model updating in 3D AEM.

After the successful implementation of the sensitivity-base model updating in 3D AEM, in future there is possibility to implement the probabilistic method of model updating. The Bayesian method can be the one which can be considered. The implementation of the Bayesian method in 3D AEM can be the future scope of this research.

7.3.3 CUDA based solver to improve the computational efficiency of the 3D AEM

The 3D AEM is a powerful numerical technique used for analyzing complex engineering problems by discretizing structures into smaller elements. However, its computationally intensive nature often demands substantial computing resources, leading to prolonged analysis times. Currently, parallel direct solver (PARDISO) is implemented in 3D AEM to solve the structural problem, that uses the capability of CPU threads but still for the large structures it is not very efficient. So, we aim to explore the potential of CUDA-based solvers to significantly boost the computational efficiency of 3D Applied Element Method (AEM) simulations. To address this challenge, we intend to leverage CUDA, the parallel computing platform from NVIDIA, to develop a high-performance solver that harnesses the power of GPUs for accelerating the resolution of large linear systems inherent in the AEM. By taking advantage of the GPU's parallel processing capabilities, we anticipate achieving substantial speedups, making 3D AEM simulations more accessible for real-world engineering applications with stringent time constraints. This research holds the potential to revolutionize the efficiency of 3D AEM simulations and pave the way for more advanced and accurate engineering analyses.

7.3.4 Modelling of structures with non-uniform elements sizes in 3D AEM

The Applied Element Method (AEM) has shown great promise in efficiently simulating complex structures, yet its full potential remains untapped when dealing with non-uniform element sizes in three-dimensional scenarios. With the non-uniform element sizes we can significantly reduce the total number of elements in complex large structures and also we can

efficiently model the non-engineered structures very efficiently. This study seeks to develop novel algorithms and methodologies that accommodate varying element sizes, enabling more accurate and realistic simulations of real-world structures. By addressing this critical limitation, the research endeavors to enhance the overall performance and reliability of the AEM for practical engineering applications, contributing significantly to the advancement of structural analysis and design in various industries.

References

[1] Central Beareu of Statistics (CBS), "National Population and Housing Census 2011, National Report," 2012.

[2] JICA, "The study on Earthquake Disaster Mitigation," 2002.

[3] T. R. Naik, V. M. Malhotra, and J. S. Popovics, "The ultrasonic pulse velocity method," in *Handbook on Nondestructive Testing of Concrete, Second Edition*, CRC Press, 2003, pp. 8–1.

[4] T. Akashi and S. Amasaki, "Study of the stress waves in the plunger of a rebound hammer at the time of impact," *Spec. Publ.*, vol. 82, pp. 17–34, 1984.

[5] J. Helal, M. Sofi, and P. Mendis, "Non-destructive testing of concrete: A review of methods," *Electron. J. Struct. Eng.*, vol. 14, no. 1, pp. 97–105, 2015.

[6] NSET, "Seismic vulnerability evaluation guideline for private and public buildings Part-1: Pre disaster vulnerability assessment, Government of Nepal, Ministry of Physical Planning and Works," 2009.

[7] N. NDMA, "Seismic Vulnerability Assessment of Building Types in India NDMAGo India." 2013.

[8] M. R. Tabeshpour, A. Bakhshi, and A. A. Golafshani, "Vulnerability and damage analyses of existing buildings," in *13th World conference on earthquake engineering*, 2004.

[9] T. Rossetto and A. Elnashai, "A new analytical procedure for the derivation of displacement-based vulnerability curves for populations of RC structures," *Eng. Struct.*, vol. 27, no. 3, pp. 397–409, 2005.

[10] A. J. Kappos, G. Panagopoulos, C. Panagiotopoulos, and G. Penelis, "A hybrid method for the vulnerability assessment of R/C and URM buildings," *Bull. Earthq. Eng.*, vol. 4, no. 4, pp. 391–413, 2006.

[11] M. Remki and D. Benouar, "Damage potential and vulnerability functions of strategic buildings in the city of Algiers," *KSCE J. Civ. Eng.*, vol. 18, no. 6, pp. 1726–1734, 2014.

[12] F. Wang and T. Chan, "Review of vibration-based damage detection and condition assessment of bridge structures using structural health monitoring," in *Proceedings of the Second Infrastructure Theme Postgraduate Conference: Rethinking Sustainable Development-Planning, Infrastructure Engineering, Design and Managing Urban Infrastructure*, Queensland University of Technology, 2009, pp. 35–47.

[13] F. Uehan and K. Meguro, "Assessment of seismic damage to railway structures using applied element method and microtremor measurement," in *13th World Conference on Earthquake Engineering Vancouver, BC, Canada August*, 2004, pp. 1–6.

[14] R. D. Sill, "Minimizing measurement uncertainty in calibration and use of accelerometers," *Endevco Tech. Pap. TP299*, 2010.

[15] J. Mottershead and M. Friswell, "Model Updating In Structural Dynamics: A Survey," *J. Sound Vib. - J Sound Vib*, vol. 167, pp. 347–375, Oct. 1993, doi: 10.1006/jsvi.1993.1340.

[16] C. Ventura, H. Prion, C. Black, M. Rezai, and V. Latendresse, "Modal properties of a steel frame used for seismic evaluation studies," in *Proceedings of the 15th International Modal Analysis Conference*, 1997, p. 1885.

[17] R. Brincker, L. Zhang, and P. Andersen, "Output-only modal analysis by frequency domain decomposition," in *Proceedings of ISMA25: 2000 International Conference on Noise and Vibration Engineering*, Katholieke Universiteit, Leuven, 2000, pp. 717–723.

[18] R. Brincker and P. Andersen, “Understanding stochastic subspace identification,” in *Conference Proceedings: IMAC-XXIV: A Conference & Exposition on Structural Dynamics*, Society for Experimental Mechanics, 2006.
[19] O. C. Zienkiewicz, R. L. Taylor, and J. Z. Zhu, *The finite element method: its basis and fundamentals*. Elsevier, 2005.
[20] P. A. Cundall and O. D. Strack, “A discrete numerical model for granular assemblies,” *geotechnique*, vol. 29, no. 1, pp. 47–65, 1979.
[21] M. Friswell and J. E. Mottershead, *Finite element model updating in structural dynamics*, vol. 38. Springer Science & Business Media, 1995.
[22] T. Marwala, “Finite-element-model updating using computional intelligence techniques: Applications to structural dynamics,” 2010.
[23] D. C. Zimmerman and M. Kaouk, “Eigenstructure assignment approach for structural damage detection,” *AIAA J.*, vol. 30, no. 7, pp. 1848–1855, 1992.
[24] M. Baruch, “Optimization procedure to correct stiffness and flexibility matrices using vibration tests,” *AIAA J.*, vol. 16, no. 11, pp. 1208–1210, 1978.
[25] S. Sehgal and H. Kumar, “Structural Dynamic Model Updating Techniques: A State of the Art Review,” *Arch. Comput. Methods Eng.*, vol. 23, no. 3, pp. 515–533, Sep. 2016, doi: 10.1007/s11831-015-9150-3.
[26] E. Yu, S.-N. Kim, T. Park, and S.-H. Lee, “Detection of earthquake-induced damage in a framed structure using a finite element model updating procedure,” *Sci. World J.*, vol. 2014, 2014.
[27] F. Sarvi, S. Shojaee, and P. Torkzadeh, “Damage identification of trusses by finite element model updating using an enhanced Levenberg-Marquardt algorithm,” vol. 4, no. 2, pp. 207–231, 2014.
[28] W.-X. Ren and H.-B. Chen, “Finite element model updating in structural dynamics by using the response surface method,” *Eng. Struct.*, vol. 32, no. 8, pp. 2455–2465, 2010.
[29] V. Arora, “Comparative study of finite element model updating methods,” *J. Vib. Control*, vol. 17, no. 13, pp. 2023–2039, 2011.
[30] T. Marwala and S. Sibisi, “Finite element model updating using Bayesian framework and modal properties,” *J. Aircr.*, vol. 42, no. 1, pp. 275–278, 2005.
[31] H.-F. Lam and J. Yang, “Bayesian structural damage detection of steel towers using measured modal parameters,” *Earthq. Struct.*, vol. 8, no. 4, pp. 935–956, 2015.
[32] H. Sohn and K. H. Law, “Bayesian probabilistic damage detection of a reinforced-concrete bridge column,” *Earthq. Eng. Struct. Dyn.*, vol. 29, no. 8, pp. 1131–1152, 2000.
[33] Q.-G. Fei, A.-Q. Li, and C.-Q. Miao, “Dynamic finite element model updating using meta-model and genetic algorithm,” *J. Southeast Univ. Engl. Ed.*, vol. 22, no. 2, pp. 213–217, 2006.
[34] J. Zapico, A. González-Buelga, M. Gonzalez, and R. Alonso, “Finite element model updating of a small steel frame using neural networks,” *Smart Mater. Struct.*, vol. 17, no. 4, p. 045016, 2008.
[35] K. Deb, “Multi-objective optimisation using evolutionary algorithms: an introduction,” in *Multi-objective evolutionary optimisation for product design and manufacturing*, Springer, 2011, pp. 3–34.
[36] K. Deb, *Optimization for engineering design: Algorithms and examples*. PHI Learning Pvt. Ltd., 2012.
[37] C. Gentile and A. Saisi, “Ambient vibration testing of historic masonry towers for structural identification and damage assessment,” *Constr. Build. Mater.*, vol. 21, no. 6, pp. 1311–1321, 2007.

[38] B. Sevim, A. Bayraktar, A. C. Altunişik, S. Atamtürktür, and F. Birinci, "Finite element model calibration effects on the earthquake response of masonry arch bridges," *Finite Elem. Anal. Des.*, vol. 47, no. 7, pp. 621–634, 2011.
[39] G. Lacanna, M. Ripepe, E. Marchetti, M. Coli, and C. A. Garzonio, "Dynamic response of the Baptistery of San Giovanni in Florence, Italy, based on ambient vibration test," *J. Cult. Herit.*, vol. 20, pp. 632–640, 2016.
[40] G. Osmancikli, A. Bayraktar, T. Türker, Ş. Uçak, and A. Mosallam, "Finite element model calibration of precast structures using ambient vibrations," *Constr. Build. Mater.*, vol. 93, pp. 10–21, 2015.
[41] A. C. Altunişik, A. Bayraktar, B. Sevim, and H. Özdemir, "Experimental and analytical system identification of Eynel arch type steel highway bridge," *J. Constr. Steel Res.*, vol. 67, no. 12, pp. 1912–1921, 2011.
[42] C. Gentile and A. E. Saisi, "Structural Health Monitoring of a centenary iron arch bridge: 1. Ambient vibration tests and condition assessment," in *4th Int. Conf. on Experimental Vibration Analysis for Civil Engineering Structures (EVACES'11)*, Starrylink Editrice, 2011, pp. 121–130.
[43] C. Ventura, J.-F. Lord, and R. Simpson, "effective use of ambient vibration measurements for modal updating of a 48-storey building in Vancouver, Canada," Jan. 2002.
[44] J. R. Wu and Q. S. Li, "Finite element model updating for a high-rise structure based on ambient vibration measurements," *Eng. Struct.*, vol. 26, no. 7, pp. 979–990, Jun. 2004, doi: 10.1016/j.engstruct.2004.03.002.
[45] D. Skolnik, E. Yu, J. Wallace, and E. Taciroglu, "Modal system identification and finite element model updating of a 15-story building using earthquake and ambient vibration data," *Struct. Eng. Res. Front.*, pp. 1–14, 2007.
[46] B. Weber, P. Paultre, and J. Proulx, "Structural damage detection using nonlinear parameter identification with Tikhonov regularization," *Struct. Control Health Monit. Off. J. Int. Assoc. Struct. Control Monit. Eur. Assoc. Control Struct.*, vol. 14, no. 3, pp. 406–427, 2007.
[47] S. R. Shiradhonkar and M. Shrikhande, "Seismic damage detection in a building frame via finite element model updating," *Comput. Struct.*, vol. 89, no. 23, pp. 2425–2438, Dec. 2011, doi: 10.1016/j.compstruc.2011.06.006.
[48] M. M. Akhlaghi, S. Bose, B. Moaveni, and A. Stavridis, "Bayesian Model Updating of a Damaged School Building in Sankhu, Nepal," in *Model Validation and Uncertainty Quantification, Volume 3*, Springer, 2019, pp. 235–244.
[49] O. C. Zienkiewicz and P. Morice, *The finite element method in engineering science*, vol. 1977. McGraw-hill London, 1971.
[50] B. Dutta, A. Kakodkar, and S. MAITI, "Use of Two Singular Point Finite Elements in the Analysis of Kinked Cracks," in *Proceedings of The 7th International Conference On Fracture (ICF7)*, Elsevier, 1989, pp. 2315–2322.
[51] K. Meguro and M. Hakuno, "Fracture analyses of concrete structures by the modified distinct element method," *Doboku Gakkai Ronbunshu*, vol. 1989, no. 410, pp. 113–124, 1989.
[52] K. Meguro and M. Hakuno, "Application of the extended distinct element method for collapse simulation of a doubledeck bridge," *Doboku Gakkai Ronbunshu*, vol. 1994, no. 483, pp. 17–27, 1994.
[53] T.-D. Hatem, "A new efficient method for nonlinear, large deformation and collapse analysis of strutures." PhD Thesis, The University of Tokyo, 1998.
[54] C. Farhat and F. M. Hemez, "Updating finite element dynamic models using an element-by-element sensitivity methodology," *AIAA J.*, vol. 31, no. 9, pp. 1702–1711, 1993.

[55] R. B. Lehoucq, D. C. Sorensen, and C. Yang, *ARPACK Users' Guide*. Society for Industrial and Applied Mathematics, 1998. doi: 10.1137/1.9780898719628.
[56] A. Teughels, J. Maeck, and G. De Roeck, "A finite element model updating method using experimental modal parameters applied on a railway bridge," *WIT Trans. Built Environ.*, vol. 54, 2001.
[57] J. J. Moré, "The Levenberg-Marquardt algorithm: implementation and theory," in *Numerical Analysis: Proceedings of the Biennial Conference Held at Dundee, June 28–July 1, 1977*, Springer, 2006, pp. 105–116.
[58] T. Kawai, "Recent developments of the Rigid Body and Spring Model (RBSM) in structural analysis," in *Seiken Seminar Text Book*, Institute of Industrial Science, The University of Tokyo, 1986, pp. 226–237.
[59] T.-D. Hatem, "a new efficient method for nonlinear, large deformation and collapse analysis of strutures." PhD Thesis, The University of Tokyo, 1998.
[60] K. Meguro and H. Tagel-Din, "Applied Element Method for Structural Analysis," *Doboku Gakkai Ronbunshu*, vol. 2000, no. 647, pp. 31–45, 2000.
[61] K. Muto, "Strength and Deformation of Structures." Maruzen Publishing Co. Ltd.,(in Japanese), 1965.
[62] A. Filiatrault, É. Lachapelle, and P. Lamontagne, "Seismic performance of ductile and nominally ductile reinforced concrete moment resisting frames. II. Analytical study," vol. 25, p. 11, 1998.
[63] A. Filiatrault, É. Lachapelle, and P. Lamontagne, "Seismic performance of ductile and nominally ductile reinforced concrete moment resisting frames. II. Analytical study," vol. 25, p. 12, 1998.
[64] S. H. Lo, "On bandsolver using skyline storage," *Comput. Struct.*, vol. 44, no. 6, pp. 1187–1196, Sep. 1992, doi: 10.1016/0045-7949(92)90362-4.
[65] T. A. Davis, S. Rajamanickam, and W. M. Sid-Lakhdar, "A survey of direct methods for sparse linear systems," *Acta Numer.*, vol. 25, pp. 383–566, 2016.
[66] R. Barrett *et al.*, *Templates for the solution of linear systems: building blocks for iterative methods*. SIAM, 1994.
[67] C. T. Kelley, *Iterative methods for linear and nonlinear equations*. SIAM, 1995.
[68] Y. Saad, *Iterative methods for sparse linear systems*. SIAM, 2003.
[69] O. Schenk and K. Gärtner, "Pardiso," 2010.
[70] D. S. Watkins, *Fundamentals of matrix computations*. John Wiley & Sons, 2004.
[71] I. S. Duff, A. M. Erisman, and J. K. Reid, *Direct methods for sparse matrices*. Oxford University Press, 2017.
[72] S. C. Eisenstat, M. Gursky, M. H. Schultz, and A. H. Sherman, "Yale sparse matrix package. i. the symmetric codes," Yale Univ New Haven Ct Dept of Computer Science, 1977.
[73] D. Vamvatsikos and C. A. Cornell, "Incremental dynamic analysis," *Earthq. Eng. Struct. Dyn.*, vol. 31, no. 3, pp. 491–514, 2002.
[74] A. Arias, "Measure of earthquake intensity.," Massachusetts Inst. of Tech., Cambridge. Univ. of Chile, Santiago de Chile, 1970.
[75] K. T. Shabestari and F. Yamazaki, "A Proposal of Instrumental Seismic Intensity Scale Compatible with MMI Evaluated from Three-Component Acceleration Records," *Earthq. Spectra*, vol. 17, no. 4, pp. 711–723, Nov. 2001.

Annexes

Annex 1: Structural details of the experimental frame

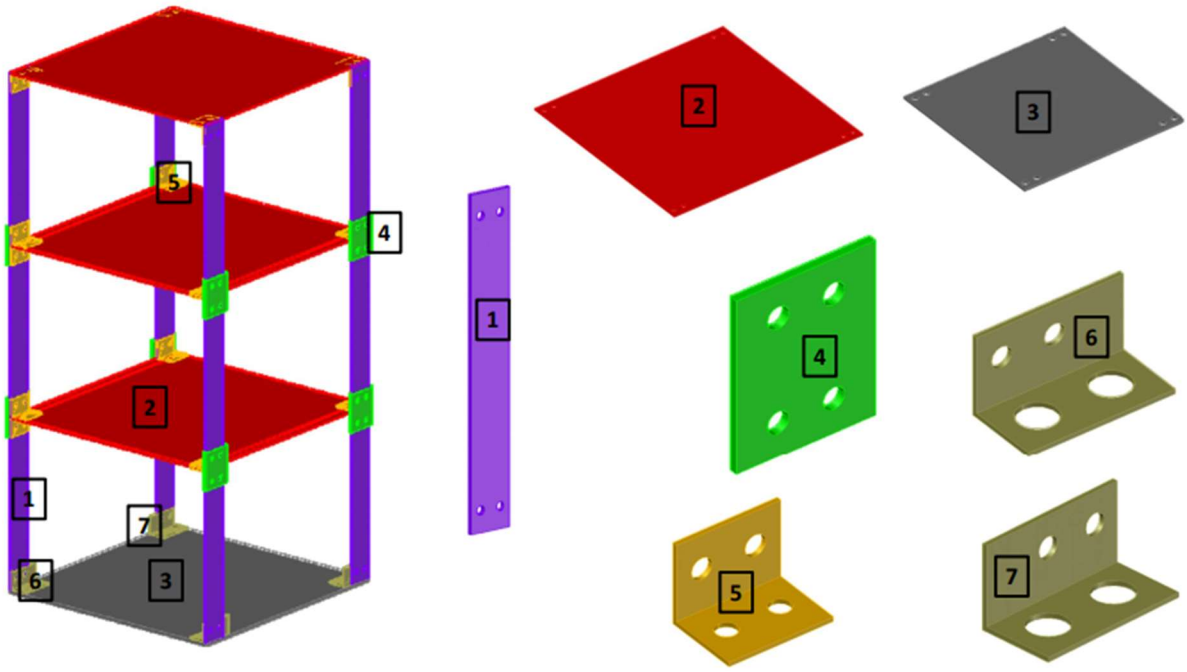

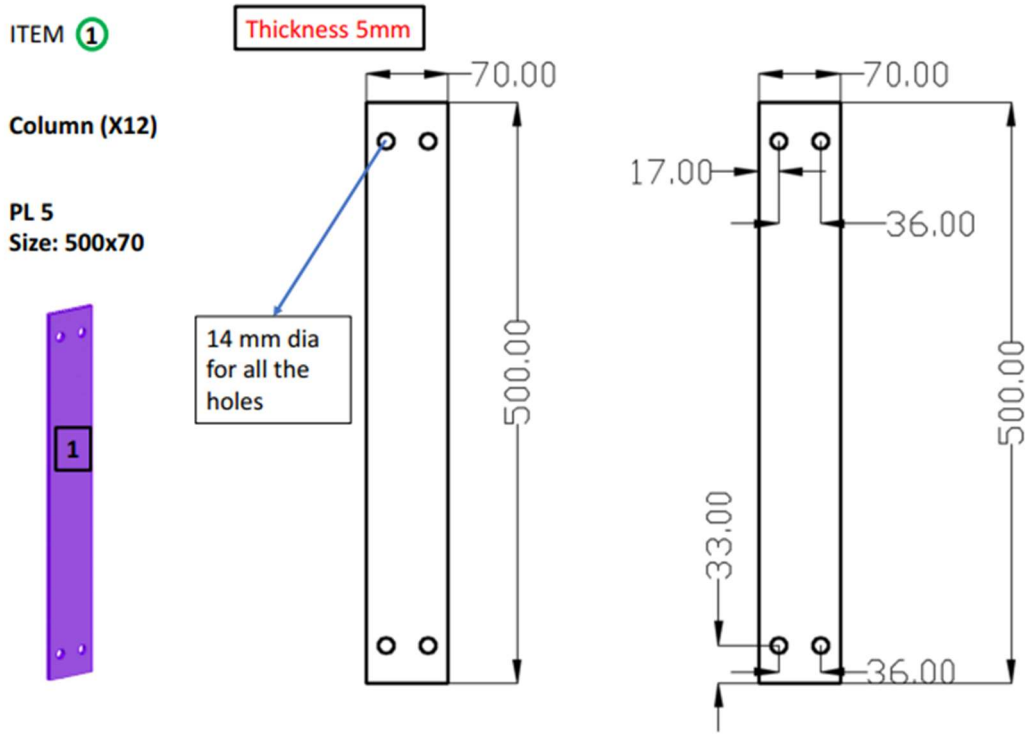

ITEM 2

Thickness 5mm

Floor Plate (X3)

PL 5
Size: 690X700

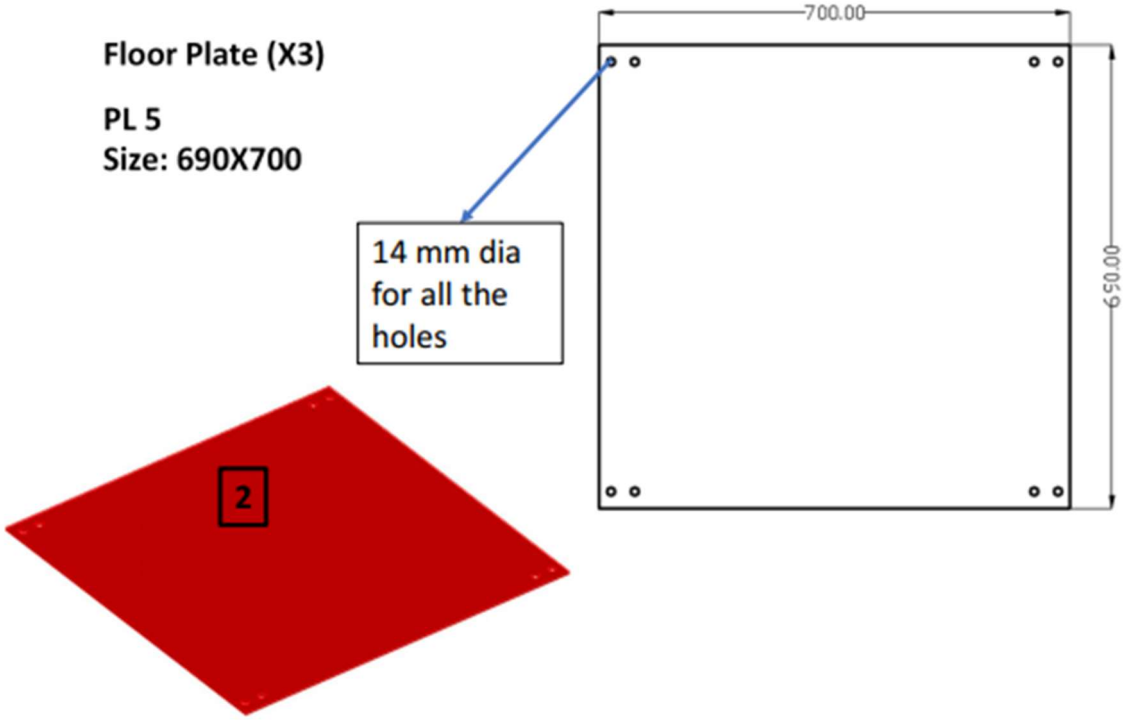

ITEM 3

Thickness 10mm

Floor Plate (X1)

PL 10
Size: 700X700

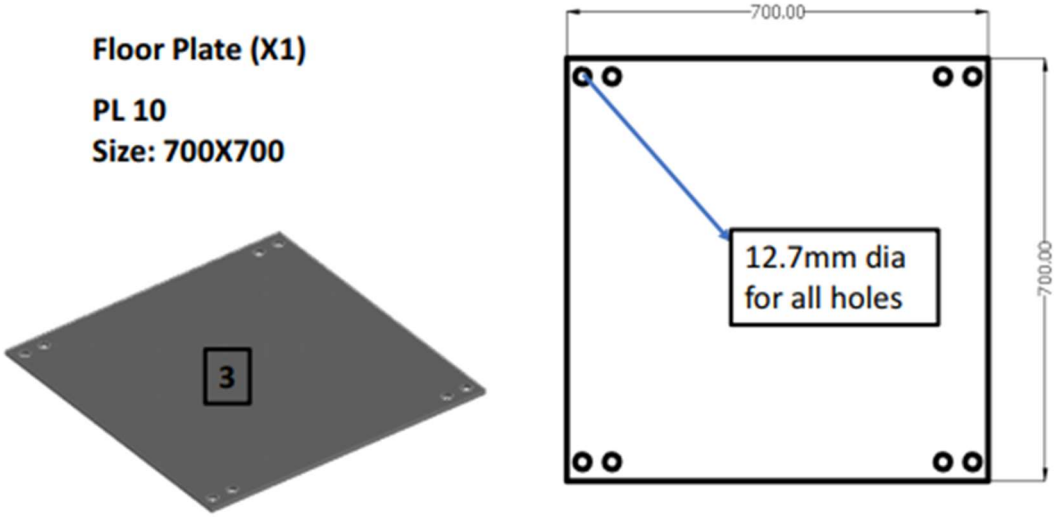

ITEM 4

Gusset Plates (X8)

PL-5

Size: 90X110

Thickness 5mm

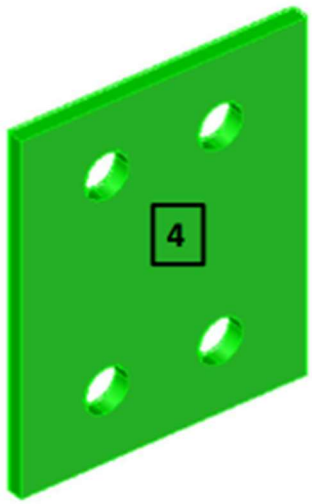

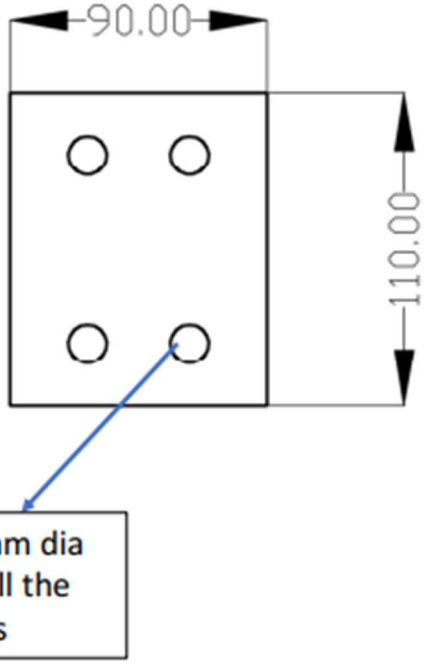

ITEM 5

Steel Angles (X20)

L-50X50X3

Length: 70mm

Thickness 5mm

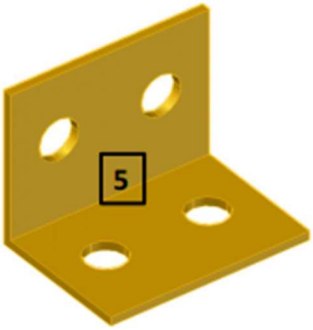

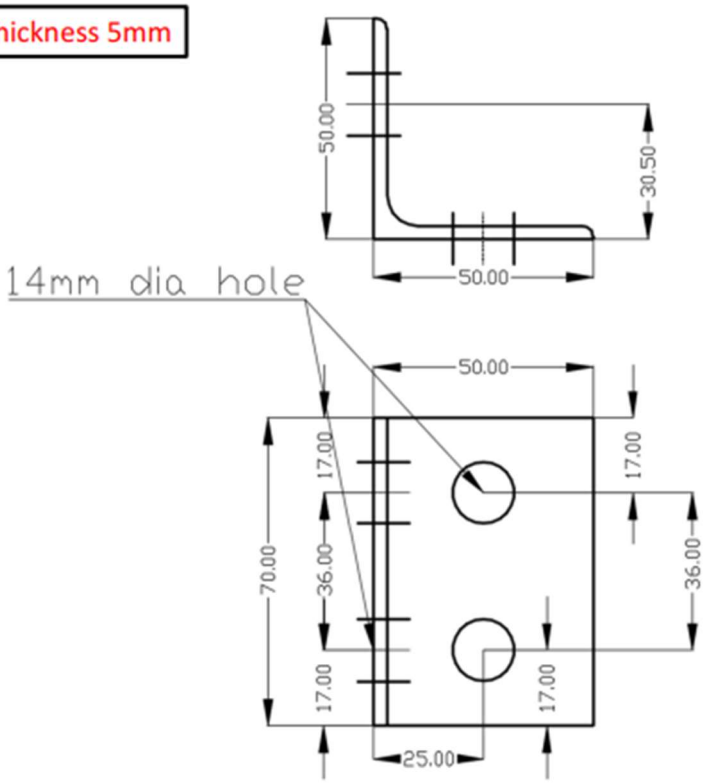

ITEM 6

Steel Angles (X2)

L-50X50X3

Length: 100mm

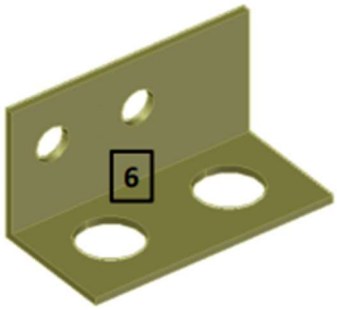

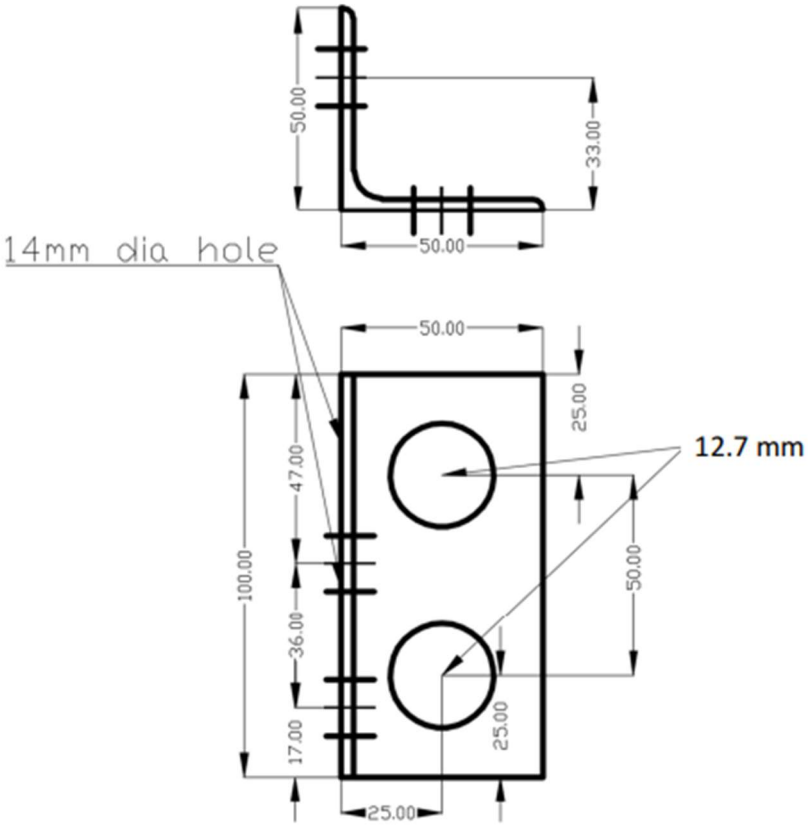

ITEM 7

Steel Angles (X2)

L-50X50X3

Length: 100mm

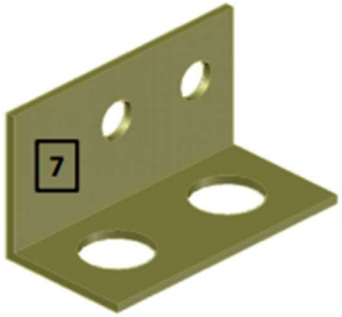

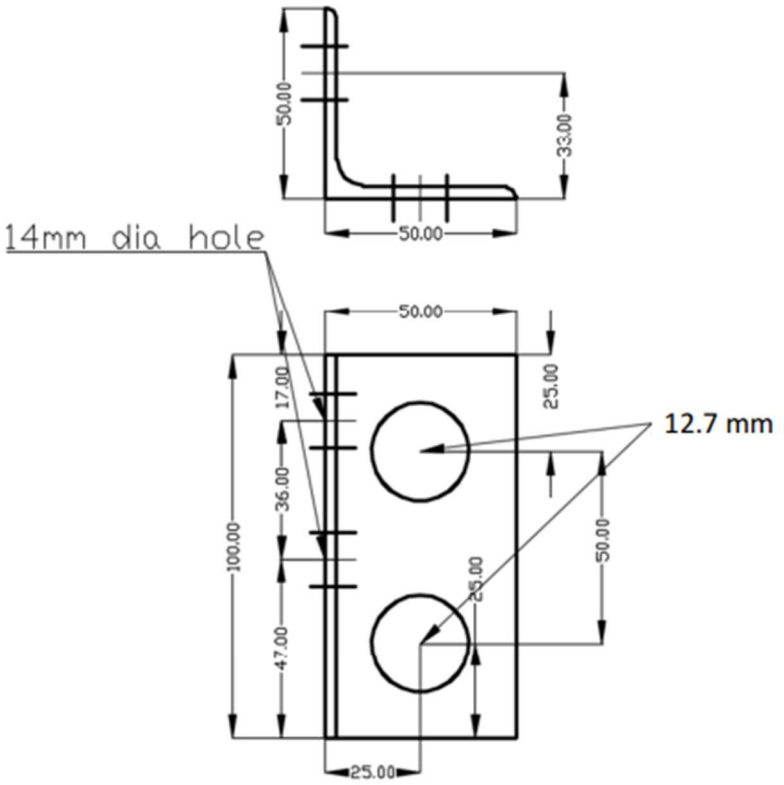

Annex 2: Structural and Architectural drawings of the field study building

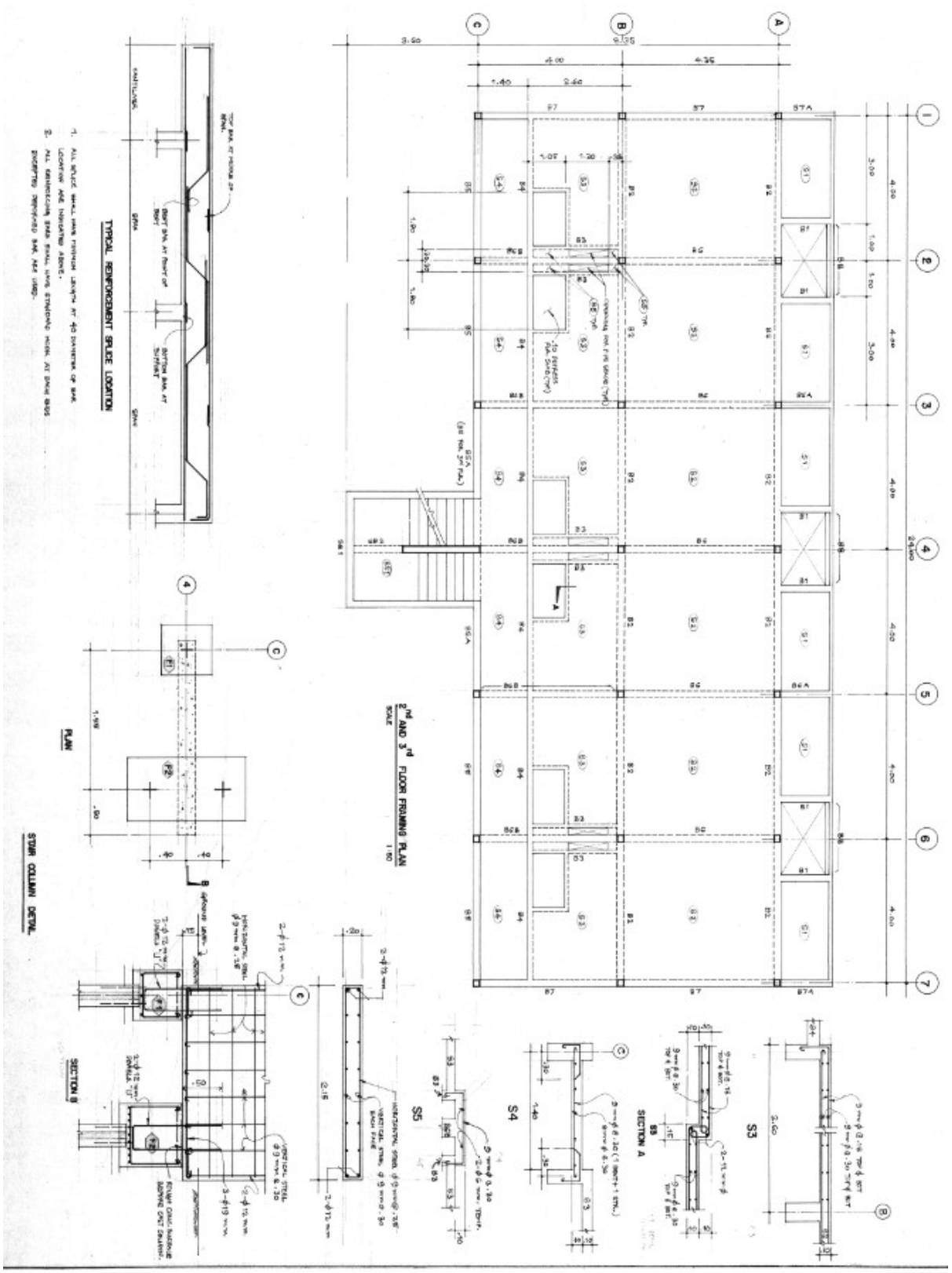

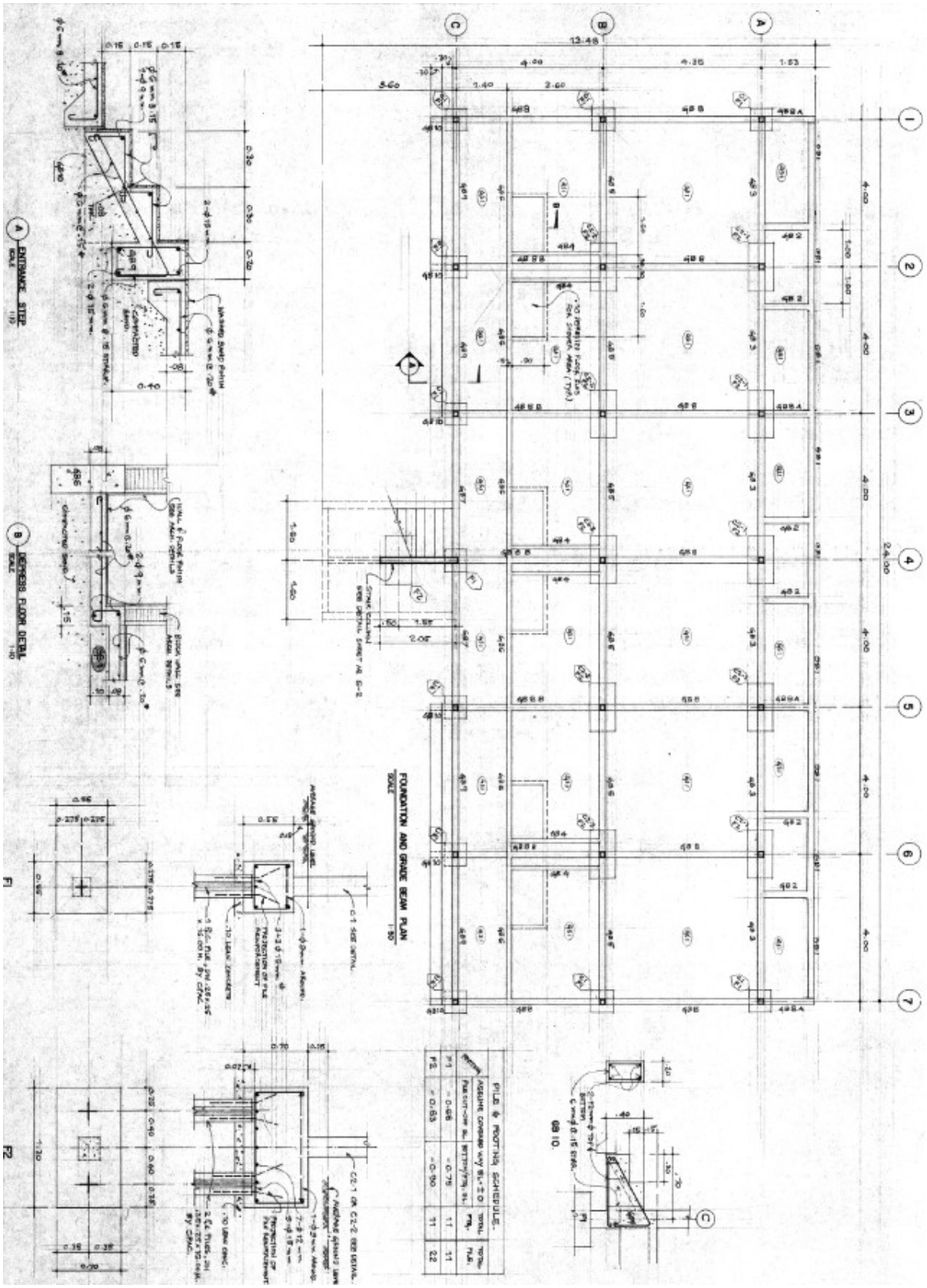
FOUNDATION AND GRADE BEAM PLAN
SCALE
1:50
A ENTRANCE STEP
SCALE
1:10
B DEPRESS FLOOR DETAIL
SCALE
1:10
PILE & FOOTING SCHEDULE
F1
F2
C2-1 OR C2-2 SEE DETAIL
SEE DETAIL SHEET NO S-2

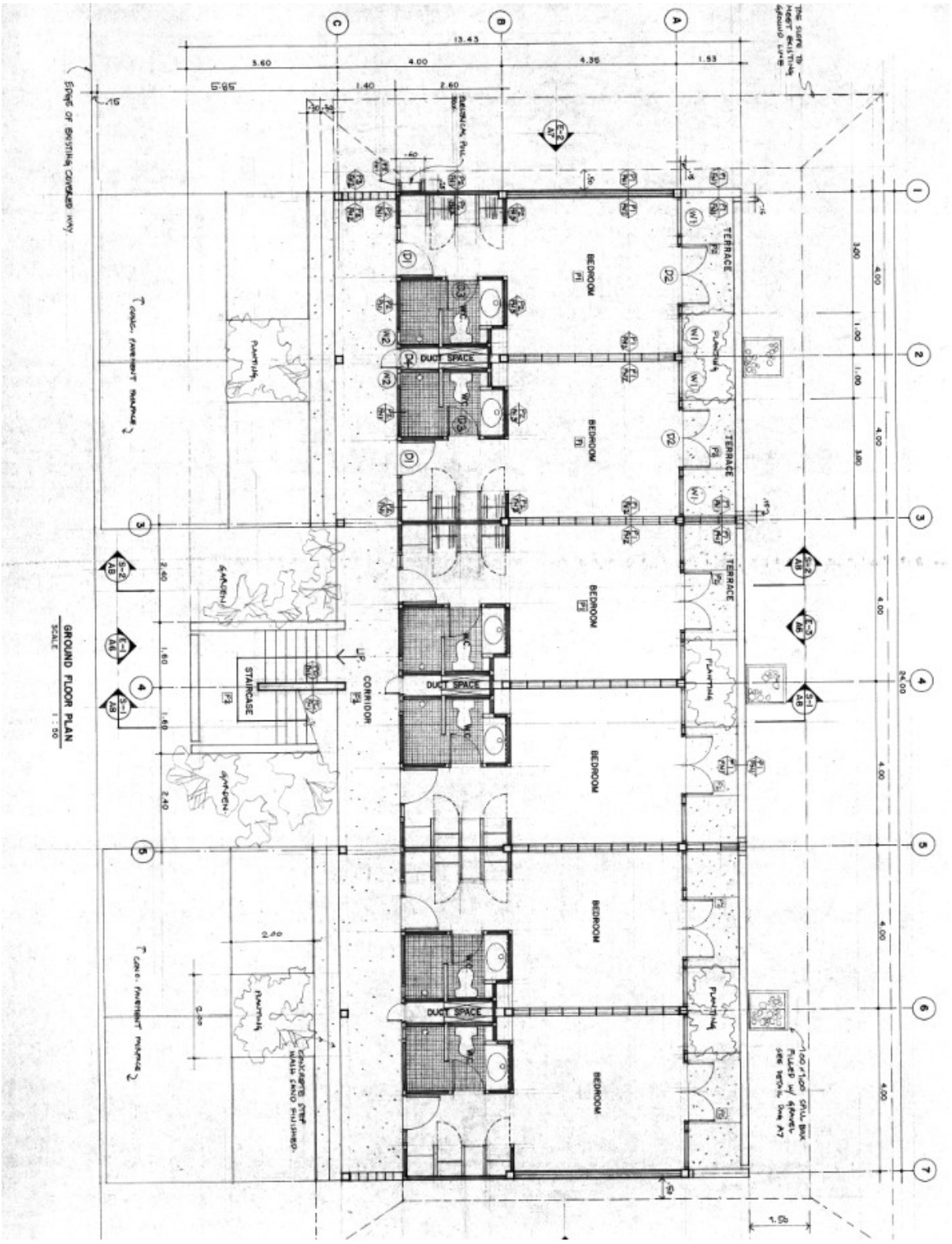
GROUND FLOOR PLAN
SCALE 1:50
BEDROOM
TERRACE
DUCT SPACE
WC
CORRIDOR
STAIRCASE
GARDEN
PLANTING
EDGE OF EXISTING CARRIAGE WAY
13.45
5.60
4.00
4.35
1.53
5.85
1.40
2.60
3.00
1.00
2.40
1.50

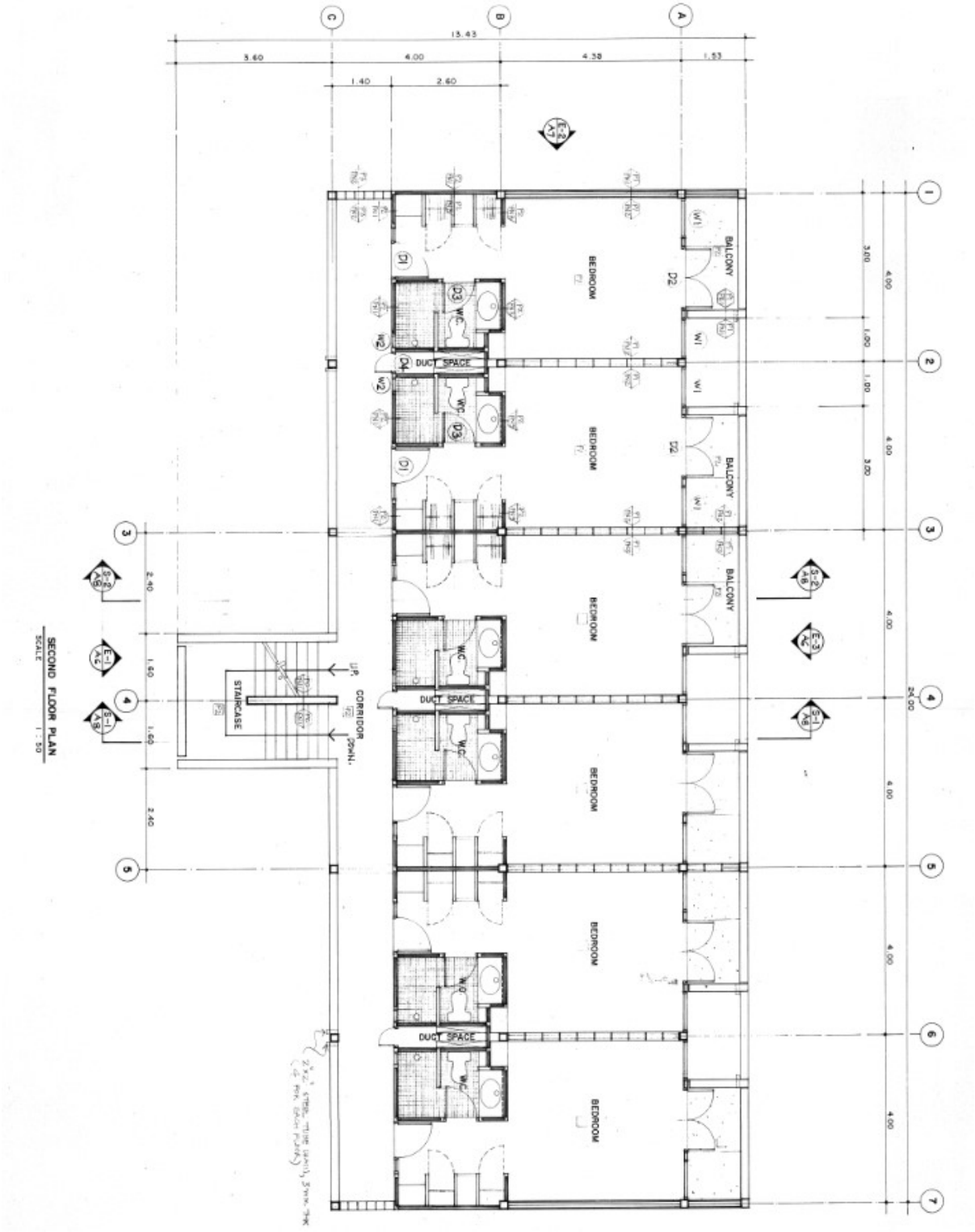
SECOND FLOOR PLAN
SCALE 1:50
BEDROOM
BALCONY
DUCT SPACE
W.C
STAIRCASE
UP
CORRIDOR
DN
13.43
5.60
4.00
4.38
1.53
1.40
2.60
2.40
1.60
24.00

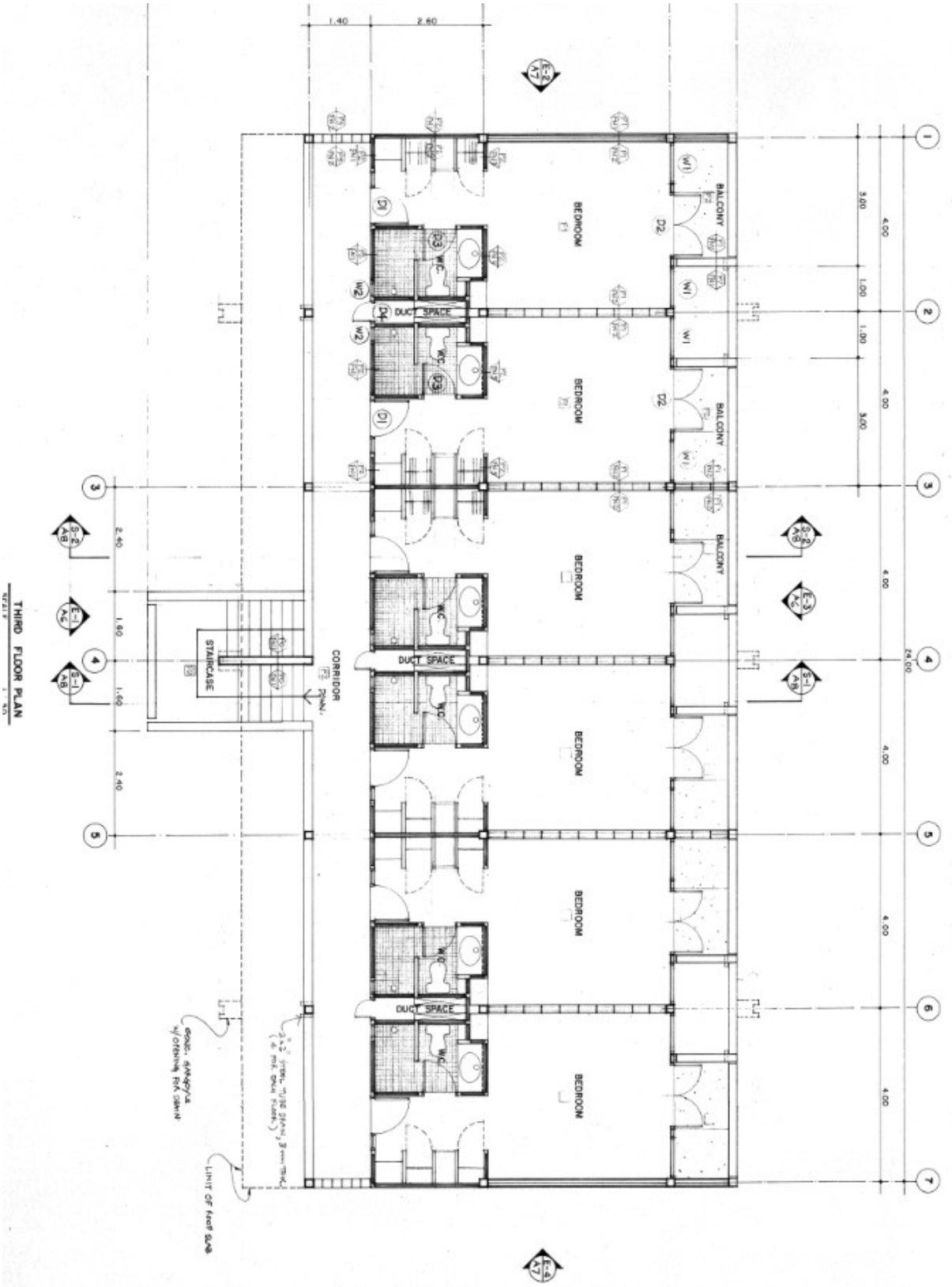
THIRD FLOOR PLAN
BEDROOM
BALCONY
DUCT SPACE
W.C.
CORRIDOR
STAIRCASE
LIMIT OF roof SLAB

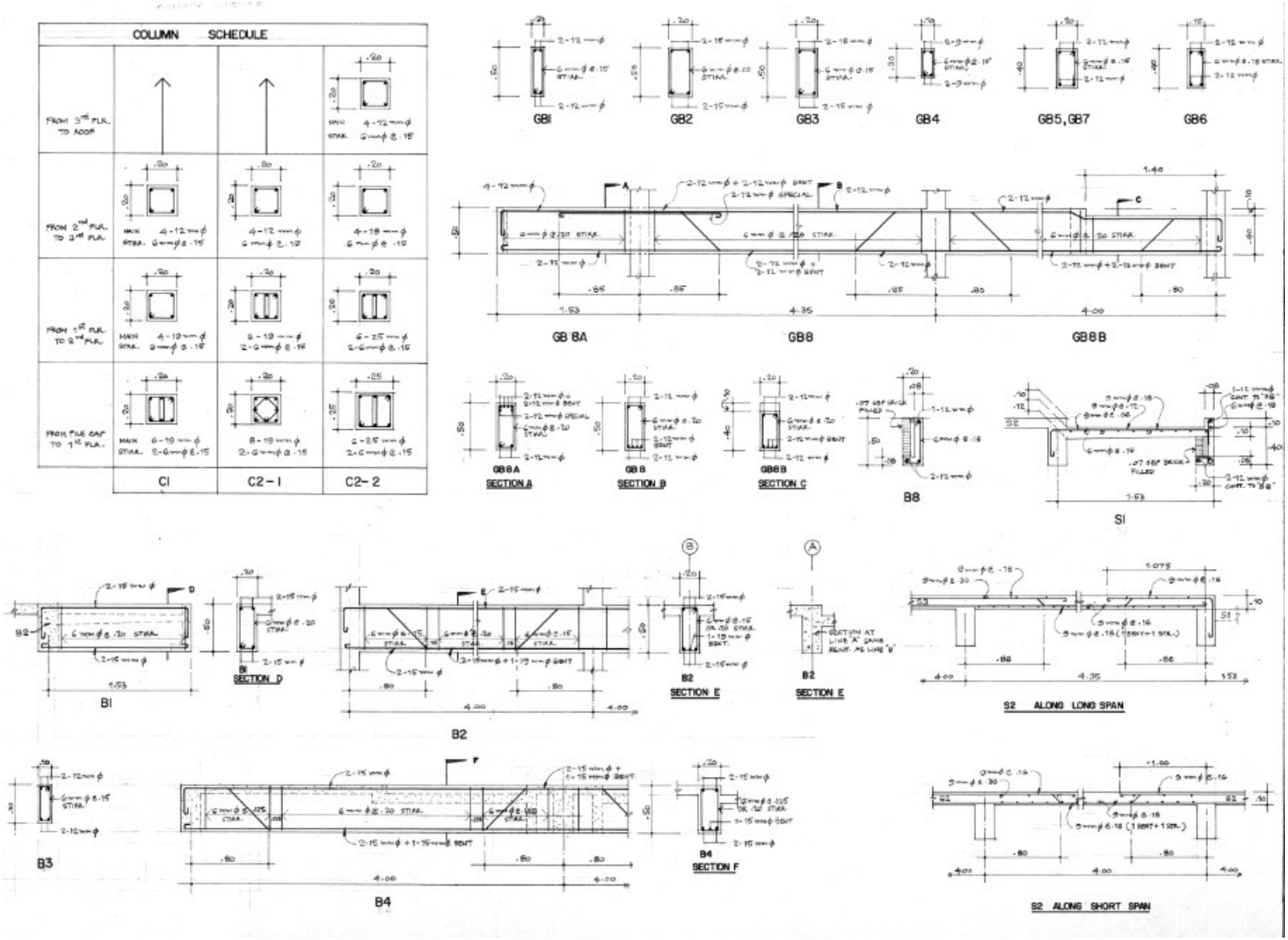
COLUMN SCHEDULE
FROM 3RD FLR. TO ROOF
FROM 2ND FLR. TO 3RD FLR.
FROM 1ST FLR. TO 2ND FLR.
FROM PILE CAP TO 1ST FLR.
C1
C2-1
C2-2
GB1
GB2
GB3
GB4
GB5, GB7
GB6
GB 8A
GB8
GB8B
SECTION A
SECTION B
SECTION C
B8
S1
B1
SECTION D
B2
SECTION E
SECTION E
S2 ALONG LONG SPAN
B3
B4
SECTION F
S2 ALONG SHORT SPAN

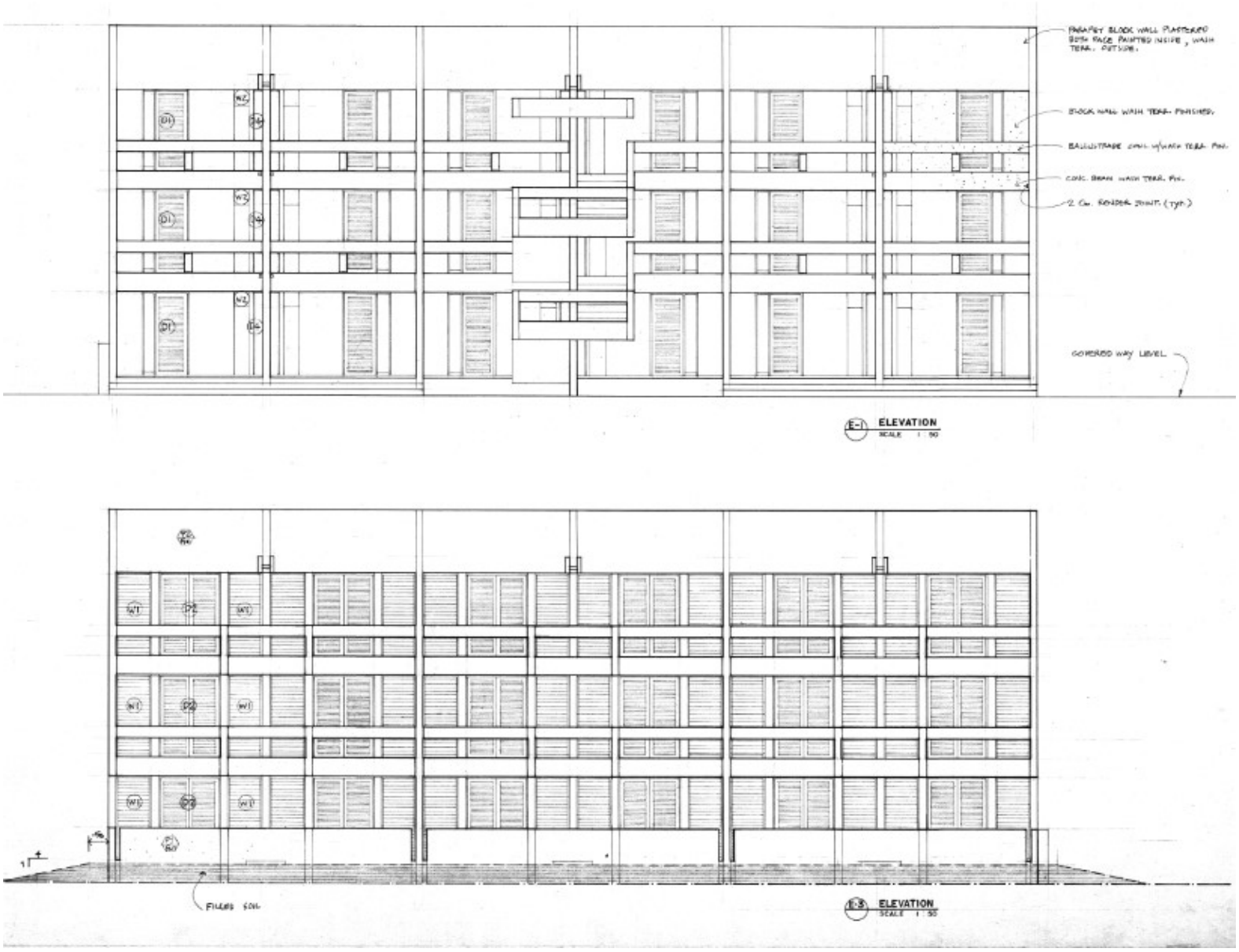
PARAPET BLOCK WALL PLASTERED BOTH FACE PAINTED INSIDE, WASH TERR. OUTSIDE.
BLOCK WALL WASH TERR. FINISHED.
BALUSTRADE CONC. W/WASH TERR. FIN.
CONC. BEAM WASH TERR. FIN.
2 Cm. REVERSE JOINT. (TYP.)
GOVERNED WAY LEVEL
E-1 ELEVATION
SCALE 1:50
FILLED SOIL
E-3 ELEVATION
SCALE 1:50

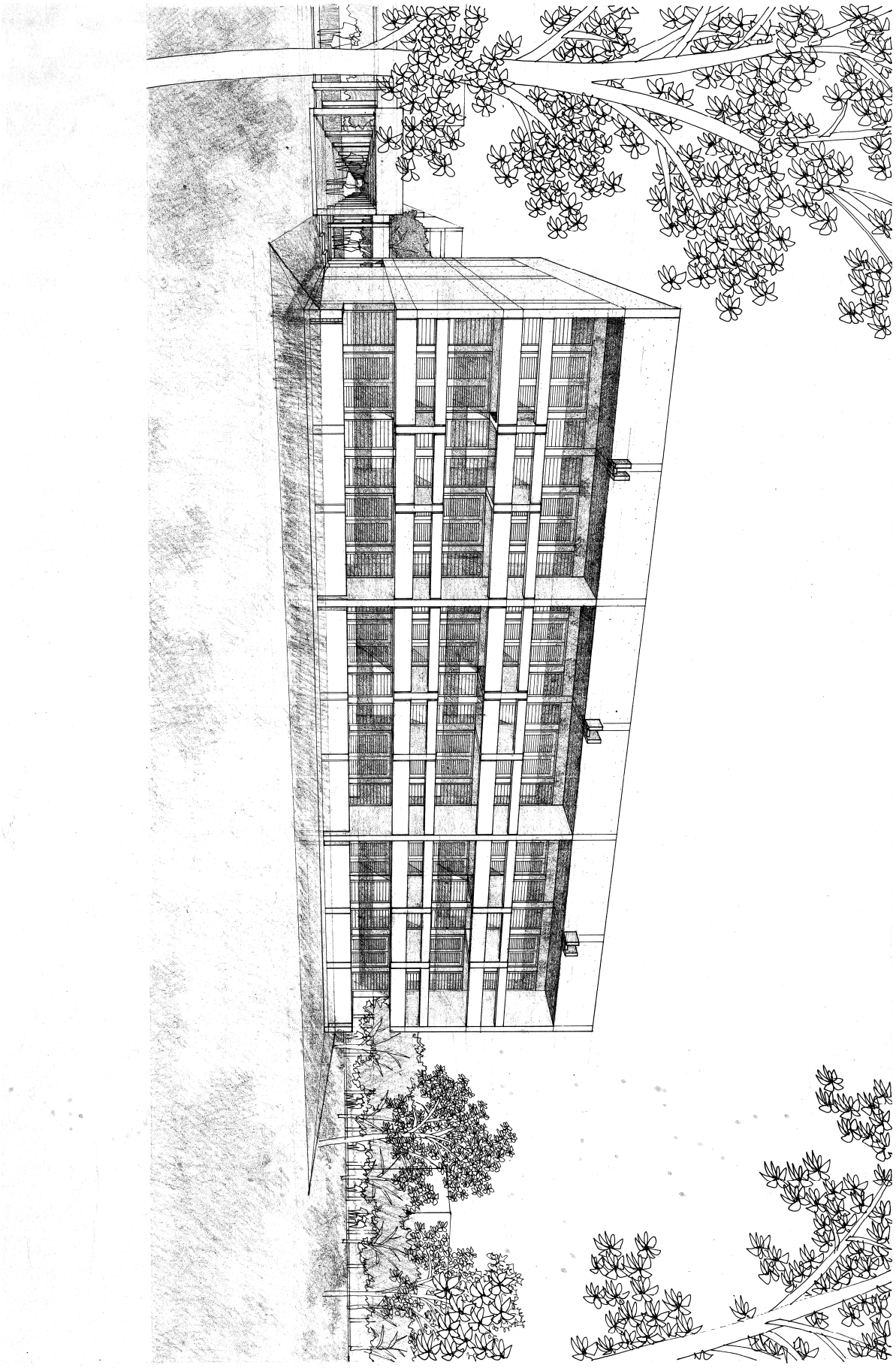

Annex 3: Ambient vibration data of the field study building

Set	Location	X-direction ambient vibration	Y-direction ambient vibration
C-1	First (ground) floor	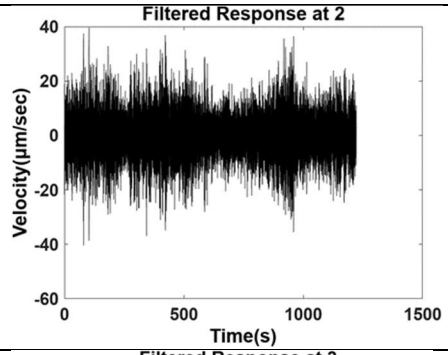	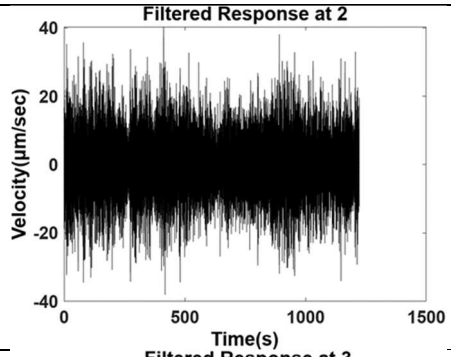
	Second Floor	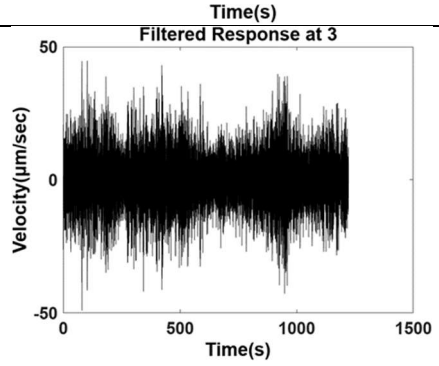	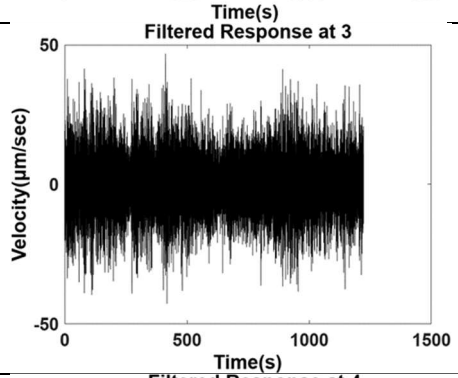
	Third Floor	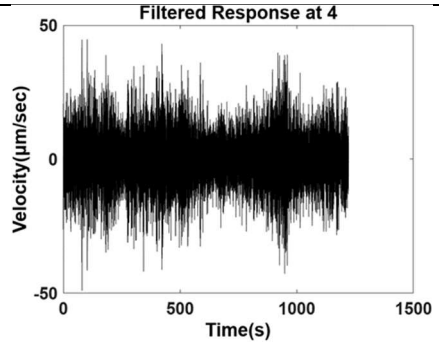	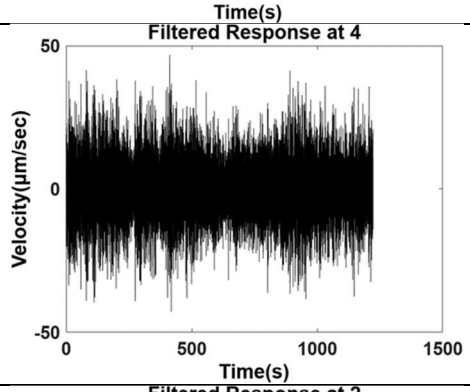
B-1	First (ground) floor	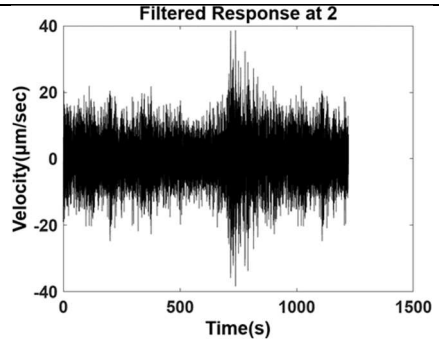	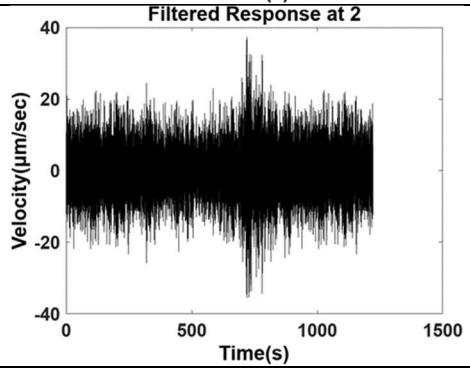

	Second Floor	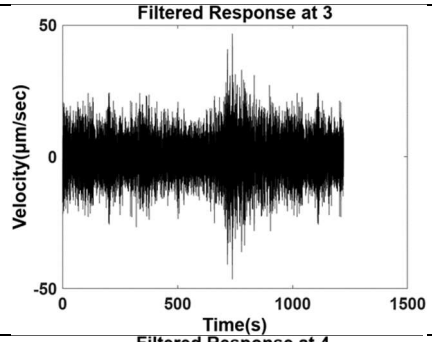	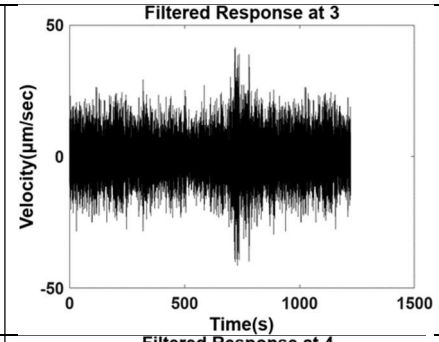
	Third Floor	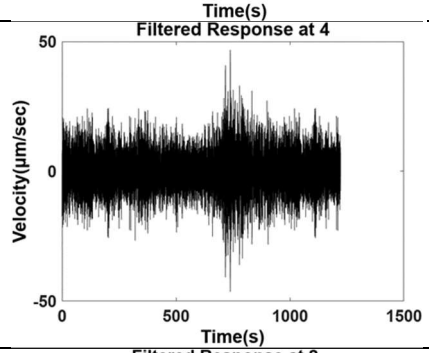	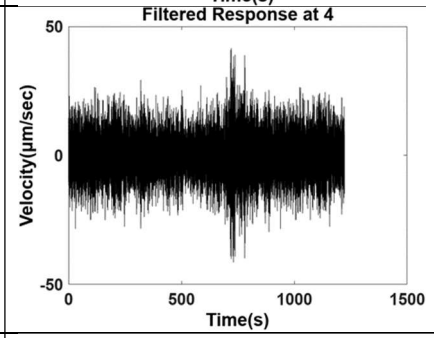
A-1	First Floor	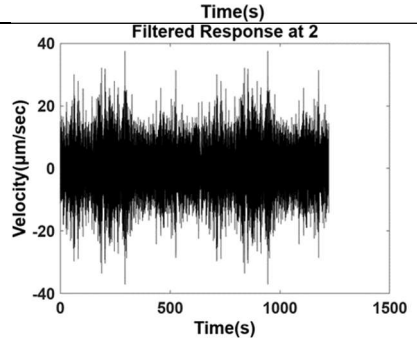	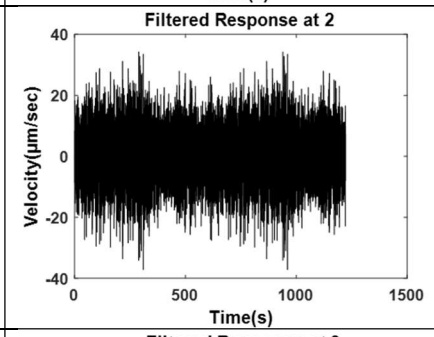
	Second Floor	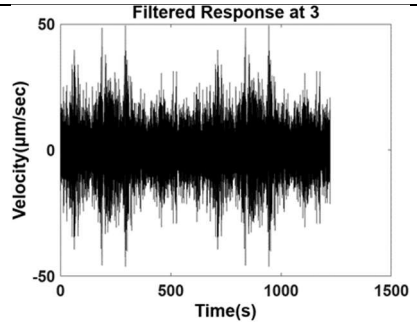	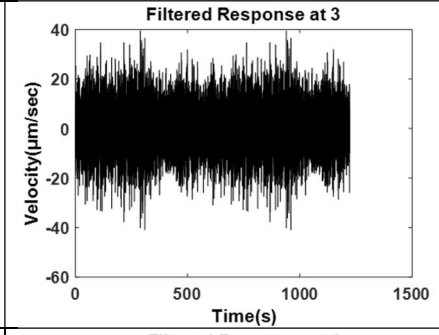
	Third Floor	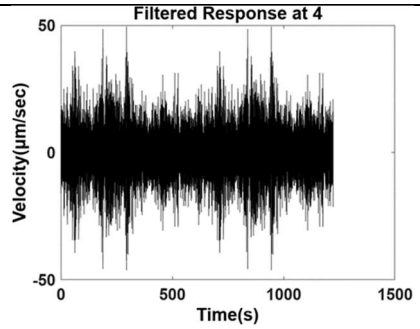	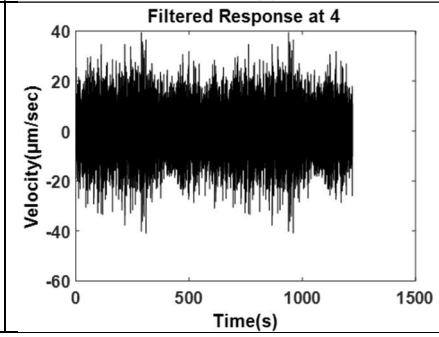

A-2	First Floor	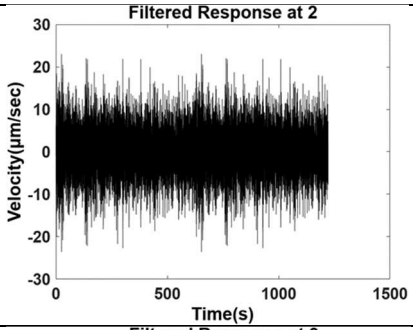	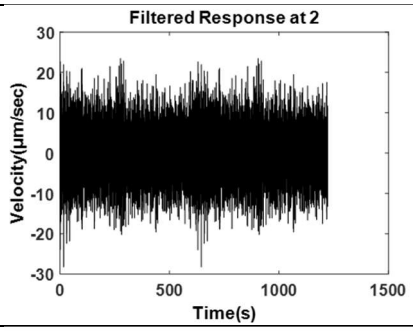
	Second Floor	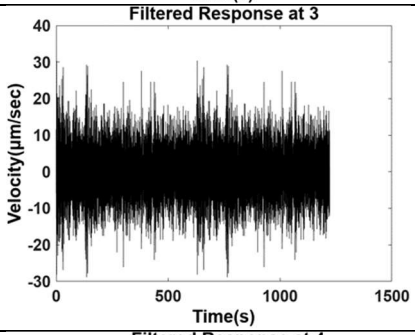	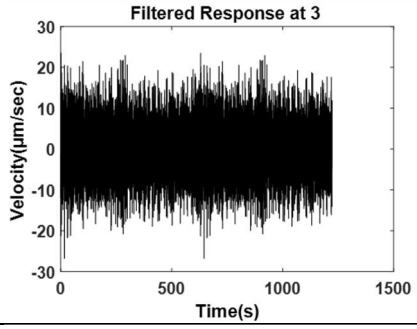
	Third Floor	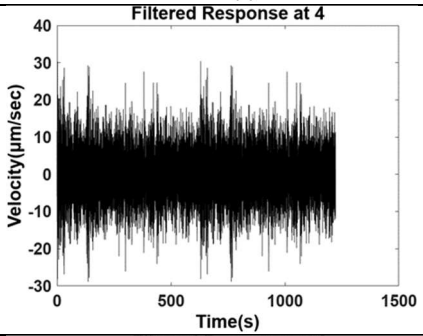	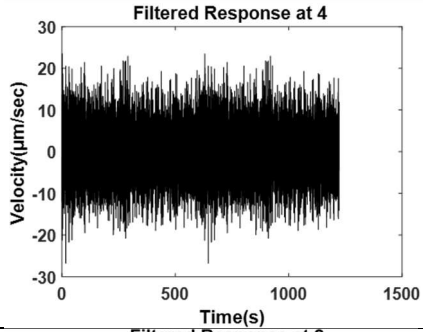
B-2	First Floor	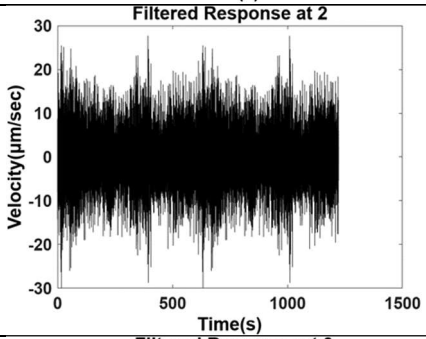	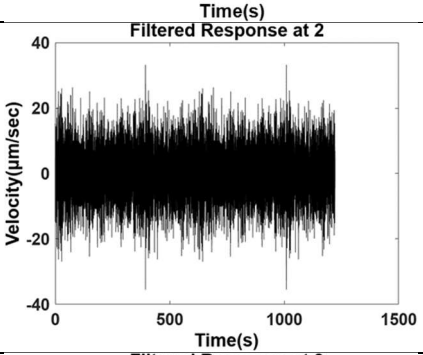
	Second Floor	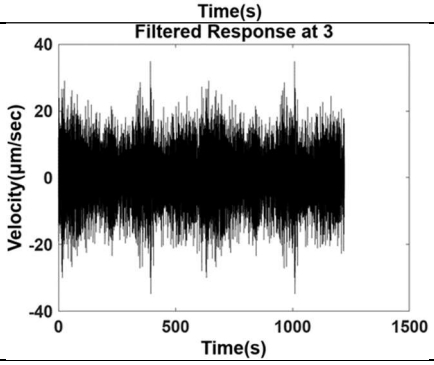	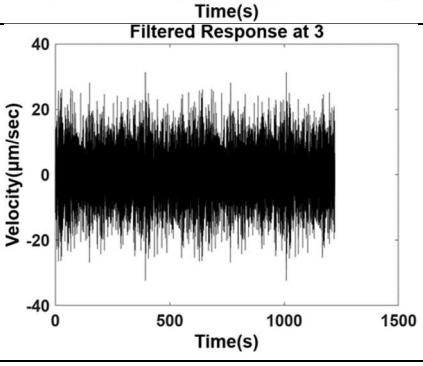

	Third Floor	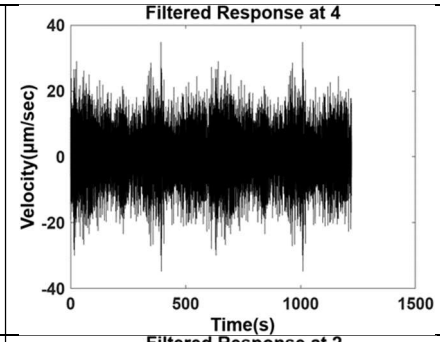	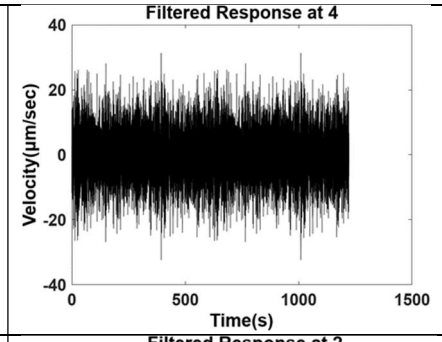
C-2	First Floor	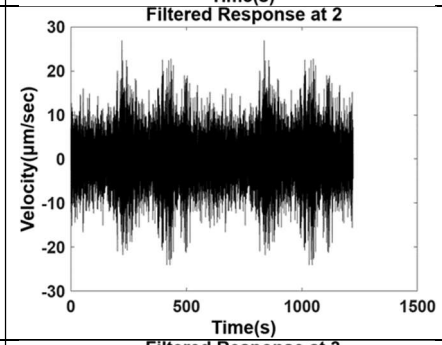	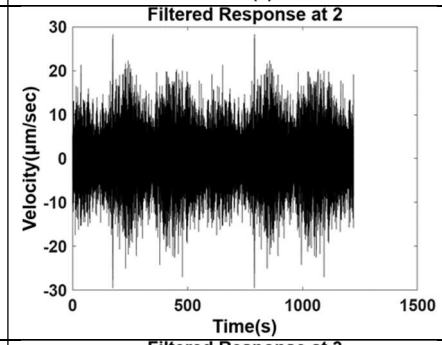
	Second Floor	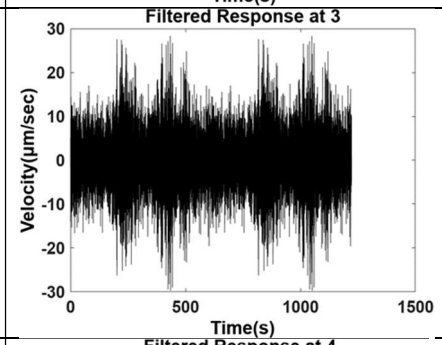	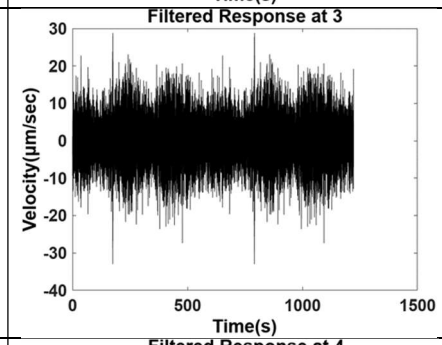
	Third Floor	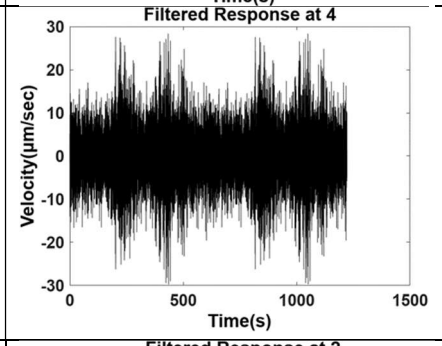	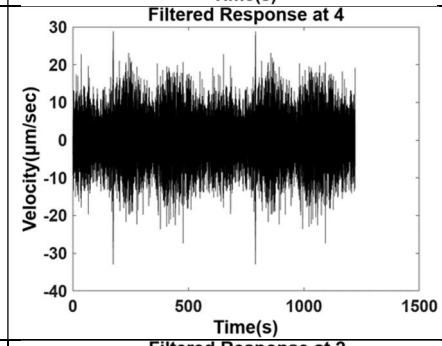
	First Floor	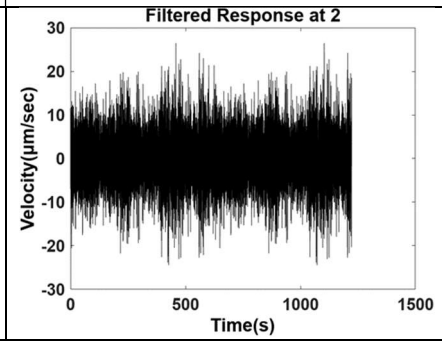	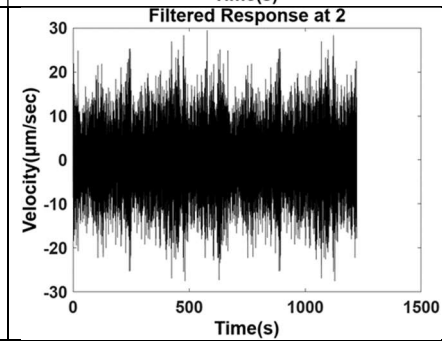

C-4	Second Floor	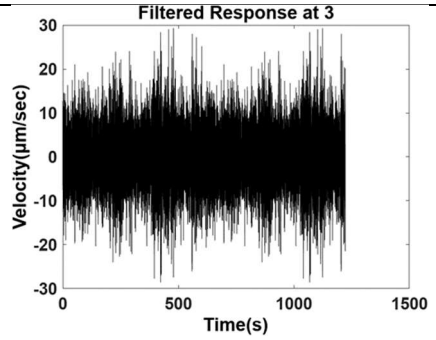	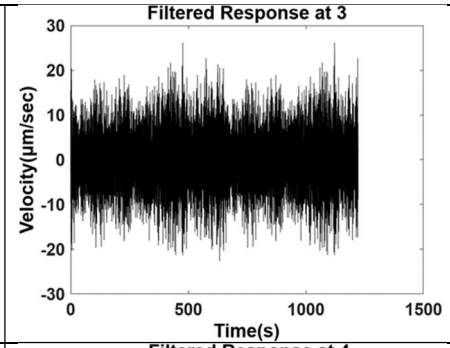
	Third Floor	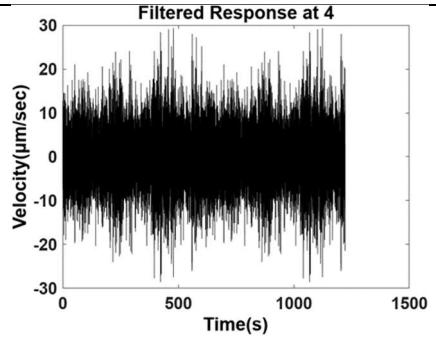	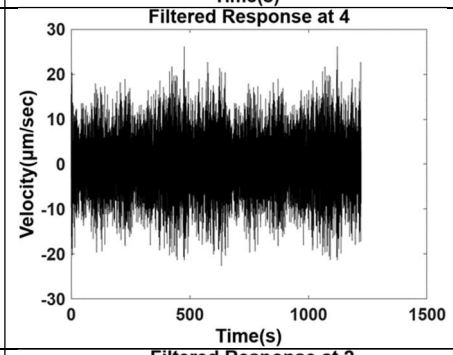
B-4	First Floor	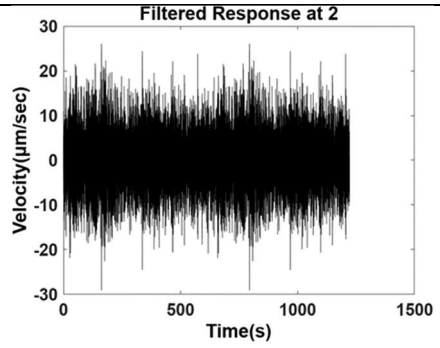	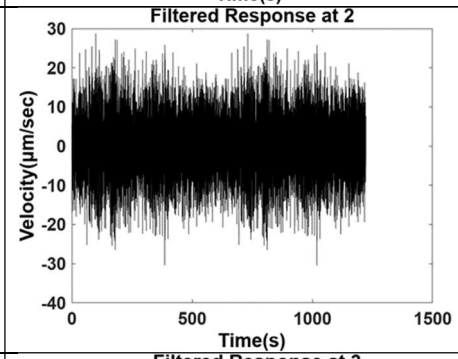
	Second Floor	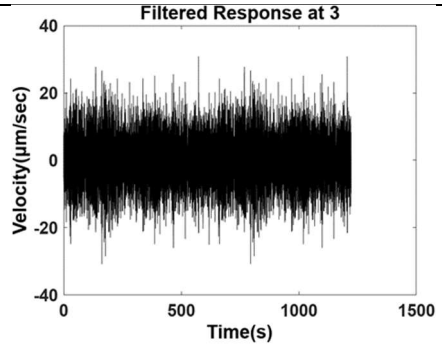	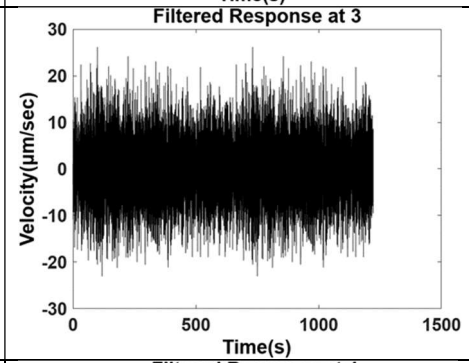
	Third Floor	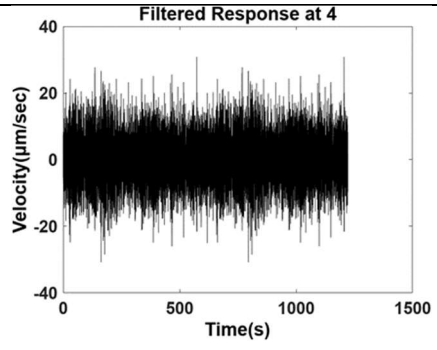	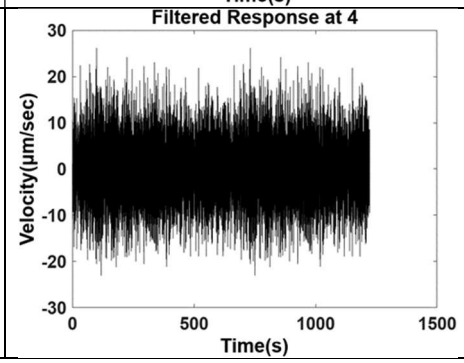

A-4	First Floor	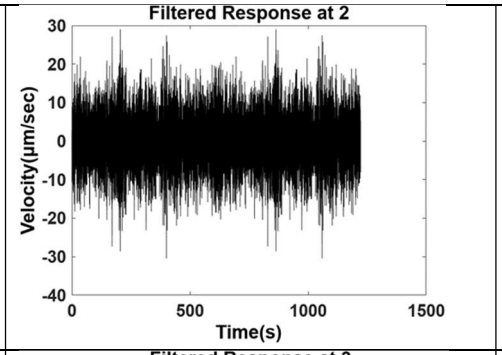	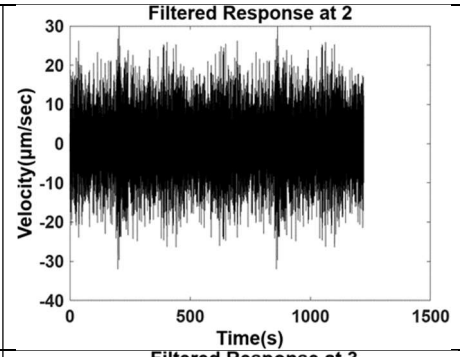
	Second Floor	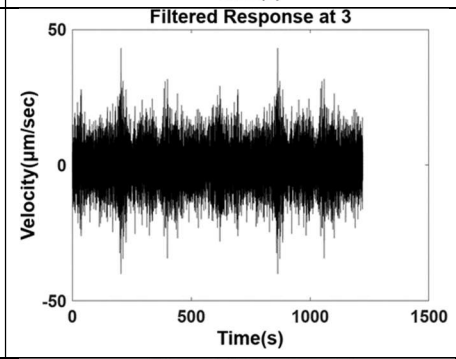	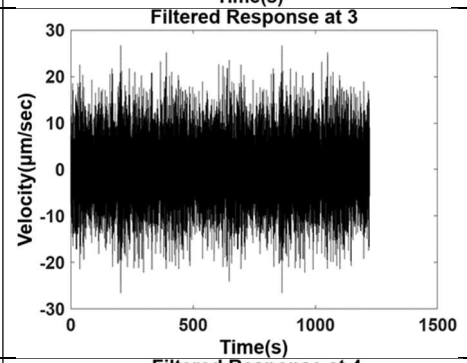
	Third Floor	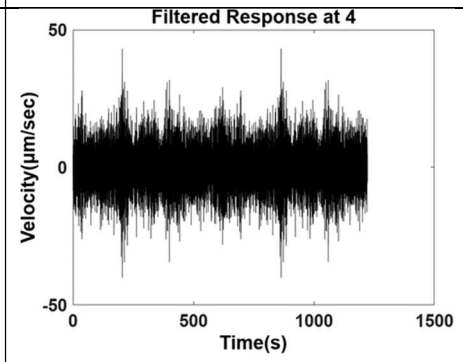	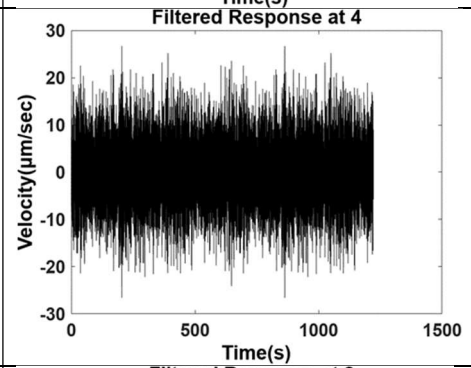
A-5	First Floor	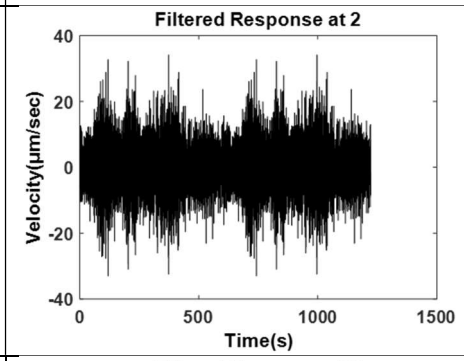	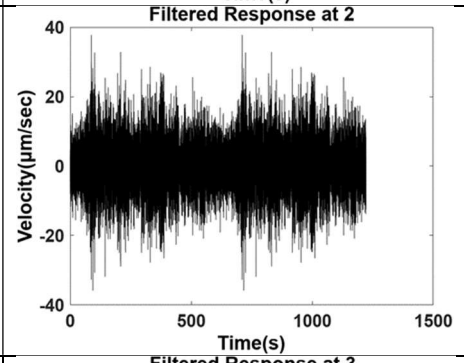
	Second Floor	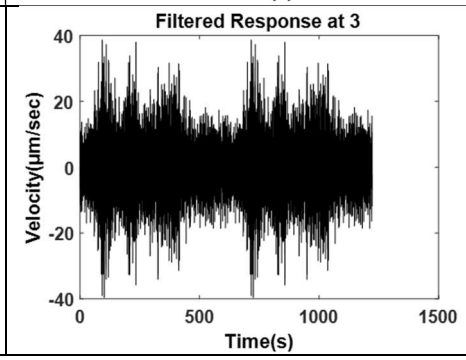	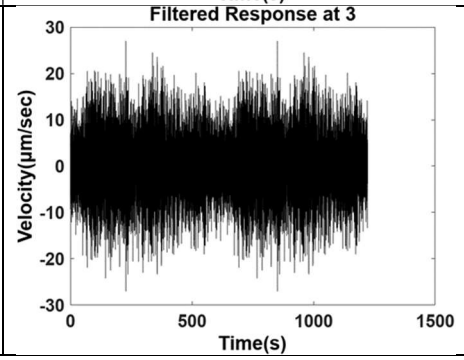

	Third Floor	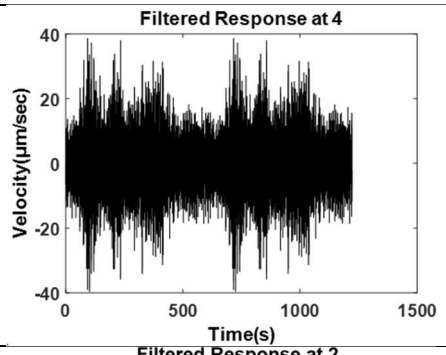	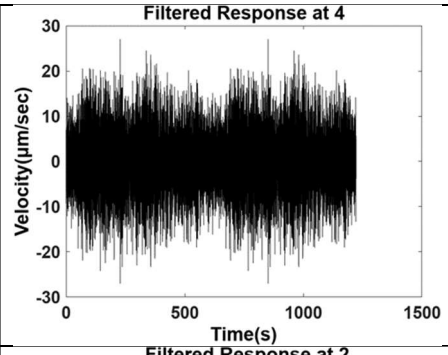
B-5	First Floor	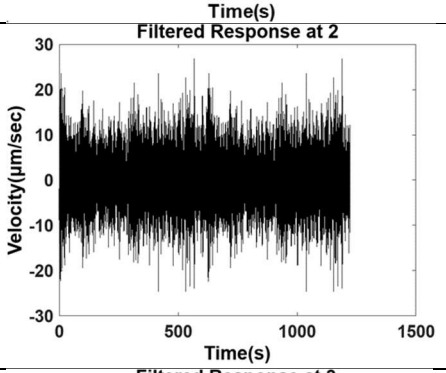	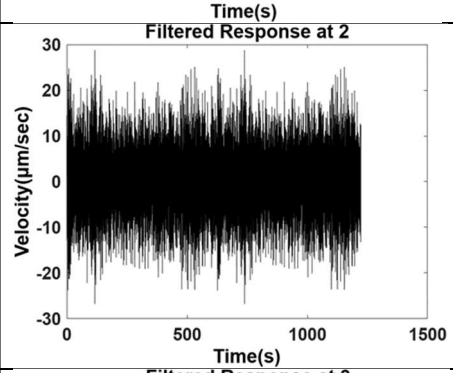
	Second Floor	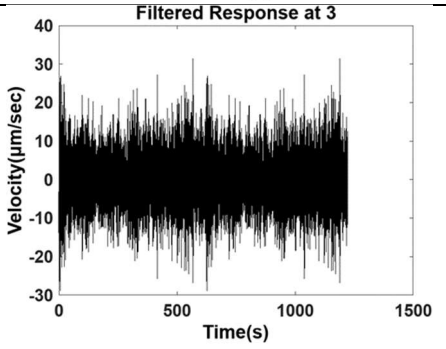	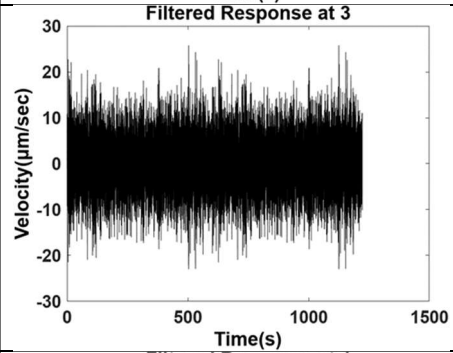
	Third Floor	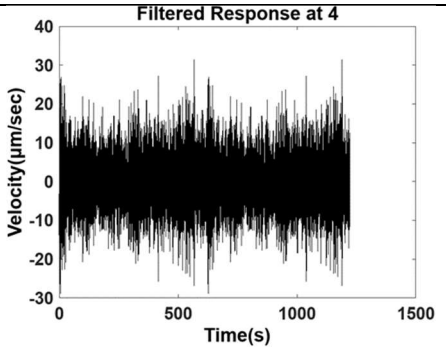	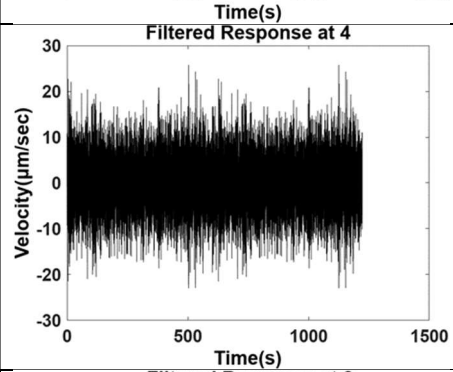
C-5	First Floor	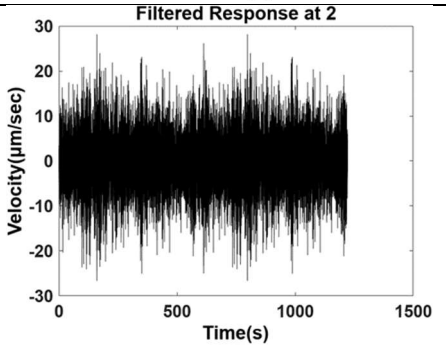	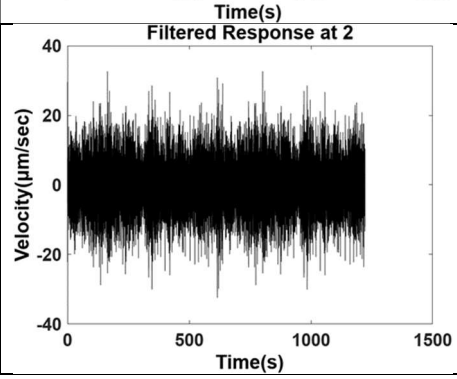

	Second Floor	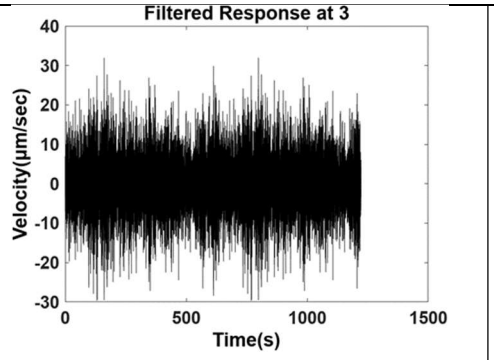	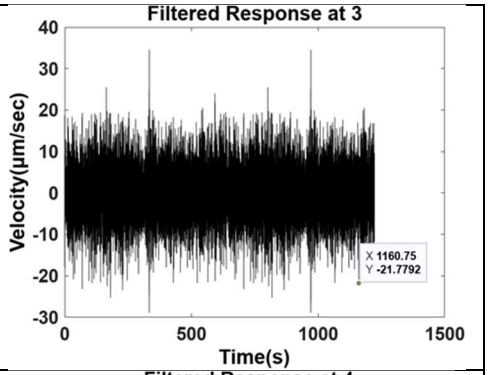
	Third Floor